

Univerza
v Ljubljani

*Fakulteta za
gradbeništvo in
geodezijo*



FRANC SINUR, univ. dipl. inž. grad.

**VZDOLŽNO OJAČANI POLNOSTENSKI NOSILCI PRI
INTERAKCIJI VELIKIH UPOGIBNIH IN STRIŽNIH
OBREMENITEV**

DOKTORSKA DISERTACIJA

Ljubljana, julij 2011

Univerza
v Ljubljani

Fakulteta za
*gradbeništvo in
geodezijo*



PODIPLOMSKI ŠTUDIJ
GRADBENIŠTVA

DOKTORSKI ŠTUDIJ

Kandidat:

FRANC SINUR, univ. dipl. inž. grad.

**VZDOLŽNO OJAČANI POLNOSTENSKI NOSILCI PRI
INTERAKCIJI VELIKIH UPOGIBNIH IN STRIŽNIH
OBREMENITEV**

Doktorska disertacija štev.: 215

**BEHAVIOUR OF LONGITUDINALLY STIFFENED
PLATE GIRDERS SUBJECTED TO BENDING-SHEAR
INTERACTION**

Doctoral thesis No.: 215

Soglasje k temi doktorske disertacije je dala Komisija za doktorski študij na 23. seji dne 9. julija 2009 in za mentorja imenovala prof. dr. Darka Bega ter dala soglasje k pisanju disertacije v angleškem jeziku.

Ljubljana, 8. julij 2011

Univerza
v Ljubljani

Fakulteta za
*gradbeništvo in
geodezijo*



Komisijo za oceno ustreznosti teme doktorske disertacije v sestavi

- prof. dr. Darko Beg,
- izr. prof. dr. Jože Korelc,
- prof. dr. Stojan Kravanja, UM FG.

je imenoval Senat Fakultete za gradbeništvo in geodezijo na 26. redni seji
dne 25. marca 2009.

Komisijo za oceno doktorske disertacije v sestavi

- prof. dr. Jože Korelc,
- prof. dr. Ulrike Kuhlmann, Stuttgart University,
- prof. dr. Laszlo Dunai, BME - Budapest University of
Technology and Economics,

je imenoval Senat Fakultete za gradbeništvo in geodezijo na 21. redni seji
dne 25. maja 2011.

Komisijo za zagovor doktorske disertacije v sestavi

- prof. dr. Matjaž Mikoš, dekan UL FGG, predsednik,
- prof. dr. Darko Beg, mentor,
- prof. dr. Jože Korelc,
- prof. dr. Ulrike Kuhlmann, Stuttgart University,
- prof. dr. Laszlo Dunai, BME - Budapest University of
Technology and Economics,

je imenoval Senat Fakultete za gradbeništvo in geodezijo na 22. redni seji
dne 22. junija 2011.

Univerza
v Ljubljani

Fakulteta za
*gradbeništvo in
geodezijo*



IZJAVA O AVTORSTVU

Podpisani **Franc SINUR, univ. dipl. inž. grad.**, izjavljam, da sem avtor doktorske disertacije z naslovom: »**VZDOLŽNO OJAČANI POLNOSTENSKI NOSILCI PRI INTERAKCIJI VELIKIH UPOGIBNIH IN STRIŽNIH OBREMENITEV**«.

Izjavljam, da je elektronska različica v vsem enaka tiskani različici.

Izjavljam, da dovoljujem objavo elektronske različice v repozitoriju UL FGG.

Ljubljana, 8. julij 2011

.....
(podpis)

ERRATA

| Page | Line | Error | Correction |
|------|------|-------|------------|
|------|------|-------|------------|

BIBLIOGRAPHIC-DOCUMENTALISTIC INFORMATION

UDC: 624.01:624.04:624.072.2(043.2)
Author: Franc Sinur
Supervisor: Prof. dr. Darko Beg
Title: Behaviour of longitudinally stiffened plate girders subjected to bending-shear interaction
Notes: 205 p., 32 tab., 136 fig., 83 eq., 2 ann.
Keywords: plated girders, bending-shear interaction, experimental tests, transverse stiffeners, numerical simulations, EN 1993-1-5

Abstract

Slender plated girders are usually composed of slender webs and compact flanges. In order to increase their capacity, they are stiffened with transverse and longitudinal stiffeners of different shapes. Thin plated girders used to support loads over long spans develop significant post-critical resistance after the plate buckling occurs. To achieve better understanding of longitudinally stiffened plated girders subjected to high bending moments and shear forces, four experimental tests on large scale test specimens were performed. The results of these tests were used to verify the numerical model, which was employed for further parametric studies. With numerical simulations the influence of initial imperfections and residual stresses on the capacity of girders was investigated. Initial imperfections were considered as actual measured initial imperfections, as positive buckling modes and as deformed shapes, based on preliminary nonlinear calculations of perfect girders. Residual stresses were considered with a simplified stress pattern where the level of compression stresses was varied. The final residual stresses were determined on the basis of residual stresses measured in the tested girder. With a verified simplified numerical model a parametric nonlinear analysis was systematically carried out to determine the resistance of longitudinally stiffened plated girders. Based on 630 numerical simulations a new equation for interaction at high bending moments and shear forces, as well as the section, where the check should be performed is proposed. An extensive reliability analysis of five different design models was made, i.e., the EN 1993-1-5 interaction model, the proposed new model, the gross cross-section bending resistance model and two models, which are a combination of the first three. The purpose of this reliability analysis is to determine partial safety factors and study the adequacy of the EN 1993-1-5 resistance model. The studies have shown, that the capacity of longitudinally stiffened plated girders can satisfactory be determined according to EN 1993-1-5 under the condition, that the check is made at a distance $h_{wi,max}/2$ and that the gross cross-section bending capacity includes safety factor $\gamma_{MI} = 1,1$. Finally, the influence of the tension field action on intermediate transverse stiffeners was studied. Two tests on a full scale girder were performed to determine the axial forces in transverse stiffeners. Parametric study, where the influence of stiffener's stiffnesses on the girders limit capacity was investigated, followed. The EN design rule for axial forces in transverse stiffeners, proved to be conservative, thereby a new design rule for rigid intermediate transverse stiffeners, based on the minimum flexural stiffness of a stiffener is proposed.

BIBLIOGRAFSKO-DOKUMENTACIJSKA STRAN

| | |
|-------------------------|---|
| UDK: | 624.01:624.04:624.072.2(043.3) |
| Avtor: | Franc Sinur, univ. dipl. inž. grad. |
| Mentor: | prof. Dr. Darko Beg, univ. dipl. inž. grad. |
| Naslov: | Vzdolžno ojačani polnostenski nosilci pri interakciji velikih upogibnih in strižnih obremenitev |
| Obseg in oprema: | 205 str., 32 pregl., 136 sl., 83 en., 2 pril. |
| Ključne besede: | polnostenski nosilci, interakcija strg-upogib, eksperimentalni testi, prečne ojačitve, numerične simulacije, EN 1993-1-5 |

Izvleček

Polnostenske nosilce običajno sestavljajo vitke stojine in kompaktne pasnice. Za povečanje nosilnosti se stojina ojača s prečnimi in vzdolžnimi ojačitvami različnih oblik. Posebnost polnostenskih nosilcev, ki se uporabljajo za premostitev večjih razponov, je izkazovanje velike postkritične nosilnosti, ki je dosežena potem, ko se pločevina že izboči. Za boljše razumevanje obnašanja vzdolžno ojačanih polnostenskih nosilcev, obremenjenih z velikimi upogibnimi momenti in strižnimi silami, smo izvedli štiri eksperimente na nosilcih naravnih dimenzij. Rezultati eksperimentalnih testov so bili uporabljeni za verifikacijo numeričnega modela, uporabljenega za nadaljnje študije vpliva različnih parametrov. Na verifikiranem numeričnem modelu smo opravili študijo vpliva začetnih geometrijskih nepopolnosti in zaostalih napetosti na nosilnost. Upoštewane so bile naslednje začetne geometrijske nepopolnosti: dejanske izmerjene, lastne oblike uklonske analize in deformirane oblike nosilca, določene s predhodno nelinearno analizo idealnega nosilca. Vpliv zaostalih napetosti smo upoštevali s poenostavljenim modelom razporeditve napetosti po prerezu, pri čemer smo spreminjali nivo tlačnih napetosti v pločevini. Končno vrednost vpliva zaostalih napetosti smo določili na podlagi nivoja zaostalih napetosti, ki smo jih izmerili v prerezu testnega nosilca. S poenostavljenim verificiranim numeričnim modelom smo z namenom določitve nosilnosti vzdolžno ojačanih nosilcev sistematično opravili parametrično nelinearno analizo. Na podlagi 630 numeričnih simulacij smo določili novo interakcijsko enačbo za območje velikih strižnih in upogibnih obremenitev ter določili prerez v panelu, kjer naj se kontrola interakcije izvede. Sledila je obširna analiza zanesljivosti petih modelov odpornosti, in sicer modela odpornosti iz EN 1993-1-5, novo določene enačbe, modela, ki določa bruto upogibno nosilnost prereza, ter dveh modelov, ki sta kombinacija prvih treh. Namen analize zanesljivosti je bil določitev delnih varnostnih faktorjev in kontrola ustreznosti modelov, ki jih določa EN 1993-1-5. Na podlagi obsežnih analiz smo pokazali, da se nosilnost vzdolžno ojačanih polnostenskih nosilcev lahko določi po EN 1993-1-5 pri pogojih, da se interakcija izvede na oddaljenosti $h_{wi,max}/2$ in da se pri bruto upogibni nosilnosti prereza upošteva varnostni faktor $\gamma_{MI} = 1,1$. V zadnjem delu naloge smo se dotaknili tudi določitve vplivov diagonalnega nateznega polja na vmesne prečne ojačitve. V ta namen smo opravili dva eksperimentalna testa na nosilcih naravne velikosti ter tako določili velikost osnih sil v prečnih ojačitvah. Sledila je sistematična parametrična študija, na podlagi katere smo raziskali vpliv togosti ojačitev na mejno nosilnost nosilca. Pokazali smo, da je določanje velikosti osnih sil po EN 1993-1-5 konzervativno, in predlagali nov način projektiranja togih prečnih ojačitev, ki temelji le na upogibni togosti teh ojačitev.

ZAHVALA

Delo, ki je bilo opravljeno v okviru disertacije, je bilo delno financirano s strani Ministrstva za visoko šolstvo, znanost in tehnologijo, v okviru programa mladih raziskovalcev.

Prof. dr. Darko Beg, hvala vam, da ste mi dali možnost in me sprejeli pod svoje mentorstvo za doktorsko delo. Hvala vam za vse koristne nasvete, spodbudo in vodenje skozi raziskovalno delo. Hvala vam, da ste mi zaupali tako obsežen projekt, verjeli vame in me vključili tudi v ostale projekte, kjer sem dobil prepotrebne izkušnje tudi na strokovnem področju.

Franci Čepon in doc. dr. Jože Lopatič, hvala vama za vajin trud in pomoč pri izvedbi eksperimentalnih testov. Posebna zahvala vam, Jože Lopatič, za vse nasvete in pripravo programov za izvedbo testov. Hvala tudi tebi Uroš Hočevar, da si se vedno odzval in mi pomagal pri pripravi testov, tudi v večernih urah.

Blaž Čermelj, vedno si mi bil na voljo in mi priskočil na pomoč. Hvala ti za vse. Niko Kristanič, prijatelj, bil si tako rekoč moj drugi mentor. Hvala ti za vse pogovore, nasvete in pomoč. Hvala tudi ostalim kolegom na katedri: Primožu Možetu, Luki Pavlovčiču, Petru Skubru in Teji Melink.

Na tem mestu bi se rad zahvalil tudi vsem mojim prijateljem, še posebno Davidu Duhu, Klemnu Rejcu, Damjanu Golobu, Zlatku Vidrihu, Maticu Poznič, Mihi Maražu, Davidu Korenu in Klemnu Podobniku. Hvala vam za vse prijetne trenutke, tebi David in Klemen pa iskrena hvala, da sta mi bila vedno pripravljena prisluhniti.

Hvala tudi moji družini, mami Anici, očetu Dragotu, sestri Mateji ter bratoma Matjažu in Blažu, ki ste mi omogočili, da sem lahko stopal po tej poti.

Na koncu bi se rad zavalil tebi, moja Meta, za vzpodbudo, pomoč in razumevanje. Hvala ti, da si kljub težkim trenutkom našla čas in mi vedno priskočila na pomoč.

Hvala tudi vsem ostalim, ki ste prispevali k mozaiku, včasih naporne, a na koncu čudovite in nepozabne poti.

TABLE OF CONTENTS

| | |
|---|-------------|
| ZAHVALA | VII |
| TABLE OF CONTENTS | IX |
| INDEX OF FIGURES | XIII |
| INDEX OF TABLES | XVII |
| 1 INTRODUCTION | 1 |
| 1.1 MOTIVATION AND OBJECTIVES | 1 |
| 1.2 THESIS CONTENT | 2 |
| 2 REVIEW OF EARLIER WORK | 5 |
| 2.1 INTRODUCTION..... | 5 |
| 2.2 SHEAR RESISTANCE | 5 |
| 2.3 SHEAR RESISTANCE OF LONGITUDINALLY STIFFENED PLATED GIRDERS | 7 |
| 2.4 BENDING STRENGTH OF PLATED GIRDERS | 7 |
| 2.5 BENDING-SHEAR INTERACTION | 8 |
| 2.6 RECENT RESEARCH WORK ON LONGITUDINALLY STIFFENED GIRDERS..... | 11 |
| 2.7 TRANSVERSE STIFFENERS | 12 |
| 3 EXPERIMENTAL PROGRAM | 15 |
| 3.1 EXPERIMENTAL INVESTIGATIONS | 15 |
| 3.1.1 <i>General</i> | 15 |
| 3.1.2 <i>Girder description</i> | 15 |
| 3.1.3 <i>Material</i> | 17 |
| 3.1.4 <i>Test procedure</i> | 18 |
| 3.1.5 <i>Instrumentation</i> | 19 |
| 3.2 INITIAL IMPERFECTIONS | 21 |
| 3.2.1 <i>Geometrical imperfections</i> | 21 |
| 3.2.2 <i>Residual stresses</i> | 26 |
| 3.3 TEST RESULTS | 28 |
| 3.3.1 <i>Resistance of tested girders</i> | 28 |
| 3.3.2 <i>Web buckling of tested panel</i> | 30 |
| 3.3.3 <i>Comparison to EN 1993-1-5</i> | 39 |
| 3.3.4 <i>Strain measurement</i> | 39 |
| 3.4 DISCUSSION | 46 |
| 4 NUMERICAL MODEL | 49 |
| 4.1 INTRODUCTION - THE FINITE ELEMENT METHOD | 49 |
| 4.2 GEOMETRY | 50 |
| 4.3 MATERIAL | 50 |
| 4.3.1 <i>The yield criterion</i> | 50 |
| 4.3.2 <i>Material idealisation</i> | 51 |
| 4.4 FINITE ELEMENTS IN ABAQUS - SHELL ELEMENTS USED | 51 |
| 4.5 ANALYSIS..... | 52 |
| 5 VALIDATION OF NUMERICAL MODEL | 55 |
| 5.1 SUMMARY OF FEM – ANNEX C OF EN 1993-1-5 | 55 |

| | | |
|----------|---|------------|
| 5.1.1 | <i>Initial imperfections</i> | 56 |
| 5.1.2 | <i>Material model</i> | 57 |
| 5.2 | MESH CONVERGENCE | 59 |
| 5.3 | NUMERICAL SIMULATIONS OF TESTED GIRDERS | 62 |
| 5.3.1 | <i>Girder SO</i> | 63 |
| 5.3.2 | <i>Girder SC</i> | 66 |
| 5.3.3 | <i>Girder UO</i> | 70 |
| 5.3.4 | <i>Girder UC</i> | 73 |
| 5.3.5 | <i>Discussion</i> | 76 |
| 5.4 | IMPERFECTION SENSITIVITY ANALYSIS | 76 |
| 5.4.1 | <i>Influence of imperfection shapes and amplitudes</i> | 77 |
| 5.4.2 | <i>Residual stresses</i> | 80 |
| 5.4.3 | <i>Discussion</i> | 82 |
| 5.5 | NUMERICAL MODEL USED IN PARAMETRIC STUDY | 83 |
| 6 | PARAMETRIC STUDY | 85 |
| 6.1 | INTRODUCTION | 85 |
| 6.2 | PARAMETERS | 85 |
| 6.2.1 | <i>Variation</i> | 85 |
| 6.3 | NUMERICAL RESULTS, FAILURE MECHANISM | 87 |
| 6.3.1 | <i>Group I - Variation of the A_f/A_w ratio</i> | 88 |
| 6.3.2 | <i>Group II - Variation of web slenderness h_w/t_w</i> | 92 |
| 6.3.3 | <i>Group III - Variation of panel aspect ratio α</i> | 95 |
| 6.3.4 | <i>Group IV - Variation of stiffness of longitudinal stiffener γ/γ^*</i> | 98 |
| 6.4 | DISCUSSION | 104 |
| 7 | M-V INTERACTION | 107 |
| 7.1 | INTRODUCTION | 107 |
| 7.2 | GIRDER RESISTANCE ACCORDING TO EN 1993-1-5 | 107 |
| 7.2.1 | <i>Resistance to shear load</i> | 107 |
| 7.2.2 | <i>Resistance to bending moment</i> | 109 |
| 7.2.3 | <i>M-V interaction</i> | 115 |
| 7.3 | EVALUATION OF CURRENT M-V INTERACTION | 116 |
| 7.3.1 | <i>Discussion</i> | 118 |
| 7.4 | NEW PROPOSAL FOR M-V INTERACTION | 121 |
| 7.5 | DETERMINATION OF THE PARTIAL SAFETY FACTOR | 126 |
| 7.5.1 | <i>Statistical evaluation of resistance models</i> | 127 |
| 7.5.2 | <i>Uncertainties in the model - determination of V_{xi}</i> | 129 |
| 7.5.3 | <i>Resistance models</i> | 130 |
| 7.5.4 | <i>Comparison and evaluation of results</i> | 137 |
| 8 | INTERMEDIATE TRANSVERSE STIFFENERS | 141 |
| 8.1 | INTRODUCTION | 141 |
| 8.2 | REQUIERMENTS IN EN 1993-1-5 | 141 |
| 8.3 | EXPERIMENTAL INVESTIGATION | 142 |
| 8.3.1 | <i>Test results</i> | 143 |
| 8.3.2 | <i>Model verification</i> | 146 |
| 8.3.3 | <i>Discussion</i> | 147 |
| 8.4 | NUMERICAL SIMULATION | 148 |
| 8.4.1 | <i>Parameters</i> | 148 |

| | | |
|-------------|--|------------|
| 8.4.2 | Results | 149 |
| 8.5 | DISCUSSIONS..... | 153 |
| 9 | CONCLUSIONS AND SUGGESTIONS FOR FURTHER WORK..... | 155 |
| 9.1 | SUMMARY AND CONCLUSIONS..... | 155 |
| 9.2 | THE ORIGINAL CONTRIBUTIONS | 158 |
| 9.3 | SUGGESTIONS FOR FURTHER WORK..... | 158 |
| I. | UVOD | 159 |
| II. | EKSPERIMENTALNI TESTI..... | 161 |
| III. | NUMERIČNI MODEL | 173 |
| IV. | PARAMETRIČNA ŠTUDIJA IN PRIMERJAVA Z RAČUNSKIMI MODELI | 176 |
| V. | TOGOST PREČNE OJAČITVE..... | 184 |
| VI. | ZAKLJUČEK..... | 185 |
| | ANNEX A: LAYOUT OF TESTED GIRDERS UNDER M-V INTERACTION | 186 |
| | ANNEX B: LAYOUT OF TESTED GIRDERS N1 - S1 AND N1 – S2..... | 198 |
| | REFERENCES..... | 201 |

INDEX OF FIGURES

| | |
|---|----|
| Figure 1: Tension field formation [22]..... | 5 |
| Figure 2: Bending stresses in the slender web plate [22] | 8 |
| Figure 3: Shear-moment interaction diagrams [22]..... | 9 |
| Figure 4: Resistance of I girder from three point bending tests [18]..... | 11 |
| Figure 5: FE parametric analysis performed on beams like the one used by Wargsjö [18]..... | 11 |
| Figure 6: Girder geometry – Symmetric cross-section..... | 16 |
| Figure 7: Girder geometry – Unsymmetric cross-section..... | 17 |
| Figure 8: Stress-strain diagram of tensile tests of 5mm thick plate..... | 18 |
| Figure 9: Test set-up – laboratory..... | 18 |
| Figure 10: Test set-up – schematic view | 18 |
| Figure 11: Loading protocol for tested girders..... | 19 |
| Figure 12: Instrumentation of tested girders..... | 20 |
| Figure 13: Setup of tested panels for photogrammetry..... | 21 |
| Figure 14: Measurements of initial imperfections of panel SO..... | 22 |
| Figure 15: Measurements of initial imperfections of panel SC..... | 23 |
| Figure 16: Measurements of initial imperfections of panel UO | 24 |
| Figure 17: Measurements of initial imperfections of panel SC..... | 25 |
| Figure 18: Position of residual stress measurement in asymmetric plated girder..... | 26 |
| Figure 19: Positions of measured residual strains | 26 |
| Figure 20: Measured residual stresses | 28 |
| Figure 21: Load-displacement curves for tested girders..... | 29 |
| Figure 22: Out-of-plane displacement development in measured points W13 and W14 | 30 |
| Figure 23: Evolution of out-of plane displacement during the test, SO | 32 |
| Figure 24: Evolution of out-of plane displacement during the test, SC..... | 34 |
| Figure 25: Evolution of out-of plane displacement during the test, UO..... | 37 |
| Figure 26: Evolution of out-of plane displacement during the test, UC..... | 39 |
| Figure 27: Principal membrane strains ($\epsilon_1 = E1$, $\epsilon_2 = E2$) in the web measured by strain gauge rosettes..... | 41 |
| Figure 28: Angle of inclination θ of the first principal deformation | 42 |
| Figure 29: The principal membrane stress orientation and values obtained at maximum load..... | 42 |
| Figure 30: Strain measurement in compression and tension flange..... | 43 |
| Figure 31: Position of strain gauges in the upper (compression) and lower (tension) flange..... | 44 |
| Figure 32: Strains measured in the transverse stiffener when SO is tested | 44 |
| Figure 33: Strains measured in the transverse stiffener when SC is tested..... | 45 |
| Figure 34: Strains measured in the transverse stiffener when UO is tested..... | 45 |
| Figure 35: Strains measured in the transverse stiffener when UC is tested..... | 46 |
| Figure 36: Unstable static equilibrium solution..... | 52 |
| Figure 37: Modelling of equivalent geometric imperfections | 57 |
| Figure 38: Modified nominal stress-strain curves of uni-axial tensile tests | 58 |
| Figure 39: Modelling of the material behaviour in the parametric study | 58 |
| Figure 40: Modelling of the material behaviour in the parametric study | 58 |
| Figure 41: Number of finite elements and used CPU time vs. size of the finite element..... | 60 |
| Figure 42: Number of increments vs. size of the finite element..... | 60 |
| Figure 43: Force-displacement curves for different mesh densities (mesh edge distance) of girder..... | 61 |
| Figure 44: Out-of-plane displacement at cross-section $x = 400$ mm from the most stressed edge..... | 61 |
| Figure 45: The influence of mesh density on displacement and capacity of girder..... | 62 |
| Figure 46: Comparison of load-deflection curves for panel SO..... | 63 |

| | |
|--|----|
| Figure 47: Evolution of the out-of-plane displacement of SO girder | 64 |
| Figure 48: Evolution of von Mises stress in the centre of the web plate - numerical simulation of the SO girder | 65 |
| Figure 49: Evolution of von Mises stress in the upper and bottom flange - numerical simulation of the SO girder | 66 |
| Figure 50: Deformed shape of tested panel SO | 66 |
| Figure 51: Comparison of load-deflection curves for girder SC..... | 67 |
| Figure 52: Evolution of the out-of-plane displacement of the SC girder..... | 68 |
| Figure 53: Evolution of von Mises stress in the centre of the web plate - numerical simulation of the SC girder | 69 |
| Figure 54: Evolution of von Mises stress in the upper and bottom flange - numerical simulation of the SC girder | 69 |
| Figure 55: Deformed shape of tested panel SC..... | 70 |
| Figure 56: Comparison of load-deflection curves for girder UO..... | 70 |
| Figure 57: Evolution of the out-of-plane displacements of the UO girder | 71 |
| Figure 58: Evolution of von Mises stress in the centre of the web plate - numerical simulation of the UO test.. | 72 |
| Figure 59: Evolution of von Mises stress in the upper and bottom flange - numerical simulation of the UO girder | 72 |
| Figure 60: Deformed shape of tested panel UO..... | 73 |
| Figure 61: Comparison of load-deflection curves for girder UC..... | 73 |
| Figure 62: Evolution of the out-of-plane displacement of the UC girder | 74 |
| Figure 63: Evolution of von Mises stress in the centre of the plate - numerical simulation of the UC test..... | 75 |
| Figure 64: Evolution of von Mises stress in the upper and bottom flange - numerical simulation of the UC girder | 75 |
| Figure 65: Deformed shape of tested panel UC..... | 76 |
| Figure 66: Imperfection shapes defined as buckling modes BM1-BM3 and as deformed shapes DS1, DS2 of SO girder..... | 77 |
| Figure 67: Points on load-deflection curves where deformed shapes were obtained (circle - DS1, triangle - DS2) | 78 |
| Figure 68: Influence of imperfection shape and amplitude on the girder resistance..... | 79 |
| Figure 69: Reduction of girders resistance for different imperfection shapes applied..... | 80 |
| Figure 70: Residual stress distribution in GMNIA analysis | 80 |
| Figure 71: The influence of residual stresses on the global girder behaviour..... | 81 |
| Figure 72: Reduction of the girder resistance for applied level of residual stresses | 82 |
| Figure 73: Influence of equivalent geometric imperfections (I1-I4), geometric imperfections (I5) and residual stresses (I6) on the girder resistance | 82 |
| Figure 74: Layout of numerical model | 83 |
| Figure 75: Girder's capacity computed by modified numerical model | 84 |
| Figure 76: Considered load cases in numerical simulations (red squares - EN 1993-1-5 interaction formulation in the range of high bending and shear load, green square - only bending check is considered)..... | 86 |
| Figure 77: Von Mises stresses for girders stiffened with one open stiffener at $h_w/4$ | 88 |
| Figure 78: Von Mises stresses for girders stiffened with one closed stiffener at $h_w/4$ | 89 |
| Figure 79: Von Mises stresses for girders stiffened with one open stiffener at $h_w/2$ | 90 |
| Figure 80: Von Mises stresses for girders stiffened with one closed stiffener at $h_w/2$ | 90 |
| Figure 81: Von Mises stresses for girders stiffened with two open stiffeners | 91 |
| Figure 82: Von Mises stresses for girders stiffened with two closed stiffeners..... | 92 |
| Figure 83: Von Mises stresses for girders stiffened with one open stiffener at $h_w/4$ | 93 |
| Figure 84: Von Mises stresses for girders stiffened with one closed stiffener at $h_w/4$ | 93 |
| Figure 85: Von Mises stresses for girders stiffened with one open stiffener at $h_w/2$ | 94 |
| Figure 86: Von Mises stresses for girders stiffened with one closed stiffener at $h_w/2$ | 94 |
| Figure 87: Von Mises stresses for girders stiffened with two stiffeners and web slenderness $h_w/t_w = 350$ | 95 |
| Figure 88: Von Mises stresses for girders stiffened with one open stiffener at $h_w/4$ | 96 |

| | |
|---|-----|
| Figure 89: Von Mises stresses for girders stiffened with one closed stiffener at $h_w/4$ | 96 |
| Figure 90: Von Mises stresses for girders stiffened with one open stiffener at $h_w/2$ | 97 |
| Figure 91: Von Mises stresses for girders stiffened with one closed stiffener at $h_w/2$ | 98 |
| Figure 92: Von Mises stresses for girders stiffened with one open stiffener at $h_w/4$ | 99 |
| Figure 93: Von Mises stresses for girders stiffened with one closed stiffener at $h_w/4$ | 99 |
| Figure 94: Von Mises stresses for girders stiffened with one open stiffener at $h_w/2$ | 100 |
| Figure 95: Von Mises stresses for girders stiffened with one closed stiffener at $h_w/2$ | 100 |
| Figure 96: Von Mises stresses for girders stiffened with two open stiffeners..... | 101 |
| Figure 97: Von Mises stresses for girders stiffened with two closed stiffeners..... | 102 |
| Figure 98: The influence of the stiffener stiffness on the girder resistance for girder stiffened with one stiffener | 103 |
| Figure 99: The influence of the stiffener stiffness on the girder resistance for girder stiffened with two stiffeners | 104 |
| Figure 100: Reduction curves for shear buckling..... | 109 |
| Figure 101: M-V interaction according to EN 1993-1-5..... | 115 |
| Figure 102: Numerical results plotted on current formulation of M-V interaction - GROUP I..... | 117 |
| Figure 103 Numerical results plotted on current formulation of M-V interaction - GROUP II..... | 117 |
| Figure 104: Numerical results plotted on current formulation of M-V interaction - GROUP III..... | 118 |
| Figure 105: Numerical results plotted on current formulation of M-V interaction - GROUP IV..... | 118 |
| Figure 106: Numerical model of the plate..... | 119 |
| Figure 107: Reduction of shear capacity of the plate under different stress states..... | 120 |
| Figure 108: Reduction of shear resistance of the plate at different stress states, calculated by numerical simulation (NUM), reduced stress method (RSM) and effective width method (EWM)..... | 121 |
| Figure 109: M-V interaction formulation – comparison..... | 122 |
| Figure 110: One stiffener, varied parameter A_f/A_w | 123 |
| Figure 111: One stiffener, varied parameter h_w/t_w | 123 |
| Figure 112: One stiffener, varied parameter γ/γ^* | 124 |
| Figure 113: One stiffener, varied parameter α | 124 |
| Figure 114: Two stiffeners, varied parameter A_f/A_w | 125 |
| Figure 115: Two stiffeners, varied parameter h_w/t_w | 126 |
| Figure 116: Two stiffeners, varied parameter γ/γ^* | 126 |
| Figure 117: Comparison of experimental (numerical) and theoretical values..... | 128 |
| Figure 118: Position of interaction check (sections 1-1 and 2-2) and gross cross-section check (section 0-0)... | 131 |
| Figure 119: Statistical evaluation of sub-set I for resistance models $r_{t,1}$ and $r_{t,2}$ | 133 |
| Figure 120: Statistical evaluation of sub-set II for resistance models $r_{t,1}$ and $r_{t,2}$ | 134 |
| Figure 121: Statistical evaluation of sub-set III for resistance models $r_{t,1}$ and $r_{t,2}$ | 135 |
| Figure 122: Statistical evaluation of sub-set IV for resistance models $r_{t,1}$ and $r_{t,2}$ | 136 |
| Figure 123: Statistical evaluation for resistance models $r_{t,3}$ | 137 |
| Figure 124: Layout of the tested girder and loading positions for tests S1 and S2..... | 142 |
| Figure 125: Load-deflection curves for tests S1 and S2..... | 143 |
| Figure 126: Strain measurements in the transverse stiffener - test S1..... | 144 |
| Figure 127: Strain measurements in the transverse stiffener - test S2..... | 145 |
| Figure 128: Cross-sections in the stiffener where the axial forces were evaluated..... | 146 |
| Figure 129: Comparison of load-deflection curves for test S1..... | 147 |
| Figure 130: Comparison of load-deflection curves for test S2..... | 147 |
| Figure 131: Comparison of the out-of-plane displacement of transverse stiffener..... | 147 |
| Figure 132: Evolution of the out-of-plane displacement of the transverse stiffener..... | 150 |
| Figure 133: Influence of stiffness of transverse stiffener on girder resistance and out-of-plane displacement of stiffener..... | 150 |

| | |
|--|-----|
| Figure 134: Out-of-plane displacement evolution over transverse stiffener for girder $h_w/t_w=250$, $\alpha=1$, $\gamma/\gamma^*=3.0$, $A_f/A_w=0.7$ | 151 |
| Figure 135: The normalized force obtained at out-of-plane displacement of $h_w/300$ for different stiffness of stiffener | 152 |
| Figure 136: Influence of stiffness on girder's capacity..... | 153 |

INDEX OF TABLES

| | |
|--|-----|
| Table 1: Experimental tests on longitudinally unsiffened girders that contain information on bending-shear interaction in the web..... | 10 |
| Table 2: Experimental tests on longitudinally stiffened girders that contain information on bending-shear interaction in the web..... | 10 |
| Table 3: Experimental data and results of longitudinally stiffened girders, Vigh | 12 |
| Table 4: Experimental data and results of longitudinally stiffened girders, COMBRI..... | 12 |
| Table 5: Geometry of the tested steel plate girders | 16 |
| Table 6: Results from tensile coupon-tests in plates..... | 17 |
| Table 7: Features of the strain gauges | 19 |
| Table 8: Comparison of measured imperfection amplitudes for panel SO with tolerances acc. to EN 1090-2 [74] | 22 |
| Table 9: Comparison of measured imperfection amplitudes for girder SC with tolerances acc. to EN 1090-2 [74] | 23 |
| Table 10: Comparison of measured imperfection amplitudes for girder UO with tolerances acc. to EN 1090-2 [74] | 24 |
| Table 11: Comparison of measured imperfection amplitudes for girder UC with tolerances acc. to EN 1090-2 [74] | 25 |
| Table 12: Comparing experimental resistance with resistance according to EN 1993-1-5 | 39 |
| Table 13: Actual dimensions of tested steel plate girders | 62 |
| Table 14: Considered levels of residual stresses in the stiffened girder | 81 |
| Table 15: Variation parameters in numerical simulations | 87 |
| Table 16: Effective width for internal compression elements [78]..... | 111 |
| Table 17: Effective width for external compression elements [78]..... | 112 |
| Table 18: Statistical evaluation of M-V interaction formulations for girders stiffened with one stiffener..... | 125 |
| Table 19: Statistical evaluation of M-V interaction formulations for girders stiffened with two stiffeners | 126 |
| Table 20: Calculation of V_{FEM} | 130 |
| Table 21: Calculated γ_M^* values for resistance models $r_{t,1}$ and $r_{t,2}$ at $\min(a, h_w/2)$ | 138 |
| Table 22: Calculated γ_M^* values for resistance models $r_{t,1}$ and $r_{t,2}$ at $h_{w_i,max}/2$ | 138 |
| Table 23: Calculated γ_M^* values for resistance model $r_{t,3}$ | 138 |
| Table 24: Calculated γ_M^* values for resistance models $r_{t,4}$ and $r_{t,5}$ at $\min(a, h_w/2)$ | 139 |
| Table 25: Calculated γ_M^* values for resistance models $r_{t,4}$ and $r_{t,5}$ at $h_{w_i,max}/2$ | 139 |
| Table 26: Axial force in the transverse stiffener at maximal girder resistance, taking into account effective part of the web $15\epsilon_t w$ | 146 |
| Table 27: Required stiffener's stiffness consider different requirements | 148 |
| Table 28: Stiffness variation of transverse stiffeners of tests S1 and S2 | 148 |
| Table 29: Required stiffener's stiffness considering different requirements | 149 |
| Table 30: Parameters taken into account for girders loaded with high bending and shear load | 149 |
| Table 31: Transverse stiffness needed to achieve displacement condition ($w < h_w/300$) | 152 |
| Table 32: Transverse stiffness needed to achieve maximal girder's capacity | 152 |

1 INTRODUCTION

Plated steel elements are used in many fields of engineering such as: aerospace engineering, nautical engineering and mechanical engineering or in the field of civil engineering. Depending on the field of application different problems considering the behaviour of these structural elements might be found.

In civil engineering the most common plated elements are plated I or box girders. The I-girder comprises of flanges and web, while the box girder comprises of flanges and two webs. The heights of such cross-section are usually between 1.5 m up to 4 m and more to resist high bending moment with less material. To reduce the weight of the girder the webs are usually very slender, stiffened with series of transverse and longitudinal stiffeners which increase resistance of the plate. These girders are extensively used for bridges, heavy industrial buildings and other structures where large spans are frequently encountered.

Stiffened plated girders possess large post-buckling resistance which was first discovered by Wilson in 1886. Nevertheless, till 1960s the elastic critical buckling load was accepted as a basis for design of plated girders. After 1960s the post buckling behaviour of plated girders was studied theoretically, experimentally and numerically to determine models which properly describe post-buckling resistance. Most of investigations were performed to obtain single characteristic resistance, such as bending resistance, shear resistance or resistance to transverse force of plated girder, while only some experiments were performed to study the interaction of different possible effects, especially for longitudinally stiffened girders. The bending-shear interaction of longitudinally stiffened plated girders is of particular interest, because only 9 experimental tests were performed in 70s and 80s, which were verified with interaction models that were developed by the authors of experiments. The results of the experiments were poorly documented, therefore to build a verified numerical model new test of longitudinally stiffened girders subjected to high bending moment and shear load were carried out.

The bending-shear interaction in the transversally and longitudinally stiffened web is studied through experimental and numerical simulations. The aim of this is to understand and explain the behaviour of plated girders under combination of high bending and shear load. The obtained numerical and experimental results are compared to design provisions of EN 1993-1-5.

1.1 Motivation and objectives

Most of research considering post-critical resistance of plated girders was done in the early sixties, seventies and some also in eighties of the last century. National norms around the world have adopted different models for the determination of plate girder resistance. In the last decades the harmonization of European norms has pushed forward research considering design of plated structures. Many experimental and numerical investigations have been performed in the field of:

- Resistance of plated girders subjected to concentrated forces (Lagerqvist [1, 2], Davaine [3], Kuhlmann and Seitz [4], Chacon [5], Kövesdi [6], Braun [7]).
- Stiffness requirement of transverse stiffeners (Lee et al. [8, 9], Xie et al. [10-12], Hendy and Presta [13, 14]).

- Determination of shear strength of longitudinally stiffened girders (Pavlovic [15, 16], COMBRI [17]).
- Bending-shear interaction of longitudinally unstiffened girders (Presta [14], Veljkovic [18]).

The tests on longitudinally stiffened girders loaded with interaction of high bending moment and shear force, were performed in the seventies and late eighties. The results of tests were found insufficient due to lack of data needed for numerical verification and further observation of girder's behaviour. The current bending-shear formulation used in EN1993-1-5 [19] is not identical to those obtained by authors who researched this field. Additionally an extended numerical study was performed by Sinur and Beg [20, 21], where discrepancy between numerical results and those according to EN 1993-1-5 was found. Therefore the current interaction formulation should be verified.

The objectives of this work are:

- To summarise existing investigations on shear, bending and bending-shear interaction formulation.
- To perform experimental investigations on longitudinally stiffened girders subjected to high level of bending moment and shear load.
- To validate the numerical model with experimental results.
- To investigate the influence of initial imperfections on girder's resistance.
- To perform an extensive numerical investigation considering bending-shear interaction and to compare numerically obtained resistance with that resistance in EN 1993-1-5.
- To determine new interaction formula and to define the cross-section, where the interaction is performed.
- To statistically evaluate interaction models by determine partial safety factors.
- To study the influence of stiffness of transverse stiffener on girder's resistance.

Within this research flanges were designed to be at least in cross-section class 2 and with no influence of shear lag present in the flanges. The transverse stiffeners are designed as rigid support to the web when bending-shear interaction is investigated.

1.2 Thesis content

The thesis is divided in 9 logical consecutive chapters. In Chapter 2 a general view of the research dealing with post-critical shear resistance, post-critical bending resistance and bending-shear interaction is given. First, the theoretical models for shear resistance are described. In this field a remarkable quantity of research was done. Secondly, the models for bending resistance are given and finally the interaction models are discussed.

In Chapter 3 the main features of experimental work are presented and discussed. The geometry, the initial imperfections and the methodology of testing are given herein. The main results of experimental work such as load-deflection curve, evolution of out-of-plane displacement in the tested panel and the displacement and strains in some characteristic points are presented and discussed.

Within Chapter 4 the numerical model in the sense of finite element description, geometry description, material description and solution technique is given.

Chapter 5 deals with evaluation of numerical model against numerical results. In the beginning the rules given in EN 1993-1-5 for numerical simulations of plated structures are illustrated and discussed. Further, the mesh convergence considering mesh size is analysed, followed by verification of numerical model with measured material property and measured initial imperfections. In the last subchapter the imperfection sensitivity analysis is given.

The numerical database and results of girders subjected to bending-shear interaction are presented in Chapter 6. The main outcome of this chapter is the described failure mechanism for different geometries of girder cross-section and different loading conditions.

The resistance to bending and shear load as well as bending-shear interaction according to EN 1993-1-5 is given in Chapter 7. The numerical results obtained in Chapter 6 are compared against those results determined with EN 1993-1-5 formulation. A new formulation of bending-shear interaction is given within this chapter. At the end the statistical evaluation of resistance model is performed.

Chapter 8 contains the analysis considering influence of stiffness of transverse stiffener on girder resistance and behaviour. Two additional experimental tests and important results are discussed and presented. Additionally, numerical model is verified against test results. Furthermore, a parametric study taking into account different stiffnesses of the stiffeners is carried out.

The conclusions of this work and suggestions for further work are given in Chapter 9. Additional data, not presented in Chapters 1 to 9 are annexed at the end of the work.

2 REVIEW OF EARLIER WORK

2.1 Introduction

Steel plated structures are commonly used to support vertical loads over long spans, where bending moment and shear force exceed the capacity of standard hot rolled beams. They are usually composed of compact flanges, slender web and stiffeners (transverse and longitudinal), connected together by welding. In the fabricated plated girder the main function of bottom and top flange is to resist bending, while the web plate resists the shear load. With series of transverse and longitudinal stiffeners the shear and bending capacity of the girder is increased. Plated girders may also be loaded with high transverse forces, which are resisted by the web and flange.

As a result of a number of bridge failures in 1970s, the design of plated structures has attracted great interest. At the beginning plated structures were designed on the allowable stress approach. Later on the design codes started to take into account substantial post-critical resistance. The limitations of the favourable behaviour of plates were not known, which resulted in some disastrous failures. To find out limits and physical explanation of the phenomenon, many large-scale research projects have been started. Increased power of computers made it possible to investigate plated structures in nonlinear range by using numerical tools. On one hand a great deal of research has been finished concerning the design of plated structures, while on the other hand there are still some open questions that should be answered.

The aim of this chapter is to present general view of the research dealing with plated girders with the emphasis on bending-shear interaction in the area of high bending and shear load.

2.2 Shear resistance

When slender web plate is subjected to pure shear, the value of principal tension stress and compression stress is the same till the buckling of the plate occur. After buckling the compression principal strain cannot increase, therefore a new load carrying mechanism is developed within the plate. In this post-buckling range, the shear is carried by inclined tensile membrane stress field as shown in Figure 1.

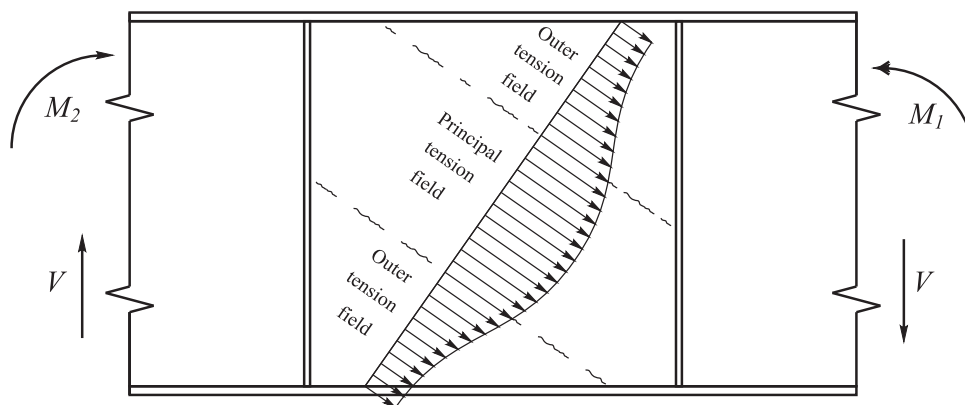


Figure 1: Tension field formation [22]
Slika 1: Formiranje nateznega polja [22]

The first explanation of post-buckling resistance of transversally stiffened girders was given by Wilson in 1886 [23]. On the basis of paper models he concluded that shear force was resisted by the formation of truss, where tension field of the web represented the tension diagonal which was anchored by flange and transverse stiffener. In 1931 Wagner [24, 25] established the first expressions for the magnitude and inclination of tension membrane field for girders usually used in aircraft construction, i.e. girders with very slender webs and rigid flanges.

Because the girder proportions in civil engineering differ significantly, these methods could not be applied directly. The flanges of civil engineering girders are usually much less rigid than those of aircraft girders, so that significant flange distortion can occur under the action of tension field, which influences the magnitude and inclination of the tension field developed in the web.

The first attempt to establish a method to predict the ultimate shear resistance for civil engineering girders was made by Basler et al. [26, 27]. They assumed, conservatively, that the flanges were flexible and that the whole tension field action was resisted by vertical stiffeners. The inclination of tension field action was determined in a way to reach maximum shear resistance.

Further investigation by Gaylord [28] and later by Fujii and Selberg [29] showed that Basler's formulation overestimates the shear strength of the web. This is due to the fact that Basler assumed complete tension field instead of a limited band. However, since the Basler-Thürlimann solution was published, many variations of tension field mechanism were developed.

The effect of flange stiffness of the yield zone in the web was considered by Takeuchi [30], where the boundaries of tension field were located at distances c_1 and c_2 from diagonally opposite corners of the panel. The distances were determined proportional to flange stiffness. The given formulation was checked with test result performed by Konishi et al. [31].

Shear resistance model of Fujii [32, 33] consists of tension field encompassing the whole panel, together with beam mechanism in each flange with hinge at mid-panel. In the direction perpendicular to tension field action, the compression stresses obtained at buckling are assumed. The magnitude of tension field is then defined with Tresca yield criterion. Later Fujii [34, 35] extended this theory to unsymmetrical girders.

In 1969 Chern and Ostapenko [36] proposed a model where tension field is determined by yielding, taking into account also the stresses that are present at buckling. The mechanism also takes into account the influence of flanges.

Four failure modes for shear resistance were proposed by Komatsu [37]. The first failure mode is achieved with inner band yielding under combination of buckling stresses and the post-buckling tension field. In the outer bands smaller tension stress which can be resisted by girder flange as a beam mechanism with hinge at distance c is assumed. The inclination of tension band is determined to get maximum shear resistance. In the second model the interior hinge develops in the mid-panel. In the third model the flanges are assumed to remain elastic and in the last failure mode Wagner field develops, taking into account mechanism of flanges.

Another tension field mechanism was proposed by Rockey and Škaloud [38], later modified by Porter et al. [39], where the tension band was taken in the direction of the panel diagonal. The final mechanism is defined with yielding of tension band taking into account also buckling stresses and plastic hinge yielding in the flanges.

Höglund [40-42] introduced so called rotated stress field method which was firstly developed for longitudinally unstiffened plated girders. He modelled the web with the system of bars with angle δ

between flanges and tension bars. The compression bars are perpendicular to tension bars. The shear buckling load is increased when angle δ decreases. Good agreement was found between measured stresses and those calculated with proposed method.

2.3 Shear resistance of longitudinally stiffened plated girders

The resistance model for longitudinally stiffened girders was firstly developed by Cooper [43] who assumes that each subpanel develops its tension field after buckling. Further, Porter et al. [39] assumed that only one tension field is developed between the flanges and transverse stiffeners. Chern and Ostapenko [44] extended Cooper's model to include frame action of the flanges and of the longitudinal stiffener.

In 1990's Höglund [45] modified his method on the basis of large amount of latest experimental tests (all together 336 tests on steel girders and 93 tests on aluminium girders) and extended it for the use on longitudinally stiffened girders. The shear resistance is defined as linear contribution of the web and flange. The rotated stress field model was checked against all experimental results and very good agreement was found for all unstiffened and longitudinally stiffened girders. This method is implemented in current European design provisions for plated steel structures EN 1993-1-5.

2.4 Bending strength of plated girders

The failure due to bending may occur by lateral-torsional buckling, local buckling of compression flange, or yielding of one or both flanges. As in the case of shear, buckling of the web due to bending does not exhaust the panel capacity and post-buckling resistance is observed. Before buckling appears, the stresses are distributed linearly. When the critical stress in the panel is attained, the post-critical resistance is realized by redistribution of stresses from flexible part to supported edges.

The first to use effective width concept for simply supported plates under compression was von Karman [46] who assumed that the entire load is carried with two strips along the simply supported edges. Later, Winter [47] and Winter et al. [48] suggested the formula of the effective width based on a result of many tests and studies of post-buckling strength. Comparing to von Karman's solution Winter included a correction coefficient which reflects the effect of various imperfections.

The effective width method developed for plates under compression was adapted also to the web of plated girders loaded with normal stresses due to bending moment. Basler and Thürlimann [49] assumed a linear distribution of stresses on effective cross-section with ultimate moment being reached when the extreme fibre in compression reaches yield strength. The effective part of the compressed web b_e was determined only at the edge of flange, the rest of the compressed part of the web was assumed to be ineffective (see Figure 2).

Höglund [42] assumed effective widths on both sides of the compressed part of the web. The effective width on the flange edge was given as $b_e = 0.76 \cdot t \cdot \sqrt{E/f_y}$ and the effective width above the neutral axis was given as $b_e = 1.64 \cdot t \cdot \sqrt{E/f_y}$.

The bending resistance was investigated also by Fujii [35, 50] and Chern and Ostapenko [51]. Fujii's formula for the ultimate bending resistance is more complicated and restricted only to laterally supported girders, while Chern and Ostapenko developed formulas for hybrid girders. The bending resistance is based on an effective width similar to Basler's proposal.

All authors proposed different formulas for the calculation of bending resistance of plated girders. In EN 1993-1-5 the bending resistance is calculated taking into account effective cross-section, where the effective widths are calculated. If the web is stiffened with longitudinal stiffeners, the interaction of

global buckling of the stiffened panel and local buckling of subpanels is considered when calculating effective characteristics. Calculation of bending resistance according to EN 1993-1-5 is given in Chapter 7.

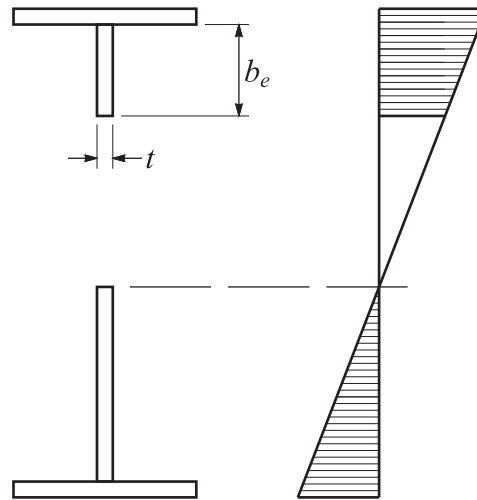


Figure 2: Bending stresses in the slender web plate [22]
Slika 2: Razporeditev upogibnih napetosti v vitki stojini [22]

2.5 Bending-Shear Interaction

Assuming that shear in a girder is carried only by the web, as assumed in Basler's model, maximum shear resistance is reached when the web is yielded uniformly and full tension field can develop. These values are independent of the bending moment in the panel as long as the moment is less than bending capacity of flanges alone. When higher bending load is applied, the moment has to be resisted also by the web, which reduces the shear resistance. When the flange contribution is taken into account in shear resistance, as in the more recent theories of shear strength, the reduction of axial force in the flange as a consequence of bending moment has to be considered (The interaction diagram that consider also interaction in the flanges is plotted in Figure 3a). In EN 1993-1-5 the reduction of flange contribution to shear resistance due to axial force in the flange is given by Höglund's formulation.

The first formulation of interaction of shear load and bending moment in the web was proposed by Basler [52] (see Figure 3b):

$$\left(\frac{V}{V_u}\right)^2 + \frac{M - M_f}{M_p - M_f} = 1 \text{ for } M > M_f \quad (1)$$

where M_f is bending capacity of flanges, M_p is the plastic bending capacity of plated girder, V_u is the shear resistance of the web, M and V are the design bending moment and shear force. The interaction formula is given for the whole range of M_f to M_p and is assumed to be invalid for thin-webbed girders when M exceeds effective bending capacity $M_{y,eff}$ of plated girder. The interaction control was performed at a distance of $h_w/2$ or at mid-panel if $a < h_w$ from the high-moment end. In this way the influence of moment gradient was considered.

Herzog [53, 54] defined a tri-linear interaction diagram (see Figure 3c) similar to Basler's. The interaction of shear load and bending moment in the web is defined when the bending load exceeds flange capacity. In this case the linear interaction formula is employed. In the same way interaction of shear and bending in the web is treated by Fujii [34].

On the other hand, Rockey et al. [55, 56] predicted the strength of the girder under combination of bending and shear through the calculation of critical buckling stress, where the influence of both actions is taken into account.

Most of experimental tests on plated girders have been performed out of interested interaction. The tests where interaction of high bending and shear is present in the web are gathered in Table 1 for longitudinally unstiffened girders and in Table 2 for longitudinally stiffened girders. The tests were verified against theoretical models that were produced by each researcher. The experimental results show very good agreement with test results. The test performed by Schueller and Ostapenko [57] were stiffened with double sided longitudinal stiffener in the compressed part of the web. The stiffener was designed to prevent global buckling of the whole panel. Evans [58] and Public Works Research Institute [59] performed tests on girders stiffened with one sided stiffeners in the compression part. The global buckling of the panel was observed in all tests.

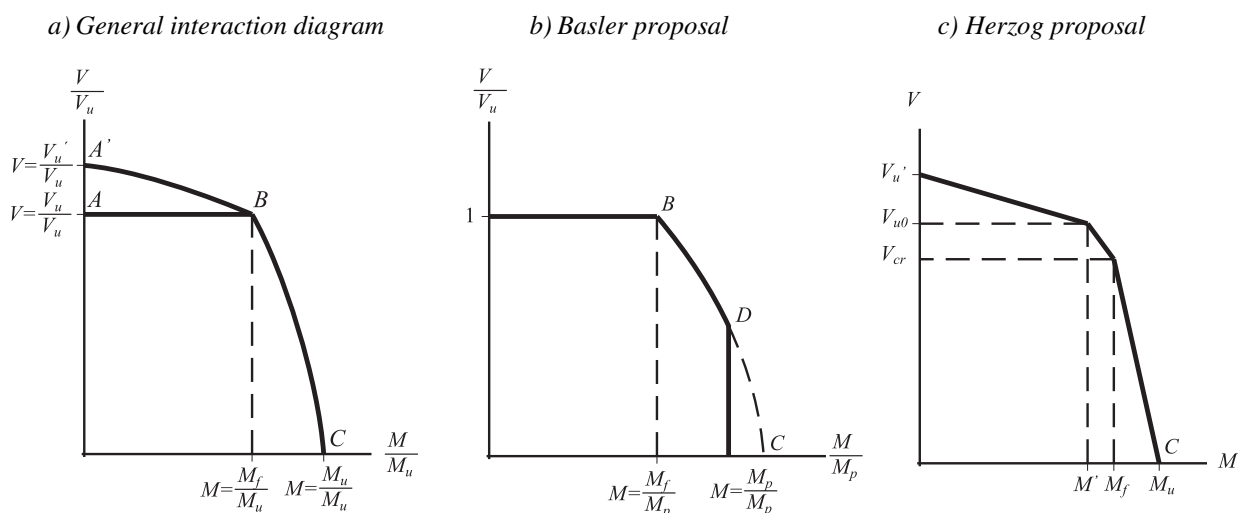


Figure 3: Shear-moment interaction diagrams [22]
 Slika 3: Interakcijski diagrami Strig-Upogibni moment [22]

In EN 1993-1-5 the interaction can be treated with two independent methods: with effective width method or with reduced stress method. The reduced stress method is based on the calculation of global slenderness of the web taking into account the effect of shear load and bending moment. After the global slenderness of the web has been calculated, the non-dimensional reduction factors are determined separately for shear and bending. Finally, the interaction check is performed with von Mises equation taking into account reduced yield stresses. With effective width method the shear resistance and bending resistance of the girder are calculated independently. Finally, the interaction of both effects is taken into account with the following expression:

$$\frac{M}{M_{pl}} + \left(1 - \frac{M_f}{M_{pl}}\right) \left(\frac{2V}{V_u} - 1\right)^2 = 1 \quad (2)$$

Preglednica 1: Eksperimentalni testi vzdolžno neojačanih nosilcev v območju strižno-upogibne interakcije v stojini

Table 1: Experimental tests on longitudinally unstiffened girders that contain information on bending-shear interaction in the web

| Test | a [mm] | h _w [mm] | t _w [mm] | b _r [mm] | t _f [mm] | M _{exp} /M _{th} | V _{exp} /V _{th} |
|--|--------|---------------------|---------------------|---------------------|---------------------|-----------------------------------|-----------------------------------|
| Basler et al. 1960 [26] | | | | | | | |
| E2-T1 | 3810 | 1270 | 12.88 | 356 | 46.23 | 1.06 | 1.06 |
| E2-T1 | 1905 | 1270 | 12.88 | 356 | 46.23 | 1.06 | 1.06 |
| G8-T4 | 1270 | 1270 | 5.00 | 305 | 19.05 | 0.97 | 1.35 |
| Cooper et al. 1964 [60] | | | | | | | |
| H1-T1 | 3810 | 1270 | 9.98 | 459 | 24.89 | 1.08 | 1.08 |
| Rockey & Skaloud 1969 [61] | | | | | | | |
| TG 20 | 305 | 305 | 2.03 | 76 | 3.25 | 1.02 | 1.02 |
| TG 21 | 305 | 305 | 2.03 | 76 | 4.88 | 1.08 | 1.08 |
| Carskaddan 1986 [62] | | | | | | | |
| C-AC3 | 2505 | 455 | 6.35 | 140 | 12.95 | 1.28 | 1.28 |
| C-AH1 | 2509 | 456 | 6.60 | 141 | 25.40 | 1.02 | 1.02 |
| Okomura & Nishino et al. 1966-1968 [63-65] | | | | | | | |
| G2-1 | 2850 | 950 | 6.60 | 250 | 19.00 | 1.04 | 1.04 |
| G1 | 1148 | 440 | 8.00 | 160 | 30.00 | 0.85 | 0.98 |
| G2 | 1148 | 440 | 8.00 | 200 | 30.00 | 0.90 | 1.01 |
| G3 | 1473 | 560 | 8.00 | 160 | 30.00 | 1.04 | 1.04 |
| G4 | 1999 | 560 | 8.00 | 250 | 30.00 | 0.94 | 1.11 |
| G2 | 1461 | 543 | 9.10 | 220 | 22.40 | 1.01 | 1.01 |
| G3 | 1906 | 722 | 9.40 | 302 | 22.20 | 0.91 | 1.08 |
| G4 | 1901 | 720 | 9.20 | 243 | 22.10 | 1.00 | 1.00 |
| G5 | 2355 | 899 | 9.00 | 291 | 22.30 | 0.93 | 1.09 |
| G6 | 2358 | 900 | 8.90 | 212 | 22.30 | 1.06 | 1.06 |
| G7 | 2851 | 1080 | 9.10 | 282 | 22.40 | 0.88 | 0.99 |
| G8 | 2851 | 1080 | 8.90 | 221 | 22.20 | 1.07 | 1.07 |

Preglednica 2: Eksperimentalni testi vzdolžno ojačanih nosilcev v območju strižno-upogibne interakcije v stojini

Table 2: Experimental tests on longitudinally stiffened girders that contain information on bending-shear interaction in the web

| Test | a [mm] | h _w [mm] | t _w [mm] | b _r [mm] | t _f [mm] | M _{exp} /M _{th} | V _{exp} /V _{th} |
|---|--------|---------------------|---------------------|---------------------|---------------------|-----------------------------------|-----------------------------------|
| Schueller & Ostapenko 1970 [57] | | | | | | | |
| UG 5.2 | 1397 | 1217 | 3.02 | 254 | 19.20 | 1.05 | 1.05 |
| UG 5.3 | 1778 | 1217 | 3.02 | 254 | 19.20 | 1.21 | 1.21 |
| UG 5.4 | 2159 | 1217 | 4.65 | 254 | 19.20 | 1.19 | 1.19 |
| UG 5.5 | 1016 | 1217 | 4.65 | 254 | 19.20 | 1.02 | 1.02 |
| Evans 1986 [58] | | | | | | | |
| PB1 | 750 | 1008 | 4.40 | 300 | 15.10 | 0.93 | 1.11 |
| PA1 | 750 | 1008 | 3.83 | 300 | 15.10 | 1.03 | 1.03 |
| Public Work Research Institute, Japan 1987 [59] | | | | | | | |
| C-26 | 1000 | 1650 | 4.73 | 250 | 12.12 | 1.03 | 1.03 |
| C-27 | 1000 | 1650 | 4.73 | 250 | 12.12 | 1.04 | 1.04 |
| C-28 | 1000 | 1650 | 4.73 | 250 | 12.12 | 1.00 | 1.00 |

The present interaction formula was verified on longitudinally unstiffened girders against experimental work by Wargsjö [66] and Axhag [67]. Wargsjö's experimental work was performed on steel grade S235 and Axhag's on steel grade S690. All experimental data shown in Figure 4 are in the range where M-V interaction in the web is present. The results of the tests show no interaction for steel grade S690, while for mild steel S235 the present interaction is covered with current interaction formulation.

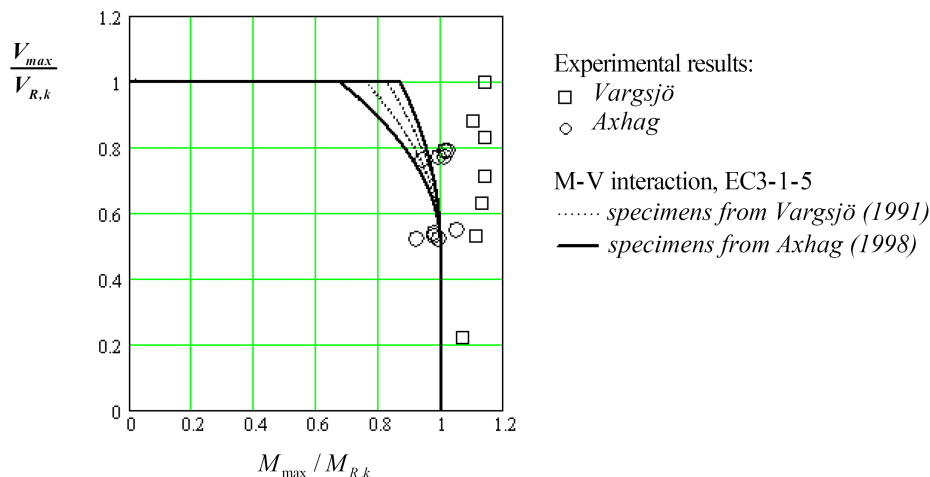


Figure 4: Resistance of I girder from three point bending tests [18]
Slika 4: Nosilnost I nosilca določen s tritočkovnim upogibnim testom [18]

A numerical study considering M-V interaction was conducted by Wargsjö. The numerical model was developed on the basis of experiments and the parametric study was performed over the whole area where M-V interaction is present in the web. The results of the parametric study are plotted in Figure 5. The numerical results show no interaction of bending and shear in the web. The results are close to prediction only for load combinations where the bending is smaller than the bending capacity of the flanges, and at very high bending moment and low shear load. In the range where interaction is determined much larger resistance was obtained.

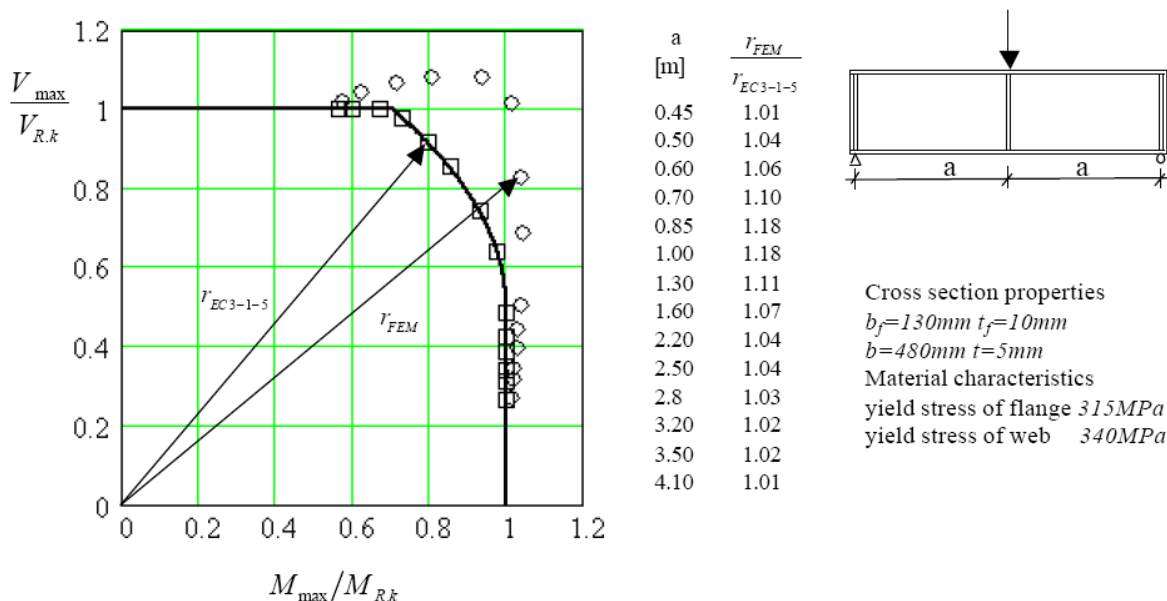


Figure 5: FE parametric analysis performed on beams like the one used by Wargsjö [18]
Slika 5: MKE parametrična študija na nosilcih, ki jih je uporabil Wargsjö [18]

2.6 Recent research work on longitudinally stiffened girders

In the last decade the tests on longitudinally stiffened girders have been performed by Vigh [68]. A new concept of longitudinally stiffened plated girders is studied through experimental (see Table 3) and numerical work. The tested girders are welded with extruded profiles with discontinuous longitudinal stiffeners. In such cases the longitudinal stiffener provides only support for out-of-plane

buckling of the plate and is not considered as part of cross-section to transfer direct stress due to bending moment. The tests were performed at high bending moments and shear forces.

Within the project COMBRI [17] two longitudinally stiffened girders have been tested in order to investigate shear buckling behaviour for different bending – shear ratios. One of them (see Table 4) was loaded in the area of high bending moment and shear load.

Preglednica 3: Parametri in rezultati vzdolžno ojačanih nosilcev, Vigh
Table 3: Experimental data and results of longitudinally stiffened girders, Vigh

| Test | a [mm] | h _w [mm] | t _w [mm] | b _f [mm] | t _f [mm] | M _{exp} /M _f |
|------|--------|---------------------|---------------------|---------------------|---------------------|----------------------------------|
| S8 | 1275 | 600 | 4 | 150 | 6+6 | 1.39 |
| S9 | 1275 | 600 | 4 | 150 | 6+6 | 1.50 |
| S10 | 1275 | 600 | 4 | 150 | 6+6 | 1.50 |
| S12 | 1275 | 600 | 4 | 200 | 10 | 1.19 |
| J1 | 1902 | 634 | 4.50 | 200 | 14 | 0.77 |
| J2 | 1902 | 634 | 4.50 | 260 | 22 | 1.01 |
| J3 | 1902 | 634 | 4.50 | 200 | 12 | 1.40 |

Preglednica 4: Parametri in rezultati vzdolžno ojačane nosilca, COMBRI
Table 4: Experimental data and results of longitudinally stiffened girders, COMBRI

| Test | a [mm] | h _w [mm] | t _w [mm] | b _f [mm] | t _f [mm] | M _{exp} /M _f |
|------|--------|---------------------|---------------------|---------------------|---------------------|----------------------------------|
| 2a | 2500 | 1000 | 6 | 350 | 20 | 1.26 |

Some tests that were performed in the range of high bending moment and shear force were found inappropriate due to the lack of input data that are needed for numerical model verification. On the other hand, some of girder geometries are not typical for those plated girders that are commonly used in practice. Therefore, for the purpose of numerical model verification, which was used later for the parametric study, experimental tests were necessary.

2.7 Transverse stiffeners

Transverse stiffener may be designed as rigid to assure buckling support to web plate, or as flexible. If the transverse stiffener is assumed to be flexible, the stiffness of the stiffener should be taken into account when critical stresses are calculated. In practice the stiffeners are usually designed as stiff to preserve straight boundaries. Stein and Fralich [69] were the first who proposed a solution for an infinitely long web with simply supported edges and equally spaced stiffeners. Bleich [22] developed a formula using numerical data of Stein and Fralich, which is given in the following form:

$$I_{st} = 2.5 \cdot h_w \cdot t_w \cdot \left(\frac{h_w}{a} - 0.7 \frac{a}{h_w} \right) \quad (3)$$

In girders with longitudinal stiffeners the transverse stiffener must support both, the web as well as longitudinal stiffeners. Cooper [43] defined the required section modulus of the transverse stiffener by:

$$S_T = S_L \cdot \frac{h_w}{a}, \quad (4)$$

where S_L is the section modulus of the longitudinal stiffener.

Basler assumes that tension field action is anchored by flanges and transverse stiffener. In such situation the transverse stiffener is loaded with compression force and should be checked for local buckling. The force according to Basler's model is given by the following expression:

$$F_s = \frac{1}{2} \sigma_t \cdot a \cdot t_w \cdot (1 - \cos \theta_d). \quad (5)$$

In case that independent tension field is developed in each subpanel for the case of longitudinally stiffened girders, as assumed by Cooper, then the effective length for buckling check of transverse stiffener is equal to the depth of the largest subpanel. On the other hand, if a panel of longitudinally stiffened girders develops global tension field, the design of transverse stiffener is the same as for longitudinally unstiffened.

In Eurocode EN 1993-1-5 [19] the stiffener is designed to resist the loads coming from tension field action and destabilizing forces arising from normal stresses in the plane. Two requirements have to be fulfilled:

- a) The maximum stresses in the stiffener: $\sigma_{max} \leq f_y / \gamma_{M1}$.
- b) The maximum out-of-plane displacement of the stiffener: $w \leq h_w / 300$.

The additional minimum stiffness requirement to resist shear buckling is defined as:

$$\begin{aligned} I_{st} &\geq 1.5 \cdot h_w^3 \cdot t_w^2 / a^2 \quad \text{for } a / h_w < \sqrt{2} \\ I_{st} &\geq 0.75 \cdot h_w \cdot t_w^2 \quad \text{for } a / h_w \geq \sqrt{2} \end{aligned} \quad (6)$$

In AASHTO [70] the minimum stiffness and the area requirement of transverse stiffener for stiffened panel in shear only are given by:

$$I_{st} = \min \left(2.5 (h_w / a)^2 - 1, 0.5 \right) \cdot a \cdot t_w^3 \quad (7)$$

$$A_{st} = \left[0.15 \cdot B \cdot h_w \cdot t_w \cdot \left(1 - \frac{\tau_{cr}}{\tau_y} \right) \frac{V}{V_u} - 18 \cdot t_w^2 \right] \frac{f_{yw}}{f_{ys}}, \quad (8)$$

Where B defines whether the stiffener is one or double sided and $18 \cdot t_w^2$ is the area of the web to act with stiffener.

In the last decades the behaviour of transverse stiffeners has been experimentally and numerically investigated by Lee et al. [8, 9]. They found out that a transverse stiffener is not necessarily subjected to axial compression in the post-buckling stage, and therefore the requirement for the minimum area according to AASHTO can be avoided. A shear transfer model called "shear cell analogy" is presented in order to describe post-buckling behaviour of the shear web panel. This analogy is used to explain why axial compressive stresses do not develop in transverse stiffeners. The study also reports that the flexural rigidity should be increased several times higher than required for elastic shear buckling in order that the web panel develops its potential ultimate shear strength. Through extensive nonlinear finite element analysis a new design rule for transverse stiffeners is proposed.

3 EXPERIMENTAL PROGRAM

3.1 Experimental investigations

3.1.1 General

The aim of four full scale tests was to examine a characteristic behaviour of longitudinally stiffened plated girders under high bending and shear load and to see, whether the current design rules given in EN 1993-1-5 are suitable. Further on, the test results also serve for the verification of numerical models.

The tests were performed on two girders stiffened with transverse and longitudinal stiffeners. On each of them two panels were investigated in the area of high bending and shear load. One girder was made of symmetric cross-section and the other one of asymmetric cross-section. The varying parameters for the test were the position, number and shape of longitudinal stiffeners, the panel aspect ratio and the slenderness of the web. The transverse stiffeners, which divided the girder into panels, were designed as rigid to prevent any interaction between adjacent panels. The transverse stiffeners were designed taking into account deviation forces and tension field action with analytical model given in Johansson et al. [71]. The system length of the girder was carefully defined in order to obtain the proper ratio of bending and shear load in the panel. The bending stiffness γ of longitudinal stiffeners was chosen so that the shear buckling resistance of the subpanel was decisive. For each of the two girders with different cross sections two types of stiffeners were chosen; open stiffener and closed stiffener. The reason for this was to obtain the influence of torsional stiffness on the behaviour of the panel resistance. All four tests can be defined as follows:

- Symmetric plated girder with open stiffener (SO)
 $h_w / t_w = 214, \alpha = 1.0, \gamma = 41.55$
- Symmetric plated girder with closed stiffener (SC)
 $h_w / t_w = 214, \alpha = 1.5, \gamma = 95.76$
- Unsymmetric plated girder with two open stiffeners (UO)
 $h_w / t_w = 300, \alpha = 1.0, \gamma = 52.12$
- Unsymmetric plated girder with closed stiffener (UC)
 $h_w / t_w = 300, \alpha = 1.5, \gamma = 137.1$

3.1.2 Girder description

The tested girders had a length of 11.160 m and 11.325 m. In Figure 6 and Figure 7 the tested panels are marked with different colours. One girder with symmetric cross-section plotted in Figure 6 with total height of 1544 mm panels SO and SC were tested. The panel SC with panel aspect ratio of $\alpha = 1.5$ is stiffened with a closed stiffener while the panel SO with panel aspect ratio $\alpha = 1.0$ with an open flat stiffener. The centre of gravity of the stiffeners was for both tested panels SC and SO positioned in the compression zone of the web, 350 mm from the upper flange. The web in the part of the tested panels SO and SC (Figure 6) was 7 mm thick, which resulted in global slenderness of $h_w / t_w = 214$. Out of investigated area, 120 mm from the intermediate transverse stiffener, the thickness of the web increased to 8 mm. Double sided transverse 20 mm thick and 156 mm wide stiffeners were used to apply external load into the girder in the region of concentrated load. With additional transverse stiffeners at both ends of the girder the rigid end post was assured. The intermediate transverse

stiffeners were designed according to EN 1993-1-5, taking into account the full effect of deviation forces (maximum bending moment in the panel was taken into account, which is conservative) and only 50% of forces which derived from the formation of the tension field (maximum shear capacity of girder was considered in calculation of tension field action). The final dimensions of the transverse stiffeners were therefore 120×15 mm. The length of the tested panels was 1500 mm for SO and 2250 mm for SC.

The panels UO and UC were tested on girder with unsymmetric cross-section with the total height of 1840 mm as shown in Figure 7. The panel UC with panel aspect ratio $\alpha = 1.5$ was stiffened with one large closed longitudinal stiffener which was classified as class 3 cross-section. The panel UO with panel aspect ratio $\alpha = 1.0$ was stiffened with two open flat stiffeners with dimensions of 10×100 mm. The web thickness of the tested panels was 6 mm, and out of investigated are the thickness was 7 mm. The unsymmetric cross-section was chosen to gain a larger compression area of the web, which consequently also resulted in higher compression force in the stiffeners. The positioning of the stiffeners at the compression part of the web can be seen in Figure 7. The length of the tested panels was 1800 mm for UO and 2700 mm for UC. The transverse stiffeners were designed in the same way as in case of symmetric girder, which resulted in stiffeners with dimensions of 122×20 mm.

To be able to perform two tests on each girder, a shift of the load application points was necessary. To ensure elastic behaviour in this transition area, part of the web between both load positions seen in Figure 6 and Figure 7 was additionally stiffened with a 7 mm thick plate.

Firstly, the test of the panel SO was carried out. Meanwhile, the web of the second panel SC was stiffened with timber diagonal to prevent any unexpected failure in this panel. For the second test, the girder was repositioned so that the load was applied to the investigated panel and the previously failed panel was additionally stiffened with a series of longitudinal stiffeners. To prevent lateral-torsional buckling the upper compressed flange was laterally supported as shown in Figure 6 and Figure 7. The geometry of each tested girder is summarised in Table 5.

Preglednica 5: Geometrijski podatki obeh polnostenskih nosilcev

Table 5: Geometry of the tested steel plate girders

| Specimen | Web | | Upper flange | | Bottom flange | | Longitudinal stiffener | | | | |
|----------|---------------|---------------|--------------|------------------|------------------|------------------|------------------------|------------------|------------------|------------------|------------------|
| | h_w [mm] | t_w [mm] | a [mm] | b_{f1} [mm] | t_{f1} [mm] | b_{f2} [mm] | t_{f2} [mm] | H_{sl} [mm] | h_{sl} [mm] | b_{sl} [mm] | t_{sl} [mm] |
| SO | 1500 | 7 | 1500 | 320 | 22 | 320 | 22 | / | / | 90 | 10 |
| SC | 1500 | 7 | 2250 | 320 | 22 | 320 | 22 | 160 | 80 | 80 | 5 |
| UO | 1800 | 6 | 1800 | 250 | 20 | 450 | 20 | / | / | 100 | 10 |
| UC | 1800 | 6 | 2700 | 250 | 20 | 450 | 20 | 300 | 180 | 80 | 5 |

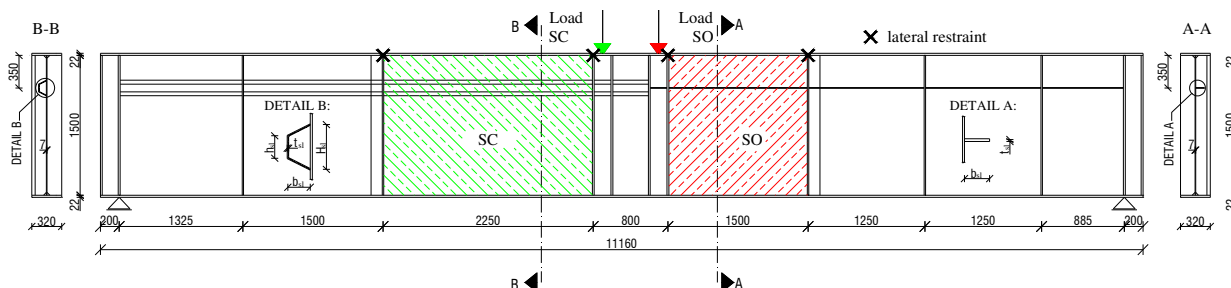


Figure 6: Girder geometry – Symmetric cross-section

Slika 6: Geometrija nosilca – simetričen prerez

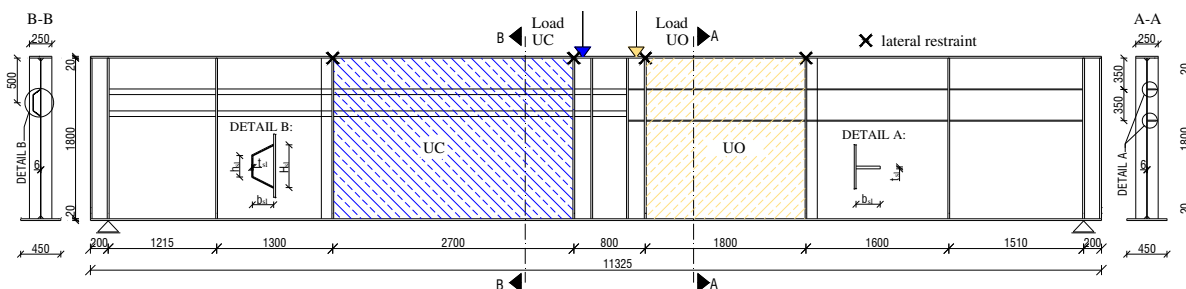


Figure 7: Girder geometry – Unsymmetric cross-section
 Slika 7: Geometrija nosilca – nesimetričen prerez

3.1.3 Material

The girders were fabricated out of eight different steel plates. Out of each plate three tensile coupons were cut out. These coupons were fabricated to determine uni-axial stress-strain behaviour and they were fabricated according to standard EN 10002-1 [72]. Two coupons were tested according to the standard tensile test and to obtain static yield stress one coupon was tested according to the modified tensile test.

The strain rates and the whole testing procedure for the standard tests were defined according to standard EN 10002-1, whereas for the modified test, the testing procedure was the same up to the yield point, i.e. is up until the plot shows that the material starts to yield. At this point where the strain is between two to five times the yield strain, the cross-head motion of the machine is stopped to record the static yield stress. A decrease in load is obtained from the load-displacement curve. It takes about five minutes for the load to become stable at zero cross-head motion. After that, the test is continued by returning to the standard testing speed for a brief interval, which depends on the strain rate at which the specimen is tested. The procedure is then repeated by stopping the cross-head motion several times. The minimum value of the load corresponding to zero strain rate indicates the static yield stress.

The strain rate in stability test and the strain rate used to obtain the yield stress should be the same. The definition of this rate when conducting stability test is difficult, therefore it is common to use static yield stress in the tension test and to use the static load in the stability test. In this way the influence of strain rate on the resistance is eliminated.

Table 6 summarises the mechanical properties obtained from the tension tests. The yield stresses and the ultimate stresses were defined as the average values of three tension tests per each plate. The average reduction was calculated as the ratio between all measured static and dynamic yield stresses. Dynamic yield stresses obtained by standard tension test were then reduced by the average reduction factor to final static yield stresses, which are later used in FEM calculations.

Preglednica 6: Rezultati nateznih preizkusov pločevine
 Table 6: Results from tensile coupon-tests in plates

| Plate | $R_{p0.02}$ Yield stress [MPa] | R_m Ultimate stress [MPa] | f_u/f_y | Average reduction of $R_{p0.02}$ [%] | Static yield stress [MPa] |
|-------|--------------------------------|-----------------------------|-----------|--------------------------------------|---------------------------|
| 5 mm | 385 | 539 | 1.40 | 7.19 | 357 |
| 6 mm | 405 | 539 | 1.33 | | 376 |
| 7 mm | 391 | 561 | 1.44 | | 363 |
| 8 mm | 399 | 552 | 1.38 | | 371 |
| 10 mm | 395 | 542 | 1.37 | | 367 |
| 15 mm | 369 | 520 | 1.41 | | 342 |
| 20 mm | 375 | 543 | 1.45 | | 348 |
| 22 mm | 354 | 536 | 1.52 | | 328 |

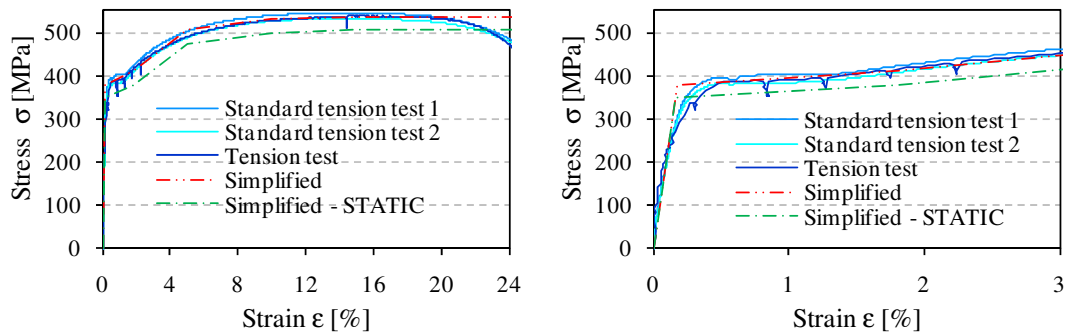


Figure 8: Stress-strain diagram of tensile tests of 5mm thick plate

Slika 8: Diagram nateznega testa 5 mm debele pločevine

3.1.4 Test procedure

The girders were set as simply supported three point bending tests under static load. At both supports, the rotation around the axis perpendicular to the web plane and movement along the longitudinal axis were allowed. The load was applied through rigid circle plate with a diameter of 200 mm and a thickness of 60 mm, hinged on hydraulic actuator with maximum capacity of 3000 kN using a displacement control. The real situation of the testing frame and the test position with a detailed schematic drawing are presented in Figure 9 and Figure 10.

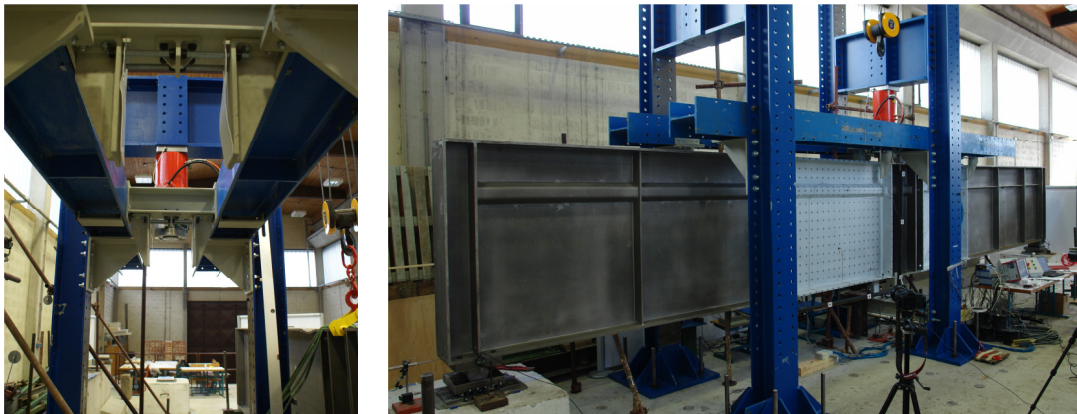


Figure 9: Test set-up – laboratory

Slika 9: Postavitev testa v laboratoriju

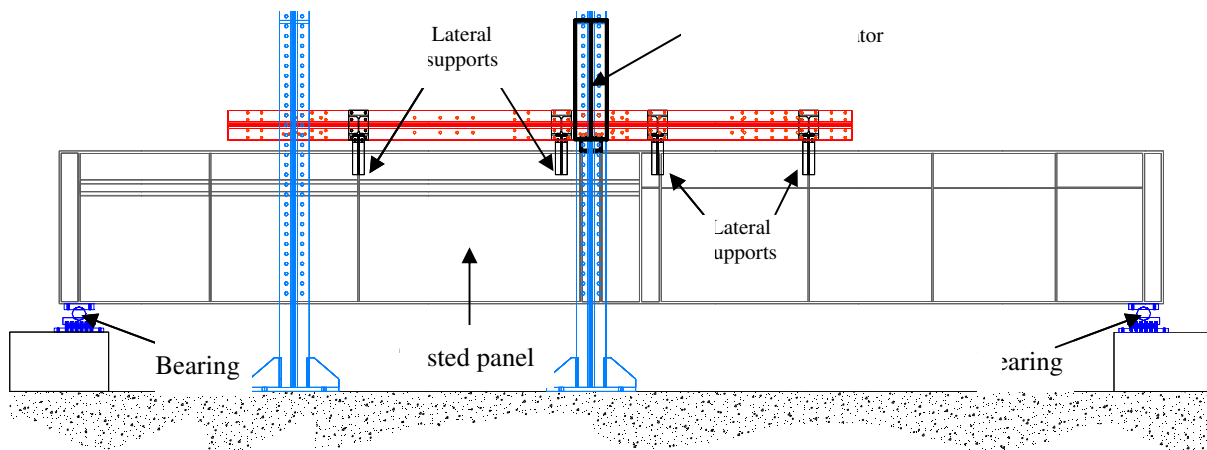


Figure 10: Test set-up – schematic view

Slika 10: Postavitev testa

The loading procedure for test SO is shown in Figure 11. The red curve represents the displacement velocity versus the vertical displacement of the girder, while the blue one indicates the time needed for each load increment and defines the stop positions.

After the test girder had been positioned in the testing frame, it was loaded up to approximately 15% of anticipated maximum load, which was still in elastic range. The preloading of the girder served on one hand to perform static and instrumentation checks and on the other hand to seat the test specimen in the proper testing position.

After the preloading phase, the real test of the girder followed by applying static load in steps. The displacement velocity of the vertical displacement under hydraulic actuator was limited by 0.05 mm/s in elastic range and it increased to 0.10 mm/s after the plastic response had been observed from the displacement-force curve. When the expected values of displacements were reached, the loading was stopped to obtain the decrease of the girder's resistance. In elastic range (only the first two steps) the stops lasted for 60 s in order to perform static checks, record measurements, make visual observations, take photographs and to record general behaviour and any unusual occurrences. In the sequel the stops depended on the time needed for stabilizing the load decrease, which was approximately 300 s.

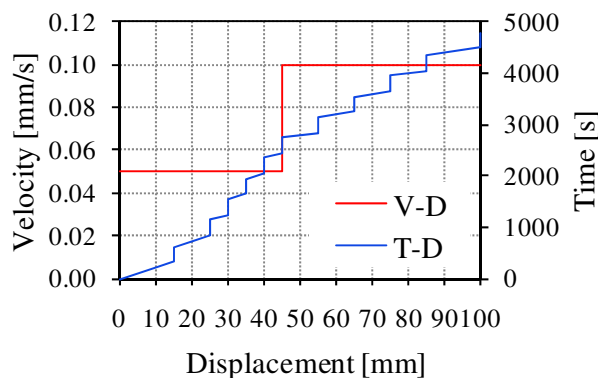


Figure 11: Loading protocol for tested girders

Slika 11: Protokol obremenjevanja nosilcev

3.1.5 Instrumentation

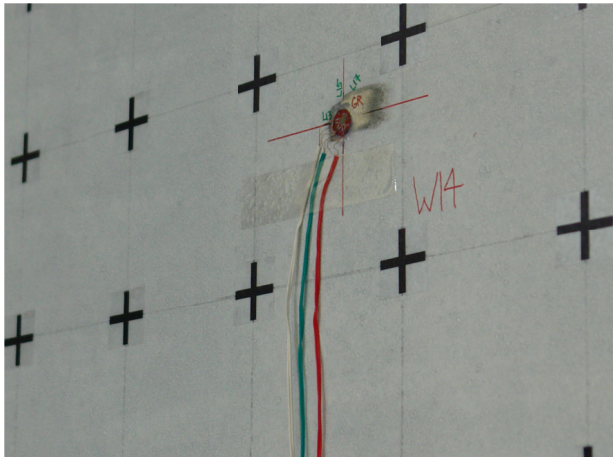
As the test progressed, strains, displacements and forces were continuously measured. The strains in flanges, transverse stiffeners and longitudinal stiffeners were measured by using uni-axial strain gauges (FLA-5-11-3L(5L), Figure 12b), whereas points of the web were monitored with rosettes (FRA-5-11-5L, Figure 12a). The gauges were placed on both sides of the web plate and transverse stiffeners, while in the flanges the strains were measured either on the top or on the bottom side only. Table 7 summarises the features of uni- and tri-axial strain gauges.

Preglednica 7: Značilnosti merilnih lističev

Table 7: Features of the strain gauges

| Type | Gauge factor | Gauge resistance | Transverse sensitivity |
|-------------|---------------|------------------|------------------------|
| FLA-5-11-3L | 2.11±1% | 120.4±0.5Ω | 0.0% |
| FLA-5-11-5L | 2.11±1% | 120.0±0.5Ω | 0.0% |
| FRA-5-11-5L | 1,2,3→2.10±1% | 120.8±0.5Ω | 0.0% |

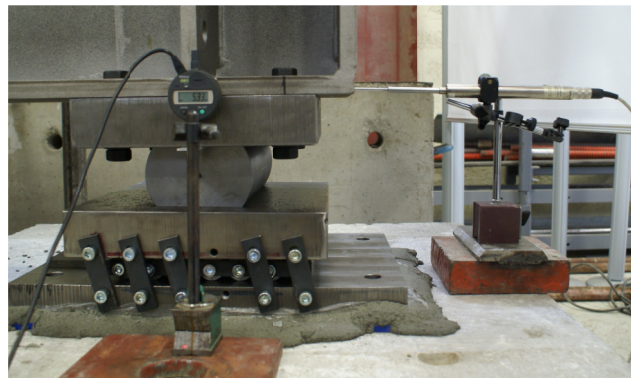
The deflections of the girder as well as out of plane displacements in some characteristic points were measured by using displacement transducers (LVDT) and digital dial indicators (see Figure 12c). The measuring ranges of LVDT were ±25 mm, ±50 mm and ±100 mm, and of digital dial indicators ±6.5 mm and ±25 mm. By employing LVDT and digital dial indicators the displacement development was known only for a few discrete points.



a) Strain gauge rosette in the web



b) Uni-axial strain gauges in the transverse stiffener

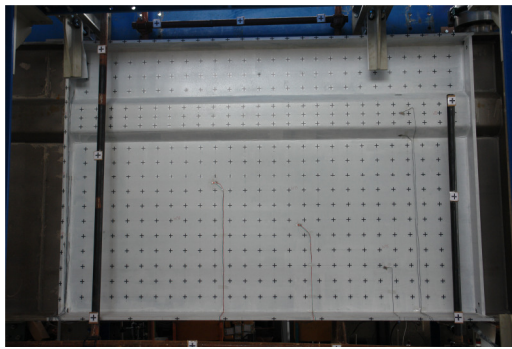


c) LVDT and Digital dial indicator at support

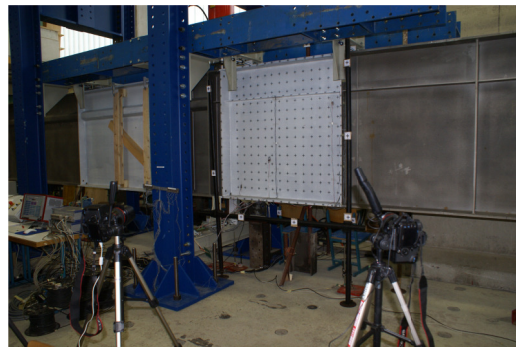
Figure 12: Instrumentation of tested girders

Slika 12: Merilne naprave na nosilcih

To get the whole displacement field of the tested panel for different loading levels, the out-of-plane displacements were measured by using photogrammetry. For this purpose the panel was painted white and marked with black crosses. Crosses were positioned to form squares with dimensions of approximately 100 mm (see Figure 13a). At these points the displacements in all three directions were tracked at each step of the loading. To do so, additional reference points positioned in the 3D space around the panel (left, right, front and back) were needed. They have to be independent of the girder and cannot change their position with loading time. Photographs were taken with three cameras EOS 5D (see Figure 13b) positioned in a way to form an angle of at least 30° between each other, which means that the first and the last camera form an angle of at least 60° . The positions of the fixed points were defined using a theodolite. The final position of the measured points was determined with direct linear transformation. Pilot measurements showed that the accuracy of photogrammetric method was below 0.2 mm.



a) Panel marked with black crosses



b) Position of the two digital cameras Canon EOS 5D

Figure 13: Setup of tested panels for photogrammetry

Slika 13: Priprava panelov in postavitev kamer za fotogrametrijo

For each test the positions of the measured key points were defined on the basis of preliminary numerical simulations. The strain gauges in the web were placed in the area where tension field action was expected. The lateral torsional buckling was controlled by monitoring strains in the compression flange. At the intermediate transverse stiffener strain gauges were applied to get information on axial stress due to formation of tension field action. The vertical deflection of the girder was monitored in six points, the longitudinal displacement in three points and the out of plane displacement in 14 points. The out of plane displacement was measured with LVDT and digital dial indicators, mostly where photogrammetry was not applied. Additional three displacement transducers were positioned to measure out-of-plane displacement in the web plate with purpose to estimate accuracy of photogrammetry. In addition, ANNEX A: Layout of tested girders under M-V interaction includes important information on the precise locations of all devices during the test.

The information regarding the applied load and displacement was obtained directly from the hydraulic actuator system. All data were recorded at 1-Hz frequency and stored in a data worksheet.

3.2 Initial imperfections

In everyday design situation, when dealing with stability, the influence of imperfections may be taken into account by using proper buckling curves if they are available. Another possibility is to perform nonlinear analysis where all relevant initial imperfections are considered in the numerical model. The most important initial imperfections present in plated girders are geometrical imperfections w_0 and residual stresses σ_R . In the numerical model both imperfections, geometrical and residual stresses can be directly considered. To simplify the numerical model, the influence of both imperfections may be taken into account with equivalent geometric imperfections w_{eq} .

To properly simulate test with numerical simulation the real initial imperfections are important, therefore it was essential to get the real 3D geometry of the tested panel and residual stress pattern along flanges and web. There are many possible ways how to determine initial geometrical imperfections and residual stresses. Geometrical imperfections of the whole girder were measured by hand, while the imperfections in the tested panels by using photogrammetry. The residual stresses were obtained by destructive sectioning method.

3.2.1 Geometrical imperfections

The initial geometry of the tested web panels was precisely determined by employing photogrammetry. In all other regions the geometry and imperfections were measured using laser

distance measuring device. The 3D data format determined by digital linear transformation was interpolated on a grid of 10×10 mm using MATLAB [73] 4 griddata method.

Figure 14 represents initial imperfection measured on a symmetric plated girder. The first two Figures show the measured imperfections in vertical and horizontal direction of the web plate at various cross sections, the third Figure represents the imperfection at the longitudinal stiffener position and finally, the last Figure presents the 3D imperfection of the whole web panel with straight black line marking the position of longitudinal stiffener. The maximum imperfection is observed in the largest subpanel with the amplitude of - 5.75 mm. The web plate is much less imperfect near to the longitudinal stiffener. Along the stiffener the maximum deviation of 0.92 mm is obtained.

Comparisons of measured initial imperfections and tolerances given in EN 1090-2 are gathered in Table 8. Measured amplitudes were much below tolerances, especially the imperfection of longitudinal stiffener where the actual amplitude represents only 24.5% of maximum allowable amplitude. The measured amplitude in the largest panel represents 50% of allowable imperfection amplitude.

Preglednica 8: Primerjava izmerjenih amplitude panela SO z tolerancami podanimi v EN 1090-2

Table 8: Comparison of measured imperfection amplitudes for panel SO with tolerances acc. to EN 1090-2 [74]

| | Measured | Tolerance | 0.8×Tolerance | Measured/Tolerance |
|------------------|-----------|-------------------|---------------|--------------------|
| Stiffener | 0.92 mm | $a/400 = 3.75$ mm | 3.00 mm | 0.245 |
| Largest Subpanel | - 5.75 mm | $b/100 = 11.5$ mm | 9.20 mm | 0.500 |

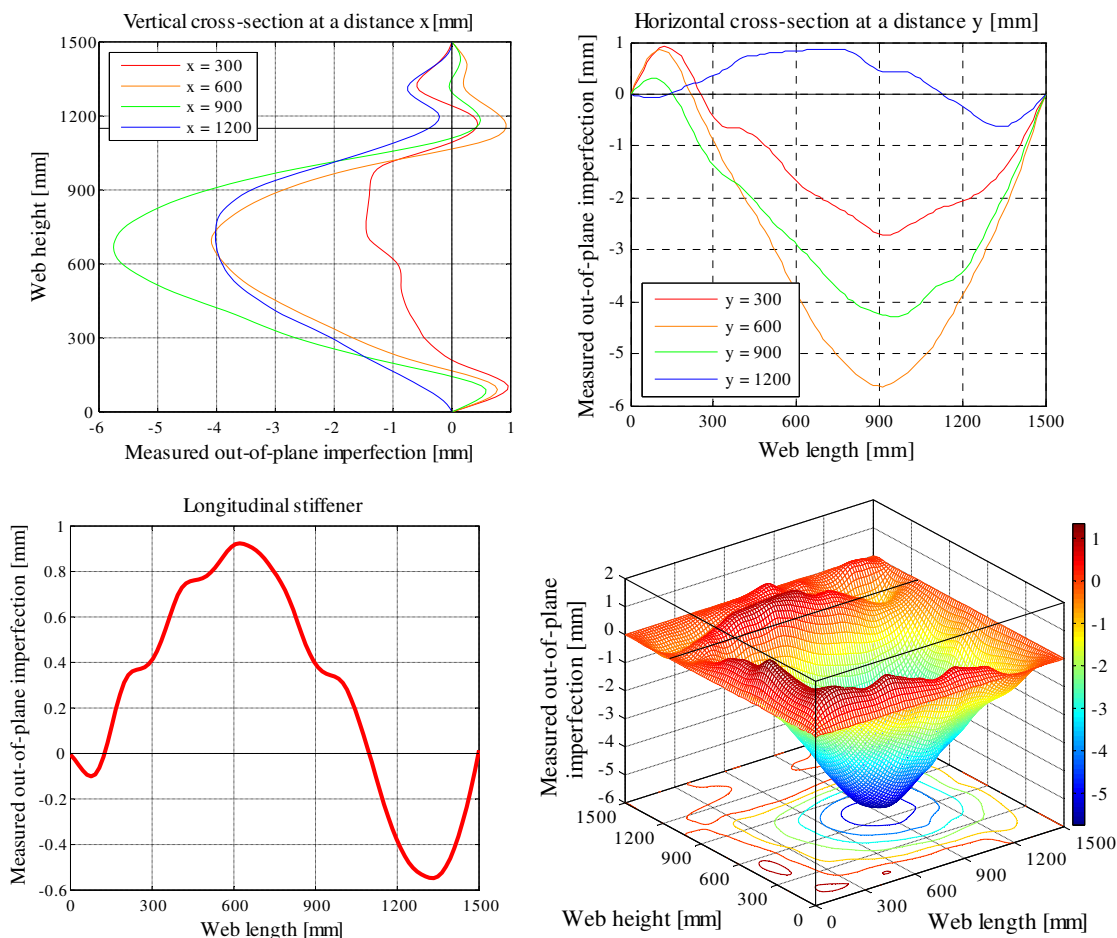


Figure 14: Measurements of initial imperfections of panel SO

Slika 14: Izmerjene začetne nepopolnosti v panelu SO

The measured imperfections of panel SC are plotted in Figure 15. The shape of initial geometry is similar to panel SO with maximum amplitude of -5.79 mm observed in the largest subpanel. The maximum amplitude of the smallest subpanel was 1.85 mm and was obtained at the left side of the plate. As in previous case, the shape of imperfections was a wave in the largest subpanel, which straightened as it approached the longitudinal stiffener and passed over to another wave in the minor subpanel, being oriented at the opposite direction. The imperfection of the longitudinal stiffener is plotted for the centre of the stiffener and is seen as an S-shape with maximum absolute amplitude of 1.49 mm.

In Table 9 the maximum measured amplitudes in the panel and along the stiffener are compared with tolerances. The actual amplitudes were below allowable and they represented 16.4%, 53.7% and 68.5% of tolerances given in EN 1090-2.

Preglednica 9: Primerjava izmerjenih amplitud panela SC z tolerancami podanimi v EN 1090-2

Table 9: Comparison of measured imperfection amplitudes for girder SC with tolerances acc. to EN 1090-2 [74]

| | Measured | Tolerance | 0.8×Tolerance | Measured/Tolerance |
|-------------------|-----------|-------------------|---------------|--------------------|
| Stiffener | 1.49 mm | $a/400 = 5.63$ mm | 4.50 mm | 0.164 |
| Largest Subpanel | - 5.79 mm | $b/100 = 10.7$ mm | 8.56 mm | 0.537 |
| Smallest Subpanel | 1.85 mm | $b/100 = 2.70$ mm | 2.16 mm | 0.685 |

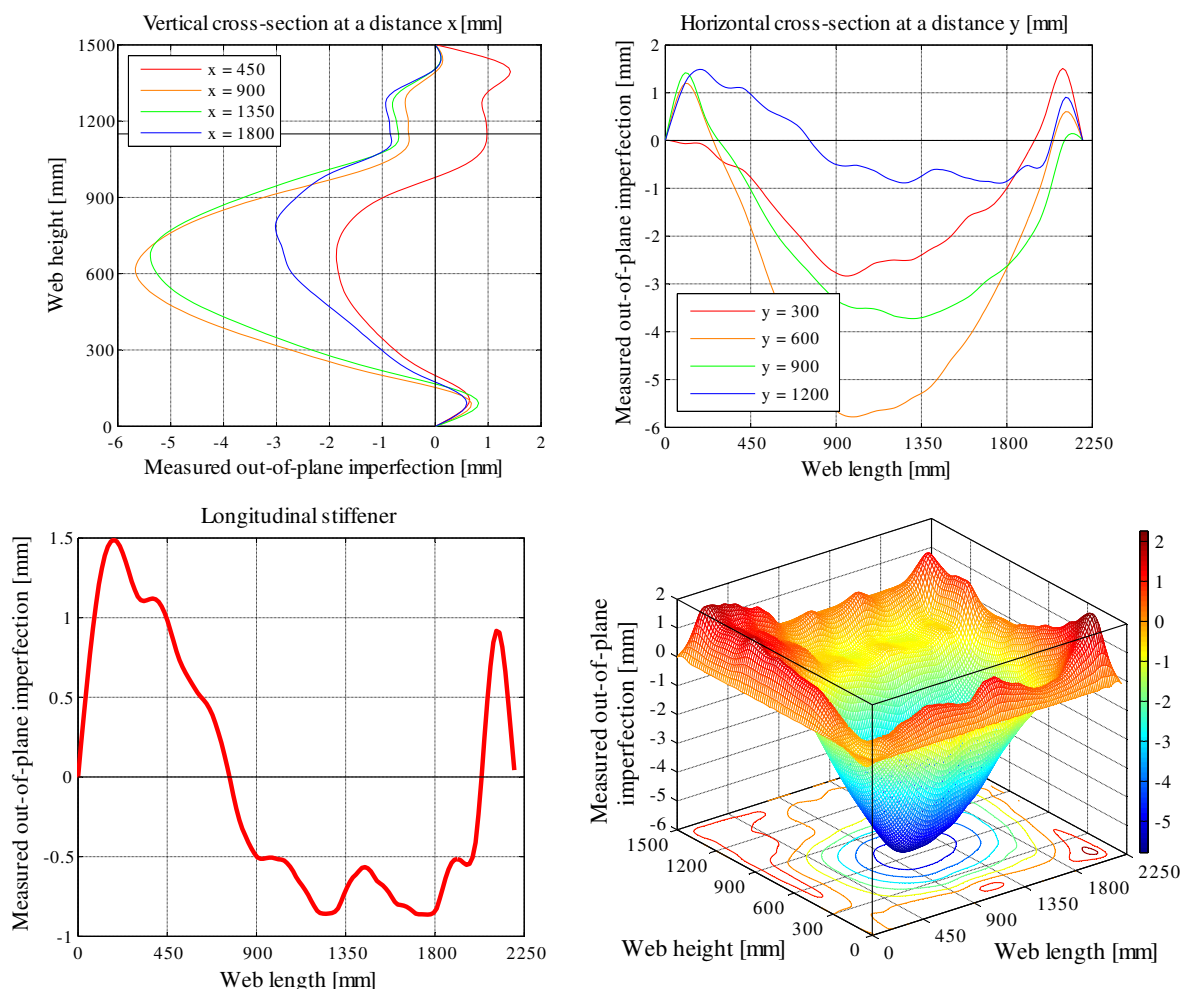


Figure 15: Measurements of initial imperfections of panel SC

Slika 15: Izmerjene začetne nepopolnosti v panelu SC

Figure 16 represents the imperfections of UO web panel stiffened with two open stiffeners. In this situation the imperfection shape is rather unusual, as the maximum amplitudes were measured in the

vicinity of transverse stiffeners. In horizontal direction an S-shape initial imperfection was observed with maximum and minimum amplitude of 3.36 mm and -4.67 mm, respectively. The imperfections of both stiffeners were of C-shape; stiffener at $x = 1450$ mm had imperfection with the maximum amplitude of 2.29 mm and stiffener at $x = 1100$ mm -2.02 mm. The overall maximum imperfection amplitude 2.51 mm of the subpanel was found in the left corner of the web. The measured imperfections were much smaller than fabrication tolerances permitted according to EN 1090-2:2008 [74] (Annex D), where the maximum amplitudes in the panel are limited to 11 mm for the largest subpanel, 3.5 mm for minor subpanels and 4.5 mm for the longitudinal stiffener.

In Table 14 the measured imperfection amplitudes were compared against tolerances of EN 1090-2. The amplitude in the smallest subpanels was closest (71.7%) to imperfection tolerance. In this case the maximum amplitude of longitudinal stiffeners represents 50.9% of allowable imperfection which was much higher than in previous cases. The amplitude measured in the largest subpanel was like for the other two amplitudes below (42.5%) allowable value.

Preglednica 10: Primerjava izmerjenih amplitude panela UO z tolerancami podanimi v EN 1090-2 [74]
 Table 10: Comparison of measured imperfection amplitudes for girder UO with tolerances acc. to EN 1090-2 [74]

| | Measured | Tolerance | 0.8×Tolerance | Measured/Tolerance |
|-------------------|-----------|-------------------|---------------|--------------------|
| Stiffeners | 2.29 mm | $a/400 = 4.50$ mm | 3.60 mm | 0.509 |
| Largest Subpanel | - 4.67 mm | $b/100 = 11.0$ mm | 8.56 mm | 0.425 |
| Smallest subpanel | 2.51 mm | $b/100 = 3.50$ mm | 2.80 mm | 0.717 |

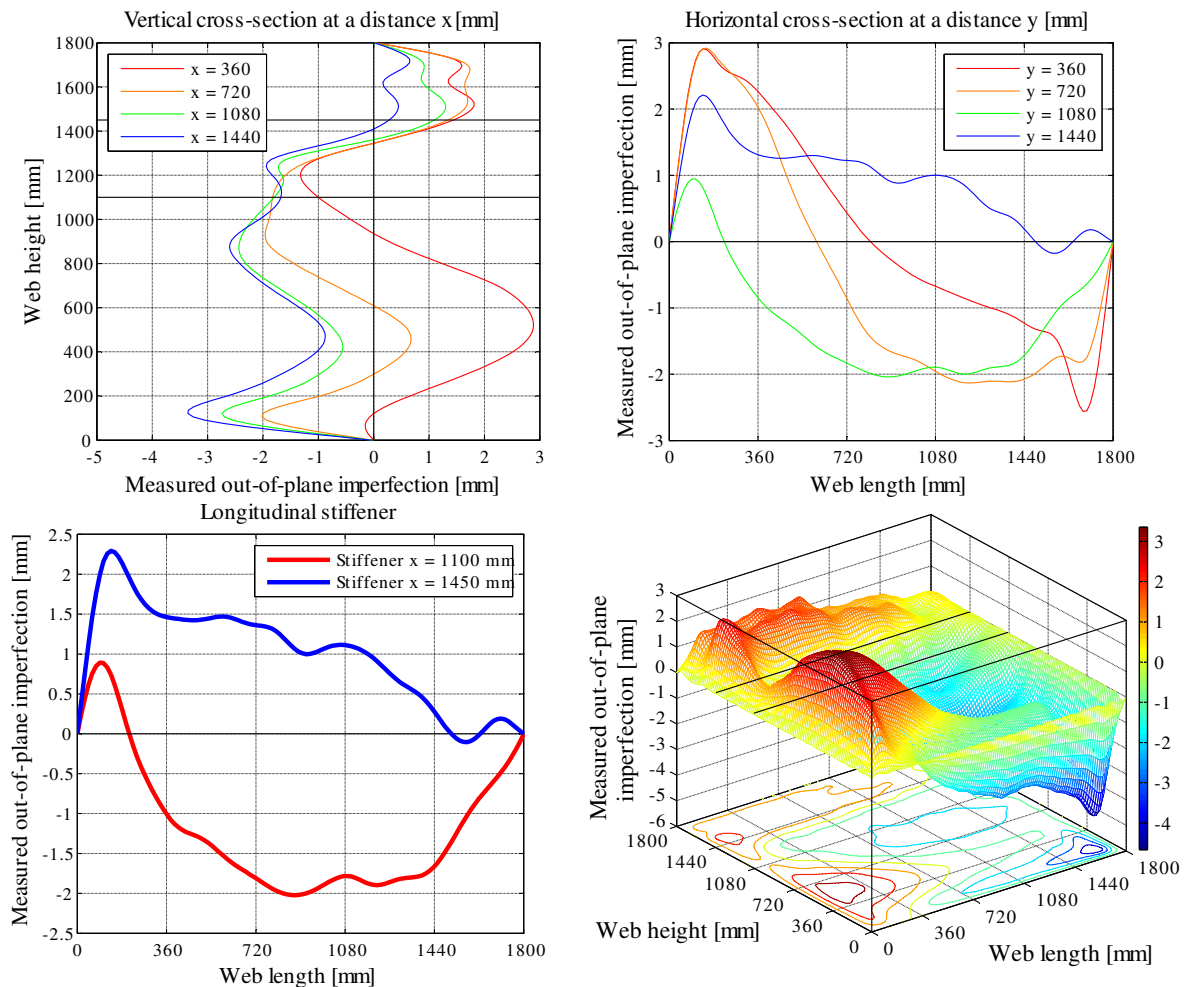


Figure 16: Measurements of initial imperfections of panel UO
 Slika 16: Izmerjene začetne nepopolnosti v panelu UO

Initial imperfections of the web panel UC do not originate only from cutting and welding during the production process itself, but also from previous testing of the UO panel. The reason for this is the fact, that after unloading of the first test, girder did not return in the initial state. Consequently, in this case the measured amplitudes were much higher. The maximum initial imperfection of 14.27 mm was obtained in the largest subpanel and -3.08 mm in the minor subpanel. The stiffener remained straight during the loading of neighbouring panel in the previous test and the measured initial imperfections were 2.49 mm.

For the largest subpanel the amplitude of measured initial imperfection was higher by 24.1% compared to tolerance. The maximum amplitudes obtained in the smallest subpanel and along the longitudinal stiffener were smaller and represented 88.0% and 36.9% of tolerance given in EN 1090-2, respectively.

Preglednica 11: Primerjava izmerjenih amplitude panela UC z tolerancami podanimi v EN 1090-2

Table 11: Comparison of measured imperfection amplitudes for girder UC with tolerances acc. to EN 1090-2 [74]

| | Measured | Tolerance | 0.8×Tolerance | Measured/Tolerance |
|-------------------|----------|-------------------|---------------|--------------------|
| Stiffeners | 2.49 mm | $a/400 = 6.75$ mm | 5.40 mm | 0.369 |
| Largest Subpanel | 14.27 mm | $b/100 = 11.5$ mm | 9.20 mm | 1.241 |
| Smallest subpanel | -3.08 mm | $b/100 = 3.50$ mm | 2.80 mm | 0.880 |

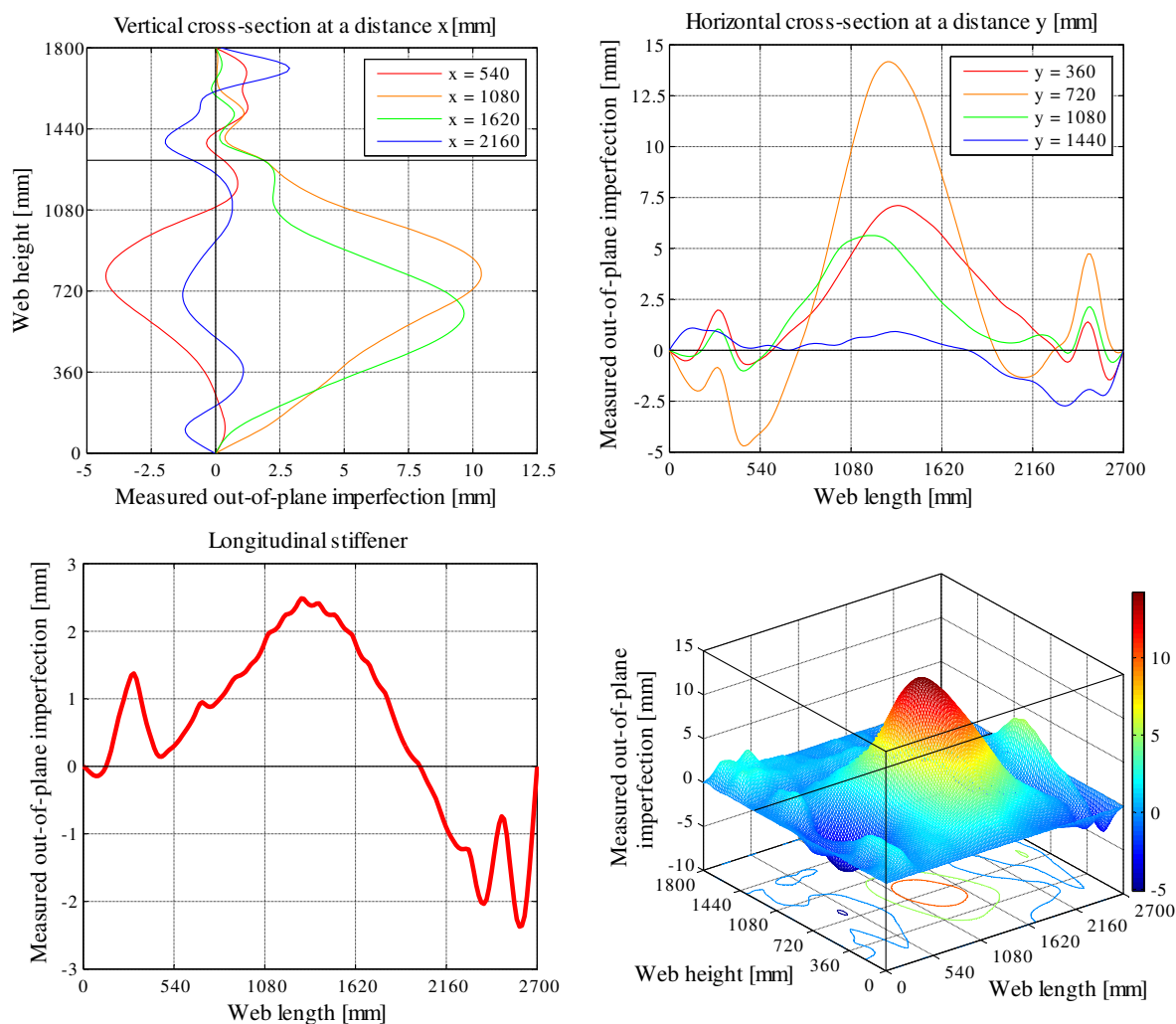


Figure 17: Measurements of initial imperfections of panel SC

Slika 17: Izmerjene začetne nepopolnosti v panelu UC

3.2.2 Residual stresses

Residual, thermal stresses arise from non-uniform temperature distribution during the fabrication. The magnitude and distribution of residual stresses in plated girders are governed by the production, cutting and welding of the plates. In the real structural elements the information about residual stresses is insufficient and the methods for their assessment are demanding, expensive and destructive.

To find out the real distribution of normal residual stresses in longitudinal direction, sectioning method was applied to the part of unsymmetric girder UC, which was during the test not exposed to high bending moments and shear forces, marked in Figure 18. After the test had been done, the residual stress measurement was performed using destructive sectioning method. The strain gauges were placed on both sides of the web and of the top flange using uni-axial strain gauges oriented in the longitudinal direction of the girder. Position of strain gauges is identified in Figure 19.

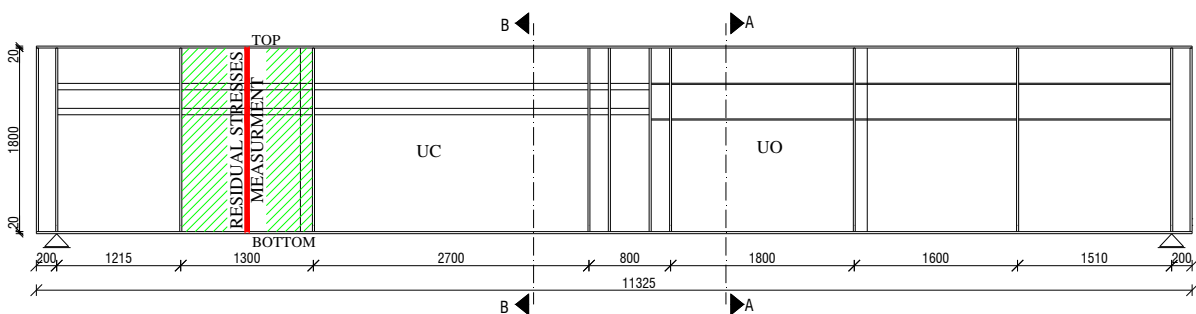


Figure 18: Position of residual stress measurement in asymmetric plated girder
Slika 18: Lokacija merjenja zaostalih napetosti na nosilcu z nesimetričnim prerezom

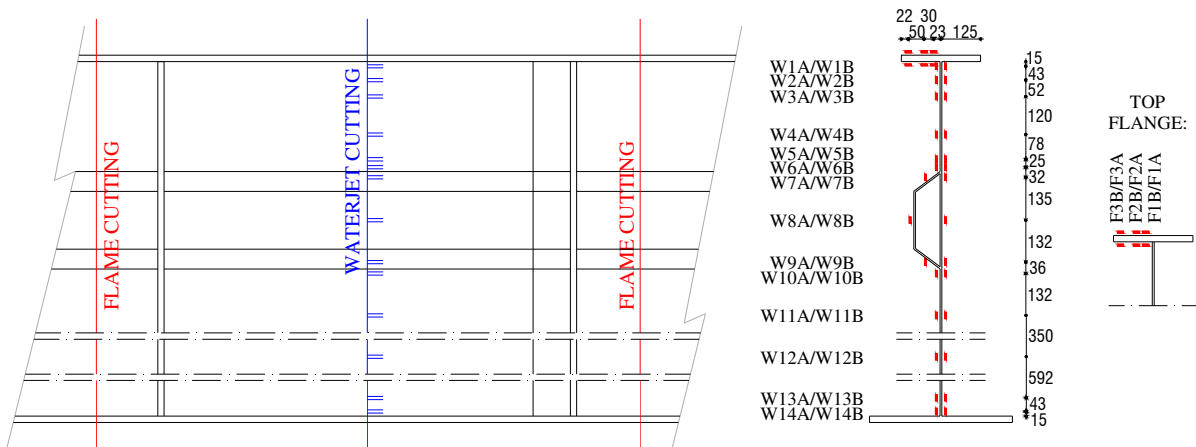


Figure 19: Positions of measured residual strains
Slika 19: Lokacija merilnih mest zaostalih deformacij

First, the investigated panel of the girder was vertically cut out next to transverse stiffeners on each side using autogenic flame cutting. During the flame cutting of the girder the strains were continuously measured. The measuring was stopped 3 hours after the flame cutting was stopped and no reduction in strains was observed. Further strain relaxation in the interested cross-section was performed by waterjet cutting where minimal increase of temperature is expected, up to 10°C from initial state. In the cutting process the following procedure was adopted: the web was firstly cut in transverse direction over its whole height, after this, cutting in the longitudinal direction of the web next to the both sides of strain gauges was performed. In this way the whole relaxation of residual strains was obtained. Also in this case the strains were continuously measured during cutting process and after, till no change in strain was observed.

Due to the size of the test specimen and its complicated geometry the strains in gauges W7A, W8A and W9A were not measured as initially planned. Further on, the strain gauge F3A was damaged during the cutting process and therefore the measured data are not reliable. For these strain gauges the measured strains at their opposite sides were adopted.

The residual stress distributions in the web plate and in the investigated half of the flange are shown in Figure 20. The stress distribution over the web depth is expected as large tension stresses in the vicinity of the welding and low compression stresses in the other area. The maximum tension stress in the web was measured 15 mm from the bottom flange and the average of both side measurements was 246 MPa. The average compression stress in the smallest subpanel was 40.60 MPa which equals to 10.25% of the measured yield stress (See Table 6, Plate 7 mm). In the largest subpanel on each side of the plate only 5 strain gauges were installed. Three of them were placed close to where the tension stresses were expected and two of them were out of this region, i.e. in the area where compression was expected. The average compression stress in this subpanel results in 7.89 MPa, representing nearly 2% of the measured yield stress.

In the flange the tension stresses can be found in the vicinity of the weld ($x = 0$ mm) as well as at the edge of the plate. Tension stress obtained at the edge was very likely caused by the cutting of the flange plate before the girder was assembled. The maximum averaged tension stress in the flange (see curve AVG in Figure 20), considering linear extrapolation from measured positions to the plate's edge (or to the middle of the plate), was 38.35 MPa, which represents only 10.23% of the measured yield stress (See Table 6, Plate 20 mm).

The residual stresses in the cross section should be in self equilibrium. However, the equilibrium of stresses was not achieved because of two main reasons; the number of measured points in the web as well as in the flange was too low and the residual stresses were measured only in the web and in one half of one flange.

The residual stresses in plated girders are rather low compared to the residual stresses in other types of steel structural elements. The main parameter which influences residual stresses is of course the ratio between the input energy and the built-in material, which is in the case of plated girders low. This results from the fact that the input heat energy mainly depends on the amount of welding. Because plated girders consist of large flanges and thin webs, the welds are relatively small.

The residual stresses in the web plate were found relatively small compared to other steel elements. In case of plate girder the actual residual stress depends on:

- Input energy of welding, which is relatively small in case of plate girders.
- Slenderness of the web plate.

In case of thin web plates some of residual stresses are transformed to the initial deformed geometry of the plate. Therefore, actual residual stresses are much lower than would be obtained for a compact plate.

In the sequel the influence of residual stresses and initial geometric imperfections are studied in connection with sensitivity analysis of initial imperfections on girder resistance. Since the influence of residual stresses was rather small (see Chapter 5.4), only geometric imperfections were considered in the validation of the numerical model.

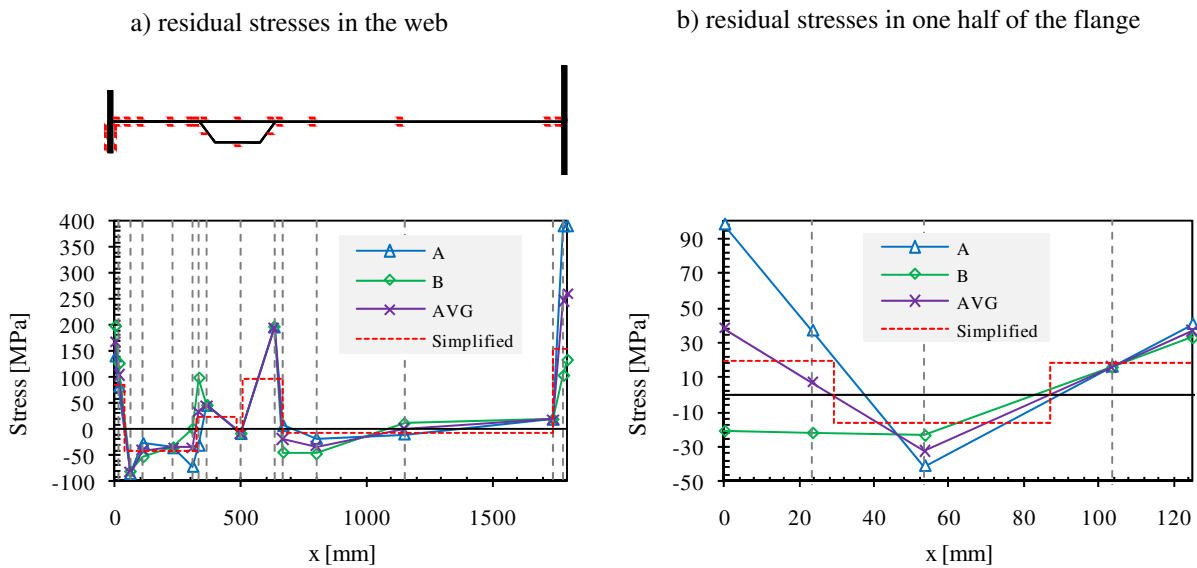


Figure 20: Measured residual stresses
Slika 20: Izmerjene zaostale napetosti

3.3 Test results

In this chapter the test results are presented. For all the tests, the first observed outstanding characteristic was the failure mechanism in the tested panel. Typical load-displacement curves with the emphasis on girders resistance, initial rigidity and ductility (rotational capacity) are presented in the first part, while in the second part, the formation of buckling and failure mode through the out-of-plane displacements of the tested web panel are described.

The out-of-plane displacement development through loading time will give detailed information of the behaviour of plated girders under combination of high bending and shear load; the transition from pure shear buckling to combined bending-shear buckling will be observed. In the last part of this chapter the measured strains will be presented and discussed. The strain information will help us gain some additional information about the formation of tension field and its influence on transverse stiffeners.

3.3.1 Resistance of tested girders

In Figure 21 load-displacement curves for tested girders are plotted. The force applied on the girder through hydraulic actuator is presented on the ordinate axis, while the deflection of the girder determined as the average of vertical deflections measured in positions V3 and V4 (see ANNEX A: Layout of tested girders under M-V interaction) are displayed on the abscissa axis. The testing procedure is the reason for the drops in girder resistance obtained in plastic zone, as the strain speed was set to 0. Because the loading speed is at these points eliminated, the lower bound of these drops represents the static response of the girder.

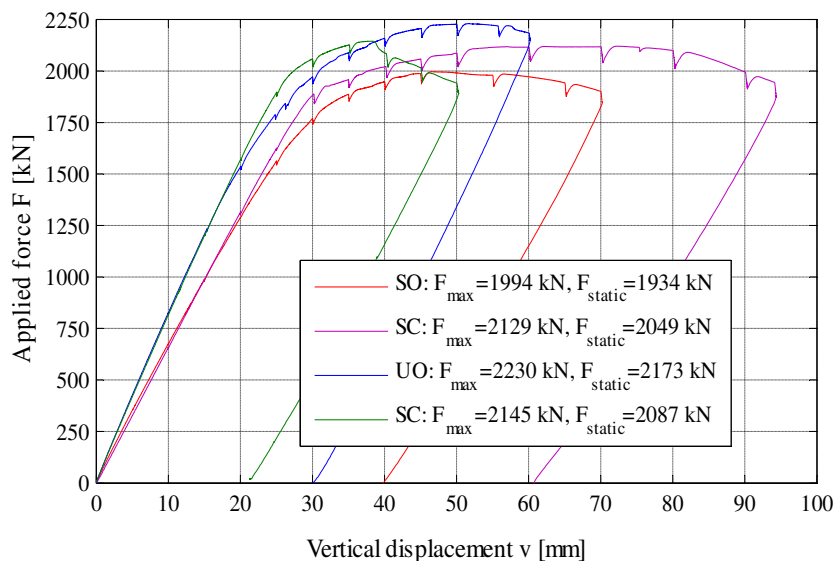


Figure 21: Load-displacement curves for tested girders

Slika 21: Krivulje sila-pomik za vse štiri teste

Since more than one parameter was varied at tests, the comparison between the girder resistances is not very consistent. However, the highest resistance was proven at unsymmetrical girder stiffened with two open stiffeners and the smallest resistance was obtained for symmetric girder stiffened with one open stiffener. All girders show a linear elastic response up to a high load level and as they pass over to the plastic range, the load gradually increases up to the maximum resistance. Once the maximum capacity is reached, the load gradually decreases. For both symmetric girders and the UO girder the decrease of their resistance after reaching the peak force is moderate, which results in high rotational capacity. At the UC test, however, an instantaneous drop of capacity due to local instability of longitudinal stiffener is obtained therefore, the rotational capacity is smaller.

Initial stiffness, i.e. incline of force-displacement curve in elastic range, was similar for the same girder and although each girder was tested twice, there was no change obtained in initial stiffness. Higher stiffness was obtained from tests of unsymmetrical girders.

In Figure 22 the development of out-of-plane displacements for two typical points W13 and W14 in the web panels are shown. The measured points were positioned in the area where the largest out-of-plane displacements were expected. For test SO the out-of-plane displacements are linear up to 1300 kN in point W13, while in point W14 a nonlinear behaviour during the whole test is found. In node W14 at a small load the out-of-plane displacement is negative and it turns in the opposite direction after the load exceeds 500 kN. For test SC the linear response of out of plane displacement was up to 1700 kN. Both displacements are negative up to the load of 2000 kN. After this load, the displacement in node W14 changes direction from negative to positive value. For test UO the linear response is found up to the load of 1400 kN and from this level forward clear nonlinear development of the out-of-plane displacement can be observed. In the last test the linear response was obtained up to the load of 1800 kN.

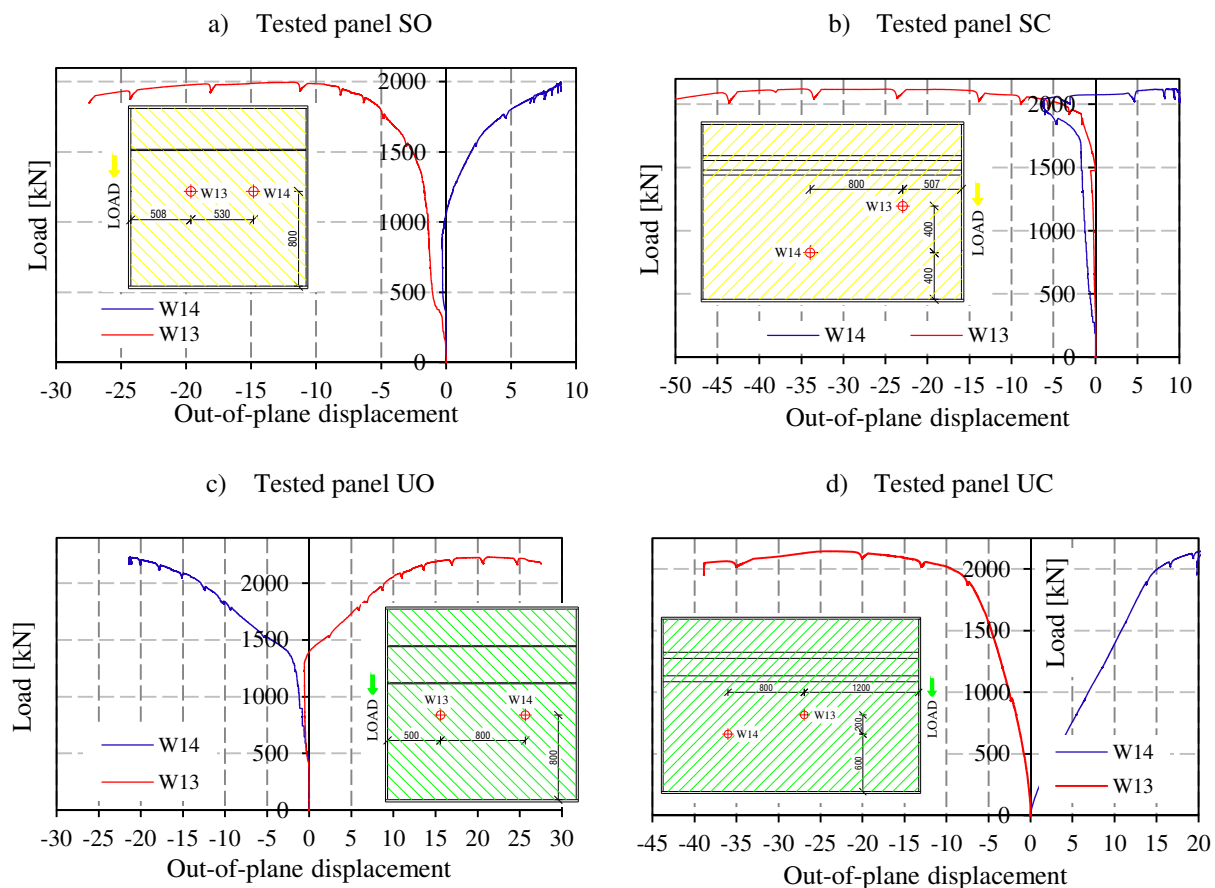


Figure 22: Out-of-plane displacement development in measured points W13 and W14

Slika 22: Razvoj pomikov izven ravnine za točki W13 in W14

3.3.2 Web buckling of tested panel

The evolution of the out-of-plane displacements of the SO tested panel is plotted in Figure 23. The displacement fields are plotted for load stages marked with red circles and letters on the force-displacement curve.

The first one was calculated for the point in which the maximum vertical deflection v of the girder was 10 mm. At this point the average shear stresses were lower than the critical stresses determined for pure shear. Nonetheless, the out-of-plane deformation caused by external load on initial imperfections can clearly be seen. At next stage ($v = 15$ mm), where the load of the panel is close to elastic critical shear force of the largest subpanel, typical shear buckling in the largest subpanel is observed. At this time also the first buckles in the smallest subpanel occur. They are caused by normal compression stresses arising from the bending moment. By increasing the shear force in the girder, the bending moment increases, but the shape of the buckling remains more or less the same, except for the change of the buckling amplitudes.

The first change of the buckling shape occurs with the transition of the girder's behaviour to the plastic range ($v = 35$ mm). The plate changes its buckling shape from three symmetric buckles to two non-symmetric buckles with absolute maximum obtained in the top left corner. The buckling shape depends on the level of shear and bending stresses. When the girder resistance is exhausted, which happens at an approximate vertical distance of $v = 45$ mm, the combination of local torsional and global flexural buckling of the stiffener is observed. At this point, the first local plate buckling of

compressed flange was observed within test. The direction and the location of the torsional buckling of the compression flange are defined by the shape and direction of the web buckling.

In the post-peak stage the local buckling expands over the whole panel and the boundary between both subpanels vanishes. The final buckling shape is a mixture of a global buckling in the diagonal direction of the web panel and of a local buckling in the area of the highest compression stresses.

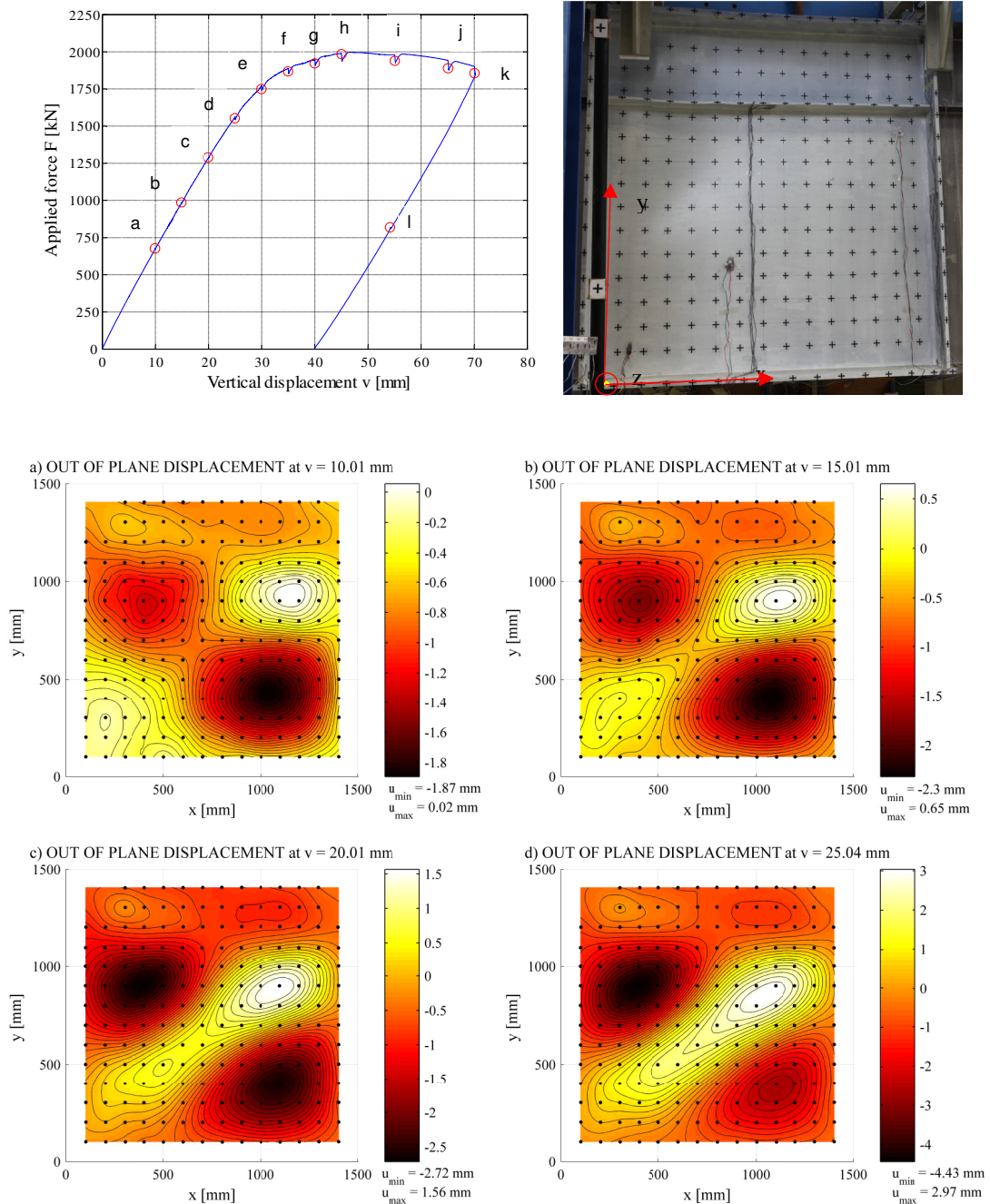


Figure 23: Evolution of out-of plane displacement during the test, SO
 Slika 23: Razvoj pomikov izven ravnine, panel SO

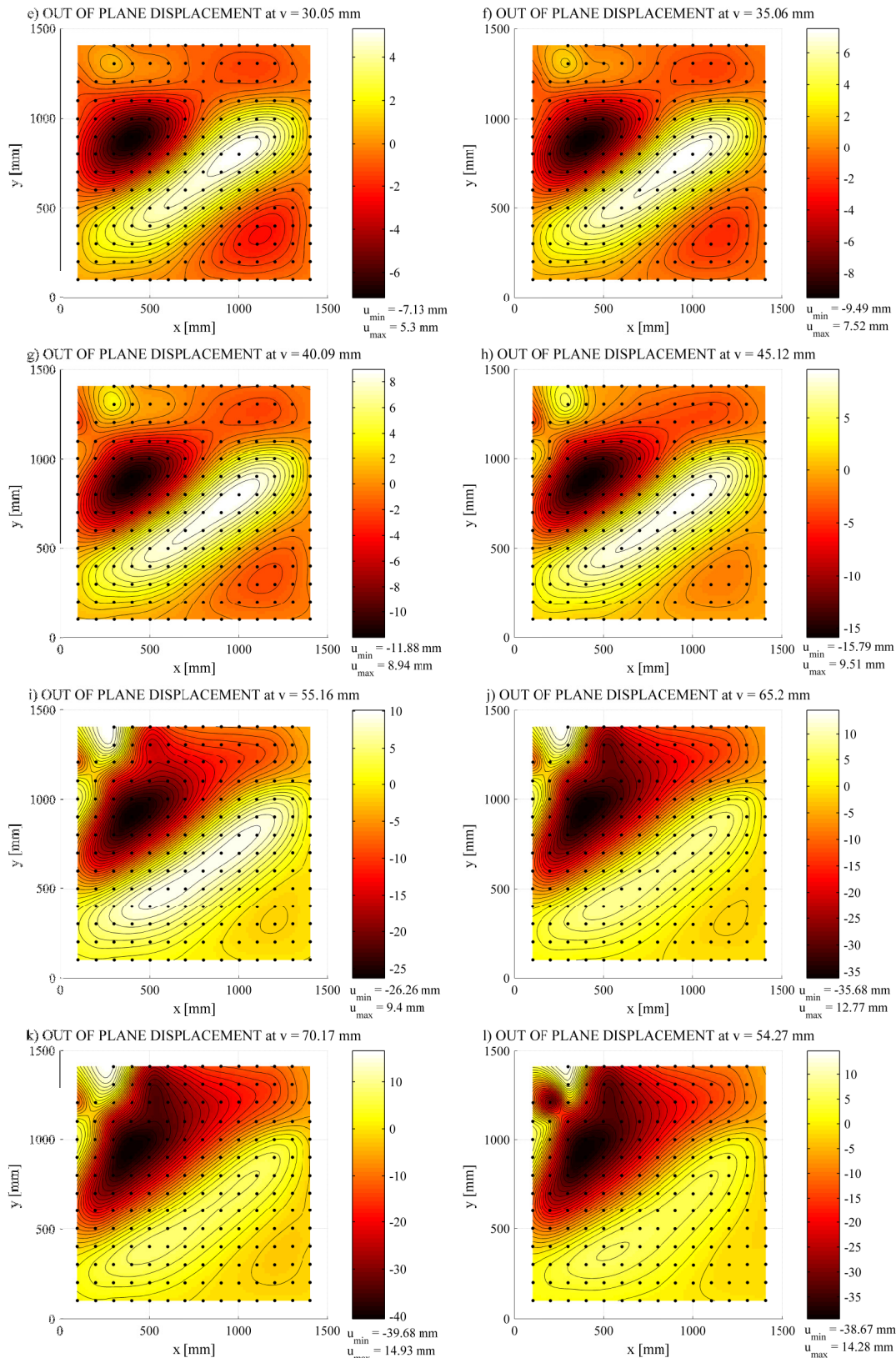


Figure 23: Evolution of out-of plane displacement during the test, SO
Slika 23: Razvoj pomikov izven ravnine, panel SO

The evolution of the web's out-of plane displacement for the second test, on the SC girder, is shown in Figure 24. The first displacement field is captured at a vertical displacement of 10.02 mm. Up to the

elastic critical shear force (up to $v = 15$ mm) only small increase in out-of plane displacements is observed.

In the second stage, where shear load in the panel is higher than elastic critical shear force, the out-of-plane displacements start to increase rapidly and the shape of the web buckling is apparently of the shear buckling type with diagonal orientation from the bottom right corner to the upper left one. In the elastic stage very little out-of plane deformations along the longitudinal stiffener are observed; the stiffener remains more or less straight. The subpanel $h_w/t_w = 270/7 = 38.57$ is for stress state due to bending with $\psi = 0.64$ classified as Class 3 cross-section, therefore the buckling in the upper panel due to normal stresses is not so evident.

When the girder approaches its maximum resistance, the longitudinal stiffener is subjected to a very high compression force due to bending moment. With every loading step the second order effects are higher, forcing the stiffener to buckle. This leads to the global buckling of the panel. In the post-peak stage the load slowly decreases and both vertical deflection and the out-of-plane displacement increase with the web failure mode remaining similar as at the peak force.

The second test shows 5.6% higher resistance than the first one, despite the fact that according to EN 1993-1-5 it should actually manifest lower capacity. This can be attributed to the high torsional resistance of the closed stiffener.

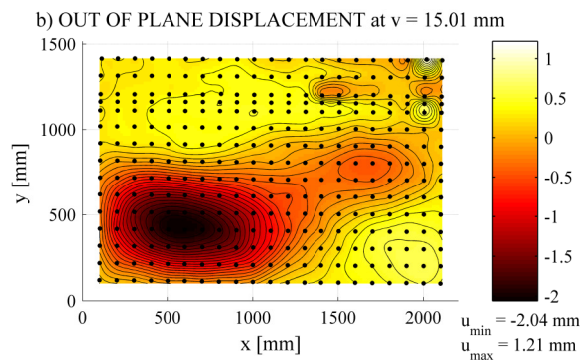
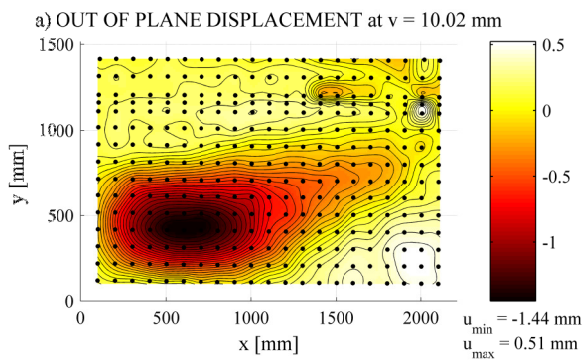
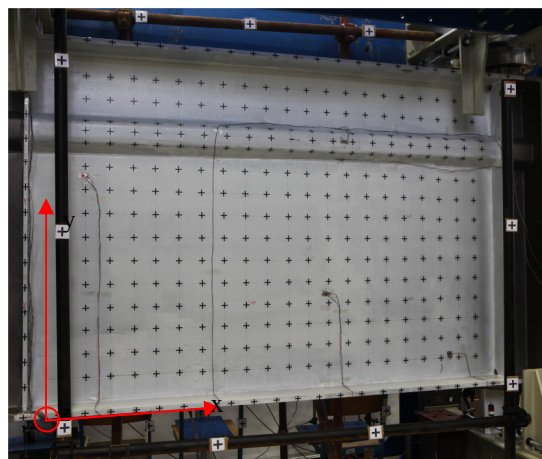
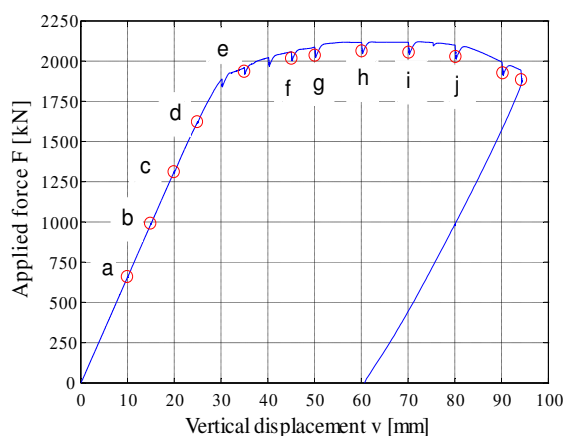


Figure 24: Evolution of out-of plane displacement during the test, SC
Slika 24: Razvoj pomikov izven ravnine, panel SC

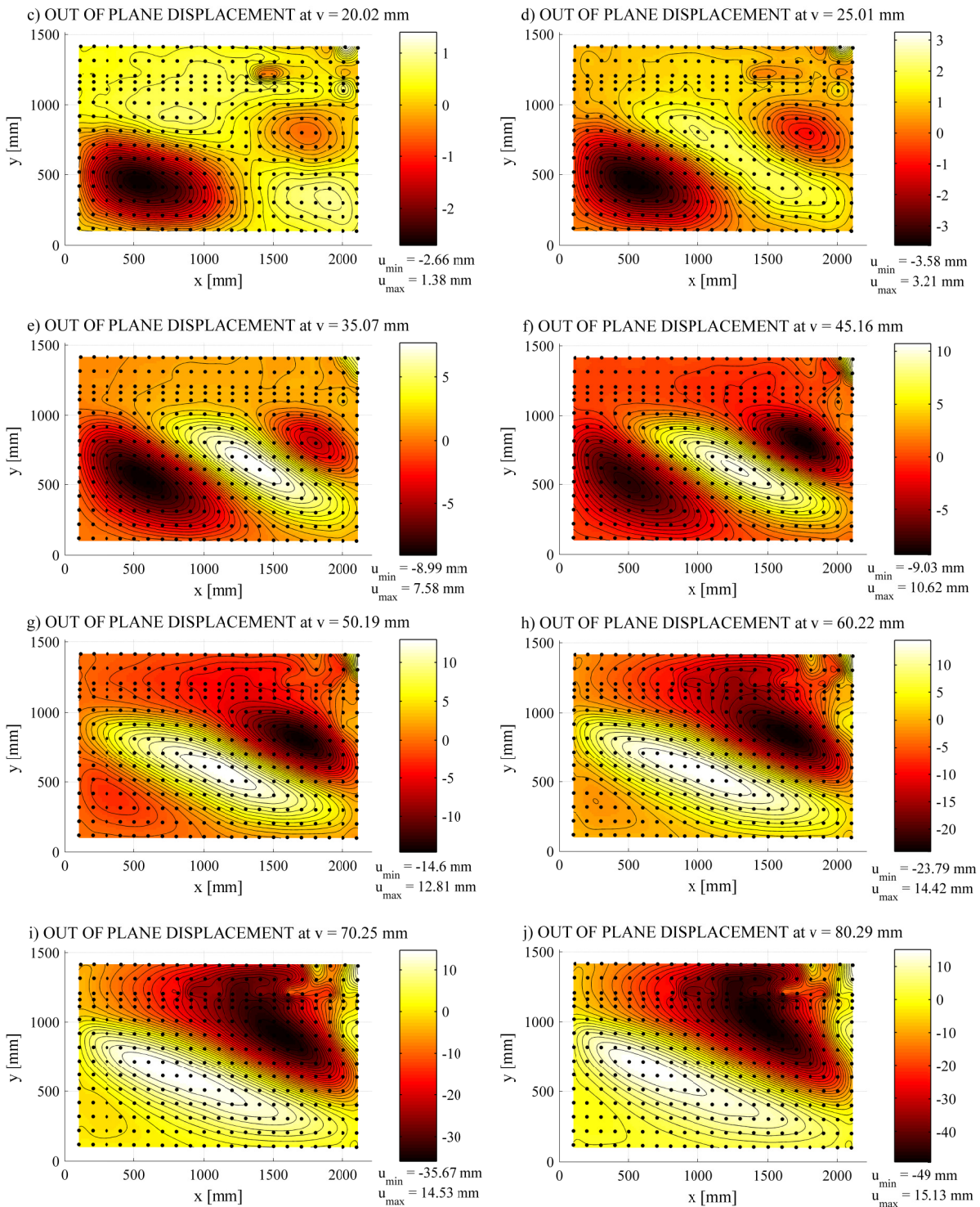


Figure 24: Evolution of out-of plane displacement during the test, SC

Slika 24: Razvoj pomikov izven ravnine, panel SC

The next two tests were performed on unsymmetric girder. Firstly, the panel stiffened with two open stiffeners in the upper part of the web (UO) was tested, while the left adjacent panel (UC) was protected against buckling. In Figure 25 the progress of the out-of-plane displacements at different levels of load applied for the tested panel are plotted. The first two pictures represent the out-of-plane displacement at a load lower than the critical shear force. The buckling shape in this load stage is undefined, as it does not belong either to shear or to bending buckling mode. By increasing the shear load and consequently also the bending moment in the panel, the highest subpanel starts to buckle due

to shear, which is seen as formation of diagonal waves. At the same time the other two subpanels start to buckle due to compression caused by the bending moment; buckling appears mainly in the area of the highest bending moment. Along the web panel away from the highest bending moment the waves alternate and the amplitudes of the waves become smaller.

The buckling is already evident in the elastic stage of the girder's response, which is up to the load of 1500 kN. The absolute maximum out-of-plane displacement at this load was 5.67 mm. In the linear stage only buckling of the web is observed, while the compressed flange and the "Open I" longitudinal stiffeners remain more or less straight. The first signs of transition from local buckling to global buckling can be seen at 2120 kN of load as the shear buckling of the highest subpanel spreads to the middle subpanel, but not to the third one. Nevertheless the local buckling still prevails at the maximum load as well as in the post peak stage.

The buckling of unsymmetrical longitudinally stiffened girder is similar as the buckling of the first two tests, the main difference being the formation of global buckling, which was in case of symmetric girders always present and was the result of the combination of high bending and shear load in the panel. In the test presented here this formation is not so evident.

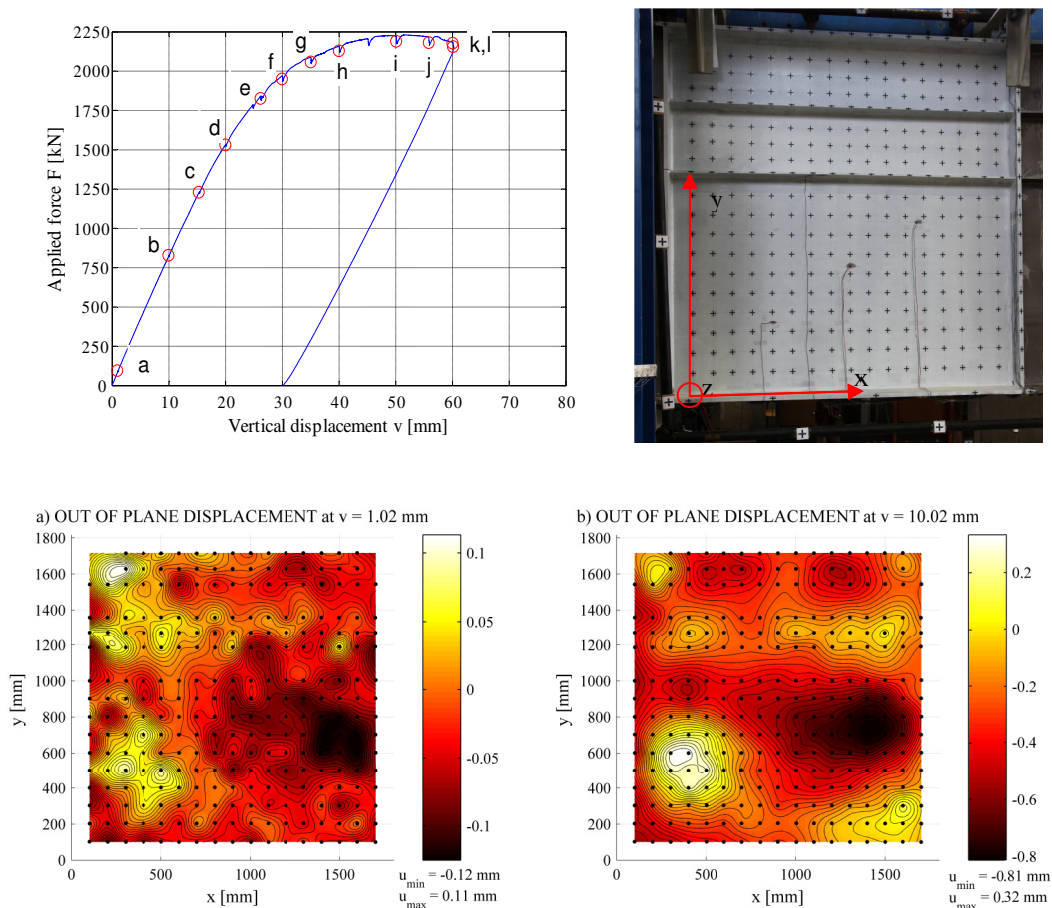


Figure 25: Evolution of out-of plane displacement during the test, UO
 Slika 25: Razvoj pomikov izven ravnine, panel UO

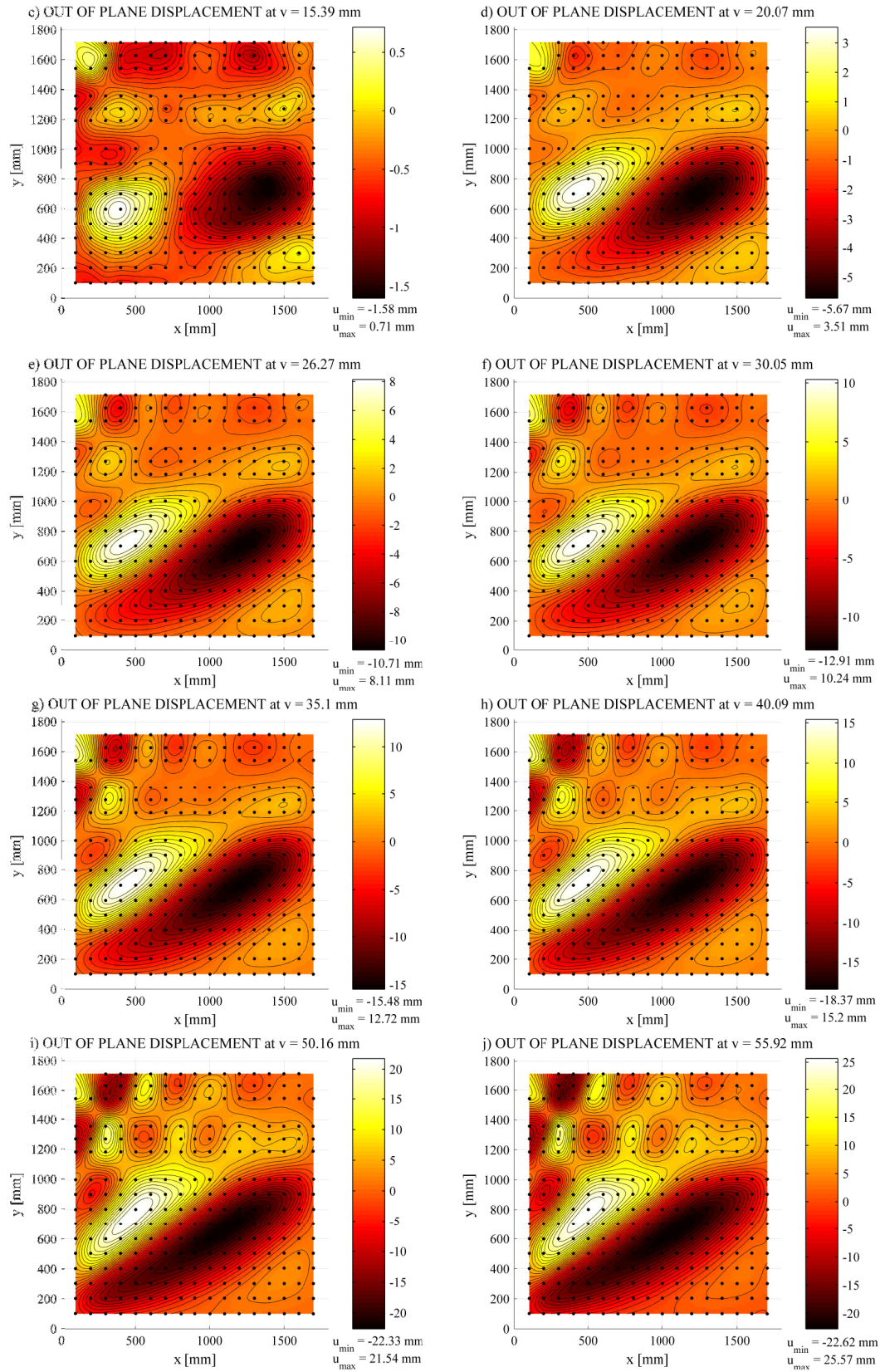


Figure 25: Evolution of out-of plane displacement during the test, UO

Slika 25: Razvoj pomikov izven ravnine, panel UO

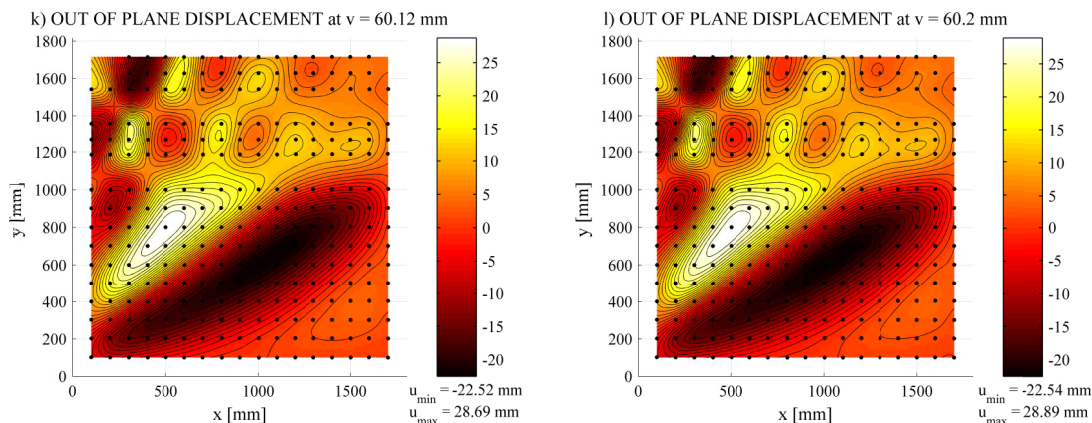


Figure 25: Evolution of out-of plane displacement during the test, UO
Slika 25: Razvoj pomikov izven ravnine, panel UO

Finally, the last test was performed on unsymmetric plated girder stiffened with closed stiffener. The initial conditions for this test were in the sense of geometrical imperfections much different than for the first three test situations. The shape of initial imperfections as well as amplitude were mainly the result of the previous test on UO panel and only partially of the fabrication process. Even though the amplitude was much higher than obtained only after fabrication, this unpredicted situation influenced neither the girder's behaviour nor its resistance.

The out-of-plane buckling in the beginning, when shear load in the panel is bellow elastic critical force, is very similar as in all previous tests. The buckling in the highest subpanel due to shear force is obtained first (see Figure 26). The web buckles in diagonal direction in three waves with absolute maximum amplitude on the other side of the panel, where the maximum bending moment is obtained. The evident local buckling in the smallest subpanel can be obtained at a force of 1200 kN. The longitudinal stiffener remains almost straight up to the load of approximately 1900 kN. Up to this point the response of the girder was elastic. By increasing the load in the panel the second order effects in combination with large compression force in the stiffener induce the stiffener to buckle. This can clearly be seen from the force displacement curve where a sudden drop in girder resistance occurs.

Up to this state the buckling of the web was separated for each subpanel. In one subpanel shear buckling occurred and in the second one buckling due to compression stresses occurred. Once the longitudinal stiffener had buckled, the whole panel formed a new buckling shape with maximum amplitude in the line of longitudinal stiffener.

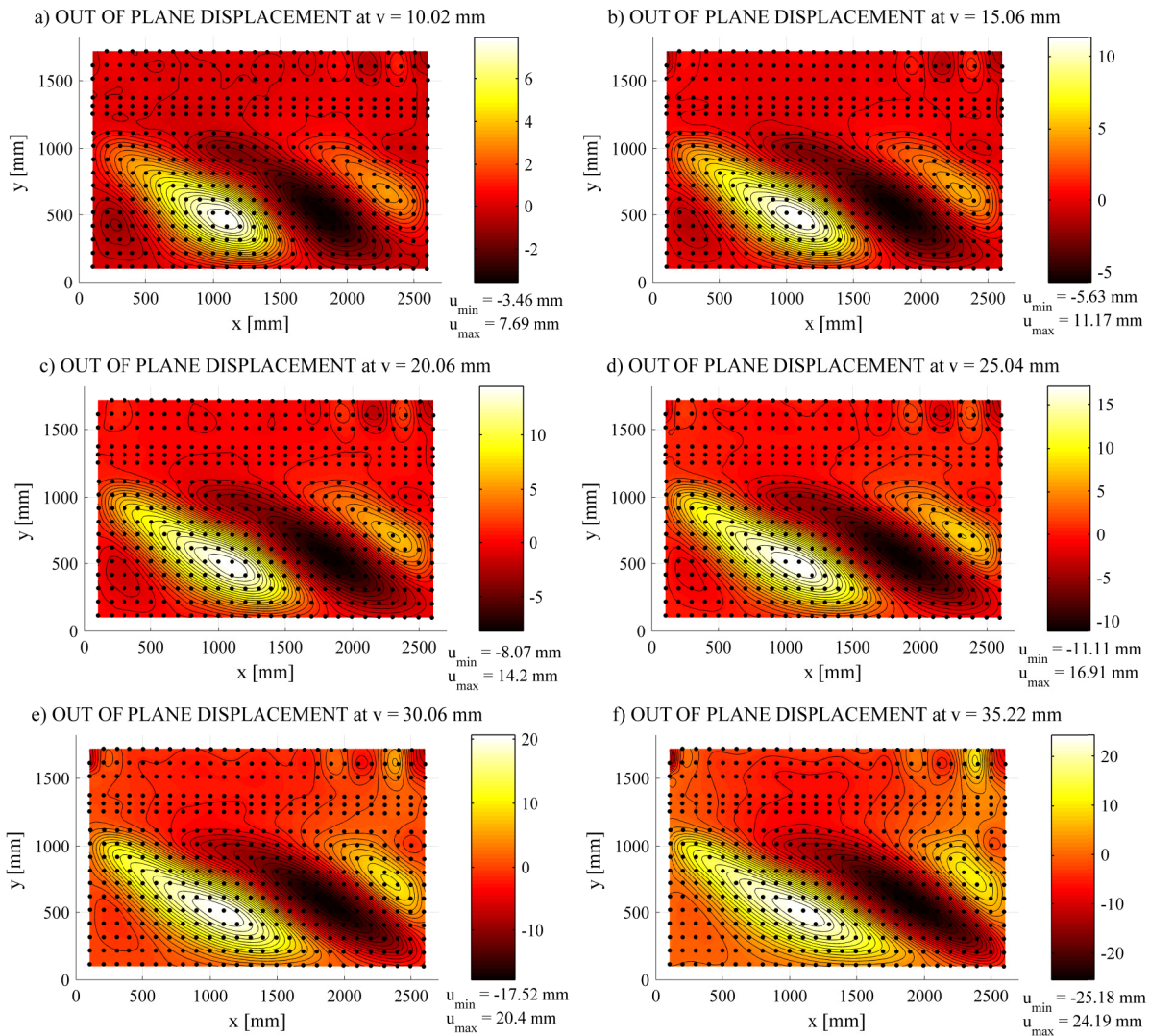
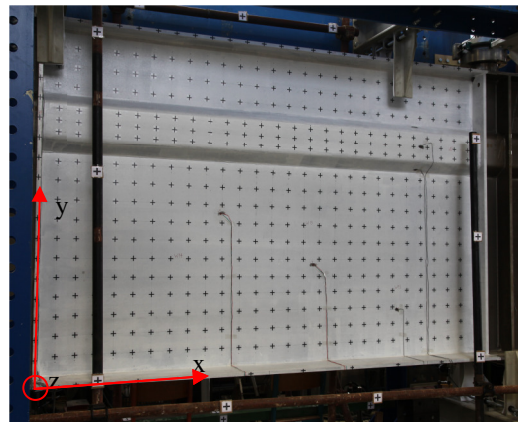
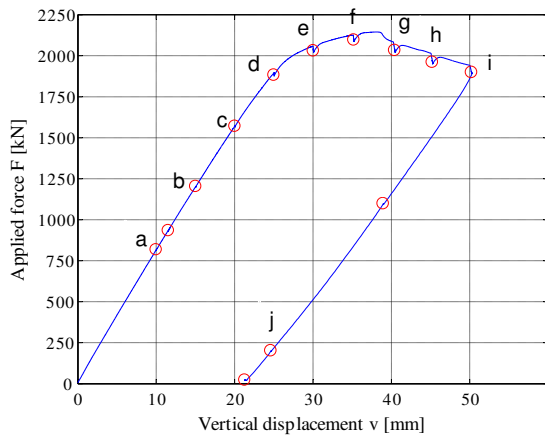


Figure 26: Evolution of out-of plane displacement during the test, UC
 Slika 26: Razvoj pomikov izven ravnine, panel UC

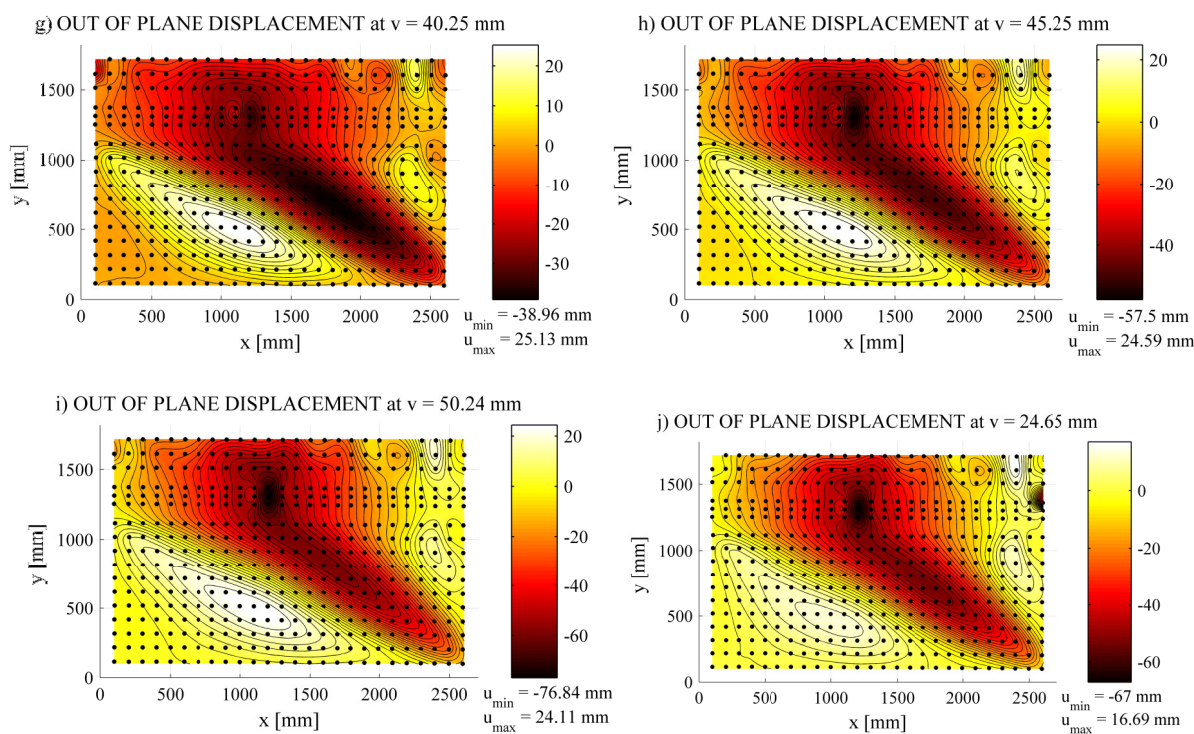


Figure 26: Evolution of out-of plane displacement during the test, UC
Slika 26: Razvoj pomikov izven ravnine, panel UC

3.3.3 Comparison to EN 1993-1-5

The ultimate characteristic resistance according to EN 1993-1-5 is determined by using effective width method (see Chapter 7.2). In Table 12 the experimental resistance of the girder is compared against calculated characteristic resistance. It can be seen that all tested girders exhibit higher resistance than the one obtained by EN 1993-1-5. It should be stressed that this additional resistance is the result of positive influence of the tension stresses in the largest subpanel, which is decisive for the determination of global shear resistance of the girder.

Preglednica 12: Primerjava eksperimentalne nosilnosti z nosilnostjo določeno po EN 1993-1-5
 Table 12: Comparing experimental resistance with resistance according to EN 1993-1-5

| | SO | SC | UO | UC |
|---|-------|-------|-------|-------|
| $F_{\text{Eksperiment}} [kN]$ | 1934 | 2049 | 2173 | 2087 |
| $F_{\text{EN 1993-1-5}} [kN]$ | 1792 | 1782 | 1746 | 1770 |
| $F_{\text{Eksp.}} / F_{\text{EN}} [\%]$ | 107.9 | 115.0 | 124.5 | 117.9 |

3.3.4 Strain measurement

The most demanding tasks of this part are, firstly, to perform the exact measurement of the position and orientation of strain gauges, and secondly, to understand the results and make the right interpretation.

The strains were measured in the following plates with the intention:

- In the web to see the development of the tension field.
- In the flanges to check any unpredicted out of plane buckling of the compressed flange.

- c) In the transverse stiffeners to determine the load in the stiffener.

During the test execution some of the strain gauges were torn due to large strains, so in these cases the strains are presented to that level only. The oscillation of strains represents a difficulty in the result interpretation; therefore in these cases the results were suitably filtered.

3.3.4.1 Triaxial strain gauges in the web

The position of strain gauge rosettes in the web is shown in ANNEX A: Layout of tested girders under M-V interaction. In panel SO the strains are measured in three points by strain gauge rosettes, while in the other tests, the strains are measured in two points by a strain gauge rosette and in one point by a linear strain gauge. In the measuring points the strain gauge rosettes were put to both sides of the plate. The presented strains are calculated as the average of strains measured on both sides of the plate and transformed to the principal strain. The direction of the measured strain is shown in ANNEX A: Layout of tested girders under M-V interaction.

From the measured surface strains the membrane strains can be calculated as follows:

$$\begin{aligned}\varepsilon_x &= (\varepsilon_{x,front} + \varepsilon_{x,back}) / 2 \\ \varepsilon_y &= (\varepsilon_{y,front} + \varepsilon_{y,back}) / 2, \\ \varepsilon_{xy} &= (\varepsilon_{xy,front} + \varepsilon_{xy,back}) / 2\end{aligned}\quad (9)$$

where ε_x represents strain in horizontal - x direction, ε_y strain in vertical - y direction (perpendicular to x direction), and ε_{xy} strain in direction 45° from horizontal x direction.

The equations for calculating principal strains from three rosette strain measurements are derived from what is known as a "strain-transformation" relationship. The normal strain at any angle θ from the major principal axis is simply expressed by:

$$\varepsilon_\theta = \frac{\varepsilon_1 + \varepsilon_2}{2} + \frac{\varepsilon_1 - \varepsilon_2}{2} \cos 2\theta, \quad (10)$$

where ε_1 and ε_2 represent the principal strains, and θ the angle between principal strain ε_1 and strain ε_x . If the measured strains and their orientation are considered in equation (10), we get three equations with three unknown quantities: principal strains ε_1 , ε_2 and direction angle θ of first principal strain:

$$\begin{aligned}\varepsilon_x &= \frac{\varepsilon_1 + \varepsilon_2}{2} + \frac{\varepsilon_1 - \varepsilon_2}{2} \cos 2\theta, \\ \varepsilon_{xy} &= \frac{\varepsilon_1 + \varepsilon_2}{2} + \frac{\varepsilon_1 - \varepsilon_2}{2} \cos 2(\theta + 45^\circ), \\ \varepsilon_y &= \frac{\varepsilon_1 + \varepsilon_2}{2} + \frac{\varepsilon_1 - \varepsilon_2}{2} \cos 2(\theta + 90^\circ).\end{aligned}\quad (11)$$

By solving equations (11) simultaneously, the principal strains and the angle can be expressed in terms of three measured strains:

$$\varepsilon_{1,(2)} = \frac{\varepsilon_x + \varepsilon_y}{2} + (-) \frac{1}{\sqrt{2}} \sqrt{(\varepsilon_x - \varepsilon_{xy})^2 + (\varepsilon_{xy} - \varepsilon_y)^2}, \quad (12)$$

$$\theta = \frac{1}{2} \arctan \left(\frac{\varepsilon_x + \varepsilon_y - 2\varepsilon_{xy}}{\varepsilon_x - \varepsilon_y} \right). \quad (13)$$

The membrane principal strains in the web panel for all four tests are plotted in Figure 27. As mentioned, strains were measured in three points of the panel in the first test. Due to technical problems the strains were not measured from the beginning of the test SO. Therefore, a linear stage up to the load of 1000 kN for the first test is missing. For other tests the principal strains are plotted for two points, one in the middle and the other in the top corner of the largest subpanel, where the tension field is anchored to the transverse and longitudinal stiffener. On each diagram, the vertical lines denote the yield strain.

From the principal deformation development the following observation can be pointed out:

- The tension principal strains measured in the centre of the panel, where the influence of normal stresses due to bending moment is very small, denoted with R2, always prevail compared to the compression principal strain. From the measured strain development the tension field formation in this point is clearly seen.
- In point, denoted as R3, in all tests except in the test of the UC and UO panel contrary phenomenon is found. The strain distribution is very complex in this area, first because of different actions, i. e. shear load and bending, and second because of longitudinal and transverse stiffeners which influence strain and stress distribution in the web.

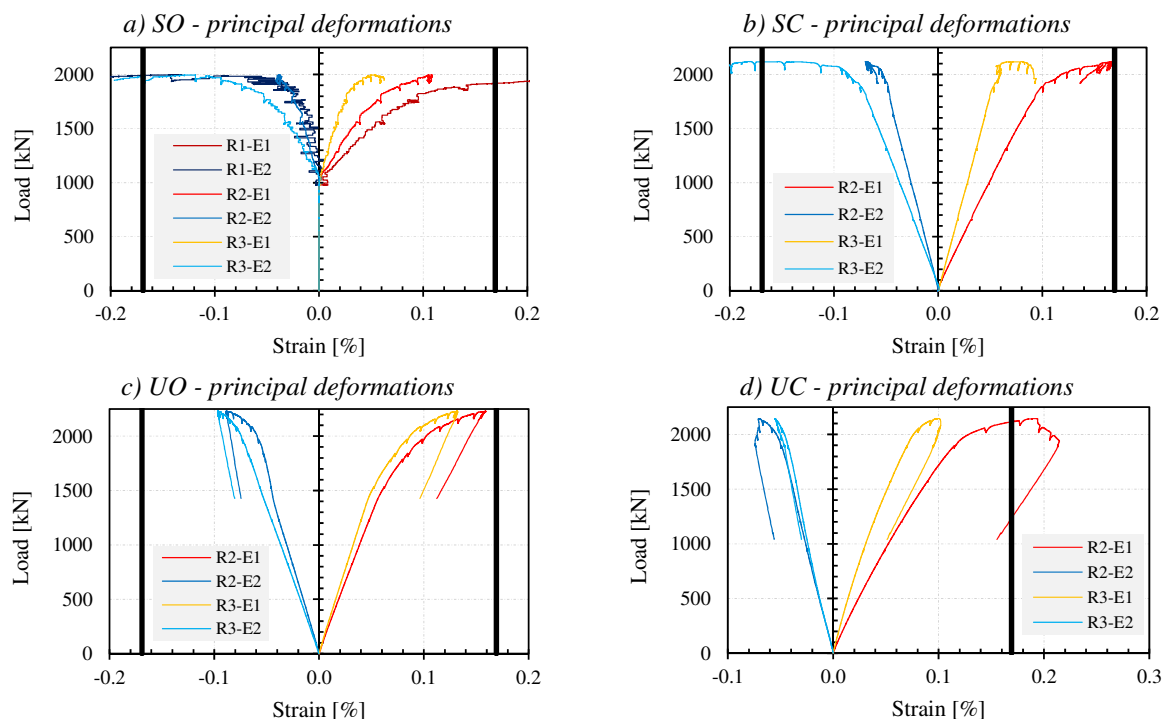


Figure 27: Principal membrane strains ($\varepsilon_1 = E1$, $\varepsilon_2 = E2$) in the web measured by strain gauge rosettes

Slika 27: Glavne membranske deformacije v stojini ($\varepsilon_1 = E1$, $\varepsilon_2 = E2$)

In Figure 28 the angle of inclination θ of the first principal strain in each measured point is shown. Each diagram corresponds to one of the tested panel. The principal strain measured in the centre point R2 is oriented in the diagonal direction of the tension field; the calculated angle is between -20 to -40° .

The angle changes its orientation in point R3, where the direction of the principal strain turns to the opposite diagonal direction compared to point R2. This happens in all cases except for girder UC, where the principal strain orientation is similar as in point R2.

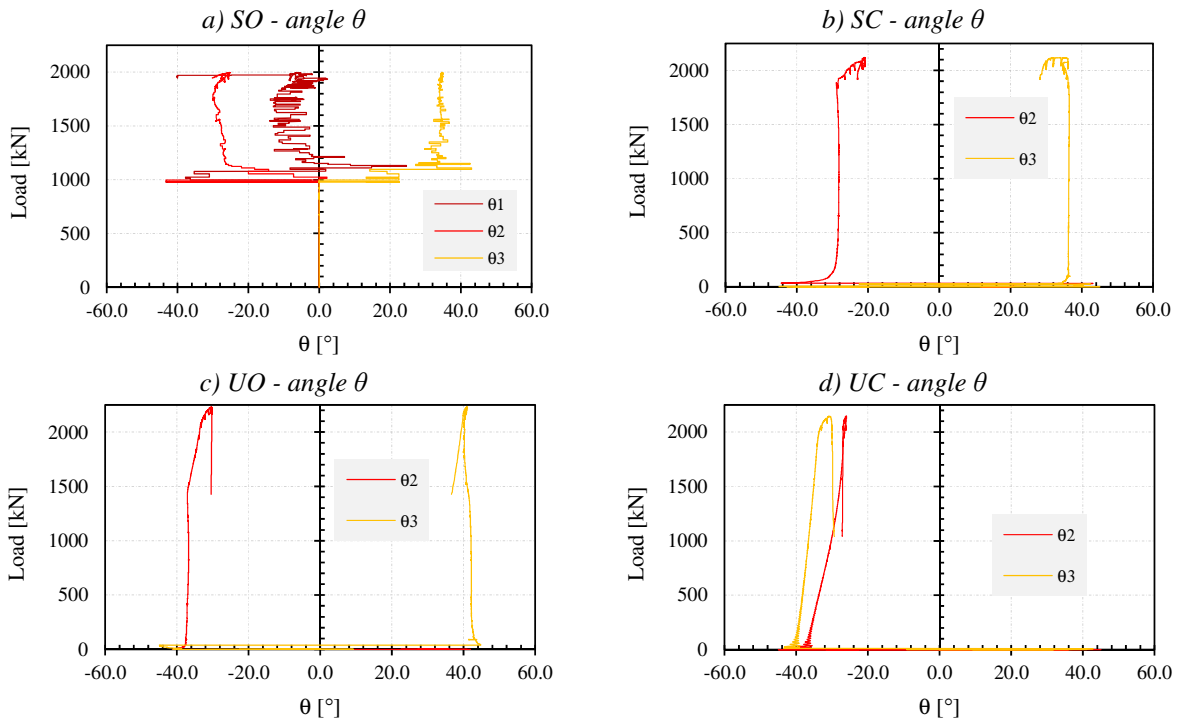


Figure 28: Angle of inclination θ of the first principal deformation
Slika 28: Naklonski kot θ prve glavne deformacije

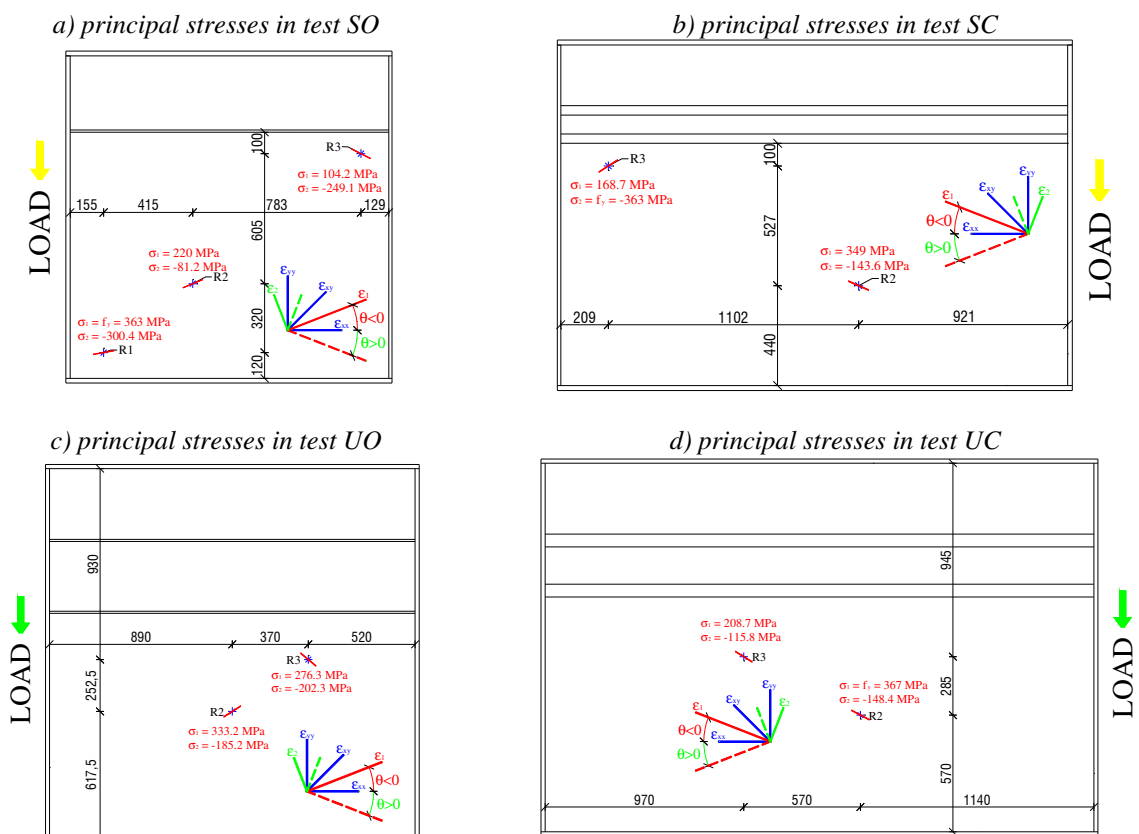


Figure 29: The principal membrane stress orientation and values obtained at maximum load
Slika 29: Vrednosti in naklon glavnih deformacij določenih pri največji obremenitvi

The orientation of principal membrane stresses and values at the maximum load are plotted in Figure 29. The orientation of nodes R1 and R2 is in the diagonal direction of the subpanel. The inclination is smaller in node R1 where the influence of tension stresses due to bending is the largest. The same orientation is also found in node R3 of the tested panel UC. In all other cases the orientation of principal tension strain in node R3 is almost perpendicular to the diagonal direction of the tension field.

3.3.4.2 Uniaxial strain gauges in the flange

The strains in the compressed and tension flange were measured in two points on each side of the flange, as shown in Figure 31, at a distance of $h_{wi,max}/2$ from the most stressed edge of the panel. The vertical lines on the diagram denote the yield strain calculated from the measured yield stress of the plates. For all tests the compressed strains are much larger than tension strains, especially at the maximum load. From the strain development in compression flange the local buckling of the flange can be clearly obtained. The local buckling occurs when one of the strains stops to increase and starts to decrease. In all cases this buckling happened on the plateau of the global response.

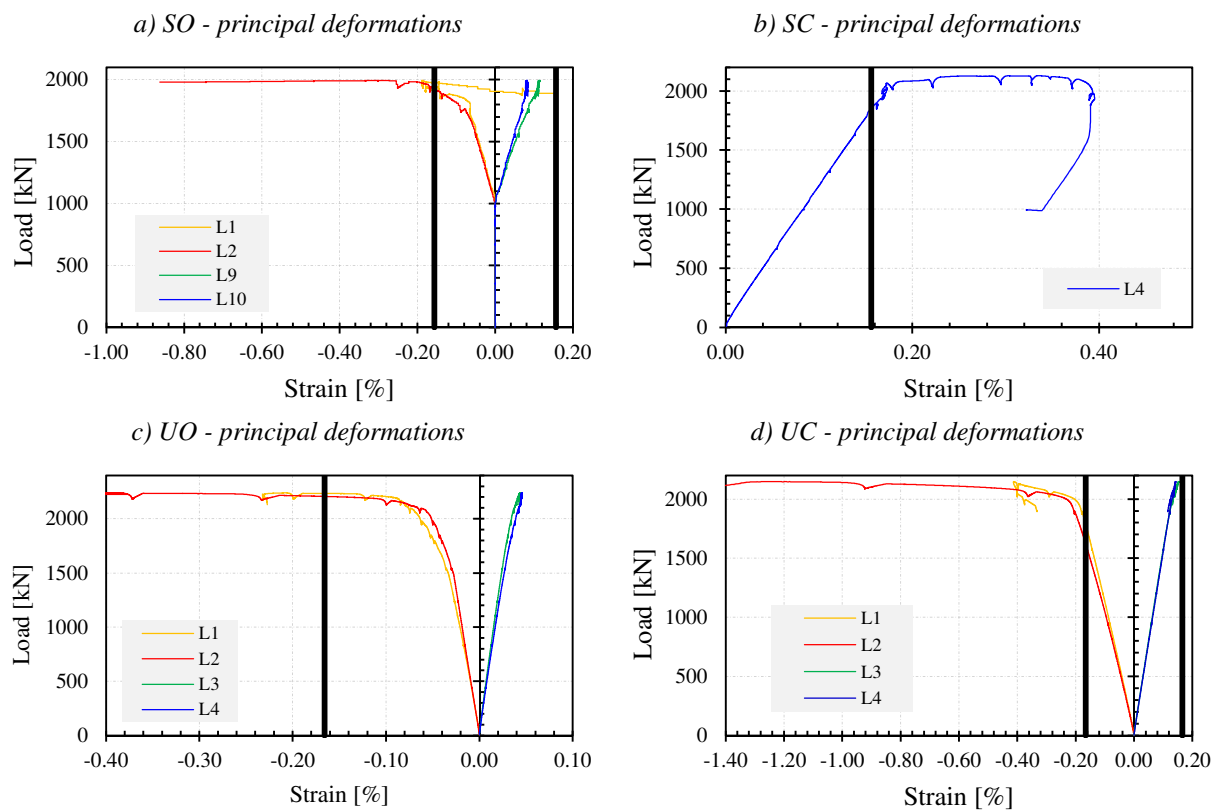


Figure 30: Strain measurement in compression and tension flange
Slika 30: Deformacije v tlačeni in natezni pasnici

3.3.4.3 Linear strain gauges on the intermediate transverse stiffener

The intermediate transverse stiffeners can be subjected to transverse bending due to deviation forces, to compressive force due to the tension field action and to an external concentrated load. In the applied tests the transverse stiffener was subjected to deviation forces and to compressive force due to tension field action. According to available literature and the numerical simulations (Presta [14], Lee et al. [8, 9]) it was established that axial force due to tension field action is much lower than the one given in EN 1993-1-5. The test results on transverse stiffener of Basler et al. [26] and Evans et al. [75] were

evaluated by Höglund and compared against rules in EN 1993-1-5. The formulation in EN 1993-1-5 for determination of axial force from tension field action was found conservative.

To get an insight into the strain distribution in the transverse stiffener, linear strain gauges were installed on the stiffener. The strains were measured along the stiffener at three cross-sections; at each cross-section the strains were evaluated in either one, two or three points. The progress of strains in the transverse stiffeners for all four tests is plotted in Figure 32 to Figure 35.

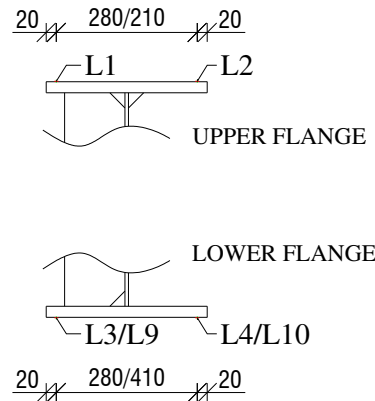


Figure 31: Position of strain gauges in the upper (compression) and lower (tension) flange
Slika 31: Pozicioniranje merilnih lističev v zgornji in spodnji pasnici

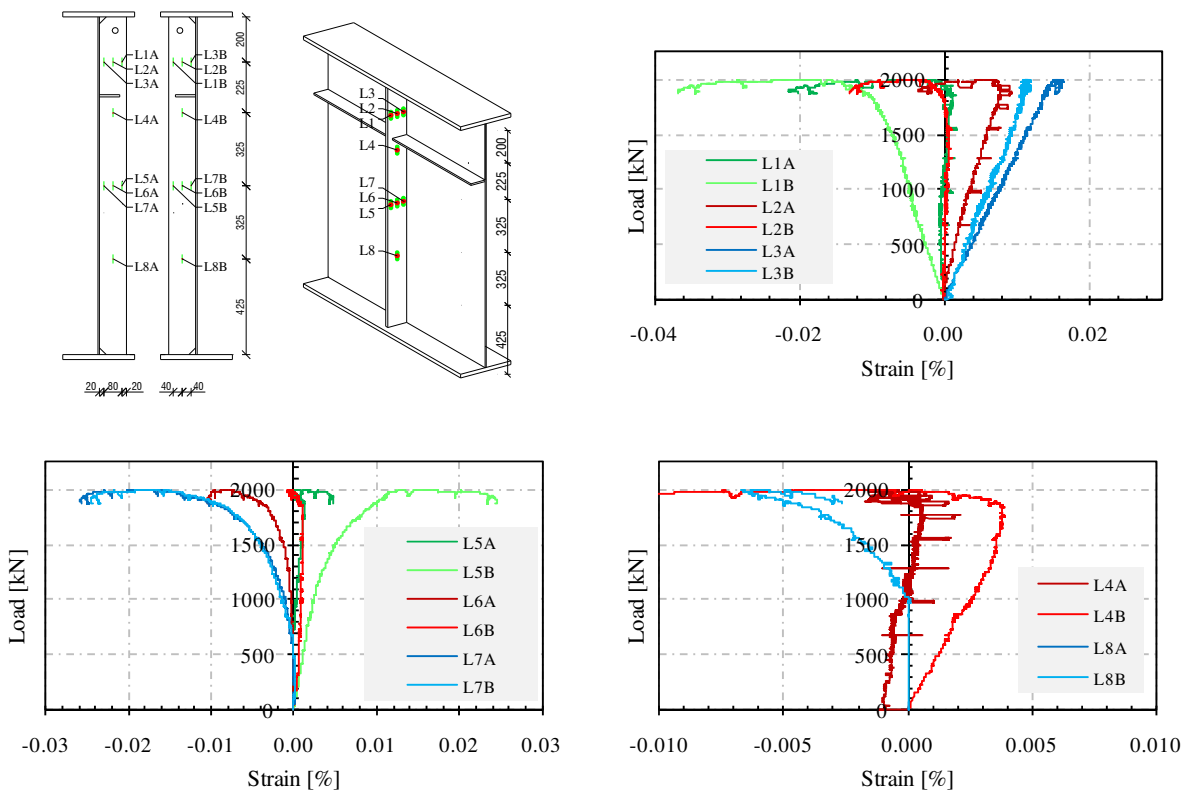


Figure 32: Strains measured in the transverse stiffener when SO is tested
Slika 32: Deformacije v prečni ojačitvi, panel SO

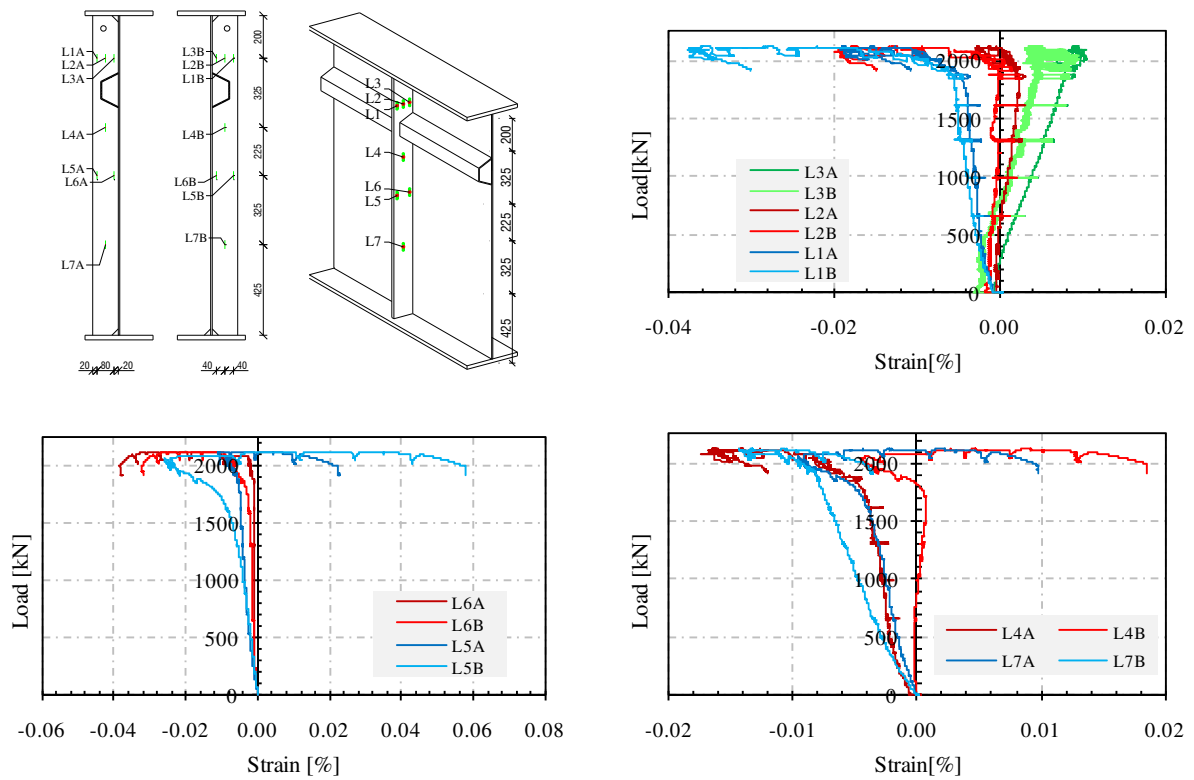


Figure 33: Strains measured in the transverse stiffener when SC is tested

Slika 33: Deformacije v prečni ojačitvi, panel SC

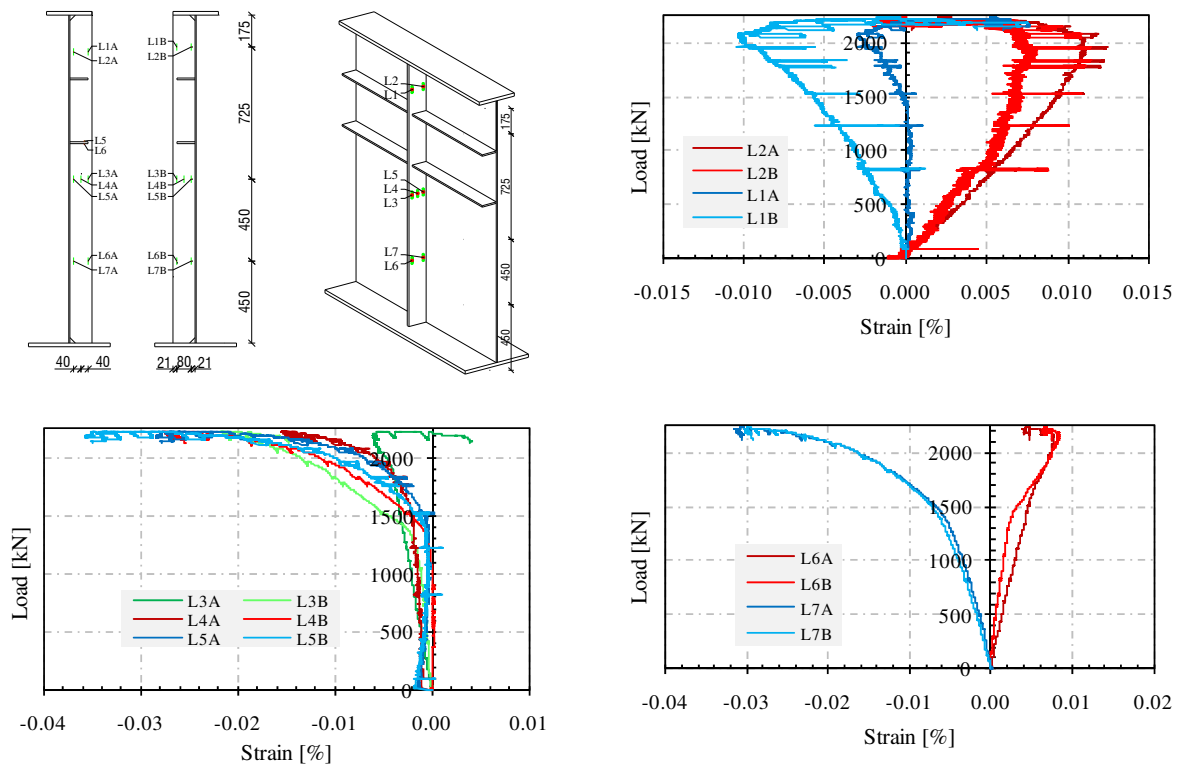


Figure 34: Strains measured in the transverse stiffener when UO is tested

Slika 34: Deformacije v prečni ojačitvi, panel UO

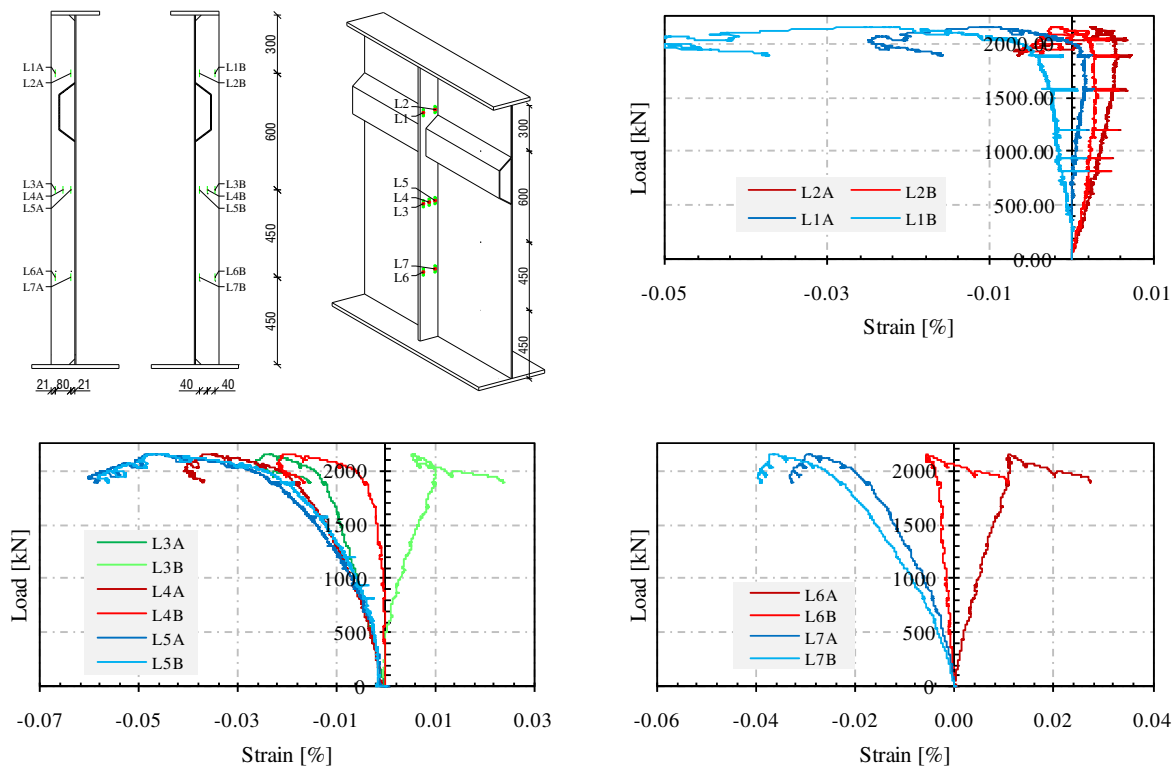


Figure 35: Strains measured in the transverse stiffener when UC is tested
Slika 35: Deformacije v prečni ojačitvi, panel UC

The measured strains in the transverse stiffeners were rather below the yield strain 0.17%. The maximum obtained strain was 0.058% which results in stress of 121.8 MPa. In most cases the outer strain point showed tension strains and the inner strain point next to the web plate compression strains. These results prove that the actual effect of tension field action on the transverse stiffener is overestimated and needs to be further investigated.

3.4 Discussion

This chapter presents an overview of experimental work on bending-shear capacity of plated girders. It includes the experiment preparation, testing and presentation of noteworthy results.

The geometry of the tested specimens was chosen to simulate the natural size of bridge composite girder at an internal support with a span around 30 m. The final dimensions were a compromise between the laboratory capacities and the desired proportions. The tests were not designed to investigate only one parameter, but to get overall information about the behaviour of longitudinally stiffened girders taking into account completely different parameters, such as web slenderness, panel aspect ratio, geometry of the stiffener (open, closed) and symmetry of the cross-section.

The experimental tests form the background for further parametric studies in the sense of calibration of numerical model. In this way the developed numerical model proved to be reliable for all further permutations of parameters of the girders.

The actual geometry considering real dimensions as well as initial out-of-plane imperfections of girders was measured with special care. The out-of-plane imperfections of all tested panels were determined by using photogrammetry.

The tested girders were fully equipped with series of electronic devices and strain gauges to follow the strains and displacements development during loading. The first significant observation was the out of plane buckling development and final failure mode. After testing the interaction of shear buckling and bending buckling of the web was visually noticeable.

Three girders showed a load-deflection response with large ductility, with slow decrease of the load capacity following the obtained peak capacity. The fourth girder, stiffened with a large closed stiffener, however, showed much smaller ductility due to instantaneous buckling of the longitudinal stiffener. This can be clearly seen from the force-deflection curve where an immediate drop of the girder resistance was obtained.

The main conclusions found through experimental work are:

- In all cases the largest lower subpanel buckled first due to shear stresses, afterwards the bending in the panel caused buckling due to normal stresses in the upper subpanel and finally global buckling of the panel was observed with the stiffener involved.
- In all tests the compressed flange buckled locally at large plastic deformations, except in the case of unsymmetric girder UC, where due to buckling of the longitudinal stiffener global buckling occurred.
- No plastic deformations were observed in the transverse stiffener.
- The torsional buckling of the open longitudinal stiffener was clearly observed at the most stressed edge of the panel.
- The rules given in EN 1993-1-5 prove to be conservative for these configurations of plated girders with the difference between experimentally obtained capacity and the one calculated by EN 1993-1-5 between 8 and 25%. The key reason for this difference comes from neglecting the positive influence of tension stresses in the lower subpanel according to rules in EN 1993-1-5.

4 NUMERICAL MODEL

Numerical methods, such as finite element method and finite differential method, were developed with the purpose to solve large, complex physical phenomena which cannot be solved theoretically. Today, the numerical methods are basic tool to solve different kinds of problems in any field of natural and engineering sciences.

4.1 Introduction - The finite element method

Most of practical problems arising in engineering applications must be solved in an approximate way by some numerical methods, since closed-form exact solutions exist only for a narrow category of problems. Nowadays, the most universal technique applicable also to structural problems is the finite element method (FEM). This method is the basic tool for most of the software packages used for engineering computations.

The possibility and advantage of using numerical methods as a tool for the simulation of physical problems often enables the researchers to avoid expensive experimental tests. Continuous development of finite elements and solution techniques as well as progress of computer capabilities enabled to solve almost any size of engineering problem.

The experimental tests, described in the previous chapter, were simulated by means of finite element method, so in this chapter an overview of the basic theory behind the finite element method used for our research will be presented. The structural modelling has proved useful not only for conducting large parametric studies but also for thorough understanding of the phenomena associated with the resistance mechanism, stress and strain distribution and buckling development of the longitudinally stiffened girders subjected to high shear and bending load.

The use of FE-method for structural problems requires a careful formulation of the mathematical model which takes into account the actual external factors such as the geometry, the material, the load and the initial conditions like supports, temperature, etc. It is of key importance in what way the real structural model is formulated as a mathematical model and whether it will properly describe the actual natural behaviour. Therefore, it is recommended when dealing with numerical tools, not only to understand the theoretical background of the finite element method, but also to have experience with numerical simulations in order to properly interpret the numerical results.

The usual methodology starts with a definition of the nature of the problem. The continuous structure is then transformed into discrete systems. Once the model has been defined, the structure is meshed with appropriately small finite elements. These elements are then properly connected at their boundary nodes. The elements can be one-, two- or three-dimensional depending on the problem being dealt with and the needed information of the structure. Some physical phenomena can be modelled with adequate accuracy by employing any kind of finite elements. In such cases the logical choice is the one dimensional element which is the most cost-effective.

In the case of nonlinear analysis of plated elements, where local buckling is of the main concern regarding the element's stability and behaviour, the mathematical model has to be described by two-dimensional elements. The complexity of the problem, the modelling as well as computation time and eventually computation cost are increased.

4.2 Geometry

Plated girders are assembled of thin plates: flanges, web, transverse and longitudinal stiffeners. Generally, the body is modelled by defining the geometry of the plates at a reference surface and the thickness through the section property definition. To obtain plate buckling effect the girders have to be mathematically modelled with shell or solid finite elements.

Although the plates are loaded in their plane, the buckling of the plate and the second order effect also cause bending in the plates. From this point of view the plate can be discretised with three dimensional shell elements, which can be subjected to both bending and in-plane force resulting in the middle of the plate.

The main assumptions of the thin plate theory (Kirchhoff plate theory) which is used for our shell formulation are:

- The plate is thin in the sense that the thickness is small compared to the characteristic length,
- because the plate thickness is either uniform or varies slowly, the three-dimensional stress effects are ignored,
- the stresses in the normal direction of the plate are zero,
- the plane section remains plane and normal to the deformed longitudinal axis (linear strain distribution due to bending over the thickness of the plate - equivalent to Euler-Bernoulli beam theory).

4.3 Material

With elastic-plastic model, calculation of stress and strain distributions at low strain is based on linear elasticity. The onset of non-linearity is attributed to plastic deformation and occurs at a stress level regarded as the first yield stress.

The structural steel was modelled as an isotropic elastic-plastic material considering yielding and strain hardening (isotropic).

4.3.1 The yield criterion

The yield criterion, defined with yield function, determines at which strains the material starts to yield. Most common yield criteria in the engineering practice are: yield criteria of von Mises, Tresca, Mohr-Columb and Drucker-Prager. One very important aspect of all these yield criteria is their isotropy, which means that plastic yield criteria are defined in terms of an isotropic yield function of the stress tensor. Since the von Mises yield criterion was employed for the numerical simulations, details of this yield function will be presented.

4.3.1.1 The von Mises yield criterion

The von Mises yield criterion is used to predict yielding of materials under any loading conditions from the results of simple uniaxial tests. According to the von Mises criterion, plastic yielding begins, when the stress deviator invariant J_2 reaches a critical value:

$$\Phi(J_2) = \sqrt{J_2} - k = \sqrt{J_2} - \tau_y = 0, \quad (14)$$

where $\tau_y = f_y / \sqrt{3}$ is the shear yield stress of the material. In terms of principal stress the stress invariant can be expressed as:

$$J_2 = \frac{1}{6} [(\sigma_1 - \sigma_2)^2 + (\sigma_2 - \sigma_3)^2 + (\sigma_3 - \sigma_1)^2]. \quad (15)$$

Under plane stress condition the yield condition reads:

$$\sqrt{\sigma_1^2 - \sigma_1\sigma_2 + \sigma_2^2} = f_y. \quad (16)$$

The stress state is characterized by the condition $J_2 \leq k^2$, with plastic flow possible only when $J_2 = k^2$.

4.3.2 Material idealisation

The material model input given in ABAQUS has a uniaxial stress-strain relation. Two different material idealisations were used in this work; one for model verification and the other for extended parametric study. These are:

- Stress-strain curve from tension tests - for model verification.
- Elastic-plastic material with a nominal plateau slope - for parametric study.

The input data defining elastic-plastic material were:

- Module of elasticity $E = 210000 \text{ MPa}$.
- Poisson's ratio $\nu = 0.3$.
- Points of pairs defined with true stresses and logarithmic strains ($\sigma_{true}, \varepsilon_{ln}^{pl}$)

The relation between engineering stress-strain relationship and true stress and logarithmic plastic strains is given as:

$$\sigma_{true} = \sigma_{nom} (1 + \varepsilon_{nom}), \quad (17)$$

$$\varepsilon_{ln}^{pl} = \ln(1 + \varepsilon_{nom}) - \frac{\sigma_{true}}{E}. \quad (18)$$

4.4 Finite elements in ABAQUS - Shell elements used

In ABAQUS [76] a wide range of shell finite elements is available for the application of different numerical problems. The library is divided in three categories and consists of general-purpose, thin and thick shell elements. In this particular study, general-purpose shell elements S4 (S3), S4R (S3R) were employed in preliminary studies.

The general-purpose elements S4 (S3) and S4R (S3R) provide robust and accurate solutions by all loading conditions for thin and thick shell problems. Thickness changes as a function of in-plane deformation. The elements do not suffer from transverse shear locking, nor do they have any unconstrained hourglass modes. The membrane kinematics is based on assumed finite strain formulation which provides an accurate solution for in-plane bending behaviour.

The employed elements were triangular three-node and four-node shells with adopted either full integration (S4 and S3) or reduced integration (S4R and S3R) over the shell element. The advantage of reduced integration elements is that the strains and stresses are calculated at the locations which provide optimal accuracy; in what is called Barlow points. Furthermore, the reduced number of integration points decreases CPU time and storage requirements. The disadvantage of the reduced integration is that the procedure can admit deformation modes which cause no straining at the integration points. To prevent this kind of excessive deformations, an additional artificial stiffness is added to the element. In this hourglass control procedure, this small artificial stiffness is associated with zero-energy deformation modes.

To calculate the shell's cross-sectional behaviour, the Simpson integration rule considering five section points is employed.

4.5 Analysis

The response of the analysed girder involves buckling and collapse behaviour, where the load-displacement response shows negative stiffness as shown in Figure 36. In such cases the structure must release strain energy to remain in equilibrium. The static equilibrium state can be found by using arc length method.

Within this method it is assumed that the loading is proportional - that is, that all load magnitudes vary with a single scalar parameter and that the response is reasonably smooth without any sudden perturbations. The main point of the method is that the solution is viewed as the search for a single equilibrium path in a space defined by the nodal variables and the loading parameters.

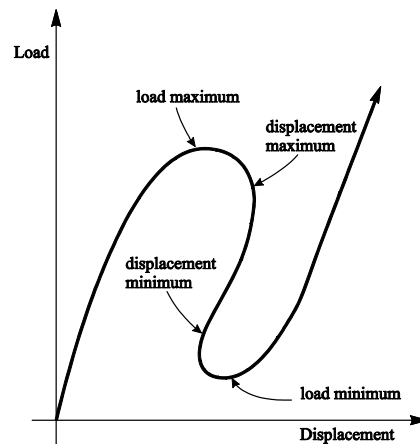


Figure 36: Unstable static equilibrium solution
Slika 36: Nestabilna ravnotežna pot

The equilibrium equation of nonlinear system can be written as:

$$\mathbf{r}_i(\mathbf{u}_i, \lambda_i) = \mathbf{f}_i^{\text{int}}(\mathbf{u}_i) - \lambda_i \mathbf{f}_i^{\text{ext}}, \quad (19)$$

where \mathbf{r}_i is the out-of-balance load vector, $\mathbf{f}_i^{\text{int}}$ vector of internal equivalent nodal forces, $\mathbf{f}_i^{\text{ext}}$ an externally applied load vector and λ_i the load level parameter. The arc-length method adds an extra constraint to the residual equation above so as to limit the length of the incremental solution. The general form of the constraint equation is given as:

$$a = \Delta \mathbf{u}^T \Delta \mathbf{u} + \Delta \lambda^2 \psi^2 \mathbf{f}^{\text{ext}T} \mathbf{f}^{\text{ext}} - \Delta l^2 = 0, \quad (20)$$

where $\Delta \mathbf{u}$ and $\Delta \lambda$ are converged incremental quantities, l a prescribed incremental solution length and ψ a prescribed scaling parameter. The system of nonlinear equations (19) together with the relevant arc-length constraint is solved by Newton iterative algorithm. The linearised system to be solved for $\delta \mathbf{u}^{(k)}$ and $\delta \lambda^{(k)}$ at the k^{th} Newton iteration is:

$$\begin{bmatrix} \mathbf{K}_T(\mathbf{u}^{(k-1)}) & -\mathbf{f}^{ext} \\ 2\Delta \mathbf{u}^{(k-1)T} & 2\Delta \lambda \psi^2 \mathbf{f}^{extT} \mathbf{f}^{ext} \end{bmatrix} \begin{Bmatrix} \delta \mathbf{u}^{(k)} \\ \delta \lambda^{(k)} \end{Bmatrix} = - \begin{Bmatrix} \mathbf{r}(\mathbf{u}^{(k-1)}, \Delta \lambda^{(k-1)}) \\ a^{(k-1)} \end{Bmatrix}, \quad (21)$$

where $\delta \mathbf{u}$ is the iterative change in displacement vector, $\delta \lambda$ the iterative change in load factor, \mathbf{K}_T the tangential stiffness matrix and a the previous value of out-of-balance arc-length.

5 VALIDATION OF NUMERICAL MODEL

The numerical model was developed in the multi-purpose code ABAQUS [76] with the purpose to simulate parametric study of the presented investigation on the behaviour of longitudinally stiffened plated girders. With simulations the response of the real system can easily be modelled. However, it is of essential importance, when developing extensive work on the basis of numerical methods, to verify the results with exact theoretical solutions or with experimentally obtained values.

The response of the plated girder under interaction of high bending and shear load is based on appointed assumptions such as mesh design, initial imperfections of the girder (structural and geometrical) and material modelling. These three assumptions do not influence only the buckling behaviour but also the girder resistance. However, the right choice of mesh and imperfections is finally in the hands of the designer. With proper consideration of these important influences the reliability of the obtained results increases.

Within the numerical model development the following characteristics, described in previous chapter, were taken into account:

- Thin plates were meshed with 4-node shell elements with reduced integration and with 3-node triangular general-purpose shell elements.
- The theory of finite strains is implemented in finite elements.
- For the model verification, the material was taken from the modified tension test on steel coupons. For parametric study an idealised bilinear elastic-plastic material was employed with nominal plateau slope.
- The yielding surface was obtained through the von Mises yield criterion.
- The response of the girder is calculated with the arc-length method. On each increment the iterative Newton method is used to solve the set of nonlinear equations.

The numerical model was developed considering recommendations by EN 1993-1-5 Annex C, which gives guidance on the use of FE-methods for ultimate limit state, serviceability limit state or fatigue verifications of plated structures.

In this chapter, the results obtained by numerical simulation will be compared to experimental results. The influence of structural and geometrical imperfections will be taken into account in the sense of different amplitudes as well as different shapes. The purpose of imperfection sensitivity analysis was to find out the influence of shape and amplitude of the initial imperfection on girder resistance and to answer the question, whether there exists an imperfection mode that would result in the smallest resistance in most of the cases. An extended sensitive imperfection analysis on longitudinally stiffened girders was carried out by Sinur et al. [77] before the experimental tests were performed.

5.1 Summary of FEM – Annex C of EN 1993-1-5

The progress of computer technology and of user friendly software in the past decades has spread the use of FEM analysis not only to research but also to design field. The recommendation given in EN 1993-1-5 is an attempt to codify the use of nonlinear FEM for the design purpose of plated structures. The following recommendations are covered by EN 1993-1-5:

- Use of initial imperfections.
- Modelling of material behaviour.
- Definition of limit state criteria.

5.1.1 Initial imperfections

In each structure or structural element initial imperfections are always present. The most important imperfections in plated girders are initial geometric imperfections and residual stresses. These imperfections result from fabrication process (cutting and welding of the plates) of plated girders. The shape and the amplitude of initial geometric imperfections of the structural element are not known in advance.

While geometrical imperfections of the structural element can easily be measured, the residual stresses are very difficult to obtain with non-destructive methods. In general, it is known that tension stresses are expected in the vicinity of welds and compression stresses in the remaining area. The distribution of these stresses is nonlinear with very high amplitudes in tension, which are near to yielding stress of material (see Chapter 3.2.2).

These imperfections, residual stresses and geometric imperfections obviously have to be properly considered in the numerical model. They can be modelled as separate imperfections or together by using the equivalent geometric imperfections according to EN 1993-1-5. When the analysis is carried out with geometric imperfections in combination with residual stresses, the shape of geometric imperfection may be based on the shape of critical plate buckling modes with amplitude values being 80% of the geometric fabrication tolerances given in EN 1090-2. At the same time the structural imperfection in terms of residual stresses may be represented by a stress pattern over the cross-section.

Another option to consider initial imperfections is to use equivalent geometric imperfections. In EN 1993-1-5 the shapes and amplitudes of initial geometric imperfections (see Figure 37), which were later used in imperfection sensitivity analysis, are defined with:

- Global member imperfection with length l .
- EG1 = Longitudinal stiffener imperfection with length a .
- EG2 = Local panel or subpanel imperfection with short span a or b .
- EG3 = Local stiffener or flange subjected to twist.

The amplitudes of imperfection mode EG 2 might be orientated in the same or in the opposite direction.

When more than one imperfection is taken into account, the leading imperfection of the total amplitude is chosen and the accompanying imperfections may have reduced amplitudes to 70%. Furthermore, the orientation of the applied imperfections must be such that the lowest resistance is obtained.

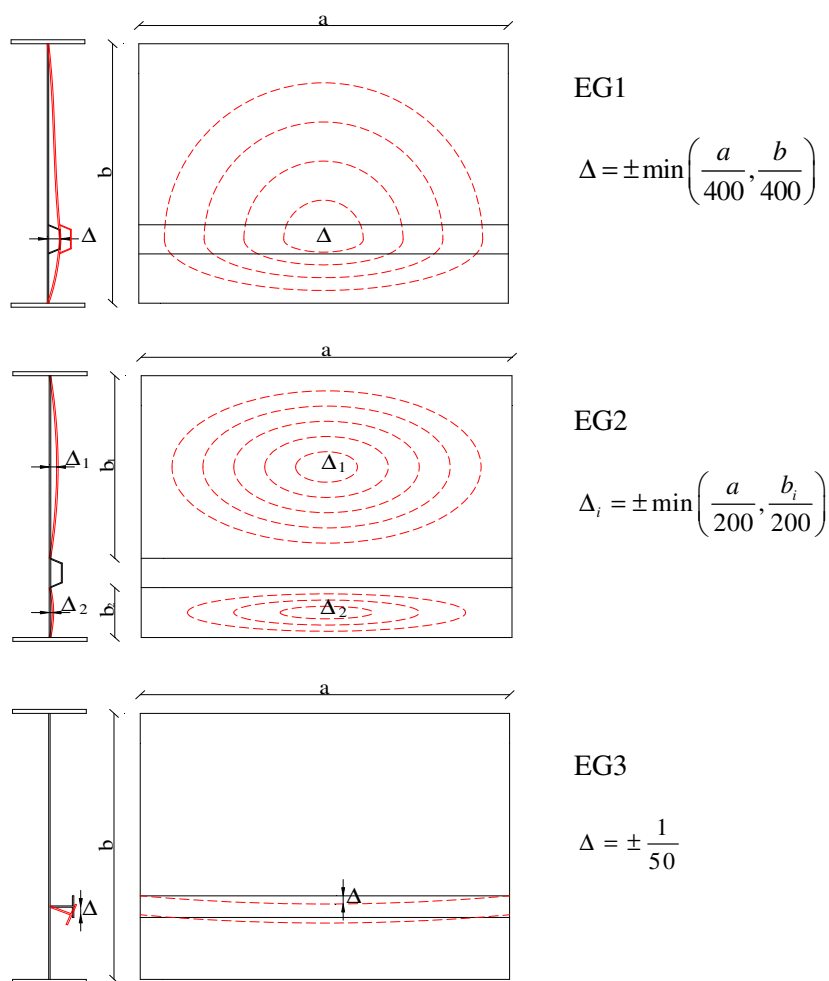


Figure 37: Modelling of equivalent geometric imperfections
 Slika 37: Modeliranje ekvivalentnih geometrijskih nepopolnosti

5.1.2 Material model

In most structural elements subjected to compressive stress local buckling will occur, either above or below the yield strength. If it comes to buckling after the yield strength has been reached throughout the whole panel, the capacity of the element above the yielding point usually increases only slightly.

In our study two material models were used. For numerical model verification true stress-strain curves according to tensile tests were adopted. They were idealized with multi-linear lines (see Figure 38), which were defined with numerical simulations of uni-axial tensile tests. In all cases the minimum strain hardening with the inclination of $E/10000$ in the area of yielding was considered.

In Figure 41 the response for girder SO modelled with two different models is shown. One material model considers strain hardening of $E/100$ after 1% of strain, while the other model is modelled as bilinear with nominal strain hardening of $E/10000$. The resistance reduction of 1.8% was found when girder was modeled with nominal strain hardening.

For parametric study an elastic-plastic material model with a nominal plateau slope was used (see Figure 39). In such material model the strain hardening is not taken into account, which influences the bending stiffness of the plate. For this reason the local buckling in the model occurs too early. Correspondingly the load and rotation capacity are also slightly smaller (see Figure 41) than would be

obtained with strain hardening model. Nominal values for structural steel S355 with elastic module $E = 210000 \text{ MPa}$ and the yield strength $f_y = 355 \text{ MPa}$ were considered. To avoid numerical problems the nominal plateau slope of $E/10000$ was assumed. Material model used in parametric study result in smaller resistance than it would with actual material hardening obtained from tension test.

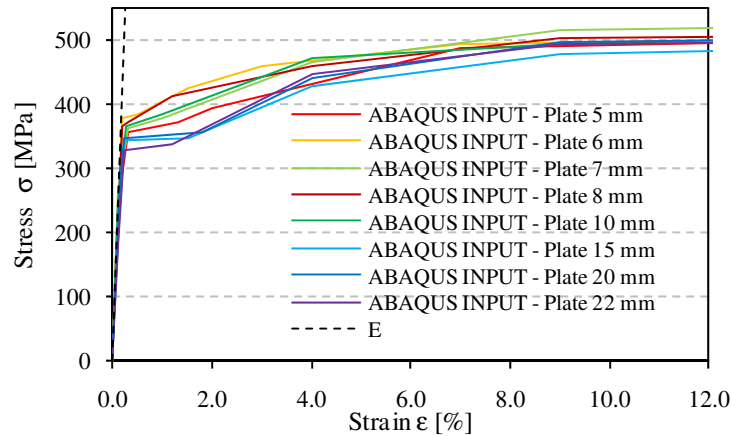


Figure 38: Modified nominal stress-strain curves of uni-axial tensile tests
Slika 38: Modificirane nominalne krivulje napetost-deformacija enosnih nateznih testov

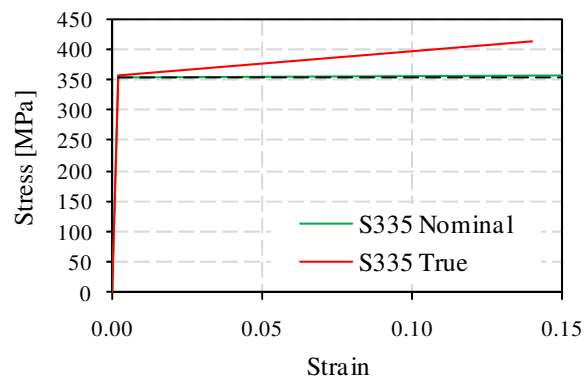


Figure 39: Modelling of the material behaviour in the parametric study
Slika 39: Materialni model uporabljen v parametrični študiji

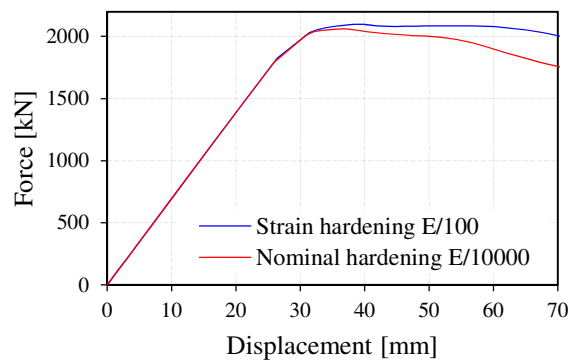


Figure 40: Modelling of the material behaviour in the parametric study
Slika 40: Materialni model uporabljen v parametrični študiji

5.2 Mesh convergence

The mesh size or mesh density of the analysed problem model also influences the numerical solution. Finer mesh is believed to produce more accurate results, but on the other hand, as the mesh density grows larger, the computation time increases. So to find the mesh density that would give satisfactory results at a reasonable computation time, a mesh convergence study was done.

The mesh convergence study was performed on a 3-point bending girder model with the following dimensions: $h_w / t_w = 1985 / 6 \text{ mm}$, $b_f / t_f = 300 / 15 \text{ mm}$. The web was stiffened with one open L stiffener positioned on $h_{w1} = 592.5 \text{ mm}$ from the compressed flange with dimensions of $b_{st} / h_{st} / t_{st} = 100 / 60 / 8 \text{ mm}$, and with series of transverse stiffeners which were designed as rigid. The distance between transverse stiffeners was $a = 2000 \text{ mm}$.

The density of the mesh depends on the size of the finite elements. Therefore, the girder was meshed with finite elements with approximate element edge size of $h_w / 80 \approx 25 \text{ mm}$, $h_w / 40 \approx 50 \text{ mm}$, $h_w / 26 \approx 75 \text{ mm}$, $h_w / 20 \approx 100 \text{ mm}$, $h_w / 13 \approx 150 \text{ mm}$ and $h_w / 10 \approx 200 \text{ mm}$. The numerical analysis, in which geometric and material nonlinearity were considered, was carried out with arc length method. The following numerical results were obtained and compared:

- The total number of finite elements used.
- The CPU time needed for the process.
- The resistance capacity of girder F_{\max} .
- The out-of-plane displacement at cross-section $x = 400 \text{ mm}$ from the most stressed edge at maximum load capacity F_{\max} and at vertical displacement $u_2 = 45 \text{ mm}$.
- The load-vertical displacement curve.

The convergence study was done on the Intel Core Duo E6850 hardware. Figure 41 represents the influence of the finite element size on the whole number of finite elements of the discretised girder and on the computation CPU time needed for the computation of the analysed case. As it can be seen, time needed to compute the response of the girder discretised with large finite elements is very short (65.1 s for element edge size of 200 mm), while on the other hand, for smaller finite elements very long computational time is needed (5763.9 s for element edge size of 25 mm). The reason for this is clearly the fact that the number of the equations which has to be solved depends on the number of degree of freedom, which is directly connected to the number of finite elements. In Figure 42 the number of increments needed to perform nonlinear analysis is plotted. The number of increments varies from 47 to 81 with maximum needed when the finest mesh is applied to girder.

As predicted, the mesh density does not influence only the CPU time, but also the girder response, the capacity of the girder and also the shape and the amplitude of buckling.

In Figure 43 the force-displacement curves for six different mesh densities are plotted. The capacity of the girder decreases with finer mesh of the girder. What might also be important for the final interpretation of the results is the post-peak behaviour of the girder. Soon after the girder shows the first signs of global plastic behaviour, an instantaneous drop in the girder resistance can be observed; the smaller the finite elements, the bigger the drop. This is found for all mesh situations except for the roughest mesh. The behaviour in plastic range influences the rotational capacity, which is the largest for the roughest mesh and decreases with finer mesh.

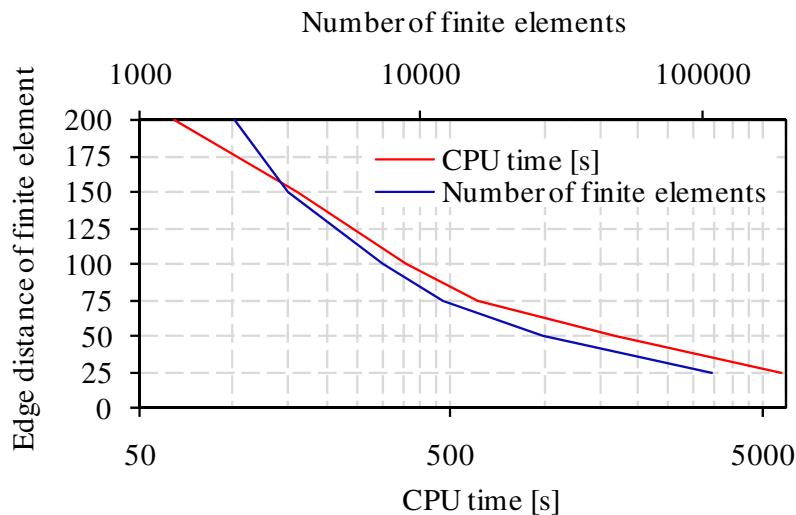


Figure 41: Number of finite elements and used CPU time vs. size of the finite element

Slika 41: Število uporabljenih končnih elementov in porabljen CPU čas v odvisnosti in velikosti končnega elementa

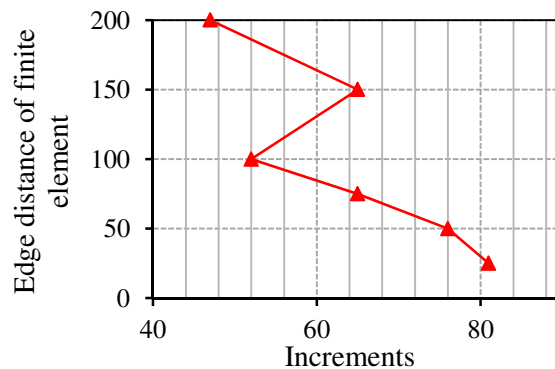


Figure 42: Number of increments vs. size of the finite element

Slika 42: Število potrebnih korakov v odvisnosti od velikosti elementa

In Figure 44 the out-of-plane displacements over the vertical cross-section, positioned at $x = 400 \text{ mm}$ from the most stressed edge for two typical situations are plotted. The first situation is where the vertical displacement ($w=45 \text{ mm}$) is in all cases the same and no difference between the load-displacement curves is present yet, and the second one where the maximum capacity of the girder is observed. The first one is much more appropriate for the comparison of the results than the second one. At this point ($w=45 \text{ mm}$) the force and vertical displacement are almost the same, while in the second case the out-of-plane displacement is compared at the maximum obtained capacity, which is for each situation reached at a different vertical displacement.

When comparing the out-of-plane displacement at the same vertical displacement ($w = 45 \text{ mm}$), the absolute maximum is obtained for the finest mesh. The opposite is found if the displacements are compared at the maximum force, where the absolute maximum is obtained for the roughest mesh. However, if out-of-plane buckling is considered, the rougher meshes prove to be stiffer than the finer ones.

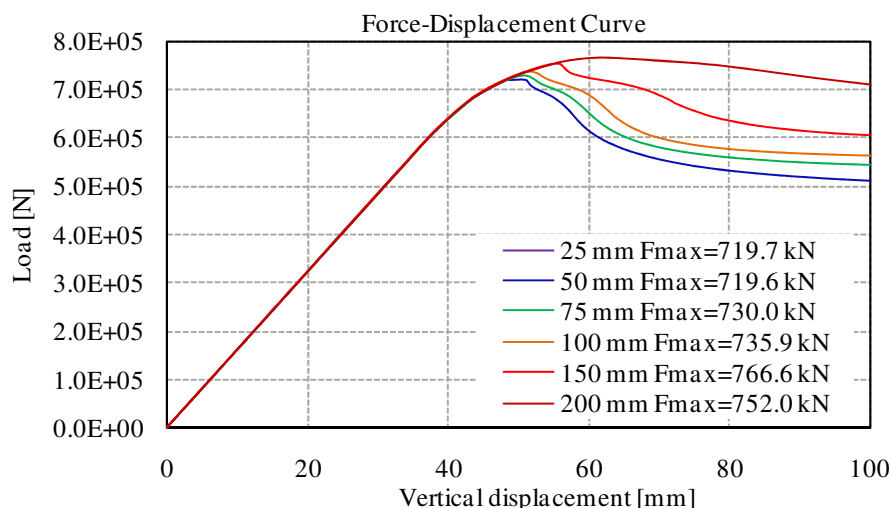


Figure 43: Force-displacement curves for different mesh densities (mesh edge distance) of girder
Slika 43: Krivulje sila-pomik za različne gostote mrež

The results are converging to the values obtained with the finest mesh, as can be seen from Figure 41, Figure 43 and Figure 44. Furthermore, these results were compared and analysed in Figure 45, where physical quantities are normalized to maximum value obtained for each group of the results. The lowest sensitivity to mesh density is found for the girder resistance, where the difference of 6% between the roughest and the finest mesh is obtained. As far as the out-of-plane (u) displacements are concerned, there is quite a big difference for various mesh densities. It can be concluded that the finest mesh results in much larger amplitude, if comparison is done at the same vertical displacement of the girder.

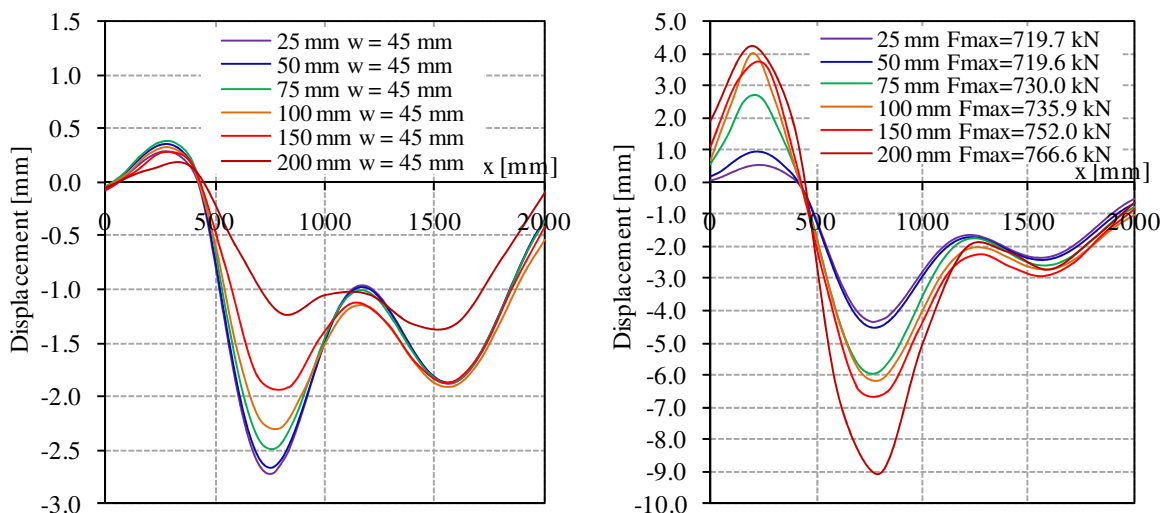


Figure 44: Out-of-plane displacement at cross-section x = 400 mm from the most stressed edge
Slika 44: Pomiki izven ravnine za 400 mm oddaljen prerez od najbolj obremenjenega roba pločevine

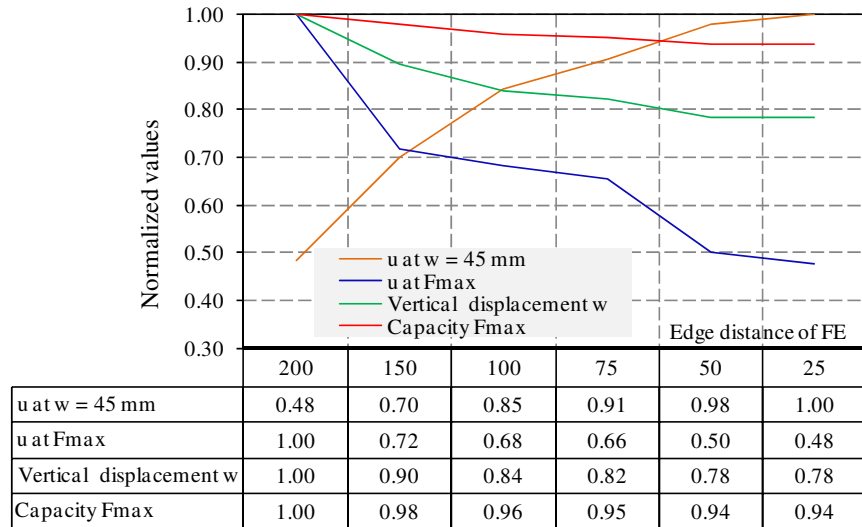


Figure 45: The influence of mesh density on displacement and capacity of girder
Slika 45: Vpliv gostote mreže na pomike in nosilnost nosilca

The mesh convergence study was performed to define the influence of mesh density on the behaviour of analysed cases. The following conclusions can be drawn:

- The highest sensitivity of mesh density is found for out-of-plane displacement and for the behaviour of the girder regarding load-displacement curve,
- The maximum capacity is less sensitive,
- Satisfactory results can be obtained, if the girder is discretised with finite elements with the average edge distance of 50 mm at most.

With reference to this study, all further simulations, verification of the numerical model and parametric study were conducted with finite elements with the edge distance of the element smaller than or equal to 50 mm.

5.3 Numerical simulations of tested girders

The numerical simulations of the tested girders were performed in accordance with the above mentioned features. The results were compared to those gathered from experimental tests. At this point the real measured dimensions of the girders are of essential importance. In Table 13 the main measured dimensions of tested girders are given.

Preglednica 13: Izmerjene dimenzije testnih nosilcev
Table 13: Actual dimensions of tested steel plate girders

| Specimen | Web | | Upper flange | | Bottom flange | | Longitudinal stiffener | | | | |
|----------|---------------|---------------|--------------|------------------|------------------|------------------|------------------------|------------------|------------------|------------------|------------------|
| | h_w [mm] | t_w [mm] | a [mm] | b_{f1} [mm] | t_{f1} [mm] | b_{f2} [mm] | t_{f2} [mm] | H_{sl} [mm] | h_{sl} [mm] | b_{sl} [mm] | t_{sl} [mm] |
| SO | 1498 | 7.18 | 1498.2 | 320.9 | 22.29 | 318.7 | 22.28 | / | / | 90 | 9.8 |
| SC | 1498 | 7.18 | 2246.3 | 320.9 | 22.29 | 318.7 | 22.28 | 160.5 | 80.9 | 80 | 5.06 |
| UO | 1798 | 5.9 | 1797.5 | 249.5 | 20.01 | 451.2 | 20.01 | / | / | 100.1 | 10.23 |
| UC | 1798 | 5.9 | 2699.1 | 249.5 | 20.01 | 451.2 | 20.01 | 296.4 | 177.0 | 81.3 | 5.06 |

For numerical verification the measured initial imperfections (see Chapter 3.2.1) were applied to the tested panels, while to all adjacent panels a global buckling shape was applied (imperfection EG1 in Chapter 5.1.1). In Chapter 5.4.2 the results considering the influence of residual stresses on the

behaviour of plated girders are presented and discussed. The girder resistance with geometric imperfections and residual stresses was reduced additionally by 0.8% compared to the girder where only geometric imperfections were considered. Because the post-critical resistance is only slightly affected by residual stresses, their influence in the numerical model verification is not taken into account.

5.3.1 Girder SO

In Figure 46 the load deflection curves from experimental test and from numerical simulation for SO girder are plotted. The difference between experimental test and FEM simulation is rather small. Some difference occurs in elastic stiffness of the whole system and in the maximum obtained resistance which differs by +2.9% compared to the experimental test. The initial elastic response of the numerical model is identical to the experimental test up to 600 kN, as from this point forward the stiffness of the numerical model is slightly bigger. The transition from elastic to plastic behaviour is much smoother in the test than in the numerical model, due to residual stresses which were not considered in numerical simulations. The resistance of the girder starts to decrease after the peak load has been reached; the decreasing is faster in real experimental test than in numerical simulation.

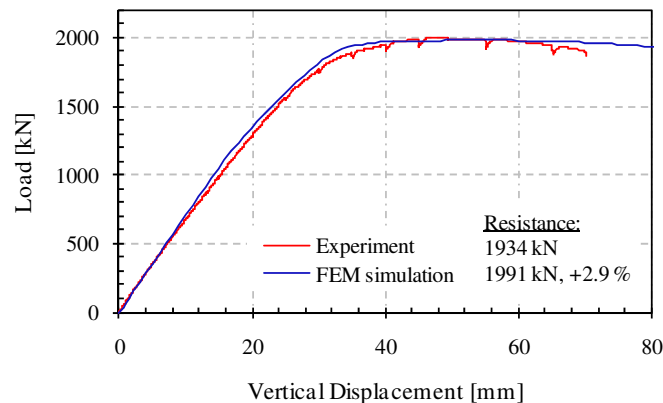


Figure 46: Comparison of load-deflection curves for panel SO
Slika 46: Primerjava krivulj sila-pomik za panel SO

The evolution of out-of-plane displacement of the web panel obtained by numerical simulation is plotted in Figure 47. Comparing these results to the experimentally measured results represented in Figure 23, the following conclusions can be given:

- In general the out-of-plane displacement is similar to the experimentally measured shape.
- The most significant difference is found in the local buckling of the upper, compressed subpanel, where the buckle is turned to the opposite direction at vertical displacement of 45.18 and 55.18 mm.
- The amplitudes of out-of-plane displacement differ up to 85% in elastic range, but the displacements are relatively small.
- In plastic range the absolute maximum amplitude calculated with numerical simulations approaches the measured experimental value.
- The local buckling of the flange in compression is turned to the opposite direction compared to the direction found in experimental test.

The numerical model sufficiently describes the behaviour of the real test. With proper consideration of significant parameters such as real material model, proper mesh density and actual initial imperfections the numerical results can get very close to the real behaviour of experimental test, as in presented situation. More noticeable difference is found only for the amplitudes of out-of-plane displacement, which differs maximally by 85%. This difference was found at very small out-of-plane displacements.

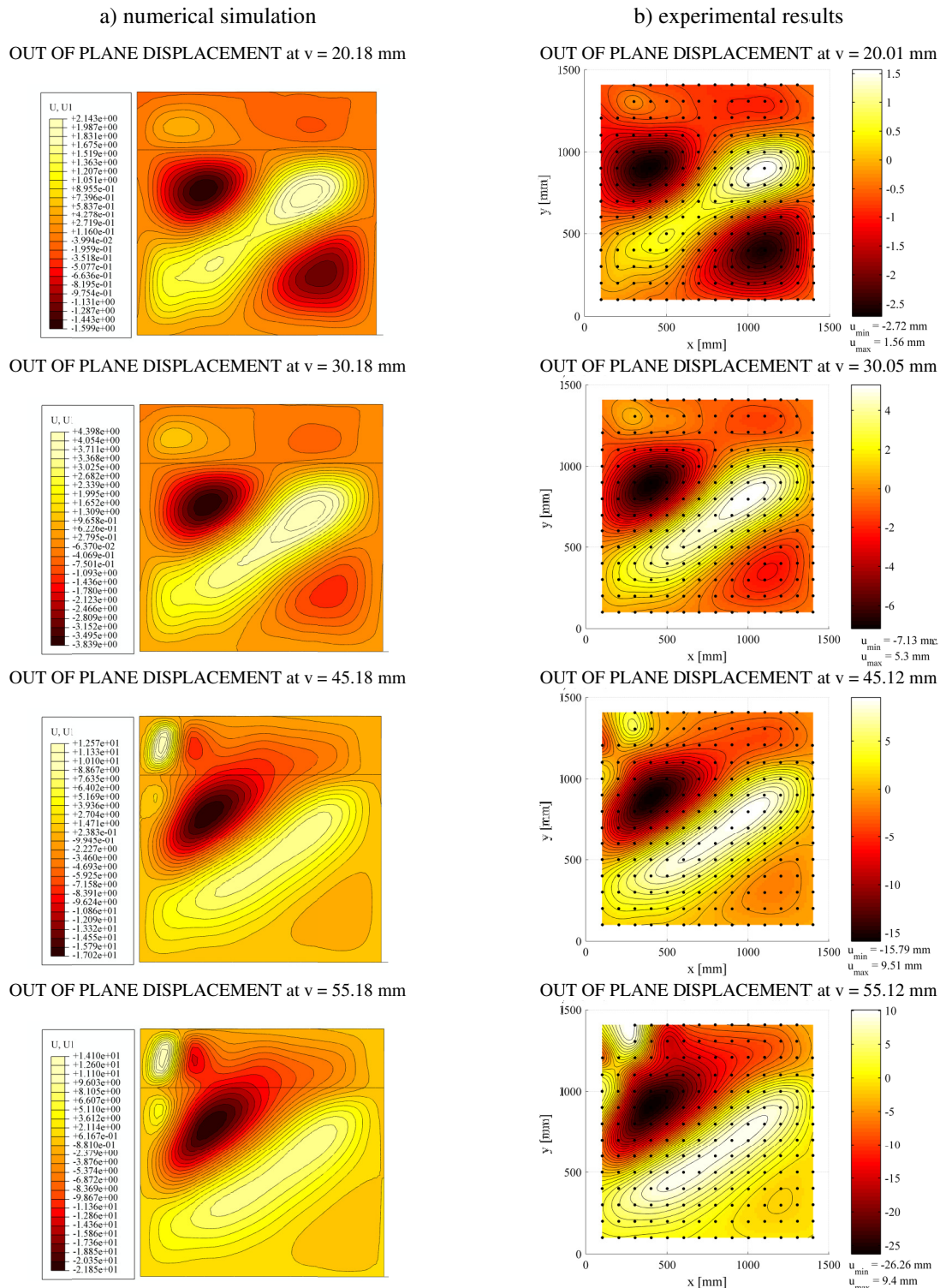


Figure 47: Evolution of the out-of-plane displacement of SO girder
 Slika 47: Razvoj pomikov izven ravnine za nosilec SO

In Figure 48 and Figure 49 the evolution of von Mises stresses for the web plate and flanges is plotted. The stresses are plotted for the middle of the plate's thickness where only membrane forces are considered. Yielding of the plate can be obtained much earlier on the top or bottom of the plate where the stress state is also influenced by in plane bending. The influence of the tension field is recognized already at vertical displacement of 20.18 mm, which can be seen from the plotted stress distribution. More evident influence of the tension field development, however, is seen at larger vertical displacement. The white colour in figures denotes equivalent von Mises stresses in the plate that are higher than yielding stress of the material. In the web plate this can be obtained at vertical displacement of 45.18 mm. The yielding appears over the cross-section height with wider area on the top and bottom of the plate. The yielding in the flanges appears already at vertical displacement of 30.18 mm.

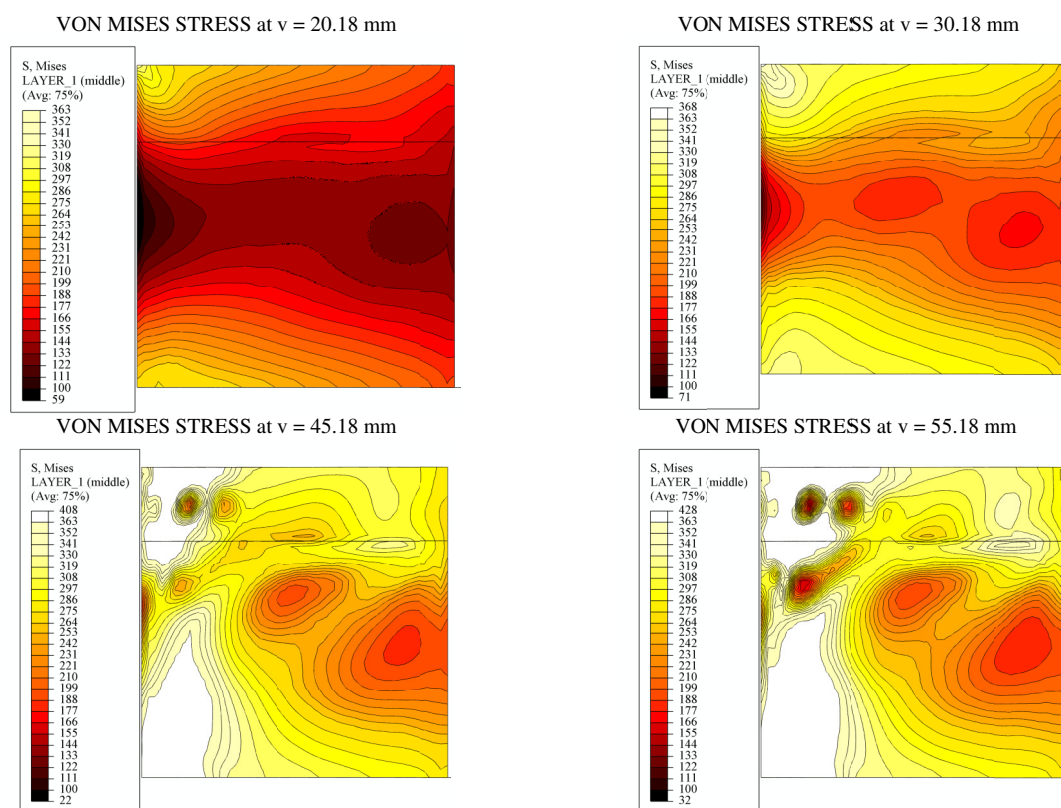


Figure 48: Evolution of von Mises stress in the centre of the web plate - numerical simulation of the SO girder
Slika 48: Razvoj Misesovih primerjalnih membranskih napetosti v stojini – numerična simulacija nosilca SO

The failure mode mechanism is a combination of buckling in compression zone due to bending and global buckling in subpanel due to shear. In Figure 50 the numerical and experimental buckling shapes are shown in axonometric view. To clearly present the formation of out-of-plane buckling the actual failure mode is 10 times enlarged in the direction perpendicular to web plate.

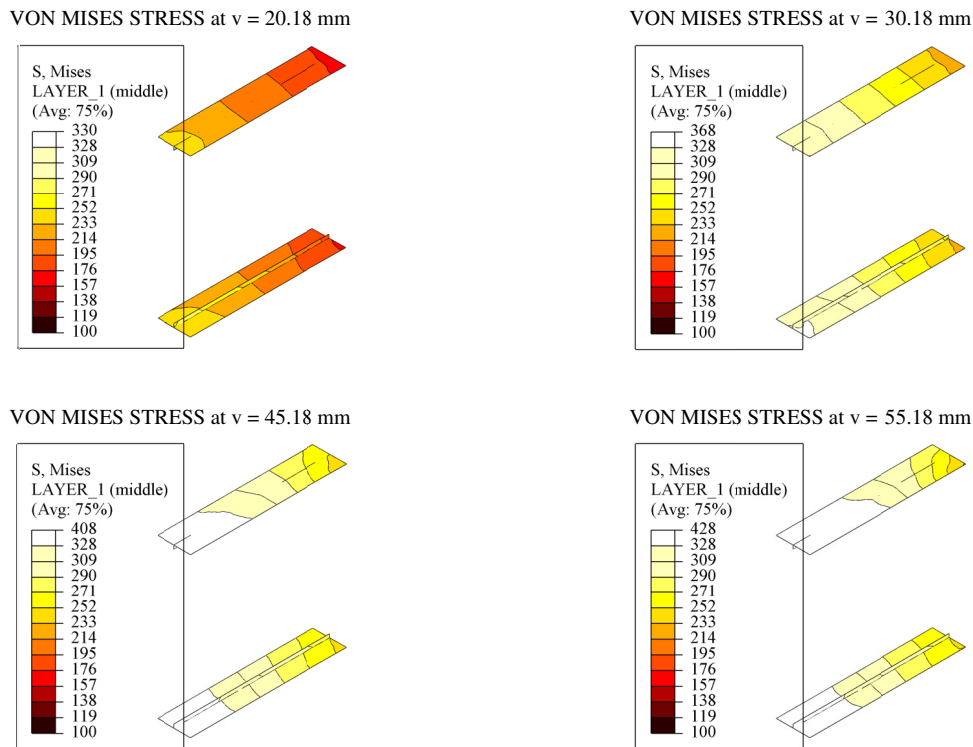


Figure 49: Evolution of von Mises stress in the upper and bottom flange - numerical simulation of the SO girder
Slika 49: Razvoj Misesovih primerjalnih napetosti v zgornji in spodnji pasnici – numerična simulacija nosilca SO

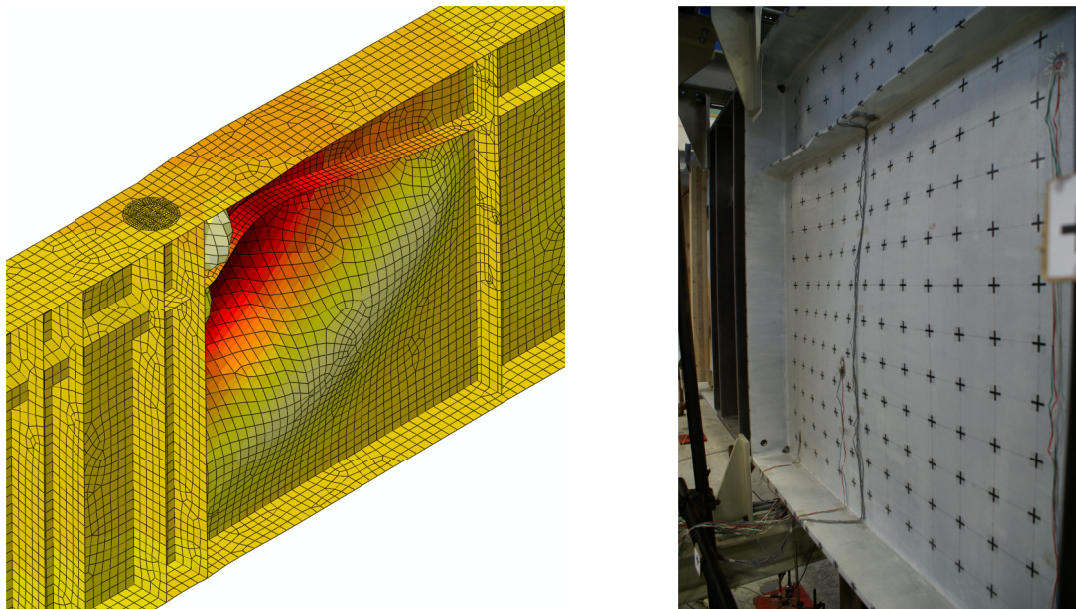


Figure 50: Deformed shape of tested panel SO
Slika 50: Deformirana oblika panela SO

5.3.2 Girder SC

Comparison of load-deflection curves of girder SC is shown in Figure 51. The numerical calculation shows very similar behaviour up to the maximum load obtained by the test (up to 65 mm). After this point the capacity of the tested girder starts to decrease, while the capacity calculated by numerical simulation still increases with the maximum capacity obtained at much larger displacement than that

of the experimental test. Nevertheless, the difference in capacities gained with numerical simulation and test is only 4.10%.

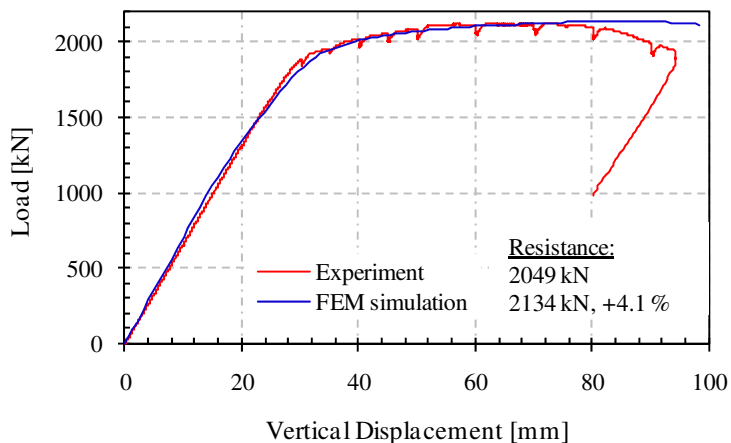


Figure 51: Comparison of load-deflection curves for girder SC

Slika 51: Primerjava krivulj sila-pomik za girder SC

The development of the out-of-plane displacement in the web panel, calculated with numerical simulation, is plotted in Figure 52. The evolution of out-of-plane displacement is similar to the measured experimental results (see Figure 24). The main difference is in elastic range, where the corresponding shape of out-of-plane displacement is found at larger vertical displacement (at higher load) than in the experiment. In plastic range the shape of the displacement is similar; larger differences occur in amplitudes at the beginning of plastic behaviour, but when approaching vertical displacement $v = 70.18$, the maximum amplitude obtained by numerical simulation (-33.96 mm) is only slightly smaller than the experimentally measured value (-35.67 mm).

Similarly, the equivalent von Mises stress distributions at the mid-thickness of the web plate for plated girder SC are shown in Figure 53 for the web plate and in Figure 52 for both flanges. In the elastic state no redistribution of stresses in the panel is obtained, but deeply in the plastic range different physical phenomena influence the stress distribution in the plates, of which the most important are the tension field action and the buckling of longitudinal stiffener. The largest stresses in the web are obtained close to the right edge and the largest stresses in the stiffener in the area of the largest out-of-plane displacements of the stiffener. Here the influence of the second order effects is significant.

In Figure 55 the failure shape of the tested girder and numerical simulation is shown. Also in this case the out-of-plane deformation is 10 times enlarged to have better picture of the buckling of the whole panel. The failure is a combination of global buckling of the whole panel due to the combination of both actions, bending moment and shear load, and local buckling of the plate at the most stressed edge due to bending moment.

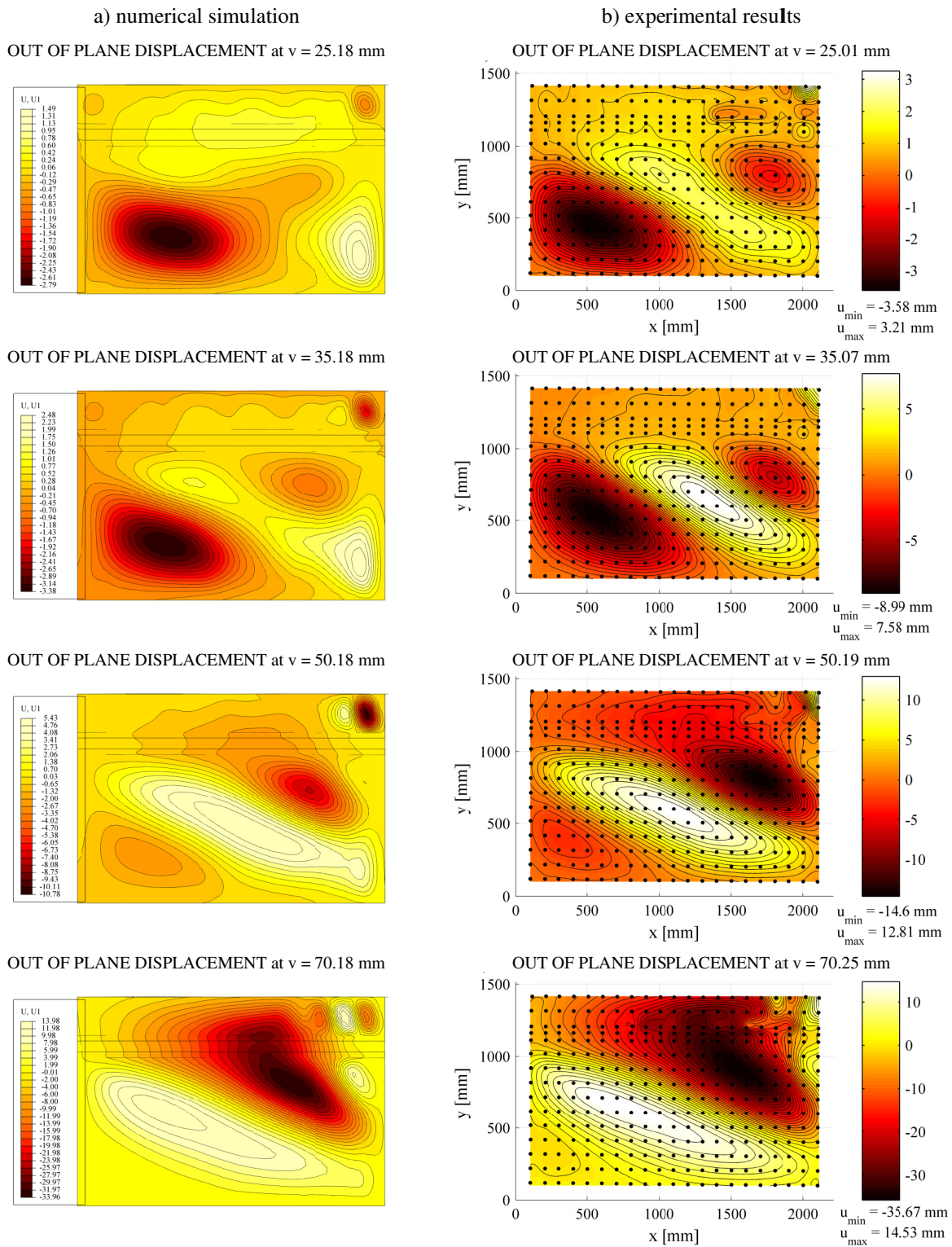


Figure 52: Evolution of the out-of-plane displacement of the SC girder
Slika 52: Razvoj pomikov izven ravnine za nosilec SC

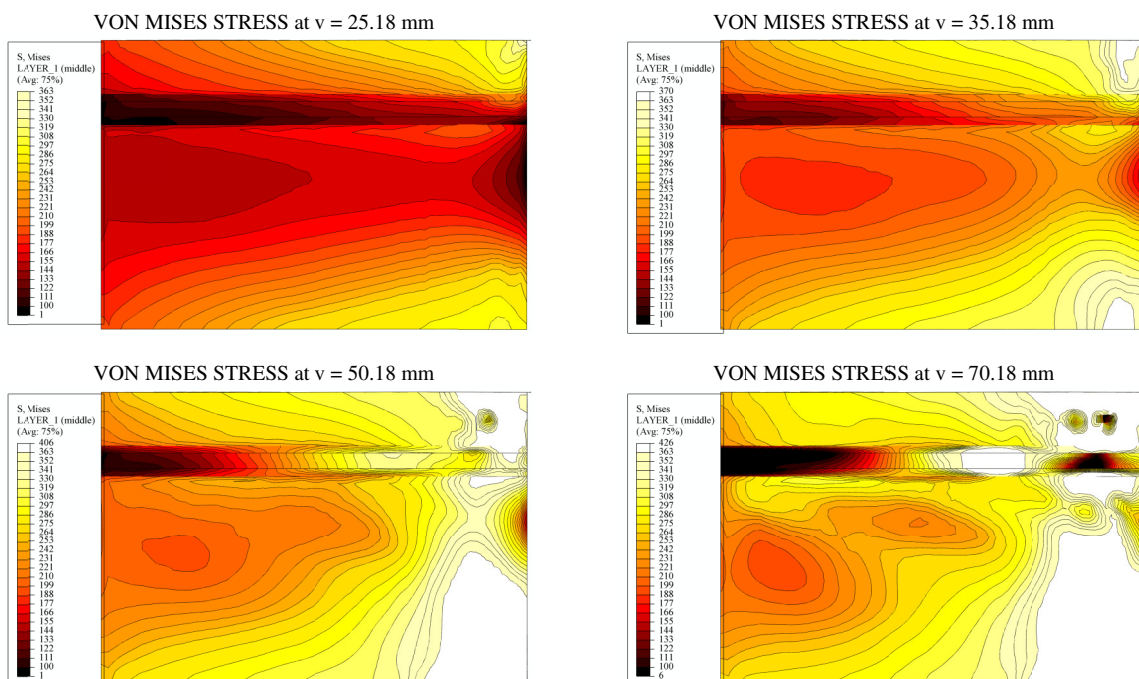


Figure 53: Evolution of von Mises stress in the centre of the web plate - numerical simulation of the SC girder
Slika 53: Razvoj Misesovih primerjalnih membranskih napetosti v stojini – numerična simulacija nosilca SC

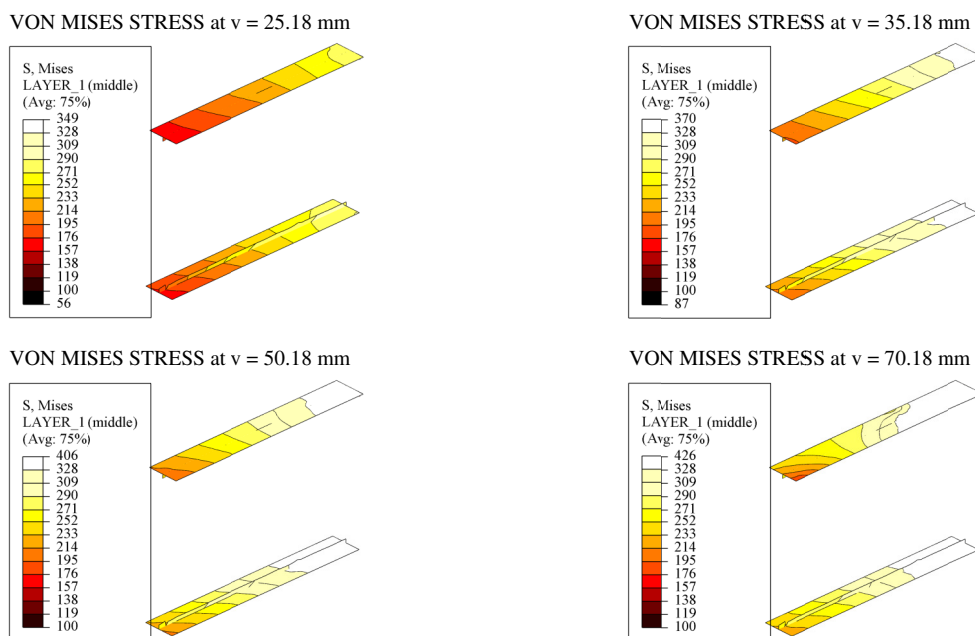


Figure 54: Evolution of von Mises stress in the upper and bottom flange - numerical simulation of the SC girder
Slika 54: Razvoj Misesovih primerjalnih napetosti v zgornji in spodnji pasnici – numerična simulacija nosilca SC

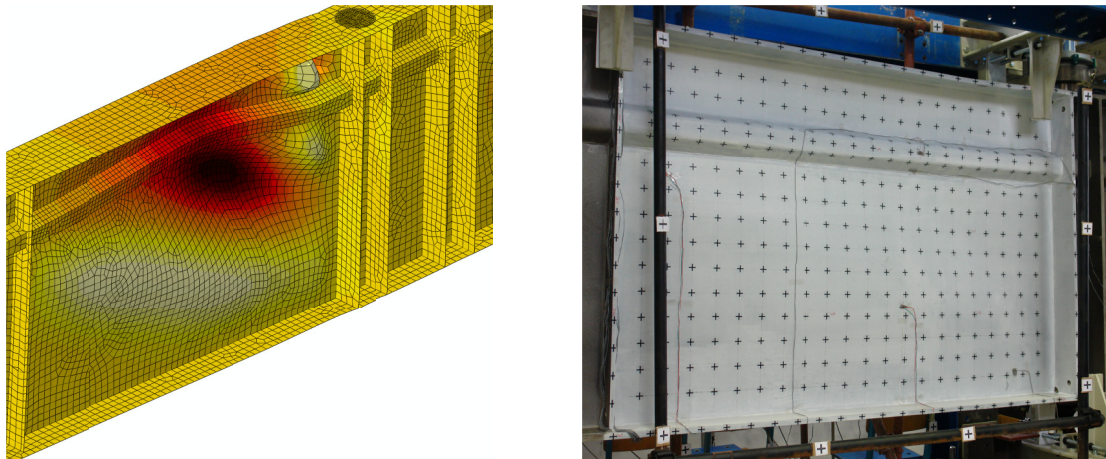


Figure 55: Deformed shape of tested panel SC
Slika 55: Deformirana oblika panela SC

5.3.3 Girder UO

The largest difference in overall behaviour obtained through numerical simulation and experimental test is found for girder UO. There is a very small difference in resistance, as only 0.6% higher resistance was obtained by numerical simulation. The response curves for the experimental tests and numerical simulation curves are plotted in Figure 56. The difference in response is obtained already in elastic range, where the numerical girder exhibits slightly higher stiffness than the tested one. Further on, the peak force is obtained much earlier than in the test. In the post-peak region the force decreases very slowly up to the vertical displacement of 60 mm. After this point the load decrease is more evident.

The evolution of out-of-plane displacements in the web panel is shown in Figure 57 and as in both previous cases their shape is similar to experimental results with one very important difference: the amplitudes are greater in the case of numerical simulation. The amplitudes of out-of-plane displacement influence the girder resistance in a way that maximum resistance is reached at much smaller vertical displacement.

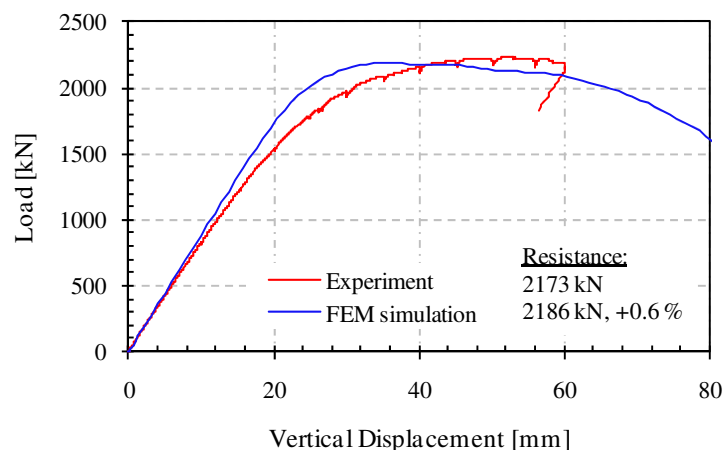
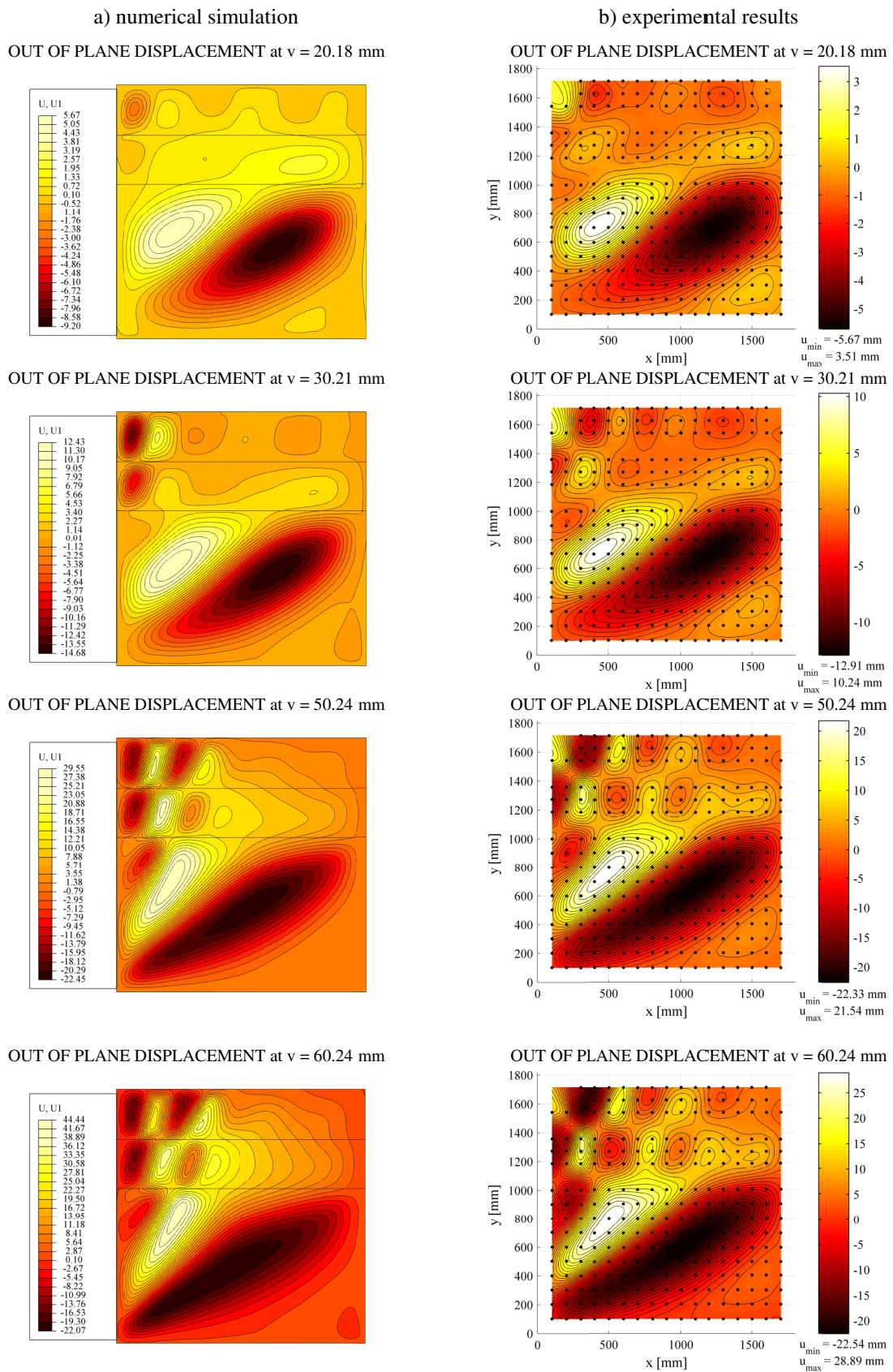


Figure 56: Comparison of load-deflection curves for girder UO
Slika 56: Primerjava krivulj sila-pomik za girder UO

Another also important difference is the out-of-plane buckling orientation in the smaller subpanels, where in numerical calculations the wave orientation alternates only in horizontal direction, while vertically the orientation of the waves at adjacent subpanels is the same.



The von Mises stress distribution over the web, flanges and stiffeners is plotted in Figure 58 and

Figure 59. In the first Figure the formation of the tension field can clearly be seen in the lower, largest subpanel. In the next Figure, at vertical displacement of 30.21 mm, the tension field is formed from the bottom left corner to the upper right corner of the subpanel. Further on, the increase of vertical load leads to local buckling and yielding of the web in the subpanels and local buckling of the longitudinal stiffeners.

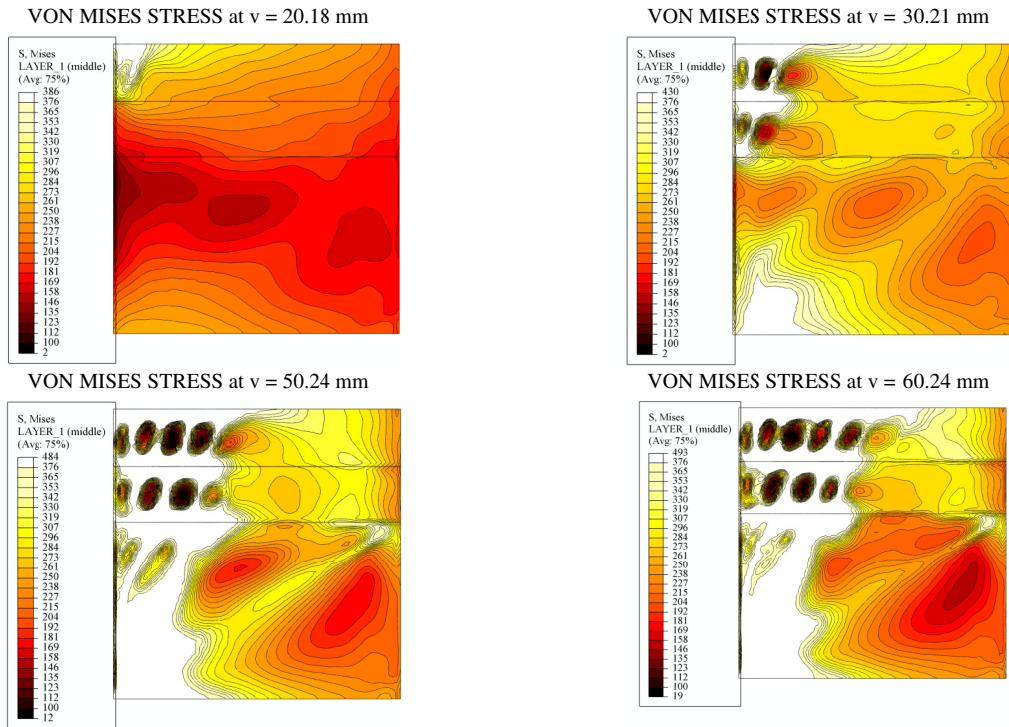


Figure 58: Evolution of von Mises stress in the centre of the web plate - numerical simulation of the UO test
Slika 58: Razvoj Misesovih primerjalnih membranskih napetosti v stojini – numerična simulacija nosilca UO

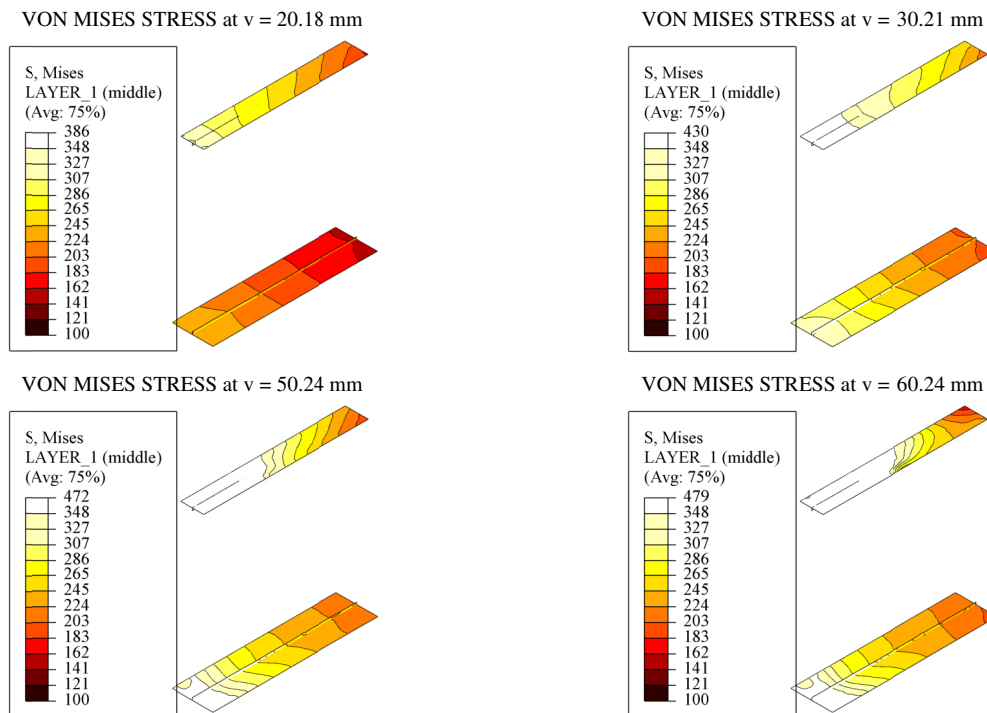


Figure 59: Evolution of von Mises stress in the upper and bottom flange - numerical simulation of the UO girder
Slika 59: Razvoj Misesovih primerjalnih napetosti v zgornji in spodnji pasnici – numerična simulacija nosilca UO

The failure mode of both, numerical simulation and experimental test is plotted in Figure 60.

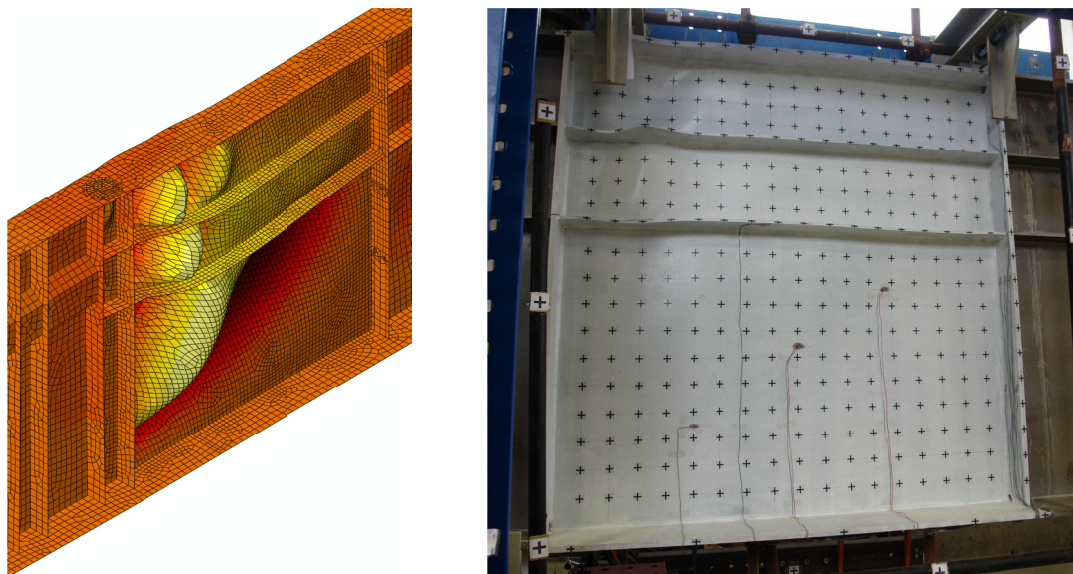


Figure 60: Deformed shape of tested panel UO
Slika 60: Deformirana oblika panela UO

5.3.4 Girder UC

The last comparison in this series is performed on un-symmetric girder UC, stiffened with one closed stiffener in compression zone. The load-deflection curve computed through nonlinear numerical analysis is compared against the test in Figure 61. The difference between numerical and test curve is very small. The first difference is in elastic stiffness of the whole system, where as in previous case the numerical stiffness is slightly higher. The numerical capacity is higher only by 1.8%. In both cases the maximum capacity is achieved just before sudden buckling of longitudinal stiffener appears. In numerical simulation this buckling happens at lower vertical displacement than in experimental test. However, due to larger stiffness of the whole system the load deflection curve is slightly shifted to the left.

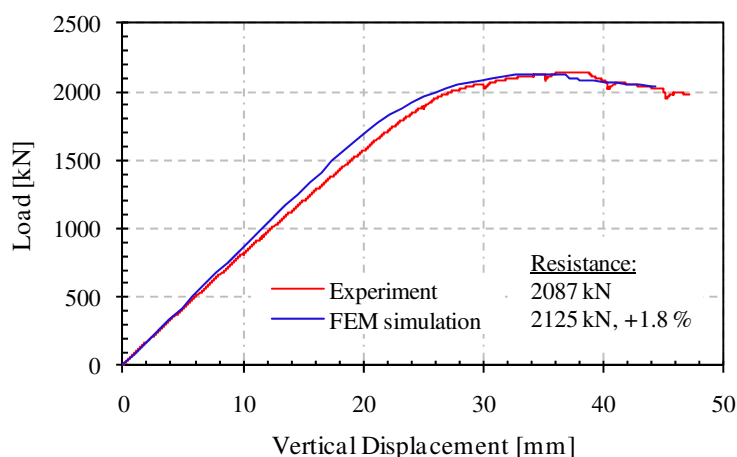
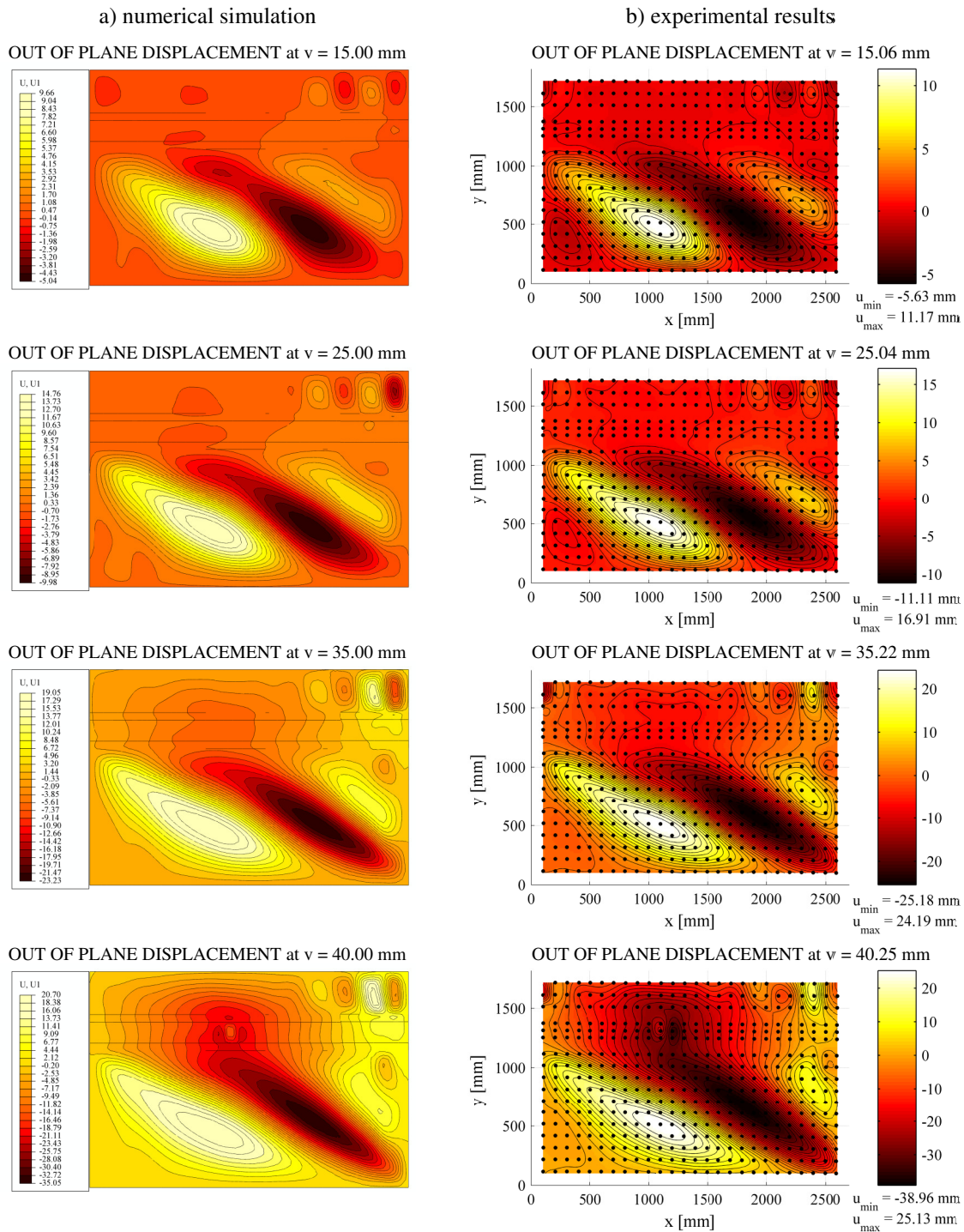


Figure 61: Comparison of load-deflection curves for girder UC
Slika 61: Primerjava krivulj sila-pomik za girder UC

As for all other girders the evolution of out-of-plane displacements is plotted in Figure 62. Two displacement fields are plotted for elastic and the other two for the plastic part of the girder's response. The numerically obtained out-of-plane displacement field is similar to the measurements in the test. In

this case also the buckling in the subpanel is alike the one in the test. The difference in the maximum amplitude of the displacement found for the worst situation is less than 21%, where the numerically obtained amplitude was 20.70 mm and the measured one in the test 25.13 mm. In general, out-of-plane displacements measured in the experimental test are larger than those calculated numerically.



Slika 62: Razvoj pomikov izven ravnine za nosilec UC

The formation of the tension field can evidently be defined through out-of-plane displacement field and can even more clearly be seen through the stress field. In Figure 63 the von Mises stresses in the observed panel are plotted for four load stages. At a vertical displacement of 15.00 mm the maximum

stresses are found at the most stressed edge in the upper, smaller subpanel (high bending moment). At this load stage the formation of tension field in the bottom subpanel is already clearly seen. The stress distribution is similar also at the next load stage (still elastic response), whereas in the next two the distribution is slightly different. After the maximum load has been reached, the highest stress can be obtained due to compression stresses from bending moment and tension field formation in the bottom subpanel and finally due to buckling, i.e. second order effect, in the middle of the longitudinal stiffener. The stress distribution in both flanges is shown in Figure 64. The stresses in the upper, compressed flange are unsymmetrical due to buckling of the flange along the whole panel.

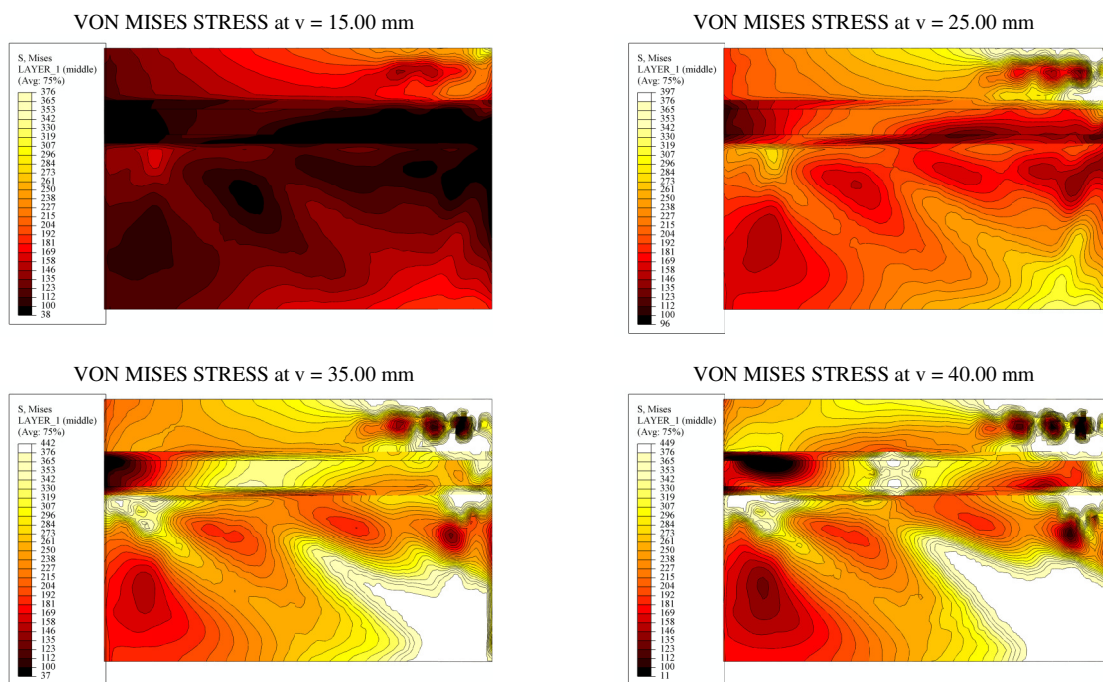


Figure 63: Evolution of von Mises stress in the centre of the plate - numerical simulation of the UC test
Slika 63: Razvoj Misesovih primerjalnih membranskih napetosti v stojini – numerična simulacija nosilca UC

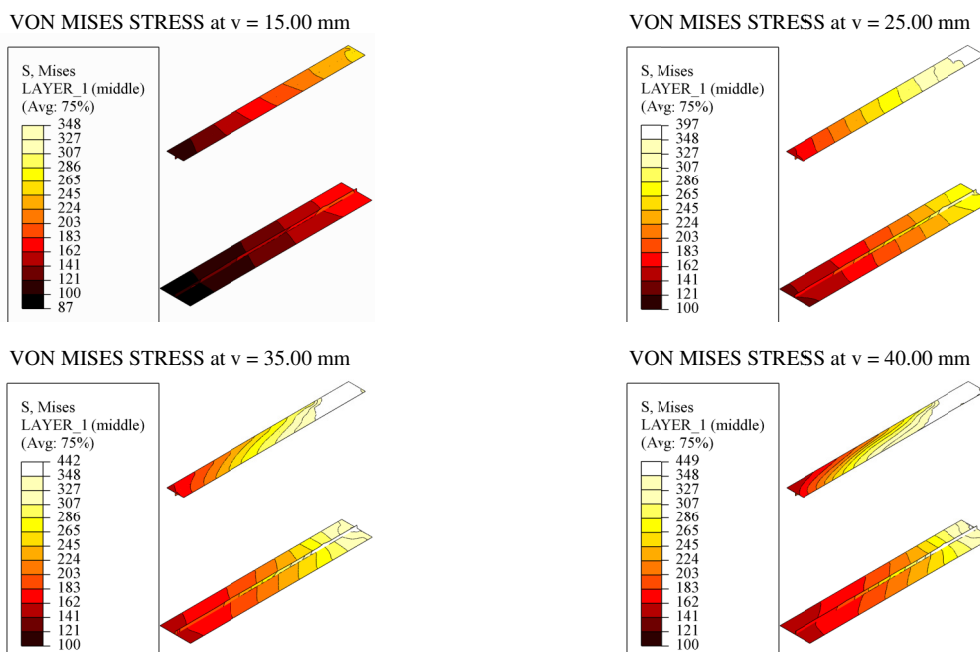


Figure 64: Evolution of von Mises stress in the upper and bottom flange - numerical simulation of the UC girder
Slika 64: Razvoj Misesovih primerjalnih napetosti v zgornji in spodnji pasnici – numerična simulacija nosilca UC

Three-dimensional presentation of the deformed shapes of the numerical model and experimental test of tested panel UC at the maximum load are plotted in Figure 65.

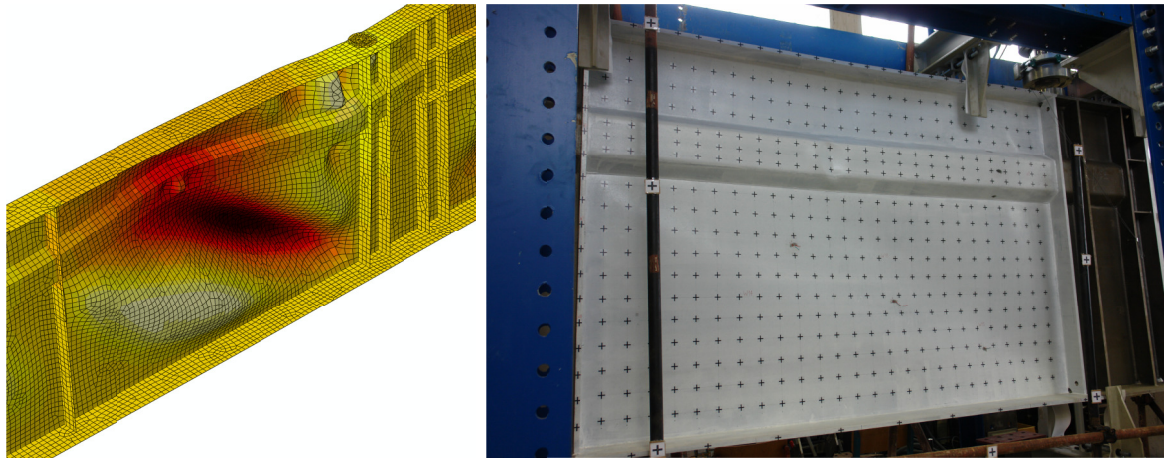


Figure 65: Deformed shape of tested panel UC
Slika 65: Deformirana oblika panela UC

5.3.5 Discussion

Very good agreement between experimental results and numerical simulation was found in the work described in previous chapters. The deviations of girder capacities were from 0.6 up to 4.1%. In all studied cases the numerical model gave slightly higher stiffness as well as capacity. The biggest difference between the numerical and the experimental results was in out-of-plane displacements, which were in the mesh convergence study also detected as the most sensitive parameter.

5.4 Imperfection sensitivity analysis

As noted in one of the previous chapters the initial imperfections have to be properly included in the numerical model, especially when dealing with stability problems. The shape of initial imperfection for particular structure or structural element is usually not known a priori. In such situation the most unfavourable imperfection, which results in the smallest resistance, should be applied to material and geometric nonlinear simulations.

A set of initial imperfections with different amplitudes was applied on the tested girders to find the sensitivity of girder resistance to initial imperfection. These imperfections were defined as positive buckling modes, as shapes according to EN 1993-1-5 and as deformed shapes defined on a preliminary nonlinear calculation of a perfect girder. For each imperfection shape the following amplitudes were taken into account: $h_w / 300$, $h_w / 200$ and $h_w / 100$.

The imperfection shapes that are defined as buckling modes or as deformed shapes may have their maximum amplitude at a different location as those prescribed in EN 1993-1-5. The amplitude of these shapes cannot be compared, therefore the overall comparison of different imperfection shapes was performed with amplitudes defined as:

- The maximum imperfection value in any investigated point was defined according to EN 1993-1-5 rules, taking into account also combinations of imperfections.
- The investigated irregular initial shape was then defined in such way that in none of the point imperfection values exceeded the maximum ones determined as described in previous point.

5.4.1 Influence of imperfection shapes and amplitudes

Eight different imperfections with three different amplitudes in positive and negative direction on each tested girder were applied, so the numerical models covered the following imperfections:

- First three positive buckling modes BM: BM1, BM2, BM3 (see Figure 66).
- Deformed shapes DS: DS1 and DS2 (see Figure 66).
- Measured imperfection MI (see Chapter 3.2.1).
- Equivalent imperfection shapes EG: EG1 and EG2 (see Figure 37).

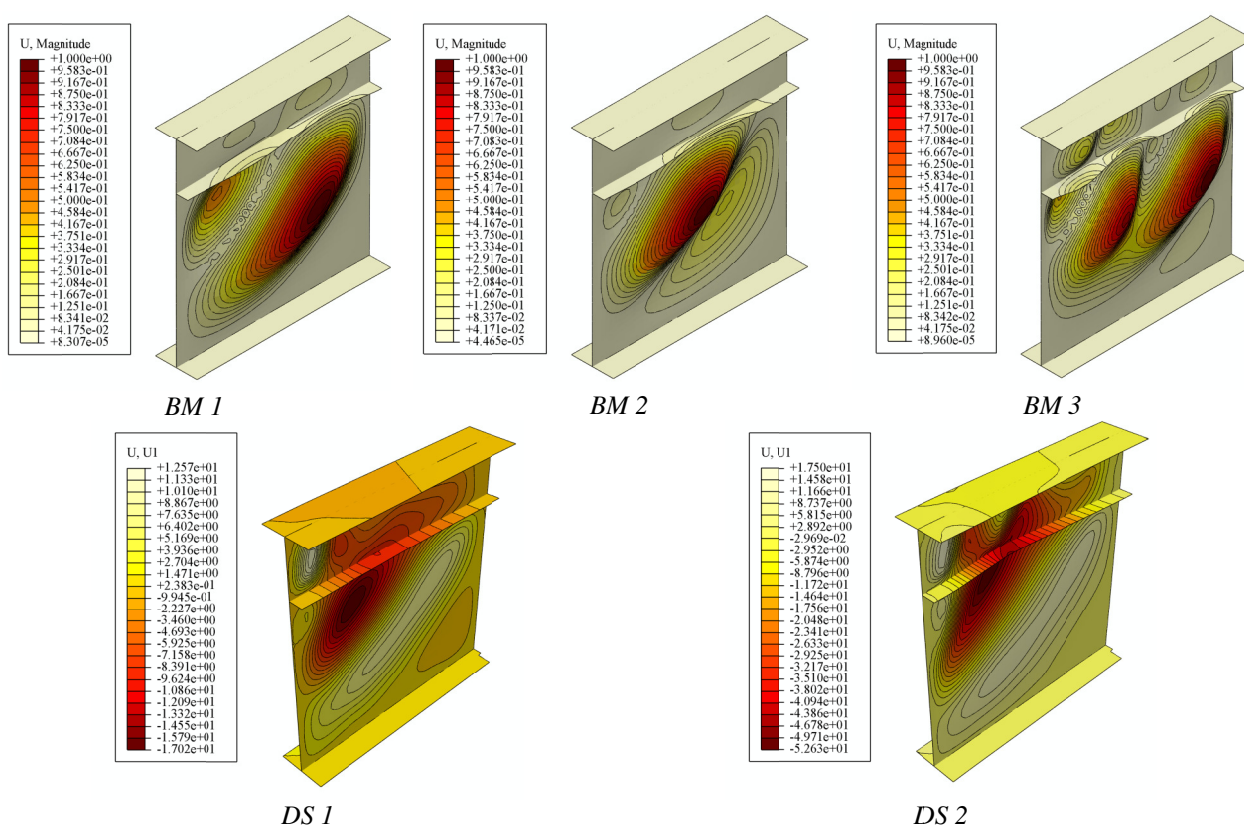


Figure 66: Imperfection shapes defined as buckling modes BM1-BM3 and as deformed shapes DS1, DS2 of SO girder

Slika 66: Oblike začetnih nepopolnosti definirane kot izbočne oblike BM1-BM3 in kot deformacijske oblike DS1 in DS2 nosilca SO

In Figure 67 the positions of deformed shapes are plotted. They were defined in two characteristic points on the load-deflection curves obtained with nonlinear calculation of the girders on which no imperfections were applied. The filled circle markers denote the first deformed shapes DS1, which were defined at the beginning of the global plastic response. The second deformed shapes considered as initial imperfections were defined at far end of plastic plateau and are marked as filled triangles on the load-deflection curves.

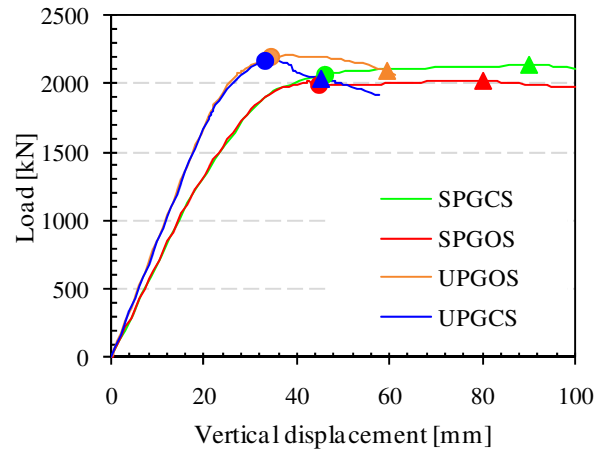


Figure 67: Points on load-deflection curves where deformed shapes were obtained (circle - DS1, triangle - DS2)
Slika 67: Točke na krivuljah sila.pomik, kjer so bile definirane deformirane oblike (krog - DS1, trikotnik - DS2)

The influence of imperfection shapes and amplitudes on girder resistance is plotted in Figure 68. The results are plotted depending on the applied imperfection amplitude (abscissa) as follows; on primary ordinate the obtained capacity of the girder and on secondary ordinate the quotient of the imperfect girder capacity and capacity of the girder without imperfections are plotted. In most cases the applied imperfections decrease the girder resistance and as expected the girder resistance also decreases by increasing the imperfection amplitude. However, some of the initial imperfections increase the resistance.

Deformed shapes DS2, defined at very large plastic deformation (see Figure 67), turn out as the worst initial imperfection for all four girders and their influence is even greater at large amplitudes of initial imperfections. All other initial imperfections prove to have quite lower influence on the girder capacity.

If the actual expected amplitudes of the initial imperfection, which are between $h_w / 200$ and $h_w / 300$, are taken into account, the following conclusions can be made:

- For girder SO the following reductions of the capacity are obtained: 1.86% for the most critical buckling mode BM, 1.41% for the most critical equivalent imperfection EG, 1.58% for measured imperfection MI and 2.96% for the more critical deformed shape DS.
- For girder SC the following reductions are obtained: 1.45% for the most critical buckling mode BM, 1.56% for the most critical equivalent imperfection EG, 1.52% for measured imperfection MI and 3.59% for the more critical deformed shape DS.
- For girder UO the following reductions are obtained: 1.95% for the most critical buckling mode BM, 1.53% for the most critical equivalent imperfection EG, 1.58% for measured imperfection MI and 4.26% for the more critical deformed shape DS.
- For girder UC the following reductions are obtained: 1.37% for the most critical buckling mode BM, 2.37% for the most critical equivalent imperfection EG, 1.02% for measured imperfection MI and 6.54% for the more critical deformed shape DS.
- Unsymmetric girders show higher reductions for most of the applied imperfection shapes, if compared to symmetric girder.

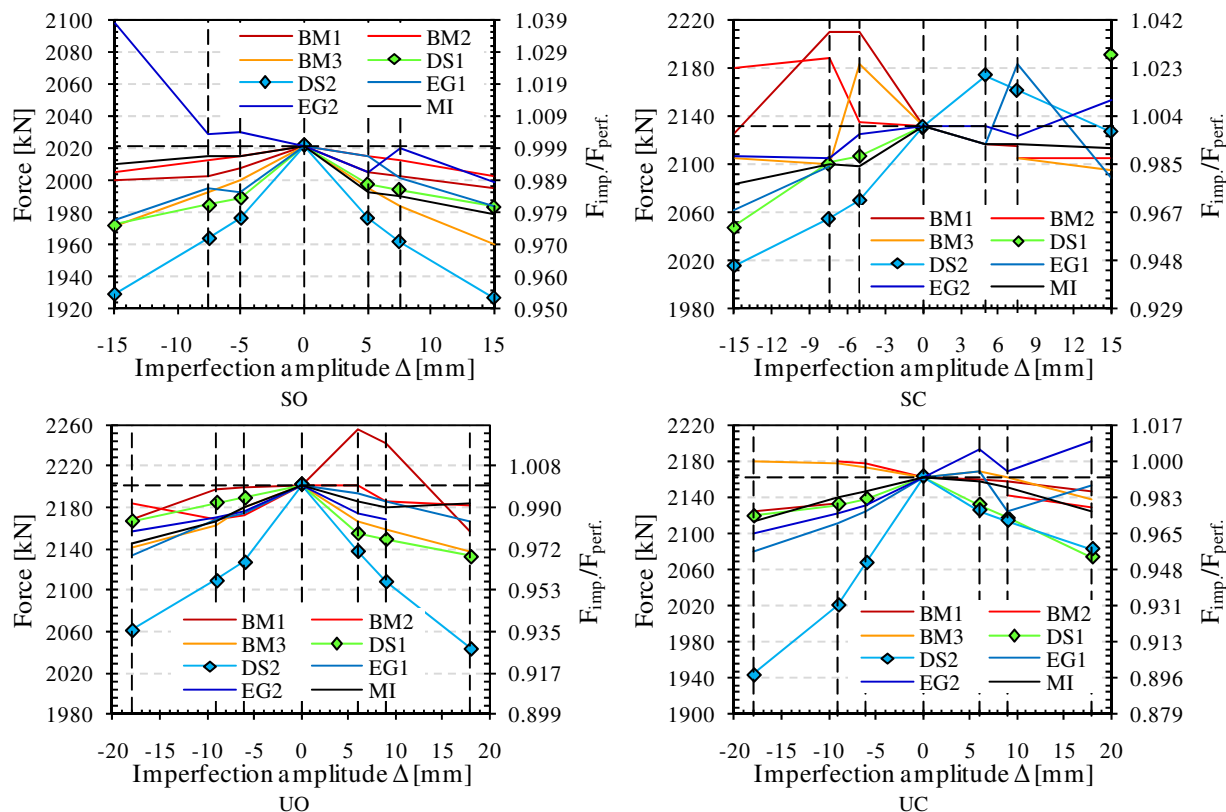


Figure 68: Influence of imperfection shape and amplitude on the girder resistance

Slika 68: Vpliv oblike nepopolnosti in velikosti amplitude na nosilnost nosilca

Finally, comparable equivalent geometric imperfections with realistic amplitudes were applied. The amplitudes were defined according to rules in Annex C of EN 1993-1-5, where in particular point the maximum amplitude of any irregular shape was limited with the maximum amplitude defined as a combination of regular imperfections in this point. Two different combinations of initial imperfections according to EN 1993-1-5 were applied:

$$EC1 = EG1 + 0.7 \cdot EG2 + 0.7 \cdot EG3, \quad (22)$$

$$EC2 = -EG1 - 0.7 \cdot EG2 - 0.7 \cdot EG3, \quad (23)$$

where EG1, EG2 and EG3 are imperfection shapes and their amplitudes given in Figure 37. In Figure 69 the capacity of imperfect girders is compared to the resistance of a perfect girder for all applied imperfection shapes. For all four girders the highest reduction of the girder resistance is obtained when initial imperfection is defined as deformed shape DS2, where the reduction of 2.8 to 4.4% for all four girders is obtained. The second most unfavourable imperfection shape is shape EC2, where the reduction of 1.1 to 1.9% is obtained. As already mentioned, some of the imperfections increase the girder resistance; higher resistance is obtained in some cases of imperfection shapes EC1, BM1, BM3 and MI. The influence of real measured imperfections results in lower resistance for tests SO, UO and UC, while for SC test the resistance is higher.

The increase in girder resistance is usually obtained in cases where the initial imperfection amplitude decreases the influence of eccentricity of the longitudinal stiffeners.

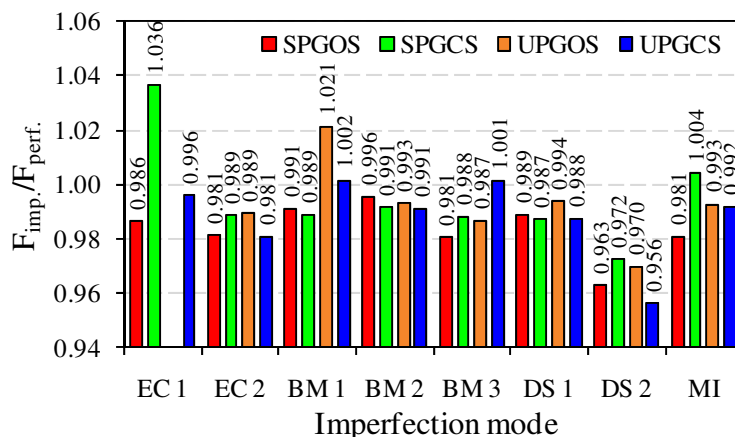


Figure 69: Reduction of girders resistance for different imperfection shapes applied
 Slika 69: Redukcija nosilnosti nosilca pri različnih začetnih nepopolnostih

5.4.2 Residual stresses

The influence of residual stresses on the girder resistance was investigated before the experimental tests were executed. This study was performed to answer, what the actual influence of residual stresses on girders behaviour and capacity is. Since the real distribution of residual stresses in the girders was not known in advance, simplification according to Figure 70 was proposed and used in numerical models. This simplification is that in the vicinity of the web - flange welds the web is in tension up to the yielding, while the other part of the web, which includes the welded area in the vicinity of the longitudinal stiffener, is in compression.

To investigate the effect of different levels of applied residual stresses, the level of compression was varied from $0.05 \cdot f_y$ to $0.20 \cdot f_y$ (see Table 14). The area of the tension zone x_f , x_w , depends on the level of assumed compression stresses k_f , k_w , and is given in equations in Figure 69. Residual stresses were taken into account together with the combination of initial geometric imperfections defined according to EN 1993-1-5 with amplitudes defined as 80% of the tolerances given in EN 1090-2.

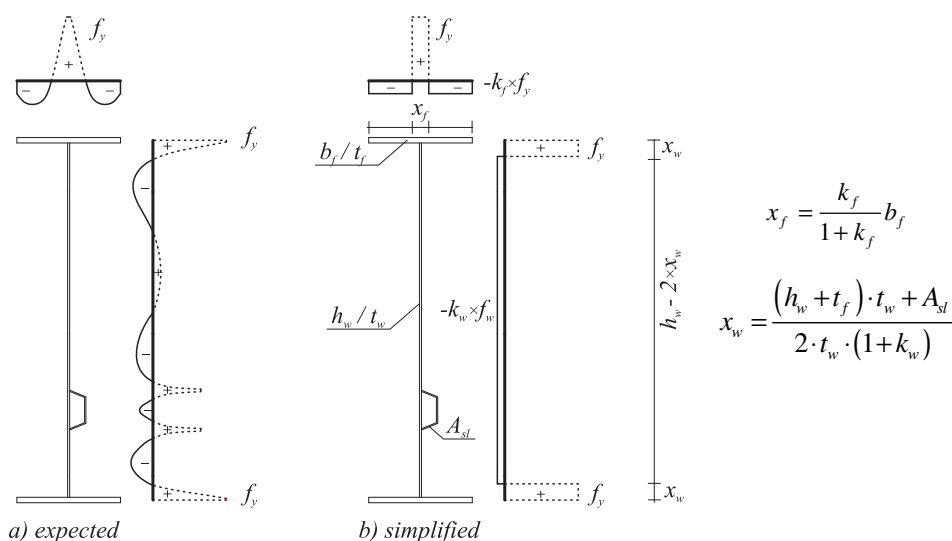


Figure 70: Residual stress distribution in GMNIA analysis
 Slika 70: Razporeditev zaostalih napetosti v GMNIA analizi

Table 14: Considered levels of residual stresses in the stiffened girder

| MODEL | k_w | k_f | MODEL | k_w | k_f |
|-------|-------|-------|-------|-------|-------|
| RW005 | 0.05 | | RF005 | | 0.05 |
| RW010 | 0.10 | | RF010 | | 0.10 |
| RW015 | 0.15 | 0.20 | RF015 | 0.05 | 0.15 |
| RW020 | 0.20 | | RF020 | | 0.20 |

In Figure 71 the load deflection curves for different levels of applied residual stresses in the girder are plotted. To get the influence of residual stresses the curves are plotted in the area of maximum capacity. In the left diagram the varied parameter is the level of the compression stresses in the web, while in the right one the level of compression stresses in the flange is varied. The black curves represent the response of the girder without any initial imperfections and the red ones the response of the girder with equivalent initial imperfections. Other curves represent the response of girder with different levels of compression stresses in combination with initial geometric imperfection. It can be seen that the main reduction in girder resistance was obtained for models RF020-C1 and RW020-C1, where the highest level of compression stresses was applied in the flanges and in the web. Residual stresses present in the element influence on:

- Global initial stiffness of the element, if the residual stresses are equal to yield stress.
- Smoothness transition from elastic to plastic stage.
- Load capacity, which is usually smaller in comparison to element with no residual stresses.
- Post-peak behaviour; the decrease in resistance is more evident, which also results in smaller rotational capacity.

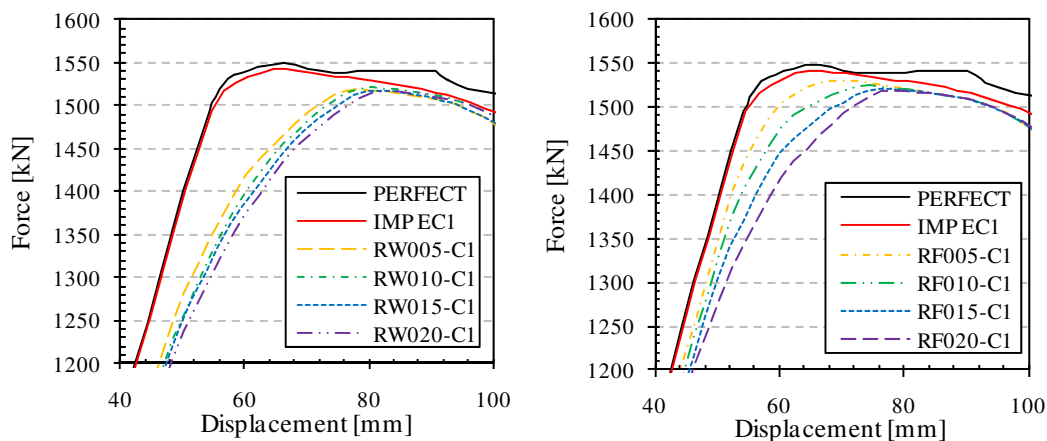


Figure 71: The influence of residual stresses on the global girder behaviour
Slika 71: Vpliv zaostalnih napetosti na globalen odziv nosilca

The reduction in girder's capacity due to presence of predicted residual stresses is plotted in Figure 72. Curve RF represents the influence of compression stresses in the flanges $a_f \cdot f_y$, while the compression stresses in the web remain the same $a_w \cdot f_y$, $a_w = 0.05$. The RW curve represents the influence of the level of compression stresses $a_w \cdot f_y$ in the web, at constant compression stresses in the flanges $a_f \cdot f_y$, $a_f = 0.20$. By increasing the level of compression stresses in the flange the girder's capacity decreases, at the lowest level of compression by 0.7% and at the highest by 1.5%. If the compression stresses were varied in the web, significant drop of capacity at minimum applied residual stress in the web was obtained; it should be stressed that the level of residual compression stresses in the flanges here is high. Additional increase of residual stresses does not affect the girder resistance.

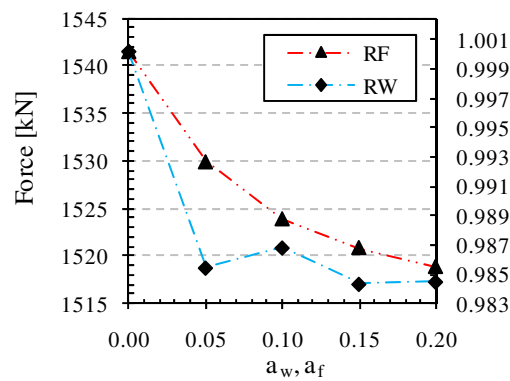


Figure 72: Reduction of the girder resistance for applied level of residual stresses
Slika 72: Redukcija nosilnosti nosilca za različne nivoje zaostalnih napetosti

Finally, the influence of residual stresses in combination with geometric imperfections was compared against equivalent geometrical imperfections. The results plotted in Figure 73 represent the capacity of the girder on which different initial imperfections are applied, normalized with resistance obtained on the perfect geometry. The influence of residual stresses is plotted for the situation where residual compression stresses in the web and flanges are equal to 5% of yield strength. This level of compressed stresses is the closest to the measured residual stresses described in Chapter 3.2.2, where the compression is near to 4% of yield strength.

The maximum decrease of the girder resistance because of equivalent geometric imperfection was found for imperfection model I1 (-0.5%). Models I2 and I3 gave similar results, while imperfection model I4 results in higher resistance (+0.4%). The combination of geometric imperfection and residual stresses leads to the smallest resistance (I6). Additional drop of 0.7% is obtained compared to the model with equivalent geometric imperfection (I1). For this particular case it was found out that the influence of initial imperfection is rather small.

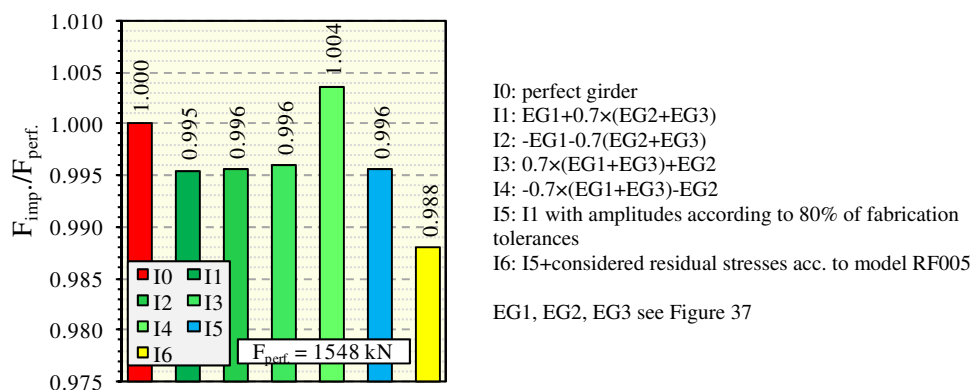


Figure 73: Influence of equivalent geometric imperfections (I1-I4), geometric imperfections (I5) and residual stresses (I6) on the girder resistance

Slika 73: Vpliv ekvivalentnih geometrijskih nepopolnosti (I1-I4), geometrijskih nepopolnosti (I5) in zaostalnih napetosti (I6) na nosilnost nosilca

5.4.3 Discussion

The behaviour of structural elements depends on all initial conditions which have to be properly considered in GMNIA analysis. Some of initial conditions, such as support conditions and load, are known, whereas the initial geometric and structural imperfections are not known in advance. When a

structure is very sensitive to initial imperfections, the right shape is of great significance, if the capacity of the element is concerned.

In this chapter the numerical analysis was performed in order to study the influence of geometric and structural imperfections on the behaviour and the capacity of girder. It was found out that geometric initial imperfections reduce the girder resistance, in the worst case by less than 4.4%. The highest reduction in girder resistance for all studied cases is found for initial imperfection defined as deformed shape (DS2) of GMNIA analysis of a perfect girder.

The influence of residual stresses was studied with a simplified stress field distribution. The presence of residual stresses reduces the stiffness as well as resistance of the girder. The reduction depends on the stress level and stress distribution. For plated girders, in which the input of the energy due to the welding is rather small, the residual stresses do not influence the girder resistance that much. Comparing results calculated only with geometrical imperfections and calculated with the combination of residual stresses and geometric imperfection, a reduction of 0.7% is established.

The presence of initial imperfections affects not only the girder resistance but also the buckling behaviour of the girder. In particular case the imperfection sensitivity is not so significant, because of the non-symmetry of the cross-section around its weak axis which results in additional bending moment with no initial imperfection. However, in the following parametric study initial imperfections EC1 and EC2 (see 5.4.1) with amplitude according to EN 1993-1-5 were taken into account.

5.5 Numerical model used in parametric study

For the sake of parametric study the numerical model was modified to reduce the size of nonlinear equations which need to be solved in each iteration. The layout of numerical model shown in Figure 74 is composed of four identical panels, supported with one vertical support in the middle of the girder length and buckling supports at each transverse stiffener. The load, bending moment and shear force are applied at each side of the girder. The direction of shear load and bending moment is orientated to make compression in the upper flange. At each girder end the edge is modelled as rigid.

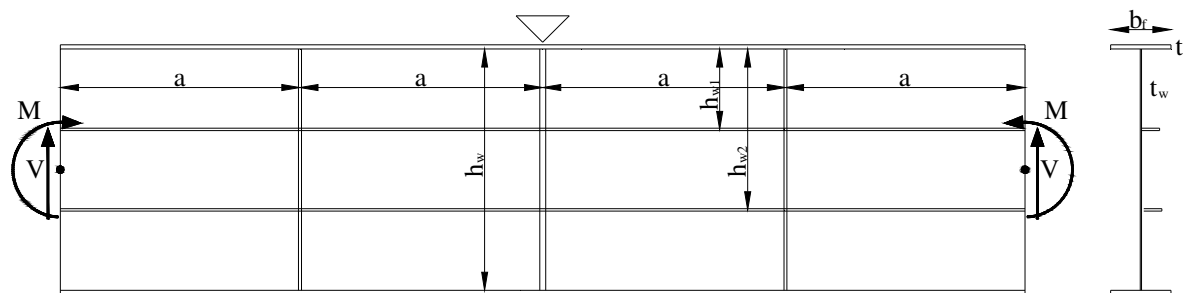


Figure 74: Layout of numerical model
Slika 74: Numerični model

The capacity determined with the modified numerical model was verified with complete three-point bending model. In Figure 75 the capacity of the girder determined with the modified model divided with capacity determined on complete model for six studied cases is plotted. The results show that the presented model gives satisfying results; the maximum deviation is 0.9% and the average 0.2%.

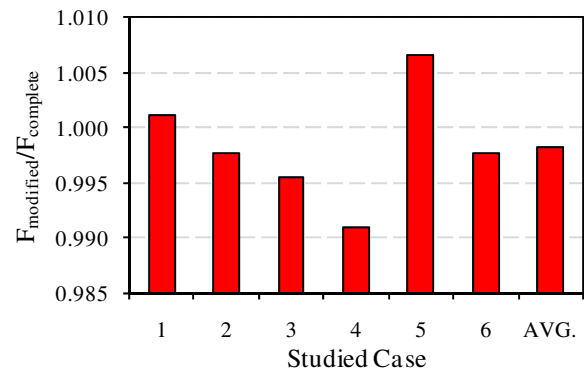


Figure 75: Girder's capacity computed by modified numerical model

Slika 75: Nosilnost nosilca izračunanega z modificiranim numeričnim modelom

6 PARAMETRIC STUDY

6.1 Introduction

In previous chapters the nonlinear model was developed and verified with experimental tests. All tests performed had their own set of parameters. To cover wider area of different parameters, a numerical database of simulations of longitudinally stiffened girders subjected to M-V interaction was developed and is presented herein. The results are aimed to fulfil the existing lack of data in this particular field.

The simulations were calculated based on the model described in Chapter 5.5. The girder was loaded up to failure by incremental nonlinear analysis. The modelling was performed according to the same principles as used in the simulations of the tests depicted in Chapter 1.

6.2 Parameters

The following parameters were considered to investigate M-V interaction of longitudinally stiffened plated girders:

- Flange to web ratio (A_f / A_w).
- Web slenderness (h_w / t_w).
- Panel aspect ratio ($\alpha = a / h_w$).
- Number and geometry of longitudinal stiffeners.
- Stiffness of longitudinal stiffeners.
- Vertical position of longitudinal stiffener (h_{w1}).
- Ratio of bending moment and shear load in the panel.

Open longitudinal stiffeners were designed to completely prevent torsional buckling due to axial load in the stiffener. The following requirement was met to prevent torsional buckling:

$$\frac{I_t}{I_p} \geq 5.3 \frac{f_y}{E}, \quad (24)$$

where I_t is the St. Venant torsional constant of the stiffener alone and I_p is the polar second moment area of the stiffener alone around the edge fixed to the plate. For open flat stiffeners and steel grade S355 the above condition can be written as:

$$\frac{b_{st}}{t_{st}} \leq \sqrt{\frac{E}{5.3 \cdot f_y}} = 10.56, \quad (25)$$

where b_{st} is the width and t_{st} the thickness of the stiffener.

6.2.1 Variation

The numerical database was constructed by varying the above mentioned parameters. Four groups formed the framework of the sample. Each group consisted of a web panel height of $h_w = 2000 \text{ mm}$ and

within each group the panel was subjected to 5 different ratios of bending to shear load as noted in Figure 76. Four of them were exposed to ($i=1, 2, 3, 4$) bending and shear load in the area where interaction according to EN 1993-1-5 should be considered. The last ratio of bending to shear load ($i=5$) was performed at shear load equal to 60% of pure shear capacity of the web V_{bw} . Within each group the following parameters are additionally varied: shape of longitudinal stiffeners (open I stiffener, closed stiffener), position and number of longitudinal stiffeners ($n=1, 2$). The vertical position of longitudinal stiffeners was varied only for one stiffener ($h_w/4, h_w/2$); in the first case the web was stiffened in the upper part, so the stiffener was subjected to high compression force, and in the second situation the stiffener was positioned at half web depth. When two stiffeners were applied, the web panel was divided in three equal subpanels ($h_w/3$). For the girder stiffened with two longitudinal stiffeners the amount of simulations for each varied parameter was reduced; evaluated values of parameters for such girder are noted with bold in Table 15. The material used in numerical simulations was modelled as depicted in Chapter 5.1.2. All parameters considered in numerical simulations are gathered in Table 15.

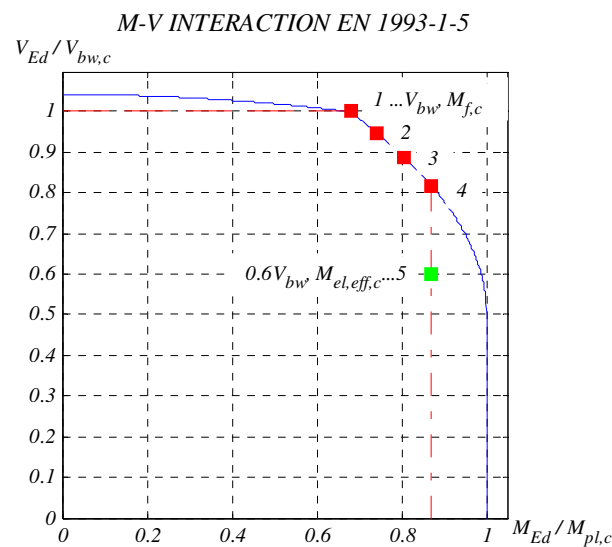


Figure 76: Considered load cases in numerical simulations (red squares - EN 1993-1-5 interaction formulation in the range of high bending and shear load, green square - only bending check is considered)

Slika 76: Upoštevane obtežne situacije v numeričnih simulacijah (rdeči pravokotniki označujejo točke v območju interakcije po EN 1993-1-5, zelen pravokotnik označuje točko, kjer je izvedena le kontrola upogibne nosilnosti)

Preglednica 15: Parametri numeričnih simulacij
 Table 15: Variation parameters in numerical simulations

| Variation parameters | GROUP | | | |
|---------------------------------------|---------|---------------------------------------|---------|---------|
| | I | II | III | IV |
| A_f/A_w | 0.3 | | | |
| | 0.5 | | | |
| | 0.7 | | | |
| | 0.9 | 0.7 | 0.7 | 0.7 |
| | 1.1 | | | |
| | 1.5 | | | |
| h_w/t_w | 250 | 150 | | |
| | | 200 | | |
| | | 250 | 250 | 250 |
| | | 300 | | |
| | | 350 | | |
| | | 400 | | |
| a | 2000 | 2000 | 1000 | |
| | | | 2000 | 2000 |
| | | | 3000 | |
| | | | 4000 | |
| | | | 5000 | |
| γ^* | 3 | 3 | 3 | 0.3 |
| | | | | 0.75 |
| | | | | 1 |
| | | | | 2 |
| | | | | 3 |
| | | | | 4 |
| Stiffener shape | Open | Open | Open | Open |
| | Closed | Closed | Closed | Closed |
| Position of the stiffener | $h_w/4$ | $h_w/4$ | $h_w/4$ | $h_w/4$ |
| | $h_w/2$ | $h_w/2$ | $h_w/2$ | $h_w/2$ |
| | $h_w/3$ | $h_w/3$ | / | $h_w/3$ |
| Number of longitudinal stiffeners | 1 | 1 | 1 | 1 |
| | 2 | 2 | | 2 |
| Presumed load | | Case 1: $M_{f,c}, V_{bw,c}$ | | |
| | | Case 2: $(2M_{f,c} + M_{el,eff,c})/3$ | | |
| | | Case 3: $(M_{f,c} + 2M_{el,eff,c})/3$ | | |
| | | Case 4: $M_{el,eff,c}$ | | |
| | | Case 5: $M_{el,eff,c}, 0.6V_{bw,c}$ | | |
| Number of numerical simulations | 140+40 | 120+30 | 100 | 160+40 |
| Total number of numerical simulations | 630 | | | |

6.3 Numerical results, failure mechanism

The collapse load of girders subjected to the combination of high bending moment and high shear load is characterised by a plastic hinge over the girders height and a plastic tension field. The tension field development depends on the normal stresses applied in the web and on the stiffness of the stiffener. The stiffness of longitudinal stiffeners influences the global behaviour of the web panel. If a slender longitudinal stiffener at the web is applied, the buckling occurs over the entire web depth, while the opposite happens for stocky stiffener, where the buckling occurs only in the subpanels. The level of bending moment and shear load defines plastic mechanisms in the girder.

The results of the numerical simulations will be presented separately for each group. The failure mechanism will be discussed for two different loads. First, for load situation, where the girder reaches the bending capacity of the flanges $M_{f,c}$, and secondly, where the girder is loaded so that it reaches the effective bending capacity of the girder $M_{el,eff,c}$.

6.3.1 Group I - Variation of the A_f/A_w ratio

In Group I the varied parameter is the A_f/A_w ratio. The results of numerical simulations will be presented and discussed for each possible position of the longitudinal stiffener and for both geometries of stiffeners, open and closed. The results are presented through the von Mises stresses; for each case for low and medium A_f/A_w ratio and for two typical load cases (see Figure 76): load case 1 ($M_{f,c}$) and load case 4 ($M_{el,eff,c}$).

6.3.1.1 Longitudinal stiffener at $h_w/4$

In Figure 77 the von Mises stresses for girder stiffened with one open stiffener in the compression zone of the web are plotted. The failure mechanism for the first load situation can be described as yielding over the whole depth of the girder due to bending and as yielding of the diagonal tension field caused by shear load. By increasing bending moment and consequently decreasing shear load the yielding of the tension field does not occur; only yielding over the whole depth of the girder due to bending can be observed. The same phenomenon is found for both A_f/A_w ratios with one difference; the shape of the local buckling of the compressed flange is in the first case (weak flange) torsional, while in the second case flange buckling in the plane of the web is obtained. The tension field formation is in all variations of numerical simulations always obtained only in the largest subpanel.

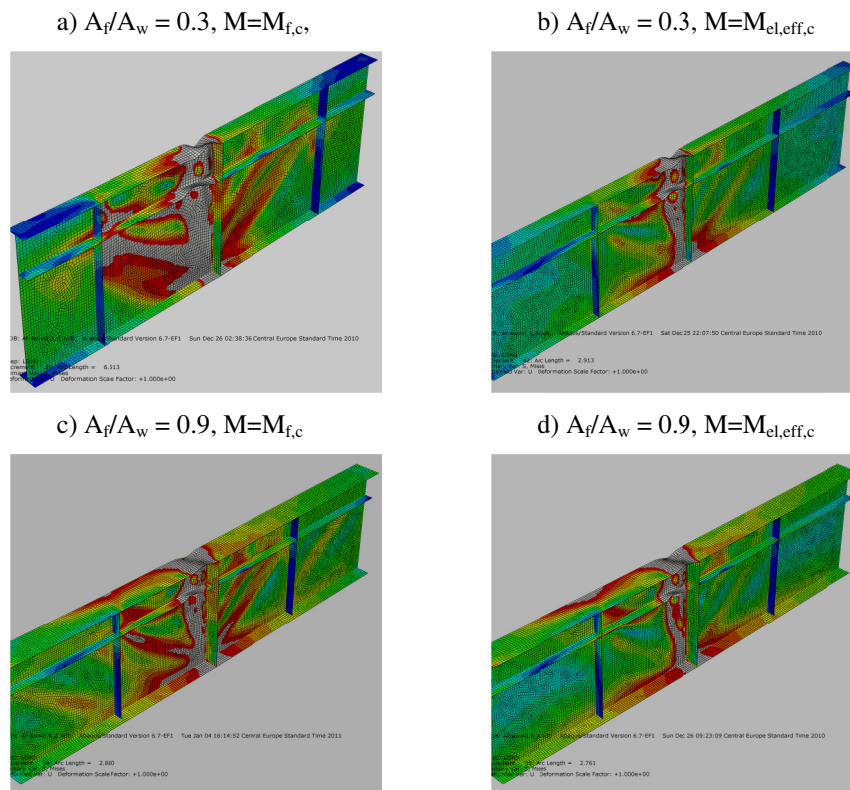


Figure 77: Von Mises stresses for girders stiffened with one open stiffener at $h_w/4$
Slika 77: Missesove primerjalne napetosti za nosilec ojačan z eno odprto ojačitvijo na $h_w/4$

In Figure 78 the same results as in the previous case are plotted for girder stiffened with closed stiffener. The failure phenomenon, the von Mises stress distribution and the buckling shape of the flanges are similar.

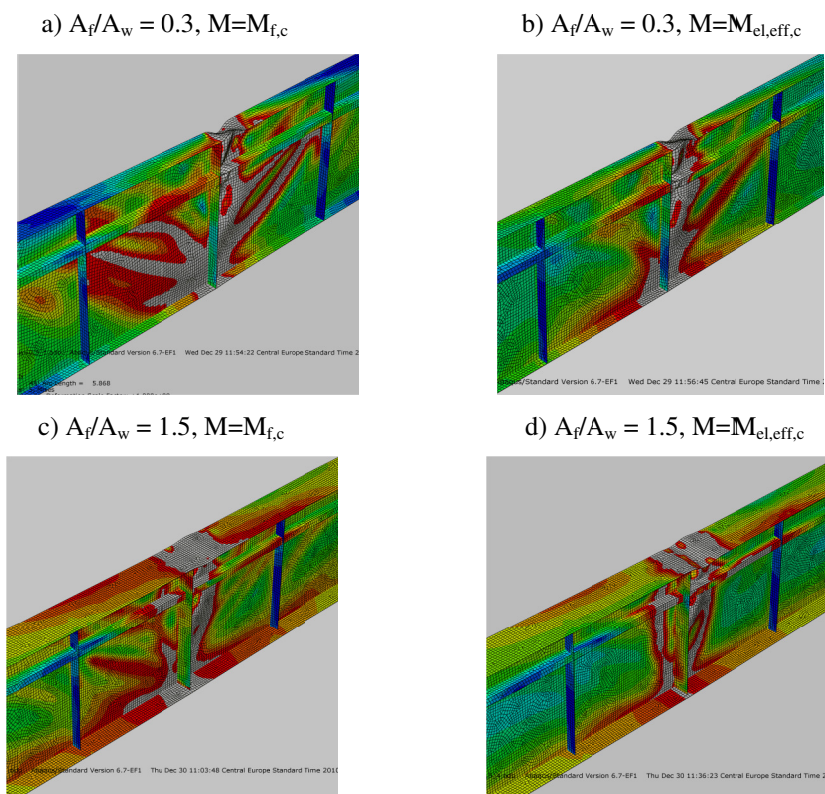


Figure 78: Von Mises stresses for girders stiffened with one closed stiffener at $h_w/4$
Slika 78: Missesove primerjalne napetosti za nosilec ojačan z eno zaprto ojačitvijo na $h_w/4$

6.3.1.2 Longitudinal stiffener at $h_w/2$

Results considering stiffener positioned in the middle of the web depth are plotted in Figure 79 and in Figure 80. For the stiffener in this position the yielding of the tension field is obtained for both load cases (load cases 1 and 4). The yielding of the tension field is as expected much more evident for high shear load (load case 1) and in the upper subpanel which is loaded with compression due to bending. At higher level of bending moment the yielding of the tension field formation occurs over a smaller length.

The stiffness of the longitudinal stiffener is sufficiently high to prevent any global buckling of the web panel. Yielding of the stiffener is present only at the most stressed edge of the panel where the bending moment is the highest.

The shape of local buckling of the flanges is for weak flanges again torsional, where for strong flanges buckling in the plane of the web occurs. The direction of the torsional local buckling is defined with buckling of the web panel which has occurred at lower load, where response of the girder was elastic.

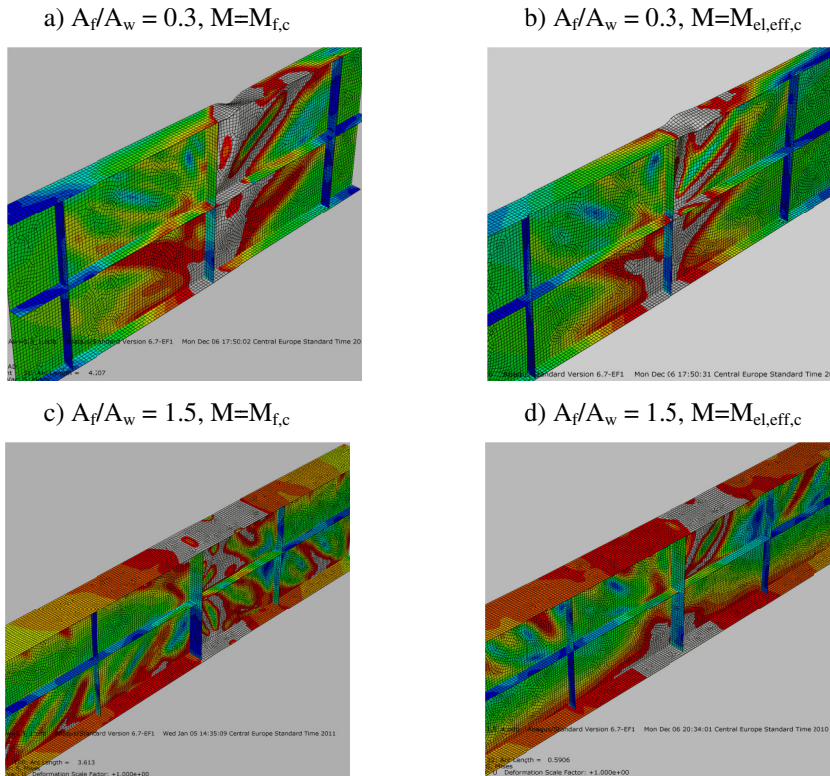


Figure 79: Von Mises stresses for girders stiffened with one open stiffener at $h_w/2$
Slika 79: Missesove primerjalne napetosti za nosilec ojačan z eno odprto ojačitvijo na $h_w/2$

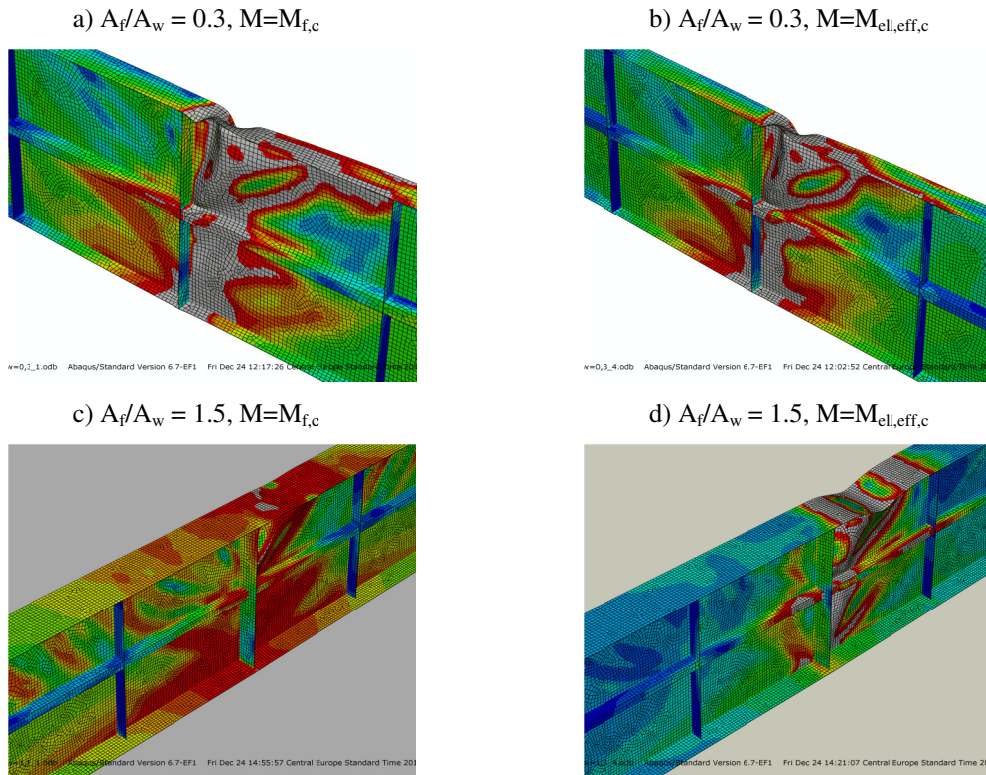


Figure 80: Von Mises stresses for girders stiffened with one closed stiffener at $h_w/2$
Slika 80: Missesove primerjalne napetosti za nosilec ojačan z eno zaprto ojačitvijo na $h_w/2$

6.3.1.3 Two longitudinal stiffeners

In the previously analysed cases the web was stiffened with one stiffener at different positions, now, in this case, two stiffeners divide the web in three equal subpanels, which is a common practice in bridge engineering. The results for these girders are shown in Figure 81 and Figure 82. The combination of yielding of the tension field and yielding over the girder's depth is clearly seen only in Figure 81 a), c) and d) and Figure 82 c). In all other cases (also in the case when a low bending moment was assumed) the yielding over the whole girder depth is obtained. Therefore, it can be concluded that the girder resistance is exhausted due to bending.

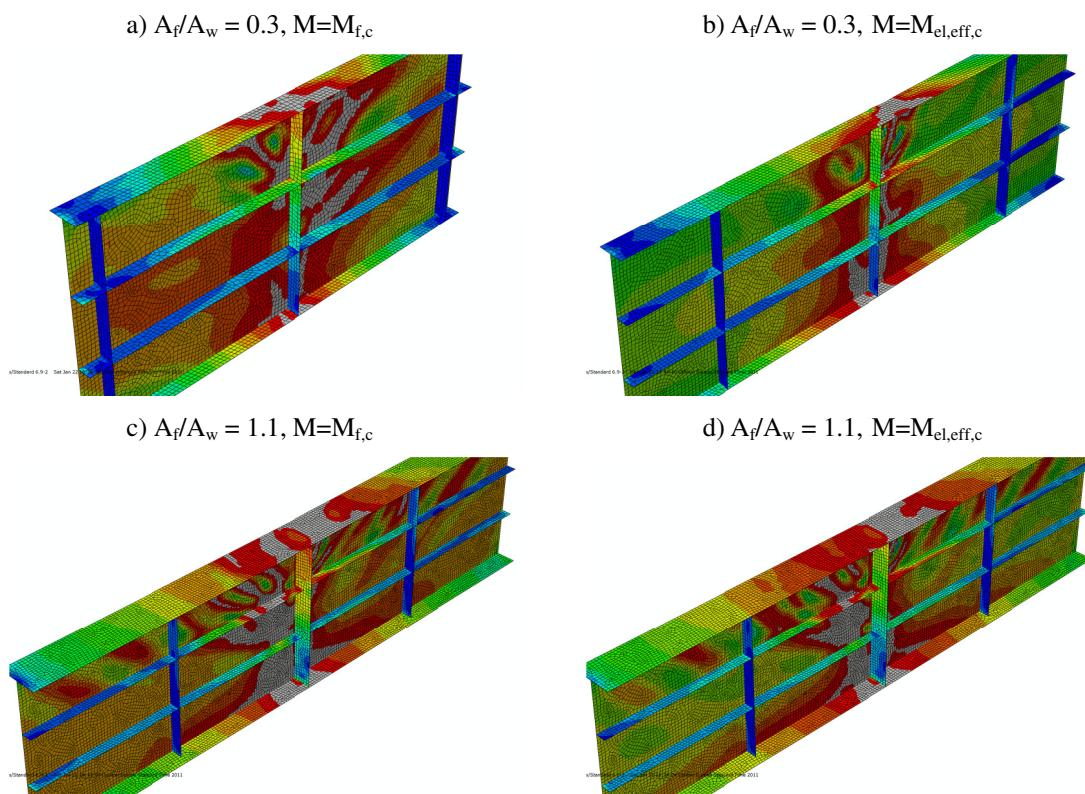


Figure 81: Von Mises stresses for girders stiffened with two open stiffeners
Slika 81: Missesove primerjalne napetosti za nosilec ojačan z dvema odprtima ojačitvama

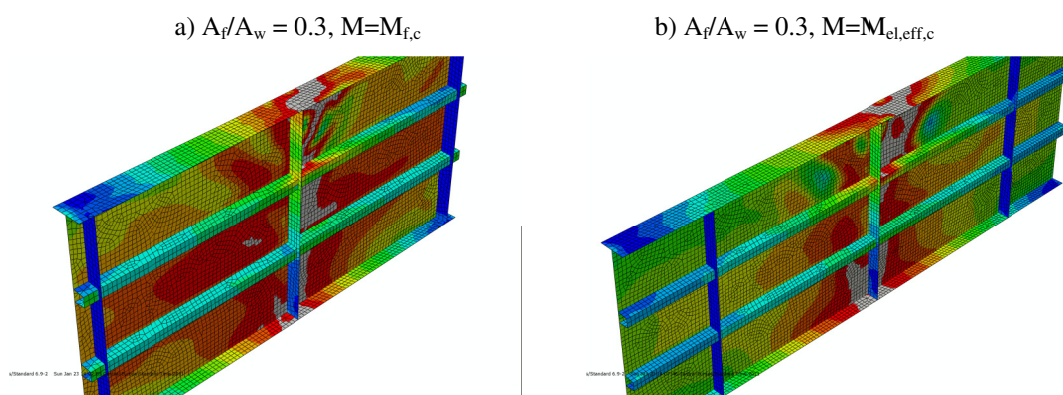


Figure 82: Von Mises stresses for girders stiffened with two closed stiffeners
Slika 82: Missesove primerjalne napetosti za nosilec ojačan z dvema zaprtima ojačitvama

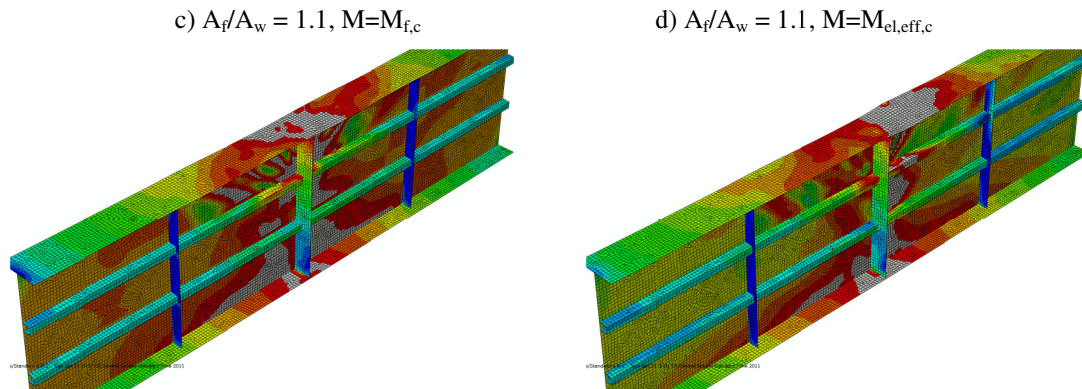


Figure 82: Von Mises stresses for girders stiffened with two closed stiffeners
Slika 82: Missesove primerjalne napetosti za nosilec ojačan z dvema zaprtima ojačitvama

6.3.2 Group II - Variation of web slenderness h_w/t_w

In Group II the varied parameter is the web slenderness h_w/t_w . The results of numerical simulations will again be presented and discussed for each possible position of the longitudinal stiffener and for both geometries of stiffeners. For each case the results are presented for two slendernesses of the webs: $h_w/t_w = 200$ and $h_w/t_w = 300$.

6.3.2.1 Longitudinal stiffener at $h_w/4$

In Figure 83 and Figure 84 the stress distributions at maximum force for girders with one open and one closed stiffener is plotted. For girders with lower bending load and higher shear load the yielding of the tension field is always clearly seen. On the other hand, when the bending moment increases, the yielding over the largest panel occurs only for larger slenderness of the web panel. The mutual influence of the tension field action and tension stresses due to bending can obviously be observed through yielding of the web in the bottom right corner of the left panels in Figure 83 b) and Figure 84 b).

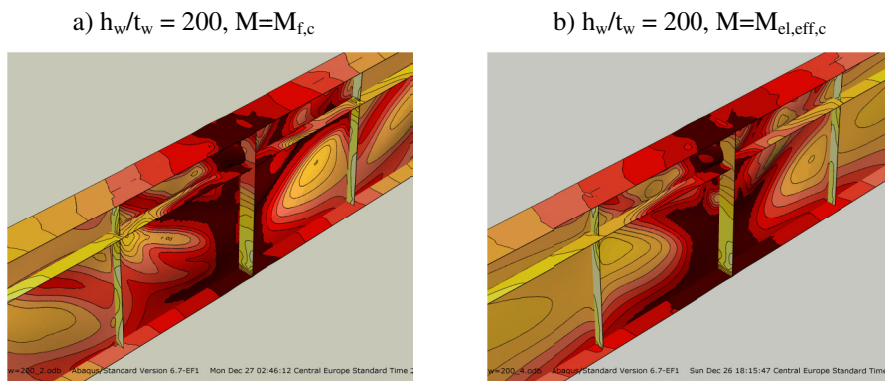


Figure 83: Von Mises stresses for girders stiffened with one open stiffener at $h_w/4$
Slika 83: Missesove primerjalne napetosti za nosilec ojačan z eno odprto ojačitvijo na $h_w/4$

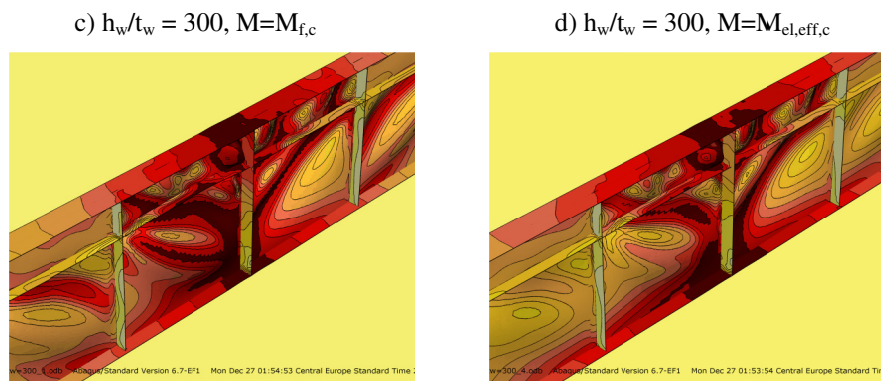


Figure 83: Von Mises stresses for girders stiffened with one open stiffener at $h_w/4$
Slika 83: Missesove primerjalne napetosti za nosilec ojačan z eno odprto ojačitvijo na $h_w/4$

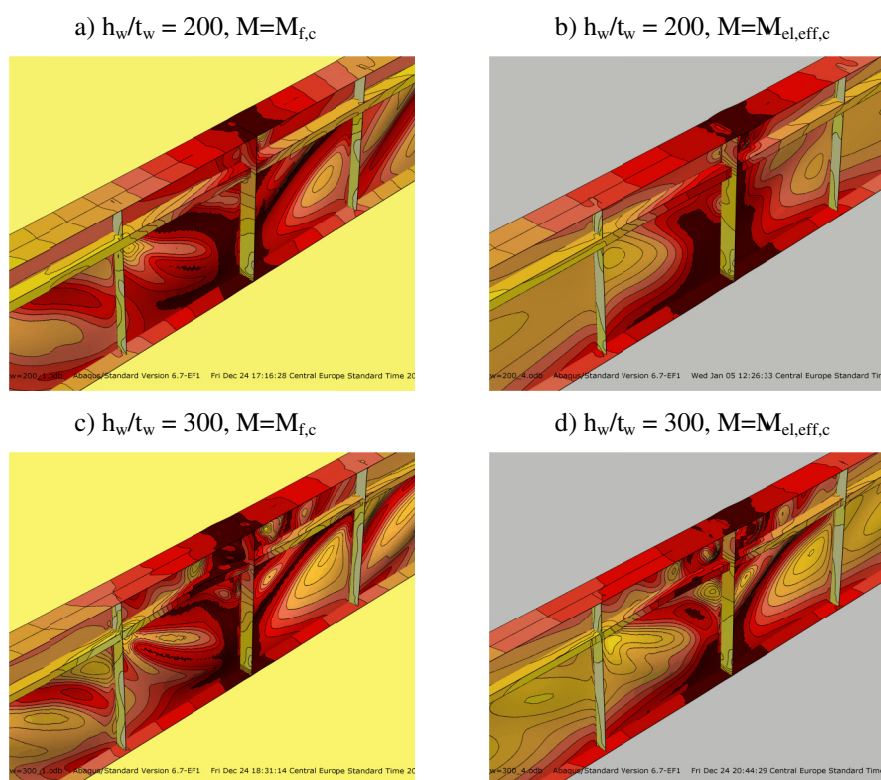


Figure 84: Von Mises stresses for girders stiffened with one closed stiffener at $h_w/4$
Slika 84: Missesove primerjalne napetosti za nosilec ojačan z eno zaprto ojačitvijo na $h_w/4$

6.3.2.2 Longitudinal stiffener at $h_w/2$

The following figures, Figure 85 and Figure 86, show the results for the same numerical simulations as in previous case with the stiffener positioned in the middle of the web. The yielding of the tension field is always present in both subpanels at high shear load, while at lower shear load the yielding of the tension field can be obtained only in the upper subpanel where compression is present. Nevertheless, the failure is always caused by the combination of both actions.

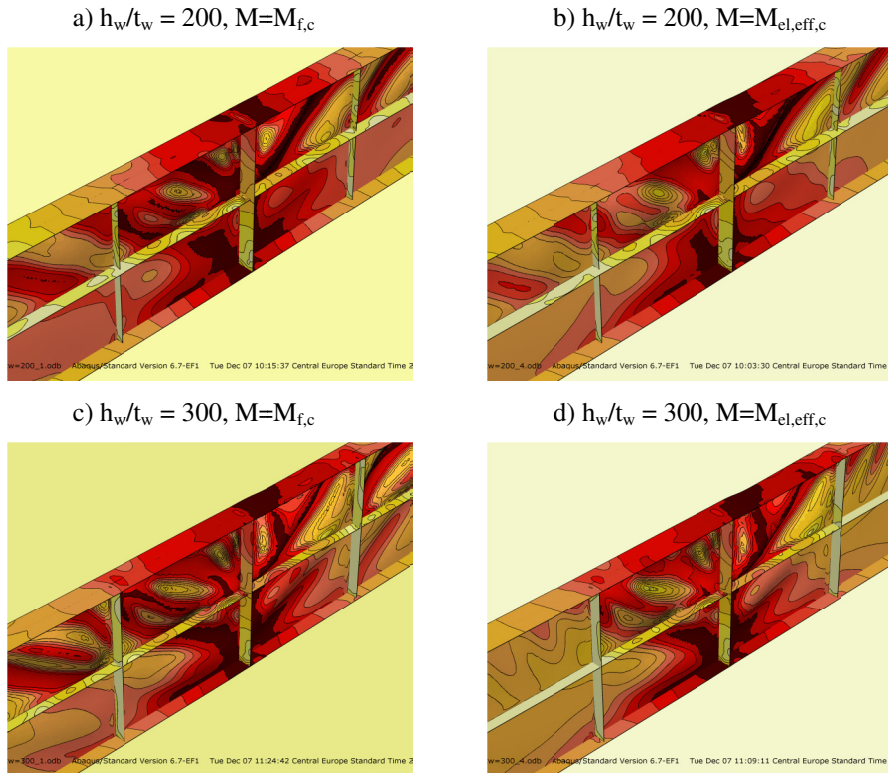


Figure 85: Von Mises stresses for girders stiffened with one open stiffener at $h_w/2$
Slika 85: Missesove primerjalne napetosti za nosilec ojačan z eno odprto ojačitvijo na $h_w/2$

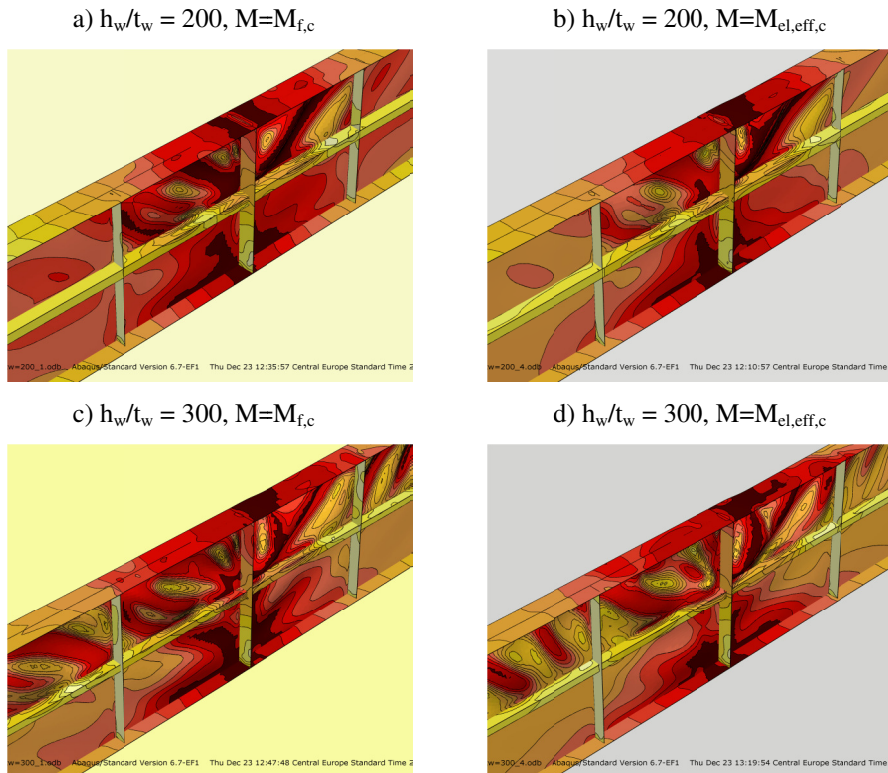


Figure 86: Von Mises stresses for girders stiffened with one closed stiffener at $h_w/2$
Slika 86: Missesove primerjalne napetosti za nosilec ojačan z eno zaprto ojačitvijo na $h_w/2$

6.3.2.3 Two longitudinal stiffeners

In Figure 87 the results for girders stiffened with open and closed stiffeners for only one web slenderness of $h_w/t_w = 350$ are plotted. The failure mechanism is very similar for all four cases, with much more obvious formation of the tension field in girders loaded with higher shear load.

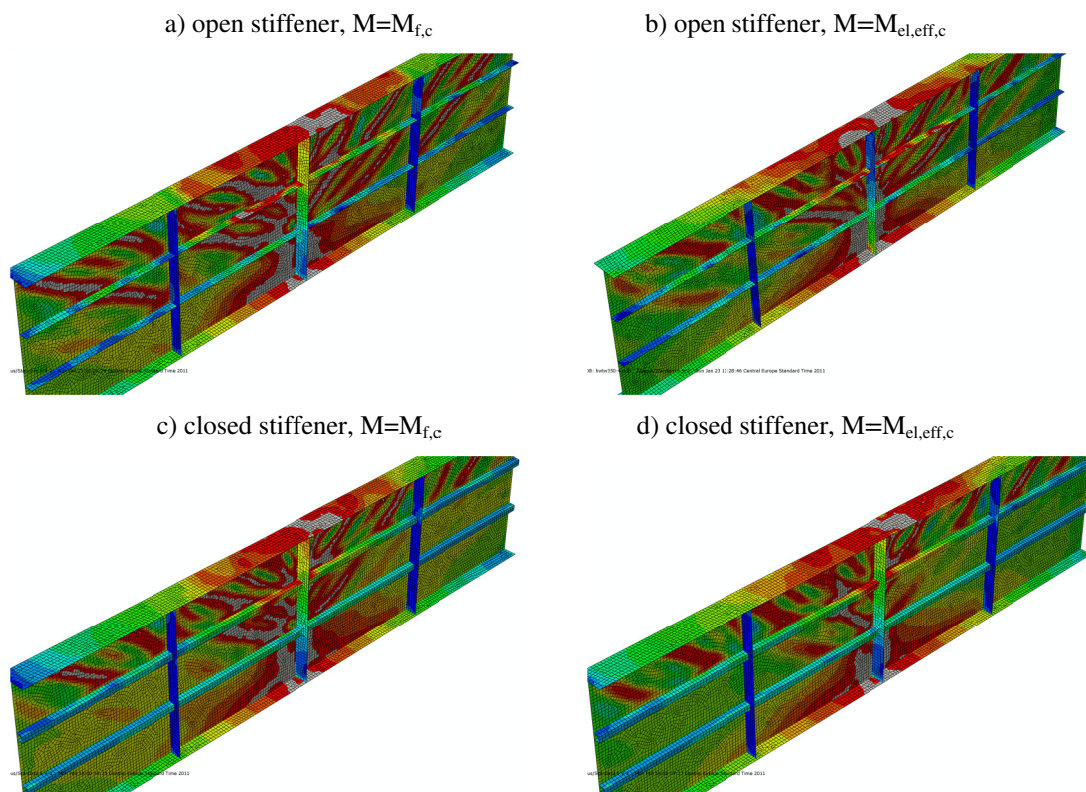


Figure 87: Von Mises stresses for girders stiffened with two stiffeners and web slenderness $h_w/t_w = 350$
Slika 87: Missesove primerjalne napetosti za nosilec ojačan z dvema ojačitvama in vitkostjo stojine $h_w/t_w = 350$

6.3.3 Group III - Variation of panel aspect ratio α

In Group III the varied parameter is the panel aspect ratio α . The results of numerical simulations will be presented and discussed for each possible position of longitudinal stiffener and for both geometries of stiffeners. For each case the results are presented for two panel aspect ratios: $\alpha = 0.5$ and $\alpha = 1.5$.

6.3.3.1 Longitudinal stiffener at $h_w/4$

In Figure 88 and Figure 89 the results for girder stiffened at $h_w/4$ are plotted. As in all previously studied cases the yielding of the formed tension field can be observed for load situation 1. At lower panel ratio $\alpha = 0.5$ the yielding of tension field is evident in all load cases, while for this load cases in girders with panel ratio of $\alpha = 1.5$ slight yielding can be obtained. The reason for the difference between the both panel ratios is that the moment gradient over the panel is steeper at lower panel ratio compared to the gradient at higher panel ratio. This plays an important role in the failure mechanism of the girder.

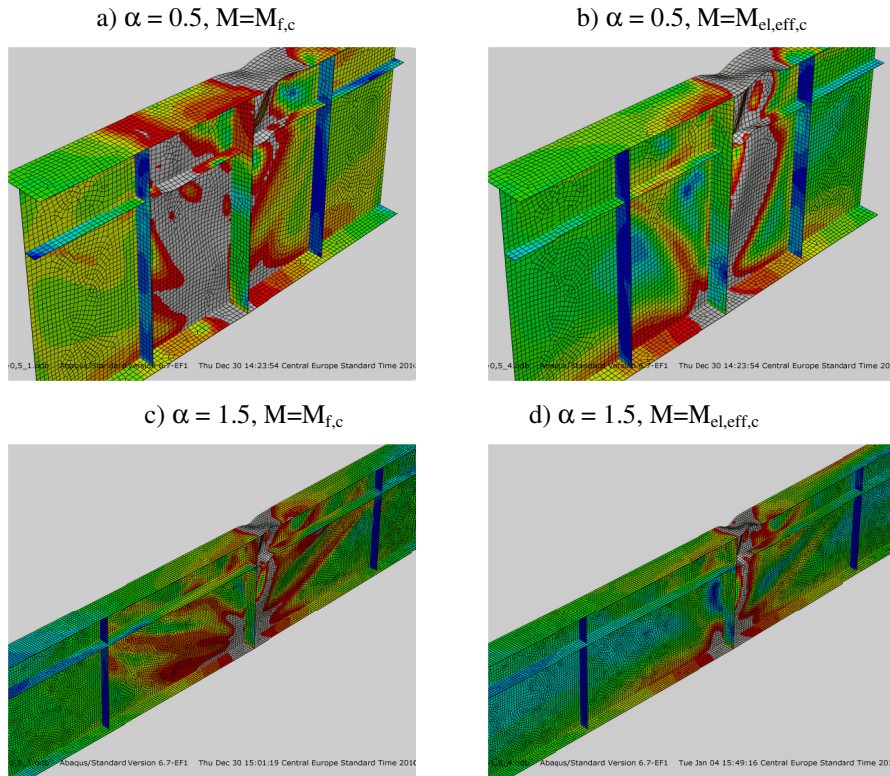


Figure 88: Von Mises stresses for girders stiffened with one open stiffener at $h_w/4$
Slika 88: Missesove primerjalne napetosti za nosilec ojačan z eno odprto ojačitvijo na $h_w/4$

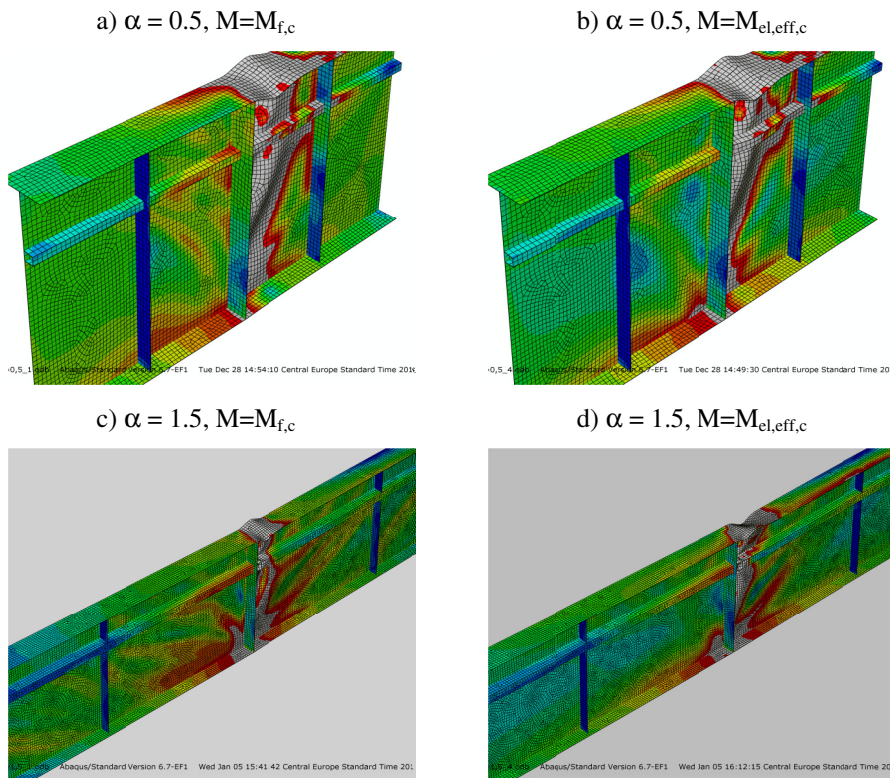


Figure 89: Von Mises stresses for girders stiffened with one closed stiffener at $h_w/4$
Slika 89: Missesove primerjalne napetosti za nosilec ojačan z eno zaprto ojačitvijo na $h_w/4$

6.3.3.2 Longitudinal stiffener at $h_w/2$

The results for stiffener positioned in the middle of the web depth are presented in Figure 90 and Figure 91. In this case, however, the yielding of the tension field occurs also in the girder with panel aspect ratio $\alpha = 1.5$ and is present only in the compressed subpanel. The angle of the tension field formation is close to 45° .

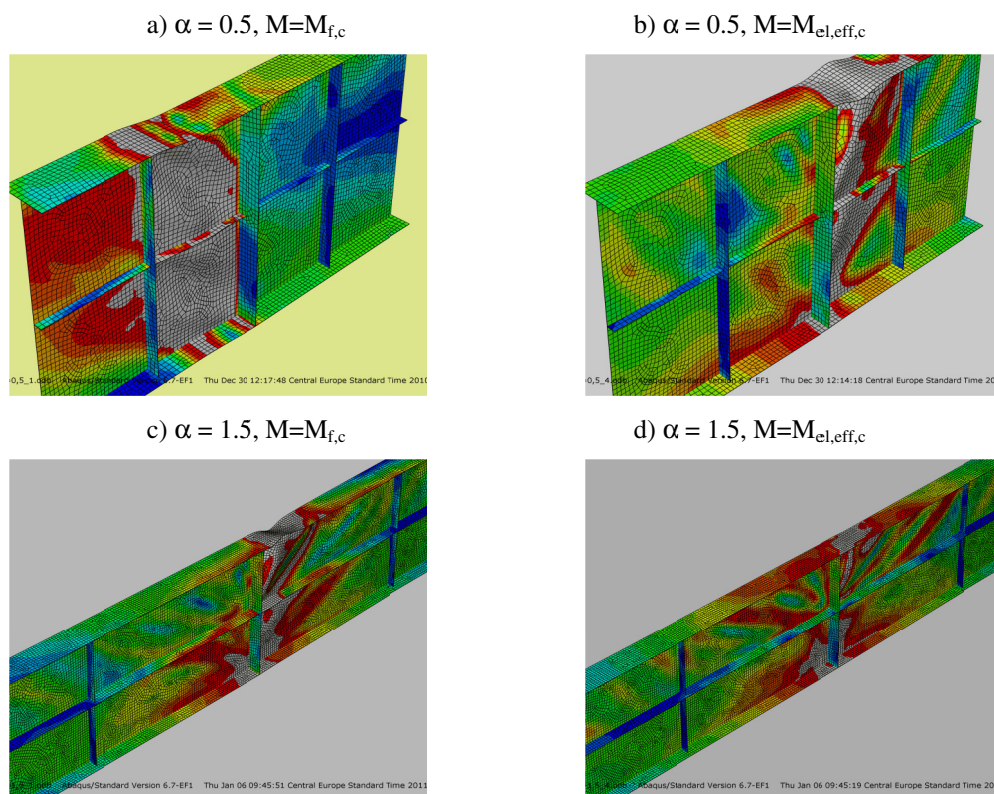


Figure 90: Von Mises stresses for girders stiffened with one open stiffener at $h_w/2$
Slika 90: Missesove primerjalne napetosti za nosilec ojačan z eno odprto ojačitvijo na $h_w/2$

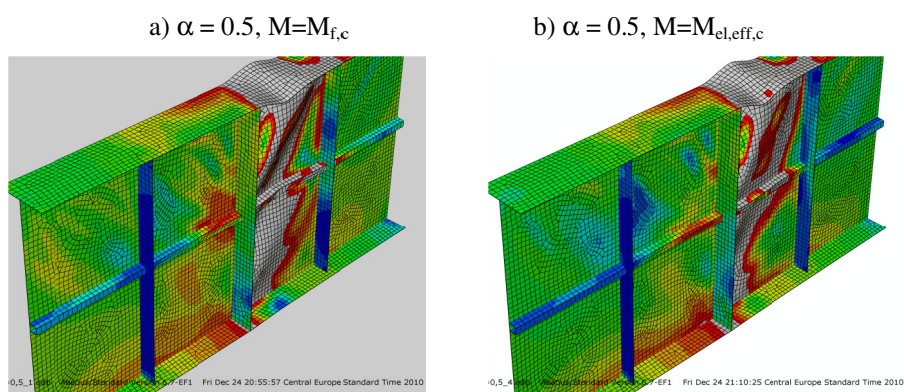


Figure 91: Von Mises stresses for girders stiffened with one closed stiffener at $h_w/2$
Slika 91: Missesove primerjalne napetosti za nosilec ojačan z eno zaprto ojačitvijo na $h_w/2$

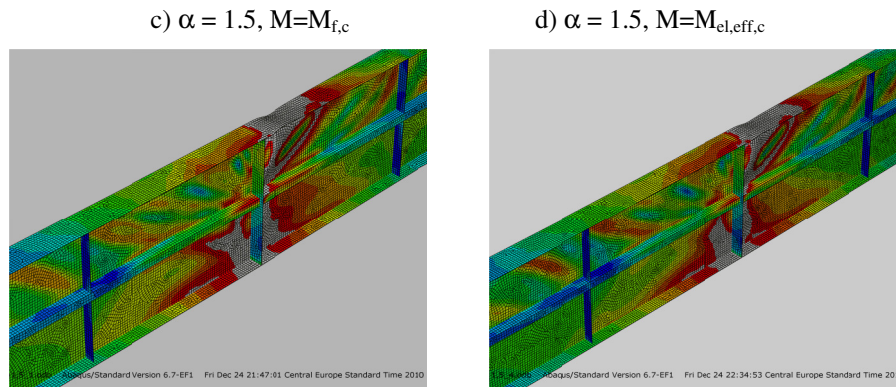


Figure 91: Von Mises stresses for girders stiffened with one closed stiffener at $h_w/2$
Slika 91: Missesove primerjalne napetosti za nosilec ojačan z eno zaprto ojačitvijo na $h_w/2$

6.3.4 Group IV - Variation of stiffness of longitudinal stiffener γ/γ^*

Stiffness of the longitudinal stiffener γ/γ^* is the varied parameter in this group of numerical simulations and like in all previous cases, the results for each case are presented for two longitudinal stiffener stiffnesses: $\gamma/\gamma^* = 0.3$ and $\gamma/\gamma^* = 1.0$.

6.3.4.1 Longitudinal stiffener at $h_w/4$

The results for girder stiffened at $h_w/4$ are plotted in Figure 92 and Figure 93. In Figure 92 the girder is stiffened with open stiffener and in Figure 93 with closed stiffener. The failure mechanism is similar for both stiffnesses. The stiffener stiffness is too small to remain straight at the maximum capacity. The buckle of the open stiffener is turned in the opposite side as the buckle of the closed stiffener. The maximum out of plane deflection of the stiffener was for all studied cases obtained at the same position. At load situation 1 three yielding lines in the web panel can be obtained. Two of them are found in the largest subpanel; the diagonal one is formed due to tension field formation, and the vertical one due to bending moment. When the bending moment increases (load situation 4), the yielding of tension field almost disappears.

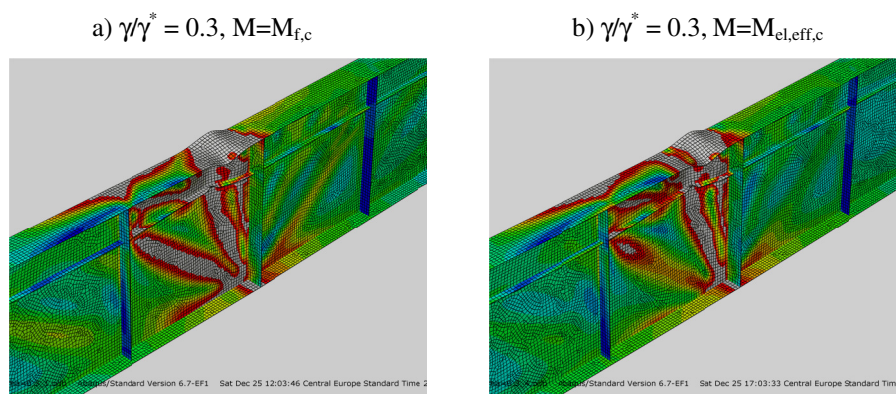


Figure 92: Von Mises stresses for girders stiffened with one open stiffener at $h_w/4$
Slika 92: Missesove primerjalne napetosti za nosilec ojačan z eno odprto ojačitvijo na $h_w/4$

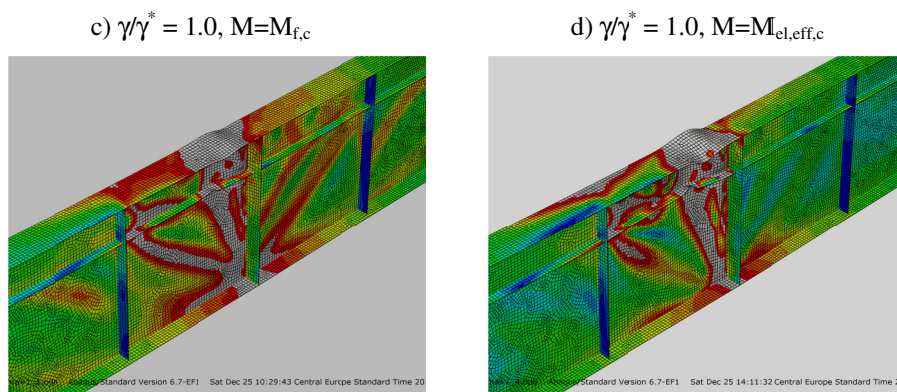


Figure 92: Von Mises stresses for girders stiffened with one open stiffener at $h_w/4$
Slika 92: Missesove primerjalne napetosti za nosilec ojačan z eno odprto ojačitvijo na $h_w/4$

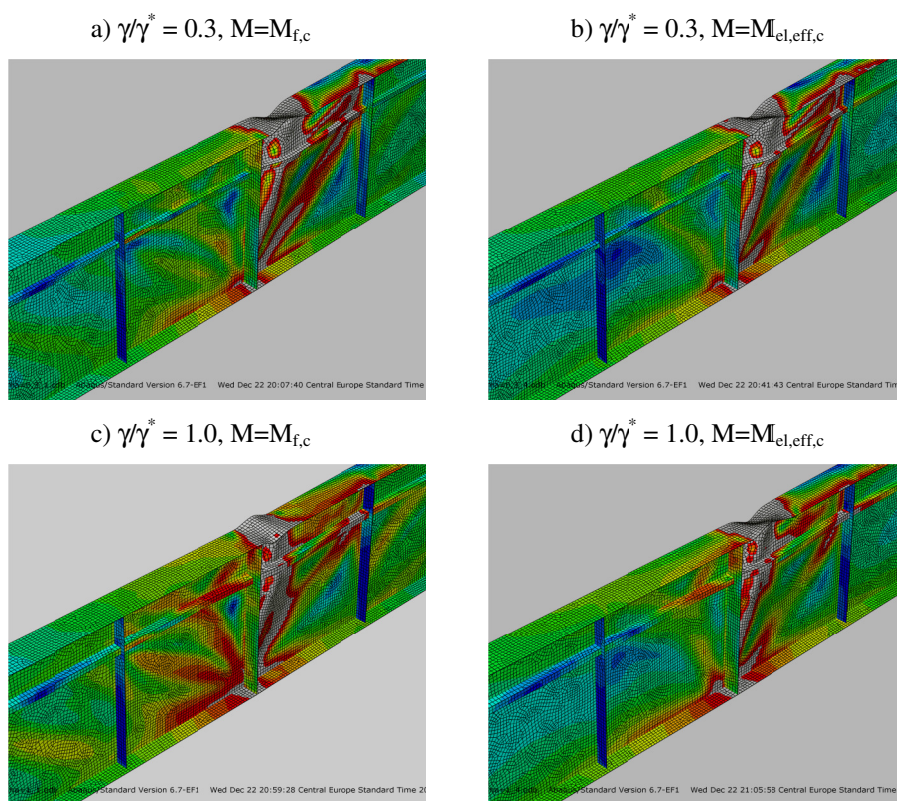


Figure 93: Von Mises stresses for girders stiffened with one closed stiffener at $h_w/4$
Slika 93: Missesove primerjalne napetosti za nosilec ojačan z eno zaprto ojačitvijo na $h_w/4$

6.3.4.2 Longitudinal stiffener at $h_w/2$

In Figure 94 and Figure 95 the results for girder stiffened in the middle of the web depth are plotted. The yielding of the formed tension field is observed over the whole panel. At the maximum obtained load the stiffener buckles in such way that the maximum out-of-plane displacement of the stiffener is where the tension field is formed. In all studied cases torsional buckling of the flange in compression is obtained.

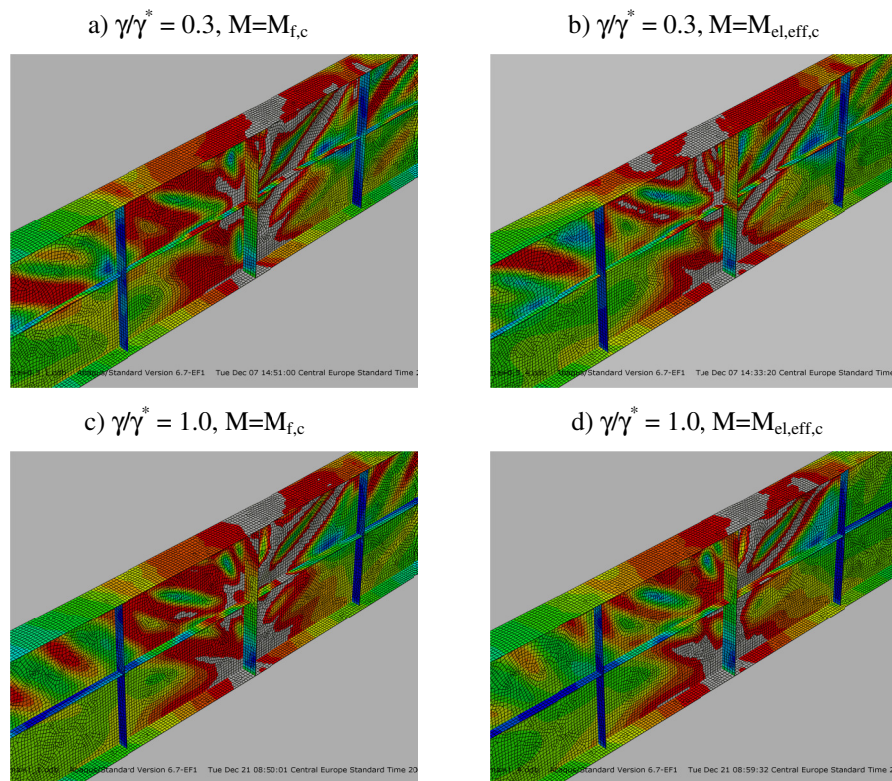


Figure 94: Von Mises stresses for girders stiffened with one open stiffener at $h_w/2$
Slika 94: Missesove primerjalne napetosti za nosilec ojačan z eno odprto ojačitvijo na $h_w/2$

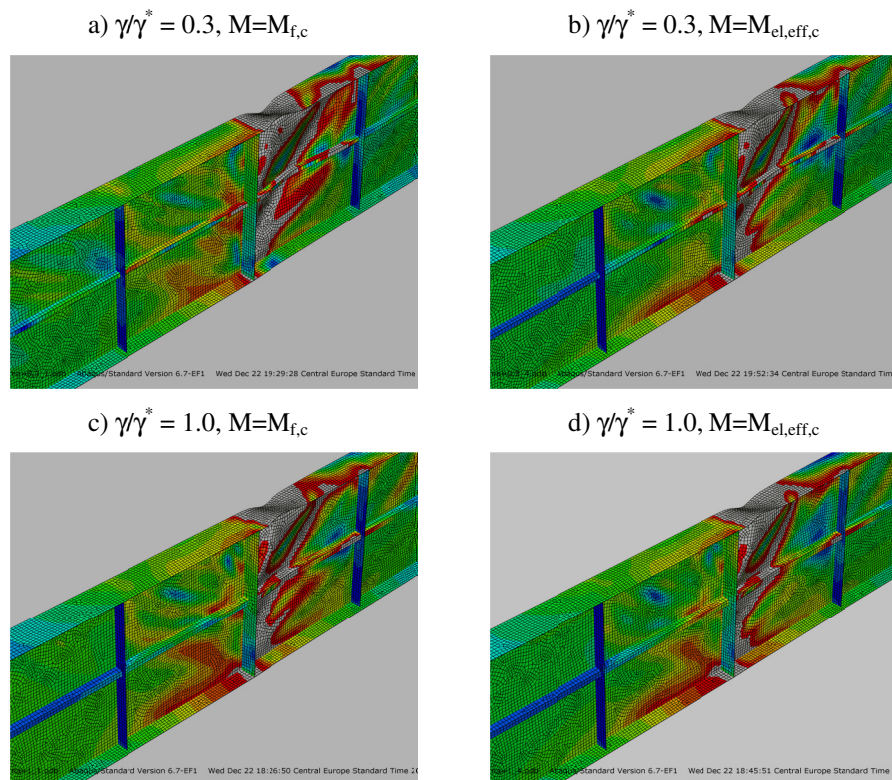


Figure 95: Von Mises stresses for girders stiffened with one closed stiffener at $h_w/2$
Slika 95: Missesove primerjalne napetosti za nosilec ojačan z eno zaprto ojačitvijo na $h_w/2$

6.3.4.3 Two longitudinal stiffeners

The results of the last set of analysed girders, where the girder is stiffened with two equally spaced longitudinal stiffeners, are presented in Figure 96 and Figure 97. In the first case the stiffness of the stiffener is set to $\gamma/\gamma^* = 0.3$ in order to obtain global buckling of the web. In the second case the stiffness is $\gamma/\gamma^* = 1.0$. The girders loaded with load situation 1 ($V_{bw,c}$, $M_{f,c}$) exhibit yielding of the tension field, while for girders loaded with higher bending moment (load situation 4) only the yielding over the cross-section depth is mainly present. In case of weak stiffeners the tension field develops over the whole web panel, whereas for stiffer stiffness $\gamma/\gamma^* = 1.0$ the local formation of the tension field is obtained.

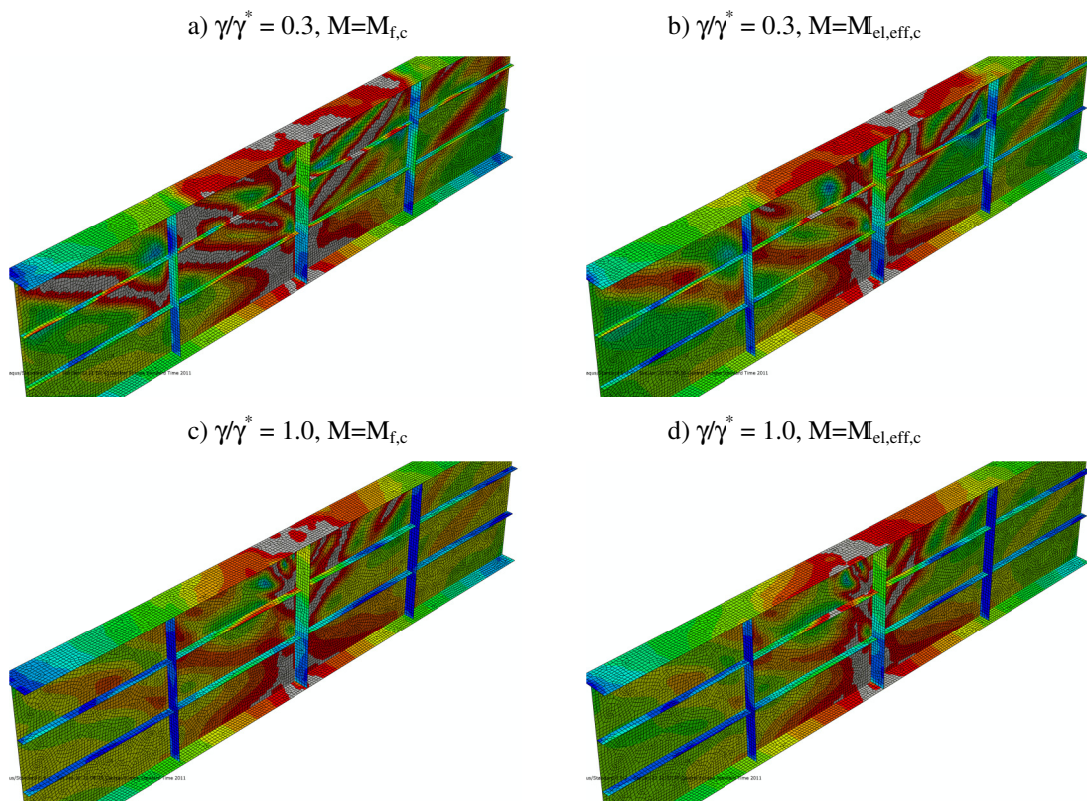


Figure 96: Von Mises stresses for girders stiffened with two open stiffeners
Slika 96: Missesove primerjalne napetosti za nosilec ojačan z dvema odprtima ojačitvama

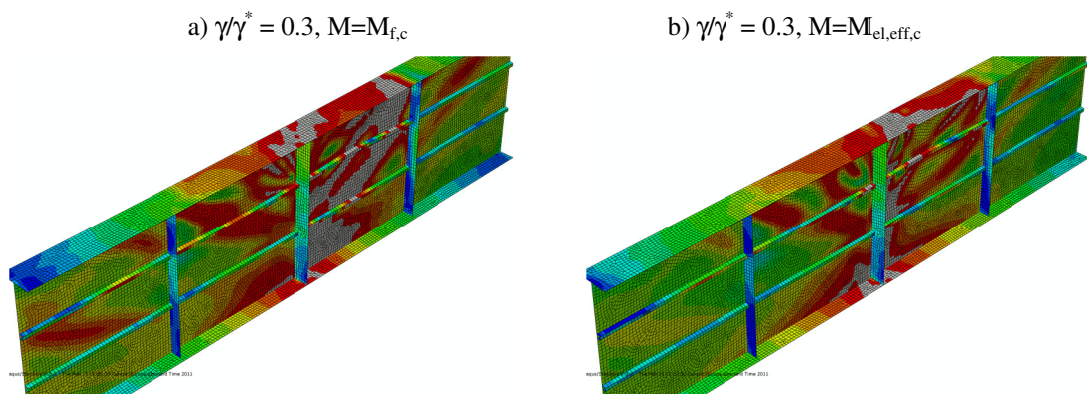


Figure 97: Von Mises stresses for girders stiffened with two closed stiffeners
Slika 97: Missesove primerjalne napetosti za nosilec ojačan z dvema zaprtima ojačitvama

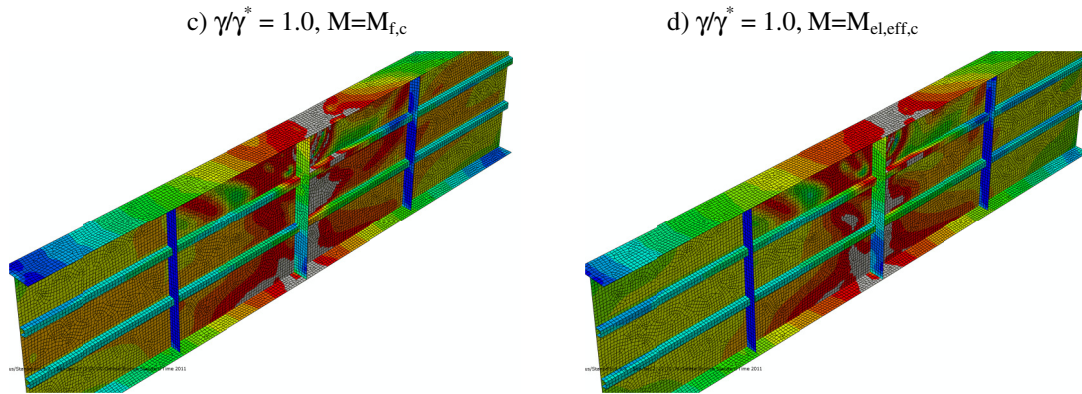


Figure 97: Von Mises stresses for girders stiffened with two closed stiffeners
Slika 97: Missesove primerjalne napetosti za nosilec ojačan z dvema zaprtima ojačitvama

6.3.4.4 Stiffness influence on girder's capacity

The stiffness of longitudinal stiffeners significantly influences the girder resistance and defines the buckling behaviour of the web panel. The increase of capacity is more obviously observed up to a certain point, up to which global buckling prevails. After this point slight additional contribution on girder's capacity is present due to a larger area and larger torsional stiffness of the stiffener.

In Figure 98 the influence of the stiffnesses on the girder resistance for girders stiffened with one open and closed stiffener at the position of $h_w/4$ and $h_w/2$, and for all load cases considered in this analysis is plotted. For girders stiffened with a stiffener at the middle of the web depth the transition stiffness, after which almost no additional resistance is gained, is clear. In all studied cases (all possible load cases) the necessary stiffnesses of the stiffener to reach this point are between 0.75 and 1.00. On the other hand this transition is not so obvious, when the stiffener is positioned in the upper part of the web ($h_w/4$) and exposed to high compression force due to bending. Surprisingly, for open stiffener in load cases 3 and 4 (see Figure 98) the girder's capacity decreases by increasing stiffness, which is not exactly clear why.

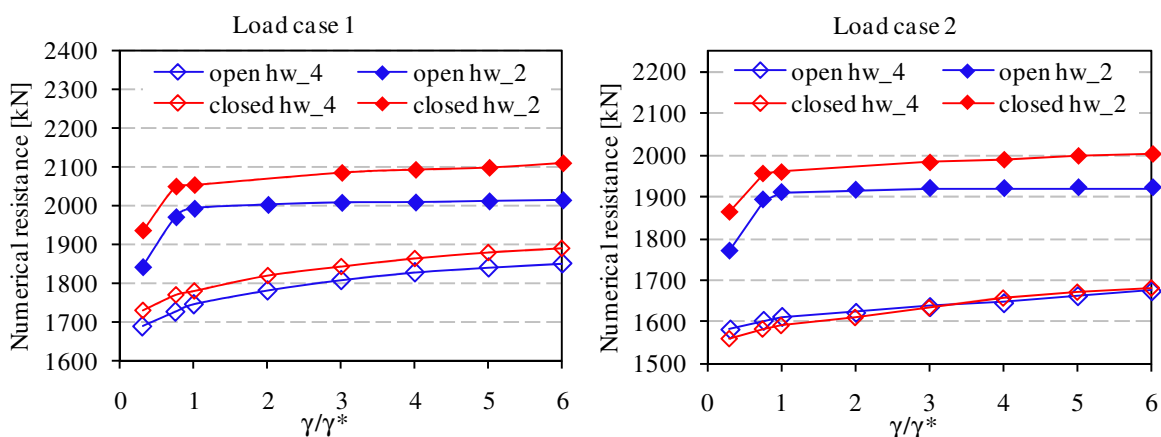


Figure 98: The influence of the stiffener stiffness on the girder resistance for girder stiffened with one stiffener
Slika 98: Vpliv togosti vzdolžne ojačitve na nosilnost nosilca ojačanega z eno ojačitvijo

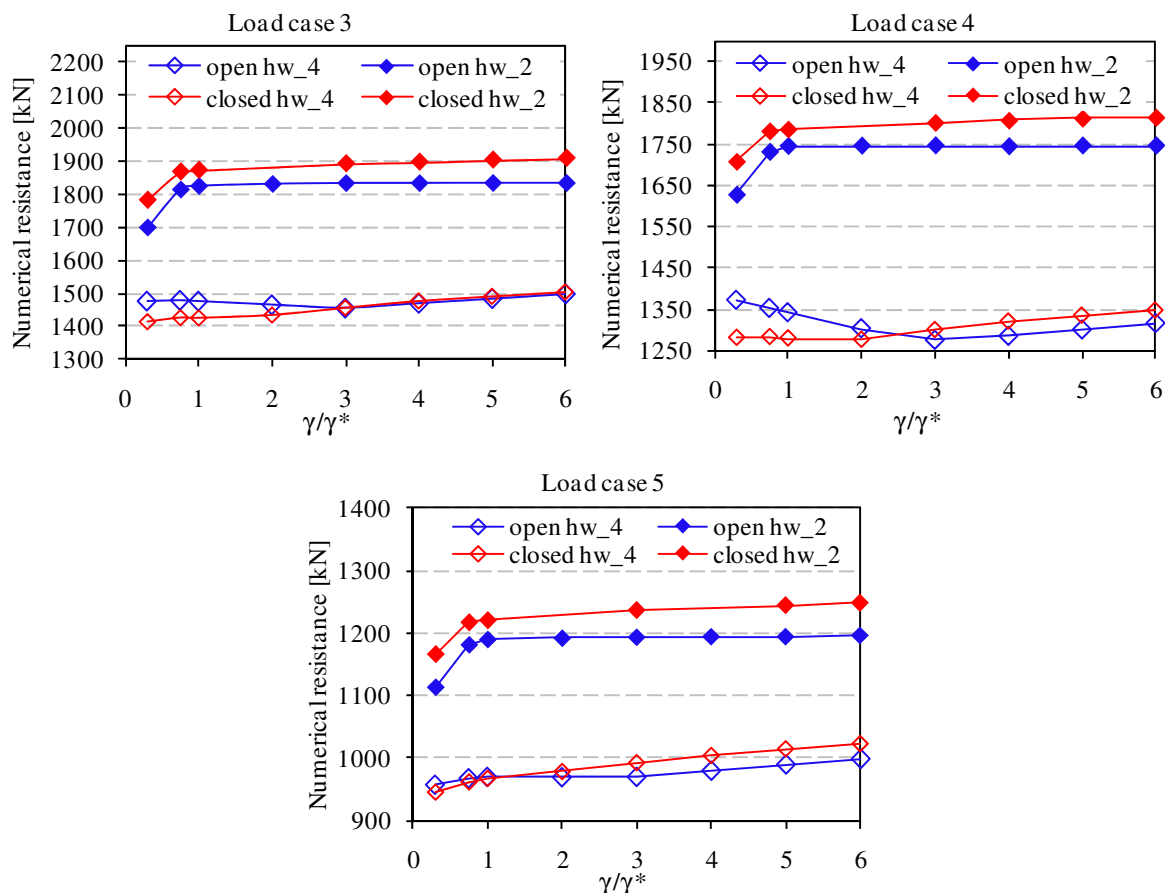


Figure 98: The influence of the stiffener stiffness on the girder resistance for girder stiffened with one stiffener
Slika 98: Vpliv togosti vzdolžne ojačitve na nosilnost nosilca ojačanega z eno ojačitvijo

In Figure 99 the influence of stiffener stiffness is shown for girder stiffened with two longitudinal stiffeners. The obtained results are similar to those obtained for the girder stiffened with one open stiffener at mid web depth. Also in this case the transition stiffness is found between values $\gamma/\gamma^* = 0.75$ and $\gamma/\gamma^* = 1.00$.

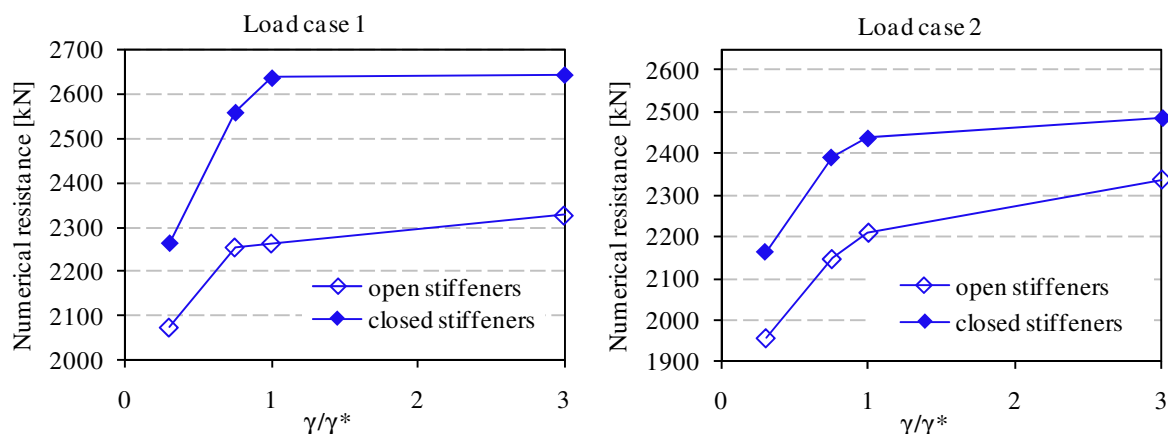


Figure 99: The influence of the stiffener stiffness on the girder resistance for girder stiffened with two stiffeners
Slika 99: Vpliv togosti vzdolžne ojačitve na nosilnost nosilca ojačanega z dvema ojačitvama

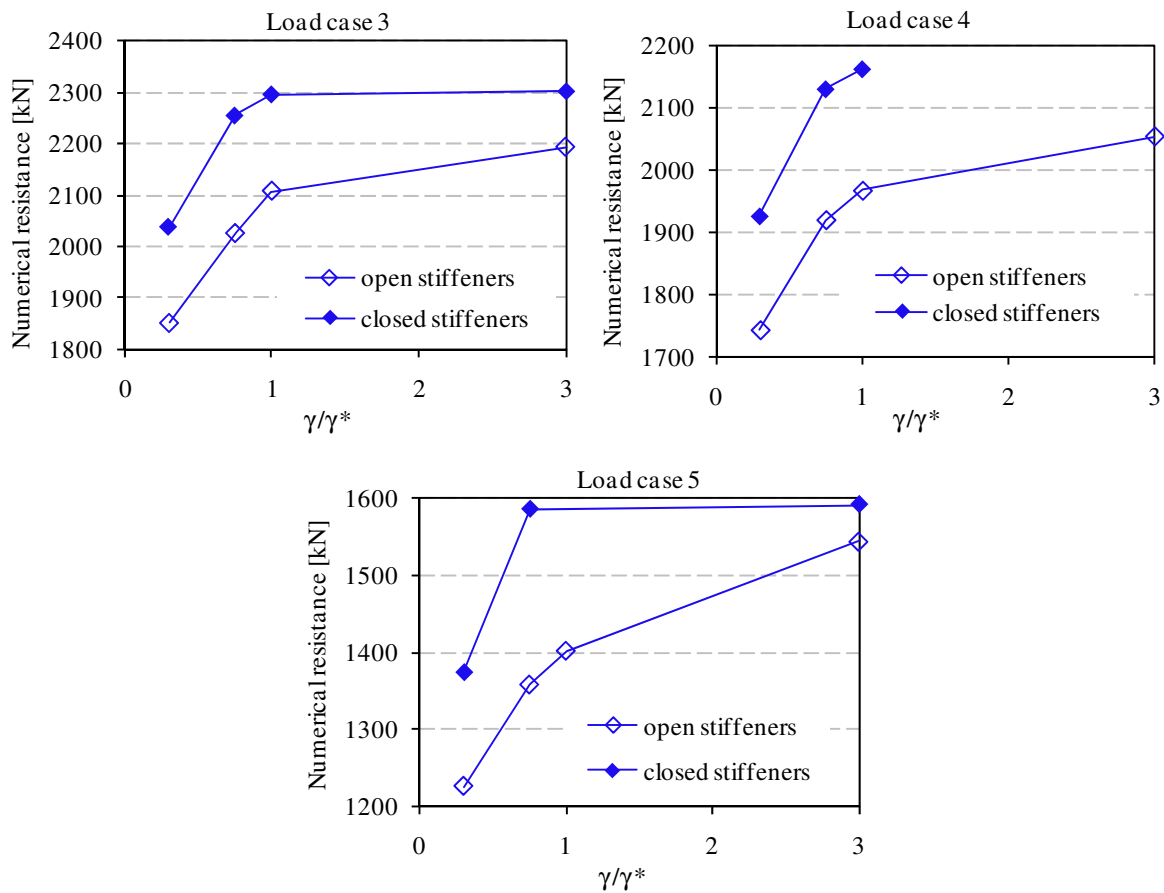


Figure 99: The influence of the stiffener stiffness on the girder resistance for girder stiffened with two stiffeners
Slika 99: Vpliv togosti vzdolžne ojačitve na nosilnost nosilca ojačanega z dvema ojačitvama

6.4 Discussion

In this chapter the results of numerical simulations for some typical parameters such as web slenderness, panel aspect ratio, stiffener stiffness and ratio of flange area to web area are presented through the stress distribution at the obtained maximum capacity of the girders. The main conclusions can be given as follows:

- At high shear load the yielding of the tension field and the yielding over the web depth is always present.
- By increasing bending moment and decreasing shear load in the web panel the yielding of the tension field in most cases disappears.
- For girders stiffened at $h_w/4$ the tension field was formed only in the largest subpanel.
- For girders stiffened at $h_w/2$ the tension field was formed in both subpanels with yielding present mainly in the upper subpanel, which is also loaded with compression stresses.
- If a weak stiffener is applied to the girder, the global buckling of the web is clearly induced.
- For two equally spaced closed stiffeners the stiffness between $\gamma/\gamma^* = 0.75$ to $\gamma/\gamma^* = 1.00$ sets a limit, after which only a slight increase of capacity by numerical simulations is

obtained. Greater stiffnesses mainly due to larger area of the stiffener are therefore not effective.

- For two equally spaced open stiffeners the transition in girder's capacity is also found between $\gamma/\gamma^* = 0.75$ and $\gamma/\gamma^* = 1.00$. After the transition point the increase of the girder resistance is still observed in all studied cases.

7 M-V INTERACTION

7.1 Introduction

The collapse behaviour of plated girders under combination of high bending and shear load has widely been studied through experimental and numerical analyses. For the sake of predicting the capacity of girders at the ultimate limit state different models were developed by researchers. In general these models are based on plastic theory and are modified on the basis of experimental tests. The interaction of both actions was established with bending moment M taken at $h_w/2$ from the high-moment end of the panel or at the mid panel if $a < h_w$ in the first case and at distance of $h_{w1,max}/2$ in the second case (see Figure 118).

In Chapter 2 the need of completing the existing database on tests specimens considering M-V interaction was discussed. Further on, a major contribution of this work was presented in Chapters 3 and 6, in which the results of numerical simulations of the total amount of 630 longitudinally stiffened plated girders were presented. The numerical results will be compared against a current formulation in EN 1993-1-5 and a new proposed model.

7.2 Girder resistance according to EN 1993-1-5

The resistance of the girder according to EN 1993-1-5 is defined separately for each effect. After the contributions of each effect have been calculated, the final resistance is obtained taking into account the appropriate interaction. Thus, in this chapter, the shear and bending resistance of longitudinally stiffened girder will be discussed.

7.2.1 Resistance to shear load

Within the behaviour of slender plates two phenomena can be observed: the state of pure shear which is present until elastic buckling stress is achieved and the tension field which starts to form after the elastic buckling stress has been reached. If the shear stresses τ , which are lower than the critical shear stresses, are transformed into principal stresses, they correspond to principal tensile stress σ_1 and principal compressive stress σ_2 with equal magnitude and inclination of 45° in accordance with the longitudinal axis of the girder. After buckling, the post-critical shear resistance by formation of a tension field is achieved. Due to buckling, no significant increase of stresses in the direction of principal compressive stresses σ_2 is possible, whereas the principal tensile stresses can still increase. The stress state in the web is in equilibrium with external shear load and no anchorage is needed to assure formation of tension field.

Different tension field theories of plates under shear have been developed to determine their resistance; for further details see Johansson et al. [71] and Beg et al. [78]. In EN 1993-1-5 the rotated stress field theory proposed by Höglund is adopted. The rotated stress field method was developed also for girder with larger panel aspect ratios ($\alpha > 3$), because in this case other existing models lead to very conservative results.

In this method, the shear resistance $V_{b,Rd}$ is determined with the contribution of the web $V_{bw,Rd}$ and of flanges $V_{bf,Rd}$ and is limited with plastic shear resistance of the web alone:

$$V_{b,Rd} = V_{bw,Rd} + V_{bf,Rd} \leq h_w \cdot t_w \cdot \frac{\eta \cdot f_{yw}}{\sqrt{3} \cdot \gamma_{M1}} \quad (26)$$

In case of M-V interaction only the contribution of the web has to be evaluated. The equation for shear resistance of the web is given by:

$$V_{bw,Rd} = \chi_w \cdot h_w \cdot t_w \cdot \frac{f_{yw}}{\sqrt{3} \cdot \gamma_{M1}} \quad (27)$$

where χ_w is the reduction factor for shear buckling. The reduction factor considers components of pure shear and tension field action. Depending on the stiffness of the transverse end stiffeners the reduction factor reads:

- For non-rigid end post:

$$\begin{aligned} \chi_w &= \eta \text{ for } \bar{\lambda}_w < \frac{0.83}{\eta} \\ \chi_w &= \frac{0.83}{\bar{\lambda}_w} \text{ for } \bar{\lambda}_w \geq \frac{0.83}{\eta} \end{aligned} \quad (28)$$

- For rigid end post:

$$\begin{aligned} \chi_w &= \eta \text{ for } \bar{\lambda}_w \leq \frac{0.83}{\eta} \\ \chi_w &= \frac{0.83}{\bar{\lambda}_w} \text{ for } \frac{0.83}{\bar{\lambda}_w} \leq \bar{\lambda}_w \leq 1.08 \\ \chi_w &= \frac{1.37}{0.7 + \bar{\lambda}_w} \text{ for } \bar{\lambda}_w \geq 1.08 \end{aligned} \quad (29)$$

where $\eta=1.2$ for steel grades up to $f_y \leq 460 \text{ MPa}$ and $\eta=1.0$ for higher steel grades.

The reduction curves according to Eqs. (28) and (29), plotted in Figure 100, are based on the plate slenderness $\bar{\lambda}_w$. For longitudinally stiffened panel the largest slenderness $\bar{\lambda}_w$ of all sub-panels and the whole stiffened panel is taken into account. $\bar{\lambda}_w$ is given by:

$$\bar{\lambda}_w = \sqrt{\frac{f_{yw} / \sqrt{3}}{\tau_{cr}}} \quad (30)$$

The critical shear stress can be determined by hand calculations according to formulas given in EN 1993-1-5. Alternatively, buckling charts and software tools may be used.

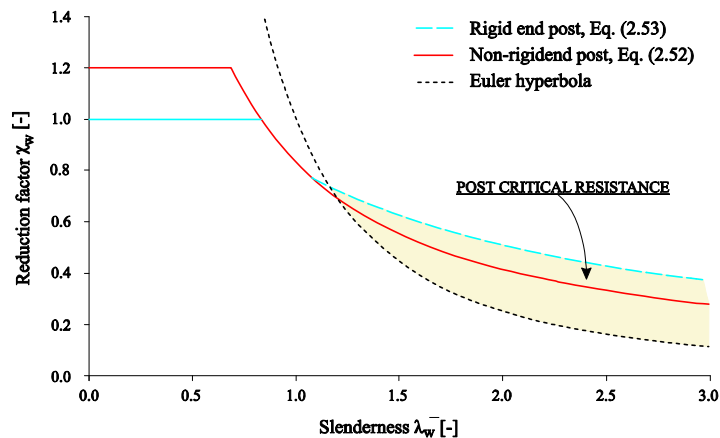


Figure 100: Reduction curves for shear buckling
Slika 100: Redukcijske krivulje za strig

7.2.2 Resistance to bending moment

The bending resistance of the longitudinally stiffened girder is determined on the basis of effective width method, where the bending resistance of the element is determined with effective characteristics of the cross-section:

$$M_{eff,Rd} = \frac{W_{y,eff} \cdot f_y}{\gamma_{M0}} \quad (31)$$

where $W_{y,eff}$ is the effective elastic section modulus, f_y is the yield stress of the material and γ_{M0} is the partial safety factor.

Three phenomena have to be considered when calculating effective characteristics of longitudinally stiffened plated I girder: shear lag effect, local buckling of the subpanels and global buckling of the whole web panel. The shear lag effect is present in both compression and tension elements, while the buckling is present only in compression elements. If both phenomena, i.e. shear lag and buckling, are present, the interaction of both influences has to be taken into account. In this particular study the flanges were designed to avoid any reduction due to shear lag effect. All considered flanges were in class 2 cross-section.

When the effective cross-section is determined, it can be treated as an equivalent class 3 cross-section, with the assumption of linear elastic strain and stress distribution over the reduced cross-section. The ultimate resistance is defined with the yielding in the centre of the plate located furthest from the centre of the cross-section. In general, the calculation of effective widths requires an iterative procedure which ends when the difference between two steps is sufficiently small.

Depending on the panel aspect ratio $\alpha = a/b$ of the plate the buckling of the plate can be treated either as "two-dimensional" plate-like behaviour or as "one dimensional" column-like behaviour. For unstiffened panels the column-like behaviour occurs at aspect ratio α much below 1.0, while for longitudinally stiffened panels with emphasized orthotropic properties such behaviour may start at aspect ratios larger than 1.0. In cases when ultimate resistance depends on both types of buckling, plate-like as well as column like, a suitable interpolation between both types of behaviour with interpolation function given in EN 1993-1-5 is considered.

The plates in column-like buckling are treated as unsupported along the longitudinal edges. Therefore, critical stresses for plate-like buckling are always larger than critical stresses for column-like buckling.

7.2.2.1 Local buckling - effective widths

Effective width b_{eff} of the slender unstiffened plates in compression is obtained with the buckling reduction factor ρ_{loc} :

$$b_{eff} = \rho_{loc} \cdot b \quad (32)$$

In EN 1993-1-5 the reduction factor ρ_{loc} is given by the modified Winter formula [79] for effective widths of slender plates and is prescribed for:

- Internal compression plate elements:

$$\rho_{loc} = \begin{cases} 1 & \text{for } \bar{\lambda}_p \leq 0.5 + \sqrt{0.085 - 0.055\psi} \\ \frac{\bar{\lambda}_p - 0.055(3 + \psi)}{\bar{\lambda}_p^2} & \text{for } \bar{\lambda}_p > 0.5 + \sqrt{0.085 - 0.055\psi} \end{cases} \quad (33)$$

- And for outstand compression plate elements:

$$\rho_{loc} = \begin{cases} 1 & \text{for } \bar{\lambda}_p \leq 0.748 \\ \frac{\bar{\lambda}_p - 0.188}{\bar{\lambda}_p^2} & \text{for } \bar{\lambda}_p > 0.748 \end{cases} \quad (34)$$

where ψ is the ratio of stresses at both edges of the plate with maximum compression stress in the denominator and $\bar{\lambda}_p$ is the plate slenderness defined as:

$$\bar{\lambda}_p = \sqrt{\frac{f_y}{\sigma_{cr,p}}} \quad (35)$$

where the elastic critical plate buckling stress $\sigma_{cr,p}$ reads:

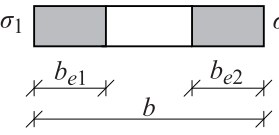
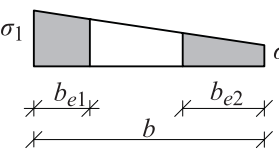
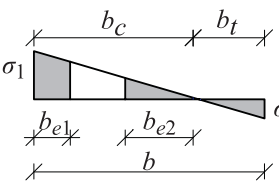
$$\sigma_{cr,p} = k_\sigma \frac{\pi^2 \cdot E}{12 \cdot (1 - \nu^2)} \left(\frac{t}{b} \right)^2 \quad (36)$$

Where b is the plate width, t is the plate thickness, E is the elastic modulus of the steel, ν is the Poisson's ratio of steel and k_σ is the plate buckling coefficient, which depends on the stress ratio ψ and boundary conditions. For plates with panel aspect ratio $\alpha = a/b \geq 1$ k_σ is given in Table 16 and Table 17, and for plates with $\alpha < 1$ and for uniform compression as:

$$k_\sigma = \left(\alpha + \frac{1}{\alpha} \right)^2 \quad (37)$$

The critical factor is calculated assuming that all four edges of the plate are simply supported. For the case of pure compression the effective widths are symmetrically distributed, while for other stress distributions the effective widths are specified with expressions in Table 16 and Table 17.

Preglednica 16: Sodelujoča širina za notranje tlačene elemente [78]
 Table 16: Effective width for internal compression elements [78]

| Stress distribution (compression positive) | | | | Effective width b_{eff} | | |
|---|-----|-------------------|-----|--|------|------------------|
|  | | | | $\psi = 1$ $b_{eff} = \rho b$ $b_{e1} = 0.5b_{eff} \quad b_{e2} = 0.5b_{eff}$ | | |
|  | | | | $1 > \psi \geq 0$ $b_{eff} = \rho b$ $b_{e1} = \frac{2}{5-\psi} b_{eff} \quad b_{e2} = b_{eff} - b_{e1}$ | | |
|  | | | | $\psi < 0$ $b_{eff} = \rho b_c = \rho b / (1-\psi)$ $b_{e1} = 0.4b_{eff} \quad b_{e2} = 0.6b_{eff}$ | | |
| $\psi = \sigma_2 / \sigma_1$ | 1 | $1 > \psi > 0$ | 0 | $0 > \psi > -1$ | -1 | $-1 > \psi > -3$ |
| Buckling coefficient k_σ | 4.0 | $8.2/(1.05+\psi)$ | 7.8 | $7.81-6.29\psi+9.78\psi^2$ | 23.9 | $5.98(1-\psi)^2$ |

Preglednica 17: Sodelujoča širina za zunanje tlačene elemente [78]
 Table 17: Effective width for external compression elements [78]

| | | | | | |
|--|------|-------------------------|--|--------------------------------|------|
| Stress distribution (compression positive) | | | Effective ^p width b_{eff} | | |
| | | | $1 > \psi \geq 0$ $b_{eff} = \rho b$ | | |
| | | | $\psi < 0$ $b_{eff} = \rho b_c = \rho b / (1 - \psi)$ | | |
| $\psi = \sigma_2 / \sigma_1$ | 1 | 0 | -1 | $-1 \geq \psi \geq -3$ | |
| Buckling coefficient k_σ | 0.43 | 0.57 | 0.85 | $0.57 - 0.21\psi + 0.07\psi^2$ | |
| | | | $1 > \psi \geq 0$ $b_{eff} = \rho b$ | | |
| | | | $\psi < 0$ $b_{eff} = \rho b_c = \rho b / (1 - \psi)$ | | |
| $\psi = \sigma_2 / \sigma_1$ | 1 | $1 > \psi > 0$ | 0 | $0 > \psi > -1$ | 1 |
| Buckling coefficient k_σ | 0.43 | $1.578 / (\psi + 0.34)$ | 1.7 | $1.7 - 5\psi + 17.1\psi^2$ | 23.8 |

7.2.2.2 Plate-like buckling

The plate buckling of longitudinally stiffened plates is the buckling of the entire panel, composed of a plate and stiffeners. If the sub-panels are slender and subjected to local buckling, the interaction of local and global plate buckling is taken into account by the modified plate slenderness for pure compression:

$$\bar{\lambda}_p = \sqrt{\frac{N_y}{N_{cr}}} = \sqrt{\frac{A_{c,eff,loc} \cdot f_y}{A_c \cdot \sigma_{cr,p}}} = \sqrt{\frac{\beta_{A,c} \cdot f_y}{\sigma_{cr,p}}} \tag{38}$$

where $\sigma_{cr,p}$ is the elastic critical buckling stress of a stiffened plate, A_c is the gross cross-section of the compression zone of the stiffened plate excluding edge parts along longitudinal edges and $A_{c,eff,loc}$ is calculated as:

$$A_{c,eff,loc} = A_{sl,eff} + \sum_i \rho_{loc,i} \cdot b_{loc,i} \cdot t \quad (39)$$

where $A_{sl,eff}$ is the sum of effective areas of longitudinal stiffeners, which takes into account local buckling, $\rho_{loc,i}$ is the reduction factor of each sub-panel i and $b_{loc,i}$ is the width of each individual sub-panel i .

The elastic critical stress $\sigma_{cr,p}$ may be determined by:

- Design charts for smeared or discretely spaced stiffeners,
- Simplified analytical expressions (two such expressions are given in EN 1993-1-5),
- Computer simulations.

Well known are Klöppel charts [80, 81] that contain critical values for discretely spaced and smeared stiffeners. The only drawback of these diagrams is that they are limited to the critical value for local buckling. Therefore, for stronger stiffeners the global critical stress cannot always be obtained from these diagrams.

Another option for the calculation of critical plate stress $\sigma_{cr,p}$ is to use general purpose FE software for structural applications or to use specialized software for plate buckling. In the framework of COMBRI project software EBPlate [82] was developed with the purpose to calculate critical stresses of the plate. By using specialized software such as ABAQUS the calculation of global buckling of the plate may become difficult when the local buckling modes prevail and the global buckling mode is very high.

Finally, the reduction factor for plate-like behaviour ρ is determined with expressions (33) and (34).

7.2.2.3 Column-like buckling

The critical elastic column buckling stress $\sigma_{cr,c}$ is determined as the buckling stress $\sigma_{cr,sl}$ of a single stiffener closest to the panel edge having the highest compression stress:

$$\sigma_{cr,sl} = \frac{\pi^2 \cdot E \cdot I_{sl,1}}{A_{sl,1} \cdot a^2} \quad (40)$$

where $I_{sl,1}$ is the second moment of area of the gross cross-section of the stiffener and adjacent parts of the plate, $A_{sl,1}$ is the gross cross-section of the stiffener and adjacent parts of the plate and a is the buckling length of a stiffener normally equal to the distance between rigid transverse stiffeners.

The critical stress of the stiffener $\sigma_{cr,sl}$ is then extrapolated to the edge of the stiffened plate using equation:

$$\sigma_{cr,c} = \frac{b_c}{b_{c2}} \cdot \sigma_{cr,sl} \quad (41)$$

where b_c is the width of the stiffened plate in compression and b_{c2} is the distance from neutral axis to the critical stiffener where $\sigma_{cr,sl}$ is evaluated. For uniform compression, the elastic critical column buckling is $\sigma_{cr,c} = \sigma_{cr,sl}$.

The column slenderness $\bar{\lambda}_c$ for stiffened plates is then defined as:

$$\bar{\lambda}_c = \sqrt{\frac{\beta_{A,c} \cdot f_y}{\sigma_{cr,c}}} \quad (42)$$

$$\beta_{A,c} = \frac{A_{sl,1,eff}}{A_{sl,1}}$$

where $A_{sl,1,eff}$ is the effective cross sectional area of the stiffener and adjacent parts of the plate with due allowance for plate buckling of the sub-panels.

The corresponding column reduction factor χ_c for stiffened plates is obtained from:

$$\chi_c = \frac{1}{\Phi + \sqrt{\Phi^2 - \bar{\lambda}_c^2}} \leq 1.0 \quad (43)$$

$$\Phi = 0.5 \left[1 + \alpha_e (\bar{\lambda}_c - 0,2) + \bar{\lambda}_c^2 \right] \quad (44)$$

$$\alpha_e = \alpha + \frac{0,09}{i/e}$$

$$i = \sqrt{\frac{I_{sl,1}}{A_{sl,1}}} \quad (45)$$

where $\alpha = 0.34$ for closed stiffener and $\alpha = 0.49$ for open stiffeners. The distance e is defined as the maximum of distances e_1 and e_2 , where for single sided stiffeners e_1 is the distance between the centres of gravity of the stiffener itself and the stiffener with the contributing plating and e_2 is the distance between the centres of gravity of the contributing plating alone and the stiffener with the contributing plating. For double-sided symmetrical stiffeners $e_1 = e_2$.

7.2.2.4 Interpolation between plate-like and column-like buckling

The interpolation between plate-like and column-like buckling becomes important for shorter plates. In order to obtain the final reduction factor ρ_c , in EN 1993-1-5 the following interpolation formula is given:

$$\rho_c = (\rho - \chi_c) \xi (2 - \xi) + \chi_c \quad (46)$$

$$\xi = \frac{\sigma_{cr,p}}{\sigma_{cr,c}} - 1, \text{ but } 0 \leq \xi \leq 1 \quad (47)$$

If reduction factor ρ_c is equal to 1.0, the stiffeners are fully effective and overall buckling involving stiffeners does not take place. At values $\rho_c < 1.0$ the stiffeners are not fully effective and they get involved in the overall buckling of the plate. The final effective area of the compression zone $A_{c,eff}$ of the longitudinally stiffened plates is determined by the following expression:

$$A_{c,eff} = \rho_c \cdot A_{c,eff,loc} + \sum_i b_{i,edge,eff} \cdot t \quad (48)$$

When calculating the geometrical properties A_{eff} , I_{eff} , W_{eff} of the final effective area of the cross-section, the thicknesses of the stiffeners t_{st} and of the contributing plating t are replaced with reduced thicknesses $t_{st} \cdot \rho_c$ and $t \cdot \rho_c$.

7.2.3 M-V interaction

The bending-shear interaction for I girders is considered if the bending load is higher than the bending capacity of the flanges $M_{f,Rd}$. The interaction is given by the following expression:

$$\bar{\eta}_1 + \left(1 - \frac{M_{f,Rd}}{M_{pl,Rd}}\right) (2\bar{\eta}_3 - 1)^2 \leq 1.0 \quad (49)$$

where

$$\bar{\eta}_1 = \frac{M_{Ed}}{M_{pl,Rd}} \quad \text{and} \quad \bar{\eta}_3 = \frac{V_{Ed}}{V_{bw,Rd}}$$

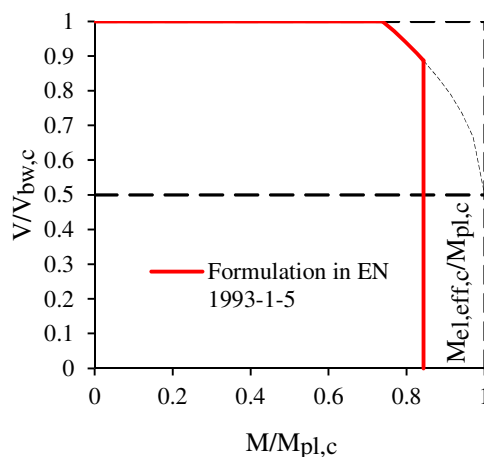


Figure 101: M-V interaction according to EN 1993-1-5
Slika 101: M-V interakcija po EN 1993-1-5

For longitudinally unstiffened girders the interaction criterion should be met in all sections other than those located at a distance less than $h_w / 2$ from the most stressed edge. For longitudinally stiffened girders Johansson et al. [71] suggested to perform interaction check at a distance of $h_{wi,max} / 2$ (see Figure 118) from the most stressed edge. This recommendation was given on the basis of engineering judgment. At this cross-section the interaction check is made to take into account a positive effect of the gradient of bending moments.

The recommended distance may lead to conservative results, especially for a large number of equidistantly spaced longitudinal stiffeners where the interaction check is performed very close to maximum value of the bending moment.

In this study the distance of $\min(0.4a, h_w / 2)$ from the most stressed edge was proposed for the interaction check. Furthermore, the interaction check was also established at a distance of $h_{wi,max} / 2$ as recommended by Johansson et al. [71].

7.3 Evaluation of current M-V interaction

The characteristic resistance was calculated and compared to results of numerical simulations. The internal forces obtained with numerical model were evaluated at the distance of $\min(0.4a, h_w/2)$ and $h_{wi,max}/2$ from the most stressed edge.

The numerical results are plotted on the M-V interaction domain from where also the general response and the influence of bending moment on the ultimate shear capacity can be seen. The markers which are below the interaction curve in the range of M_f to $M_{el,eff}$ are on the unsafe side and vice versa, if the markers are above the interaction curve, the results are safe.

The numerical results for group I (see Table 15) are plotted in Figure 102. They are plotted in non-dimensional format. The shear load is normalized with characteristic shear resistance of the web and the bending moment with characteristic plastic bending moment. For each A_f/A_w ratio a different M-V interaction curve should be plotted, but in the figure two interaction curves for ratios of $A_f/A_w = 0.3$ and $A_f/A_w = 1.1$ are plotted. Vertical lines which denote the effective characteristic resistance of the girder for the same ratios are added. The numerical results are plotted for girders stiffened with open and closed stiffeners positioned at $h_w/4$ and $h_w/2$.

All girders that were stiffened with one stiffener positioned at $h_w/4$ show higher resistance than the one predicted in accordance with EN 1993-1-5. When the stiffener is positioned in the mid web depth, the numerical resistance is found on the unsafe side for load cases 2, 3 and 4 (for load cases see Figure 76 and Table 15), when the interaction is checked at a distance of $\min(0.4a, h_w/2)$. The numerical resistance is always on safe side when the interaction is checked at a distance of $h_{wi,max}/2$. For all studied cases the linear interaction rule is found between shear load and bending moment.

The numerical results for studied group II, where the varied parameter is the slenderness of the web, are plotted in Figure 103. The difference between M-V interaction curves for various slendernesses is negligible, therefore only one interaction curve was plotted. The only difference obtained for different slendernesses of the web, though, is the vertical line which denotes elastic effective bending resistance. The first and the second vertical line belong to girders with the highest slenderness ($h_w/t_w = 400$), stiffened with stiffener at the mid web depth (first line) and at $h_w/4$ (second line). The other two vertical lines belong to girders with the lowest slenderness ($h_w/t_w = 150$).

The results are plotted for girders stiffened with only one longitudinal stiffener. The numerical results prove higher resistance than the one obtained through EN 1993-1-5 at a distance of $\min(0.4a, h_w/2)$, for girders stiffened with longitudinal stiffener in compressed part of the web ($h_w/4$), while for girders stiffened at mid web depth the resistance obtained by numerical simulations is smaller for slendernesses $h_w/t_w \leq 200$. For interaction check at $h_{wi,max}/2$ all numerical results, except girder with low slenderness $h_w/t_w = 150$ and stiffener at mid web depth, prove higher resistance. The influence of tension stresses in the largest subpanel results in higher shear resistance, which can clearly be seen in Figure 103.

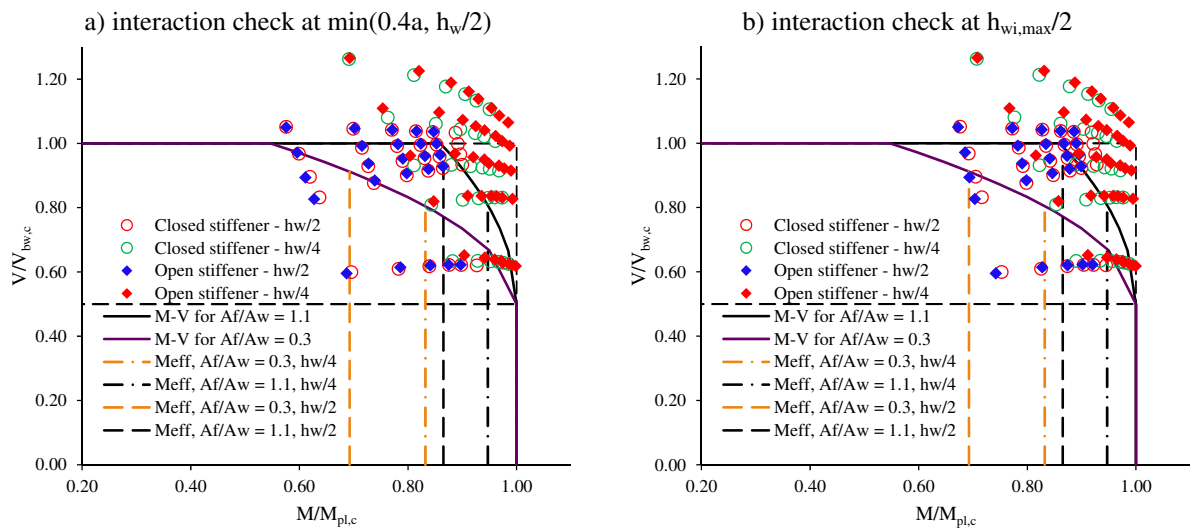


Figure 102: Numerical results plotted on current formulation of M-V interaction - GROUP I
Slika 102: Prikazani numerični rezultati na obstoječi M-V formulaciji - SKUPINA I

The shape of interaction curve depends on the slenderness of the web. For higher slendernesses $h_w / t_w \geq 200$ the shape of interaction is linear, while for slenderness $h_w / t_w = 150$ a nonlinear interaction is observed.

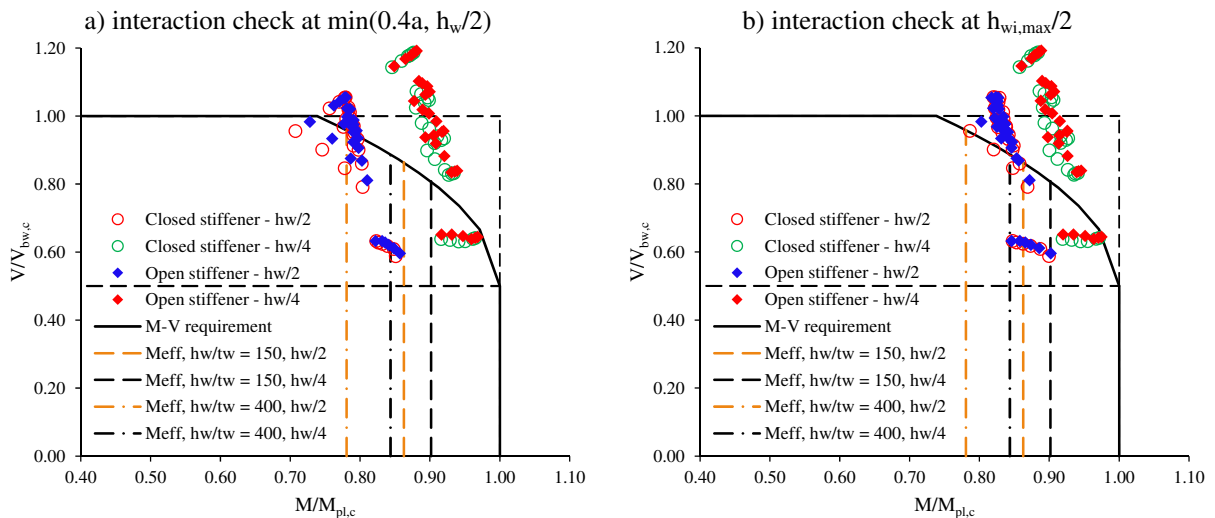


Figure 103 Numerical results plotted on current formulation of M-V interaction - GROUP II
Slika 103: Prikazani numerični rezultati na obstoječi M-V formulaciji - SKUPINA II

The numerical results of group III, where the influence of panel aspect ratio was studied, and the results of group IV, where the influence of stiffness of longitudinal stiffener was investigated, are plotted in Figure 104 and Figure 105. In both situations only one interaction curve corresponds to all calculations. The difference only exists in the vertical lines which indicate elastic effective bending resistance of the studied girders. The results are plotted only for girders stiffened with one stiffener.

The same conclusions can be drawn for these two groups. Girders, where critical shear sub-panel, which is according to EN 1993-1-5 decisive for shear resistance, is under tension, show much higher resistance. Inversely, when this sub-panel is under compression (this is found for girders stiffened with one stiffener in mid-panel and for girders stiffened with two equidistantly spaced stiffeners), the girder

resistance is smaller than the one obtained with EN 1993-1-5 for interaction check at $\min(0.4a, h_w / 2)$ otherwise for interaction check at $h_{w_i, \max} / 2$ also these results prove to be safe sided.

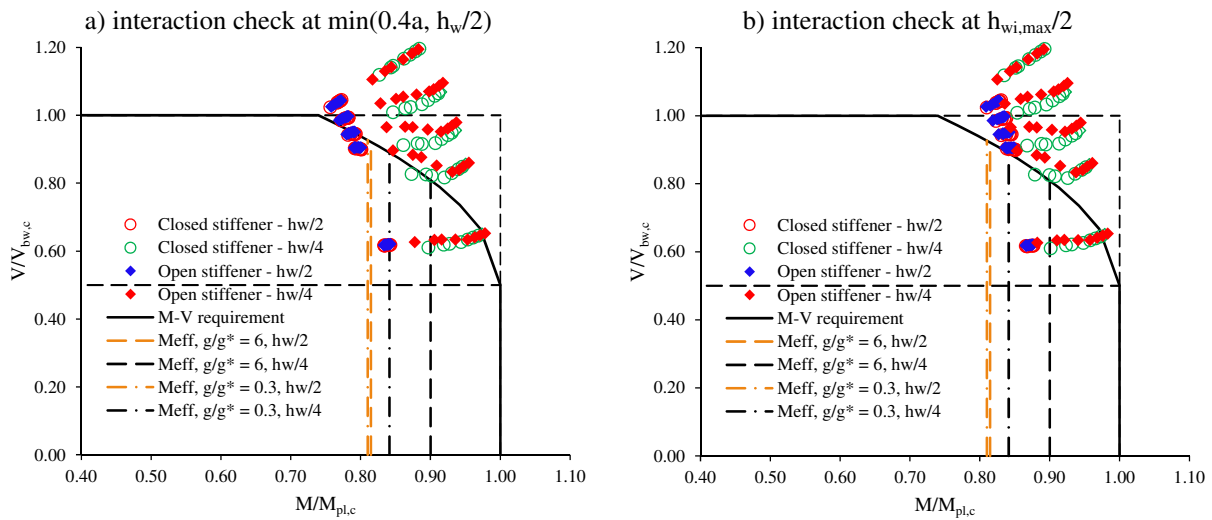


Figure 104: Numerical results plotted on current formulation of M-V interaction - GROUP III

Slika 104: Prikazani numerični rezultati na obstoječi M-V formulaciji - SKUPINA III

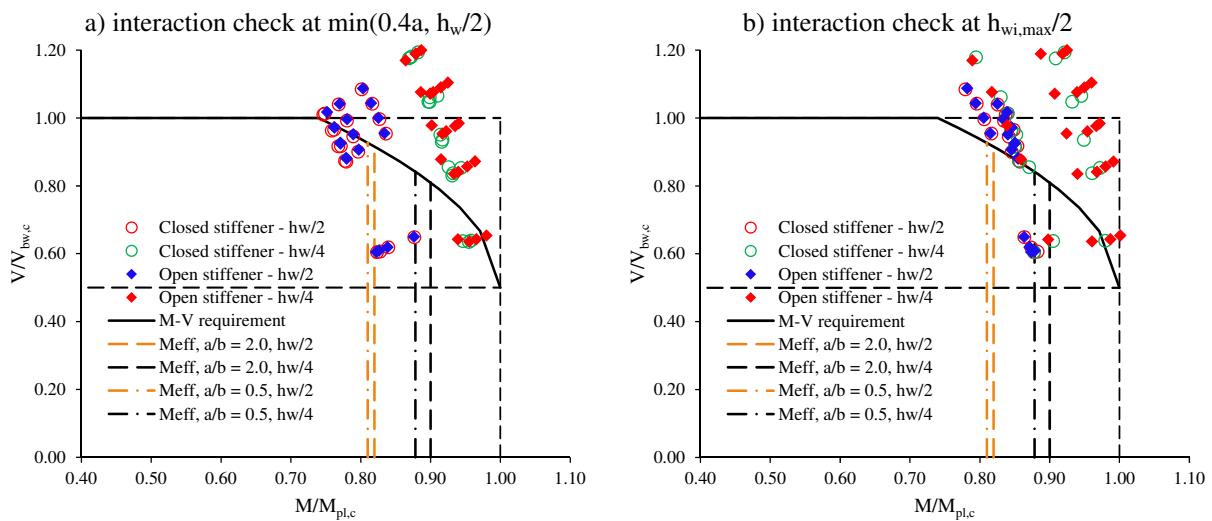


Figure 105: Numerical results plotted on current formulation of M-V interaction - GROUP IV

Slika 105: Prikazani numerični rezultati na obstoječi M-V formulaciji - SKUPINA IV

7.3.1 Discussion

The numerical results were normalized with characteristic values calculated in accordance with EN 1993-1-5 and plotted in diagrams together with the current M-V formulation. The results show some discrepancy between numerically obtained capacities and those obtained by the current formulation in EN 1993-1-5. The largest deviation is found for girders stiffened with one stiffener in compression zone. In these cases the numerical resistance is much higher due to positive effect of tension stresses in the largest subpanel which was critical for shear resistance. To explain the effect of stress state in the subpanel, the GMNIA numerical analysis was performed for a simply supported plate subjected to the combination of shear and normal stresses (see Figure 106). The analysis was performed on plates with the following slendernesses: $h_w / t_w = 55, 100, 150, 200$ and 250 . Material was modelled as bilinear

with nominal hardening slope and yield strength of 355 MPa. The global, one wave imperfection with amplitude of $\min(0.4a, h_w / 2)$ was considered in the nonlinear analysis.

The plate was simultaneously loaded with different combinations of shear and normal stresses. The maximum load obtained from the load-deflection curve defines the plate capacity. The results of numerical analysis are plotted in Figure 107. On horizontal axis the normal stresses applied on each edge are plotted. The negative values represent compression and the positive values tension stresses. On vertical axis the pure shear resistance of the plate normalized with shear resistance of the plate is plotted (the plate is loaded only with shear stresses).

It is generally well known that when dealing with compact cross-sections, the shear resistance decreases independent whether tensile or for compressive normal stresses are applied. The interaction is given by equation:

$$\left(\frac{\sigma}{f_y}\right)^2 + \left(\frac{\tau\sqrt{3}}{f_y}\right)^2 = 1.0 \quad (50)$$

Considering shear forces in equation (50) the interaction reads:

$$\left(\frac{\sigma}{f_y}\right)^2 + \left(\frac{V}{V_{f_y}}\right)^2 = 1.0. \quad (51)$$

The interaction formula (51) for compact plates is plotted with dashed line in Figure 107. Comparing results for different slendernesses of the plate the following conclusions can be drawn:

- With decreasing slenderness of the plate, the interaction between shear and normal stresses comes close to standard interaction given by equation (51), compatible with the von Mises yield criterion. This interaction is based on material yielding excluding the influence of buckling.
- The shear resistance may increase when the plate is subjected to tensile stresses. This increase depends on the plate slenderness and the normal stress amplitude in the plate. The maximum increase of 40% was obtained for a plate slenderness $h_w / t_w = 250$. At higher tensile stresses the shear resistance starts to decrease.
- When the plate is subjected to compressive normal stresses, the interaction shape depends on the slenderness of the web. At low slendernesses this interaction is quadratic; by increasing web slenderness the shape approaches to linear relationship.

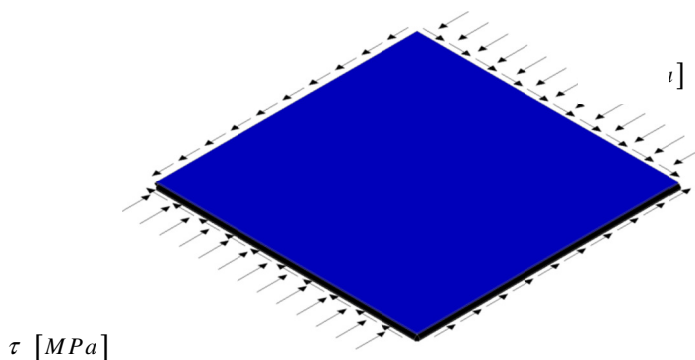


Figure 106: Numerical model of the plate

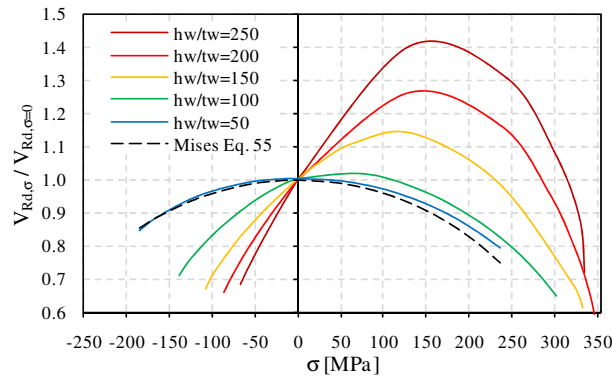
Slika 106: Numerični model pločevine

Figure 107: Reduction of shear capacity of the plate under different stress states

Slika 107: Redukcija strižne nosilnosti pločevine pri različnih nivojih normalnih napetostih

This phenomenon is reflected in the web, loaded with the combination of shear stresses and bending moments, and depends on the following parameters: stiffness of the longitudinal stiffeners and their positions which define critical subpanel slenderness. Since this phenomenon is difficult to take into account for all variables, the interaction is developed for the worst situations, in which the subpanels are loaded with the combination of shear and compressive stresses.

A comparison of the effective width method, the reduced stress method (both according to the EN1993-1-5) and numerical calculations is shown in Figure 108. The shear resistance calculated at different values of normal stresses is always normalized with pure shear resistance. The maximum resistance according to the reduced stress method (RSM) is given by the following equation:

$$\sqrt{\left(\frac{\sigma_{x,Ed}}{\rho_x \cdot f_y / \gamma_{M1}}\right)^2 + 3\left(\frac{\tau_{Ed}}{\chi_w \cdot f_y / \gamma_{M1}}\right)^2} = 1.0, \quad (52)$$

where $\sigma_{x,Ed}$ is the design stress due to normal force N_{Ed} , γ_{M1} is a partial safety factor, τ_{Ed} is the design stress load due to shear force V_{Ed} , ρ_x and χ_w are reduction factors which depend on the plate slenderness $\bar{\lambda}_p$:

$$\bar{\lambda}_p = \sqrt{\frac{\alpha_{ulr,k}}{\alpha_{cr}}}, \quad (53)$$

where $\alpha_{ulr,k}$ is a minimum load amplifier for which the design equivalent stress has to be increased to reach the characteristic yield strength f_y , and α_{cr} is the smallest factor for which the design equivalent stress has to be increased to reach the elastic equivalent critical stress.

The resistance according to the effective width method was determined considering the following expression:

$$\eta_1 + (2\bar{\eta}_3 - 1)^2 \leq 1.0, \quad (54)$$

with

$$\eta_1 = \frac{N_{Ed}}{f_y A_{eff} / \gamma_{M0}}, \quad \bar{\eta}_3 = \frac{V_{Ed}}{V_{bw,Rd}},$$

where A_{eff} is effective area of the plate determined according to Chapter 7.2.2.1, and $V_{bw,Rd}$ is a shear resistance of the plate determined in accordance with Chapter 7.2.1. Partial safety factors γ_{M0} and γ_{M1} were set to 1.0.

For small slenderness of the plate $h_w/t_w = 50$, the shape of interaction diagram is similar for all cases, while slightly higher reduction in shear resistance is found for the reduced stress method in the area of high compression stresses. For higher slenderness, the reduced stress method follows results of numerical simulation and considers the benefits of the tension stress to shear resistance. However, compared to the results of numerical simulation, the increase of shear resistance is much larger, which leads to unsafe results. The tension stresses in the plate have a stabilising effect which results in higher shear resistance.

In contrast to reduced stress method, the effective width method does not consider the benefit of tension stresses and reduces the shear resistance in the same way as for compression stresses. In the compression area the reduction according to the effective width method fits numerical results better than the reduced stress method (see Figure 108).

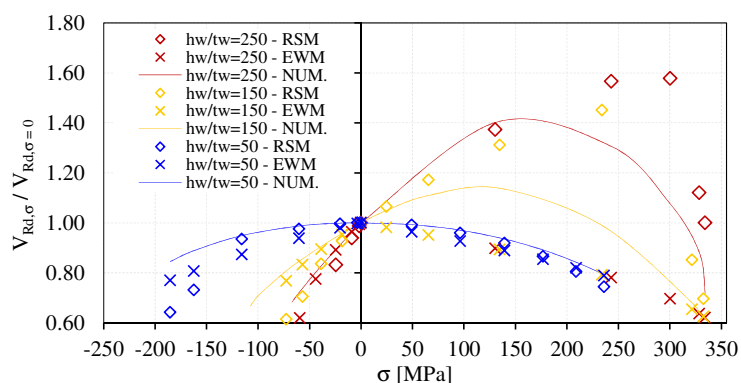


Figure 108: Reduction of shear resistance of the plate at different stress states, calculated by numerical simulation (NUM), reduced stress method (RSM) and effective width method (EWM)

Slika 108: Redukcija strižne odpornosti pločevine za različne nivoje normalnih napetosti izračunana z numerično simulacijo (NUM), z reducirano metodo napetosti (RSM) in z metodo effektivnih širin (EWM)

7.4 New proposal for M-V interaction

The results evaluated in Chapter 7.3 showed that the current interaction formula which was evaluated at a distance of $\min(0.4a, h_w/2)$ and at $h_{wi,max}/2$ from the most stressed edge was found unsuitable. First, the current interaction curve is described with quadratic formula while the obtained response of numerical results is in most cases linear. Secondly, the interaction formula at distance of $\min(0.4a, h_w/2)$ gives safe results only for girders that possess longitudinal stiffener at a distance of $h_w/4$. Therefore, for the area of large bending moment and shear force a new interaction equation is proposed and defined with:

$$\bar{\eta}_{1,new} + \left(1 - \frac{M_{f,Rd}}{M_{el,eff,Rd}}\right) (2\bar{\eta}_3 - 1)^\kappa \leq 1.0 \quad (55)$$

with

$$\bar{\eta}_{1,new} = \frac{M_{Ed}}{M_{el,eff,Rd}}$$

$$\kappa = 1$$

The differences compared to previous interaction formula are plastic bending resistance $M_{pl,Rd}$, which is replaced with elastic effective bending resistance $M_{el,eff,Rd}$, and the power κ on the second part of equation dealing with shear expression, which is removed. Both interactions valid for bending moment $M_{f,Rd} \leq M_{Ed} \leq M_{el,eff,Rd}$ are plotted in Figure 109. The new formula only gives the same resistance as the current one, when bending load is equal to bending capacity of flanges. For all other load combinations, the new proposal results in a lower resistance.

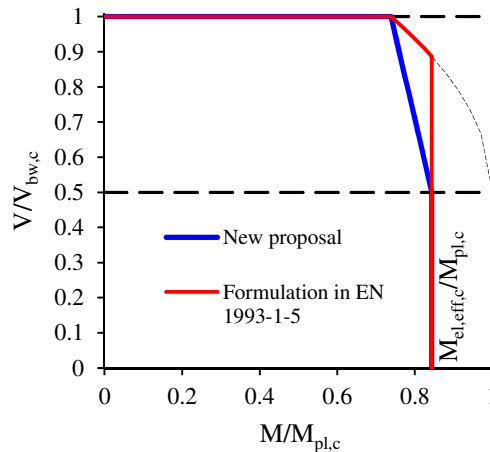


Figure 109: M-V interaction formulation – comparison

Slika 109: Primerjava M-V interakcij

In the sequel of this chapter the results considering both interaction formulas will be presented and discussed. The results will be presented as comparison of the normalized shear resistance for all five load cases (see Figure 76); the numerical shear resistance is normalized with the shear capacity obtained either by the current or by the proposed formulation. The suitability of both formulations will be discussed and estimated through statistical parameters, such as mean value and coefficient of standard deviation.

In Figure 110 to Figure 113 the comparison of results for girders stiffened with one stiffener is plotted. On the left side, the numerical results are compared against the current formulation, and on the right side against the proposed formulation. With the new formulation the bias over the load cases is eliminated, while the deviation within each load case remains the same. The largest deviation is found for load case 1, where the model was modelled to reach bending capacity of flanges $M_{el,eff,c}$. Such a large discrepancy between the girder with small flanges and the girder with large flanges can be caused by incorrectness in calculations of shear resistance. To solve this problem pure shear resistance of the girder should be determined taking into account the influence of flanges which represent the out-of-plane support to the web. For all other varied parameters the deviation for each load situation is within 10%.

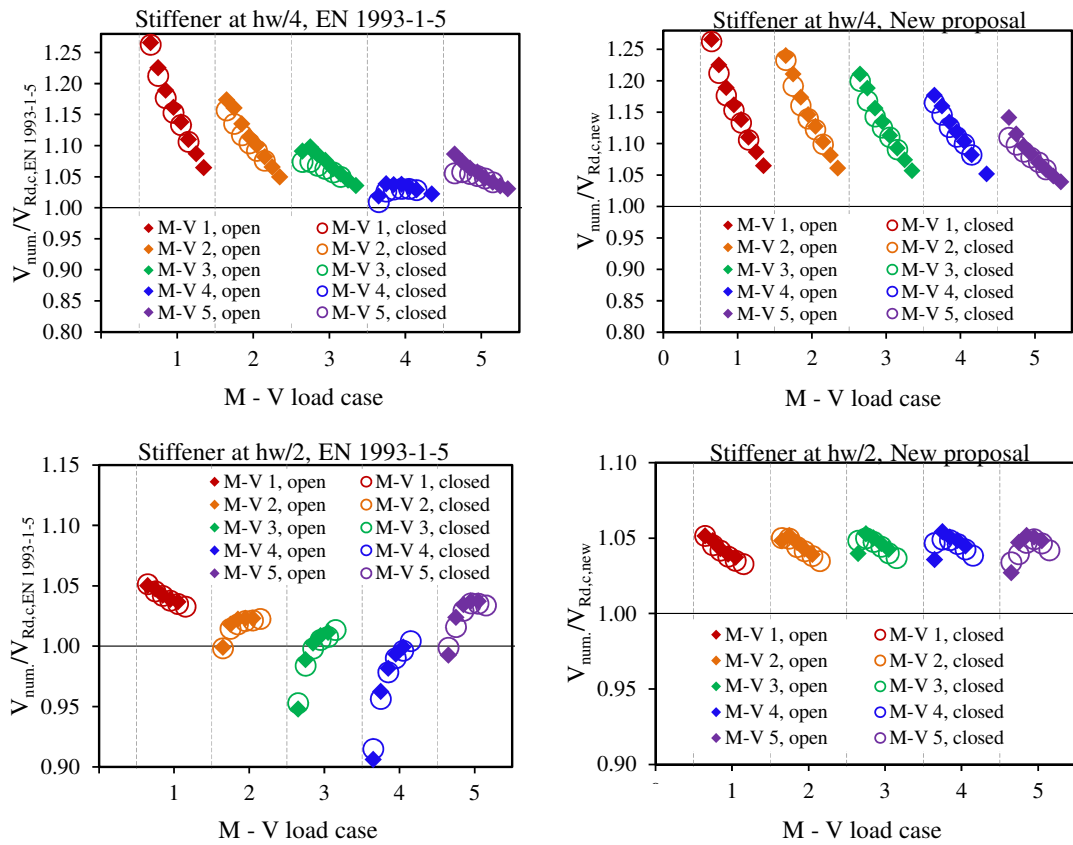


Figure 110: One stiffener, varied parameter A_f/A_w
 Slika 110: Ena ojačitev, variiran parameter A_f/A_w

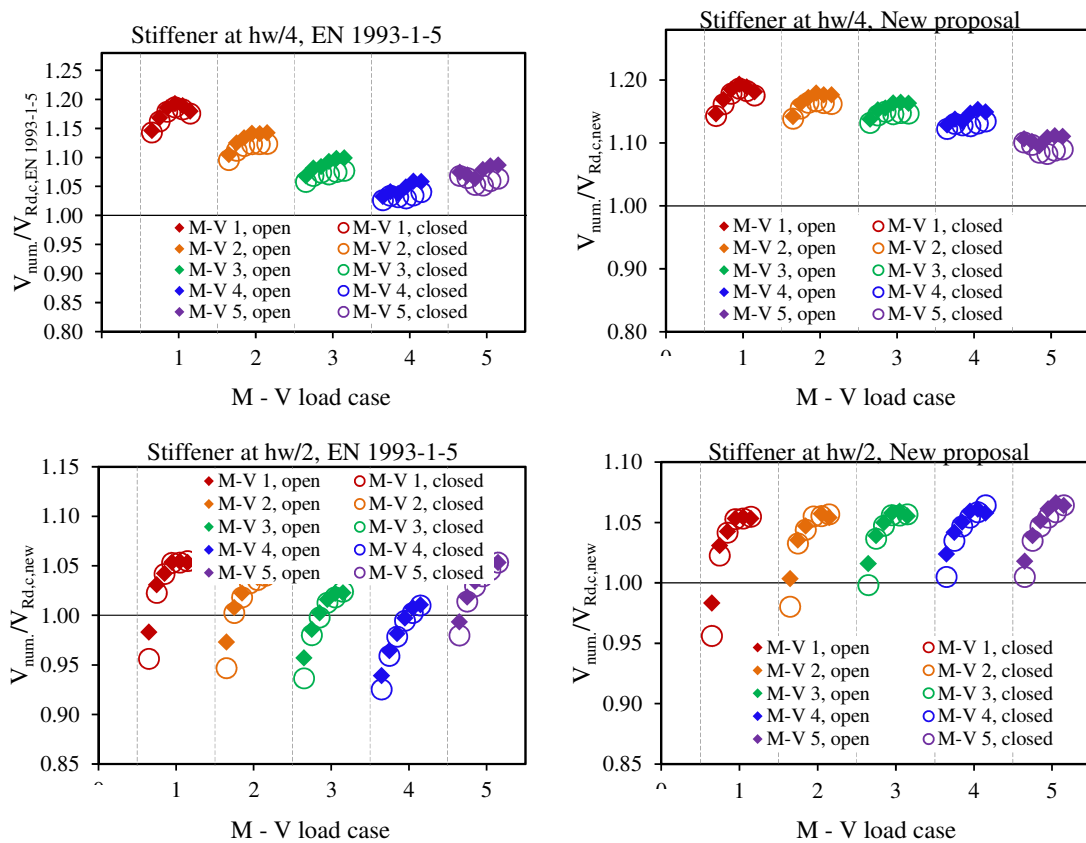


Figure 111: One stiffener, varied parameter h_w/t_w
 Slika 111: Ena ojačitev, variiran parameter h_w/t_w

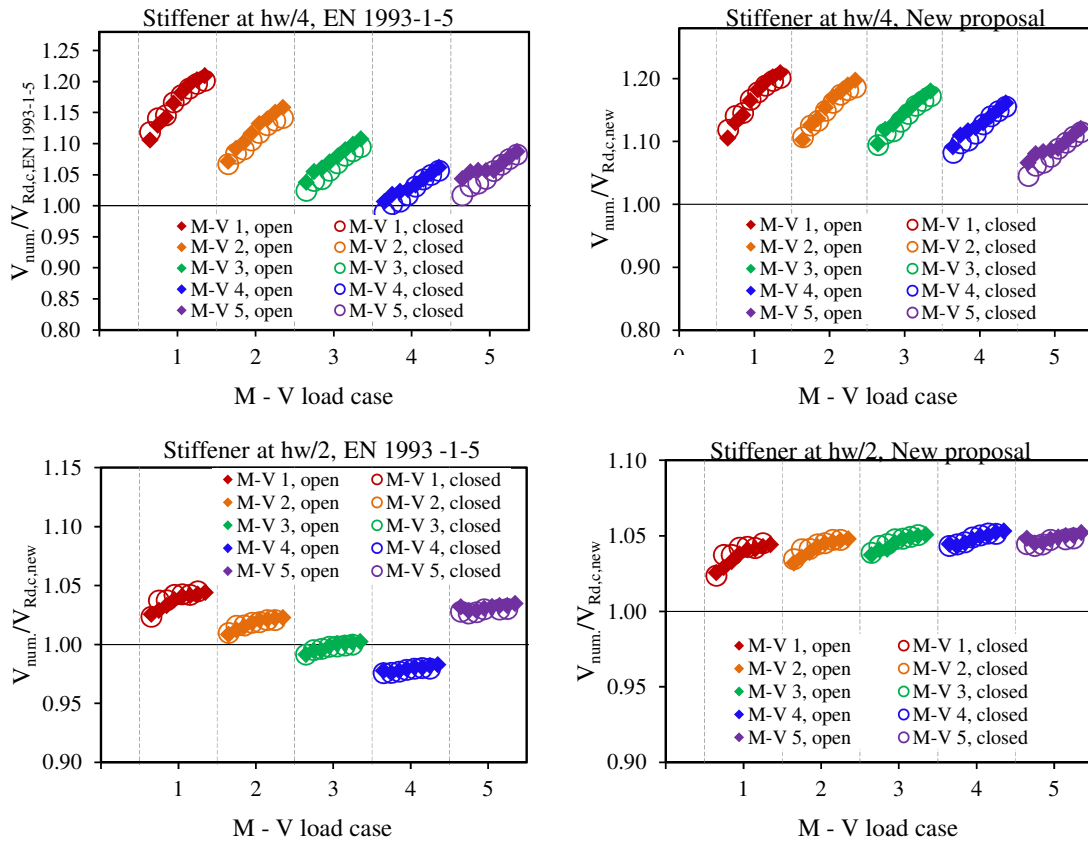


Figure 112: One stiffener, varied parameter γ/γ^*

Slika 112: Ena ojačitev, variiran parameter γ/γ^*

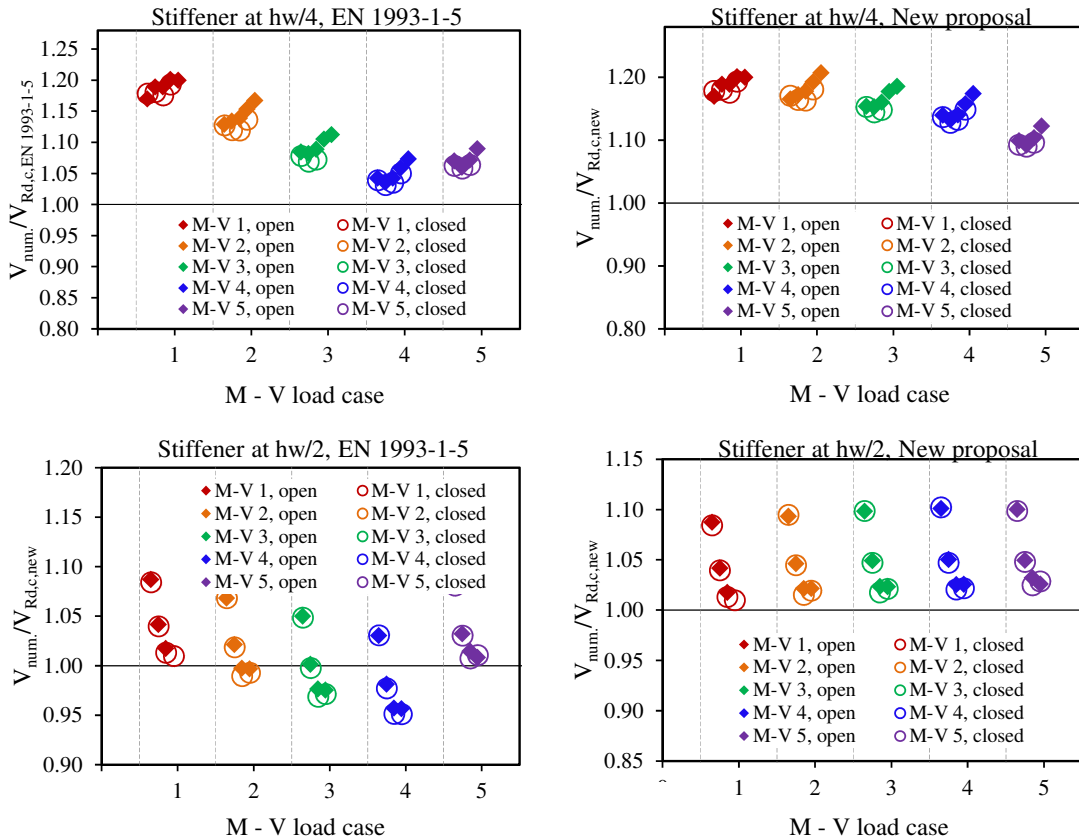


Figure 113: One stiffener, varied parameter α

Slika 113: Ena ojačitev, variiran parameter α

The results of statistical evaluation of both interaction models for girders stiffened with one stiffener are gathered in Table 18. The calculated parameters are mean value of $V_{num.} / V_{Rd,c}$, standard deviation and coefficient of variation. The proposed interaction model results in higher mean value and lower coefficient of variation for all studied variations of parameters.

Preglednica 18: Statistično ovrednotenje M-V interakcije za nosilce ojačane z eno ojačitvijo
 Table 18: Statistical evaluation of M-V interaction formulations for girders stiffened with one stiffener

| VARIED PARAMETER | POSITION AND TYPE OF THE STIFFENER | MEAN VALUE | | STANDARD DEVIATION | | COEFFICIENT OF VARIATION | |
|-------------------|------------------------------------|------------|-------|--------------------|-------|--------------------------|-------|
| | | EN 1993 | NEW | EN 1993 | NEW | EN 1993 | NEW |
| A_f/A_w | hw/4, open | 1.085 | 1.125 | 0.058 | 0.058 | 0.054 | 0.051 |
| | hw/4, closed | 1.085 | 1.135 | 0.060 | 0.050 | 0.055 | 0.044 |
| | hw/2, open | 1.009 | 1.045 | 0.034 | 0.006 | 0.033 | 0.006 |
| | hw/2, closed | 1.010 | 1.043 | 0.030 | 0.006 | 0.030 | 0.005 |
| h_w/t_w | hw/4, open | 1.103 | 1.150 | 0.048 | 0.028 | 0.044 | 0.024 |
| | hw/4, closed | 1.090 | 1.139 | 0.050 | 0.030 | 0.046 | 0.026 |
| | hw/2, open | 1.014 | 1.044 | 0.032 | 0.020 | 0.031 | 0.019 |
| | hw/2, closed | 1.009 | 1.040 | 0.037 | 0.026 | 0.036 | 0.025 |
| γ/γ^* | hw/4, open | 1.091 | 1.137 | 0.053 | 0.038 | 0.049 | 0.033 |
| | hw/4, closed | 1.083 | 1.132 | 0.056 | 0.039 | 0.052 | 0.035 |
| | hw/2, open | 1.013 | 1.044 | 0.022 | 0.006 | 0.022 | 0.006 |
| | hw/2, closed | 0.982 | 1.044 | 0.172 | 0.005 | 0.175 | 0.005 |
| α | hw/4, open | 1.112 | 1.161 | 0.054 | 0.033 | 0.048 | 0.028 |
| | hw/4, closed | 1.099 | 1.149 | 0.055 | 0.031 | 0.050 | 0.027 |
| | hw/2, open | 1.015 | 1.049 | 0.039 | 0.031 | 0.038 | 0.029 |
| | hw/2, closed | 1.012 | 1.045 | 0.039 | 0.032 | 0.039 | 0.031 |
| ALL | ALL | 1.052 | 1.094 | 0.077 | 0.057 | 0.073 | 0.053 |

The results for girders stiffened with two longitudinal stiffeners are plotted in Figure 114 to Figure 115. In these cases the current interaction formula gives higher resistances than those obtained with numerical simulations. With the new formulation the results are transferred on the safe side, i.e. the numerical results are slightly higher than predicted. According to the new interaction formulation the results are overall unsafe only for small slenderness $h_w/t_w=150$ (see Figure 115). The largest discrepancy is found for load case 1, where the bending moment is equal to bending capacity of flanges.

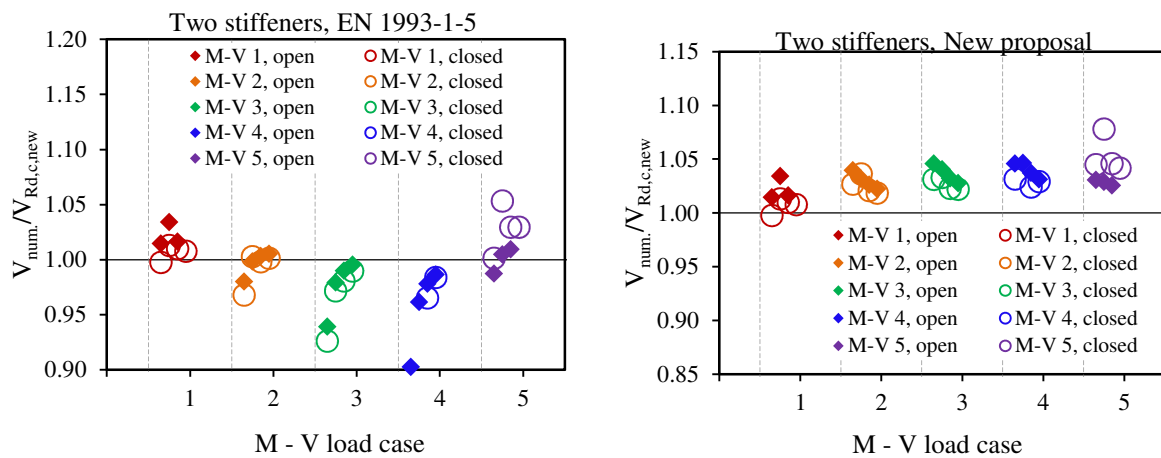


Figure 114: Two stiffeners, varied parameter A_f/A_w
 Slika 114: Dve ojačitvi, variiran parameter A_f/A_w

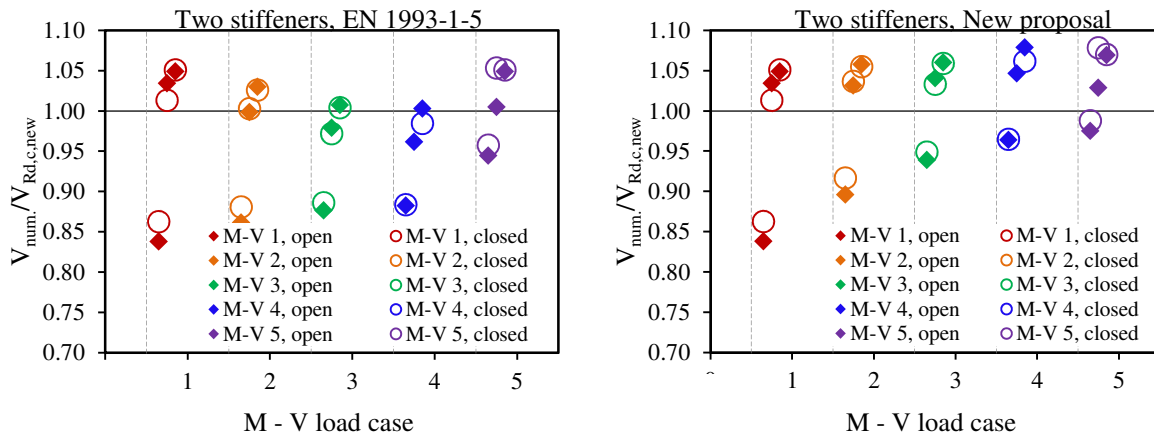


Figure 115: Two stiffeners, varied parameter h_w/t_w
 Slika 115: Dve ojačitvi, variiran parameter h_w/t_w

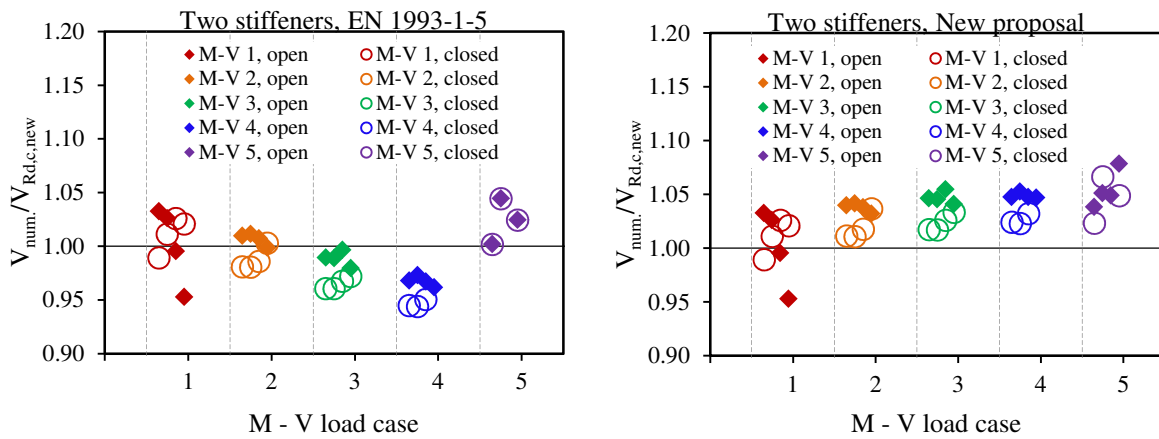


Figure 116: Two stiffeners, varied parameter γ/γ^*
 Slika 116: Dve ojačitvi, variiran parameter γ/γ^*

Preglednica 19: Statistično ovrednotenje M-V interakcije za nosilce ojačane z dvema ojačitvama
Table 19: Statistical evaluation of M-V interaction formulations for girders stiffened with two stiffeners

| VARIED PARAMETER | TYPE OF STIFFENERS | MEAN VALUE | | STANDARD DEVIATION | | COEFFICIENT OF VARIATION | |
|-------------------|--------------------|------------|-------|--------------------|-------|--------------------------|-------|
| | | EN 1993 | NEW | EN 1993 | NEW | EN 1993 | NEW |
| A_f/A_w | open | 0.995 | 1.037 | 0.035 | 0.014 | 0.035 | 0.014 |
| | closed | 0.984 | 1.023 | 0.032 | 0.010 | 0.032 | 0.010 |
| h_w/t_w | open | 0.972 | 1.011 | 0.074 | 0.072 | 0.076 | 0.071 |
| | closed | 0.969 | 1.005 | 0.066 | 0.063 | 0.068 | 0.062 |
| γ/γ^* | open | 0.999 | 1.038 | 0.027 | 0.025 | 0.027 | 0.024 |
| | closed | 0.987 | 1.024 | 0.030 | 0.016 | 0.031 | 0.016 |
| ALL | ALL | 0.986 | 1.024 | 0.045 | 0.039 | 0.046 | 0.038 |

7.5 Determination of the partial safety factor

The interaction formulation developed in previous Chapter 7.4 is determined for mean values of parameters. In engineering practice the resistance of the structure is defined with design values where uncertainties such as material, geometry and the model are considered. In this chapter the interaction model is statistically evaluated. Mean values, standard deviations and coefficient of variations are considered. The model is developed on the basis of numerical simulations, therefore the coefficient of variation which takes into account numerical model is also considered. To determine partial safety factors the rules passed in EN 1990 [83] Annex D are considered.

Two different methods for the determination of partial safety factor are given, if experimental results are available:

- Statistical evaluation of a single property.
- Statistical evaluation of a resistance model.

In this work the partial safety factors are determined considering statistical evaluation of a resistance model. Within this model the influence of other parameters which are not covered by numerical simulations or experiments is also taken into account. The short overview of the used model is presented in the sequel.

7.5.1 Statistical evaluation of resistance models

The method in EN 1990, Annex D, which gives a procedure for the assessment of the characteristic and the design value, is based on the following assumptions:

- The resistance function is a function of a number of independent variables.
- All relevant geometrical and material properties are measured.
- A sufficient number of tests is available.
- There is no correlation between the variables in the resistance function.
- All variables follow either a normal or a log-normal distribution.

The first step of the analysis is to establish a theoretical resistance model which corresponds to the numerically obtained results. The theoretical resistance model is a function of a number of independent variables \underline{X} :

$$r_i = g_{ri}(\underline{X}) \quad (56)$$

After the theoretical model has been established, the results are compared against numerical results as shown in Figure 117. The points represent pairs of corresponding values (r_{ii}, r_{ei}) .

If the resistance function is exact and complete, then all of the points lie on the line $\theta = 45^\circ$. In practice the points are slightly scattered. If any systematic errors are observed, the deviation from the line should be investigated in order to check whether this indicates mistakes in the test procedures or in the resistance function. However, in practice the points are located at gradient different than $\theta = 45^\circ$ which is taken into account with the parameter b calculated with the least square method:

$$b = \frac{\sum_i r_{ei} \cdot r_{ii}}{\sum_i r_{ii}^2} \quad (57)$$

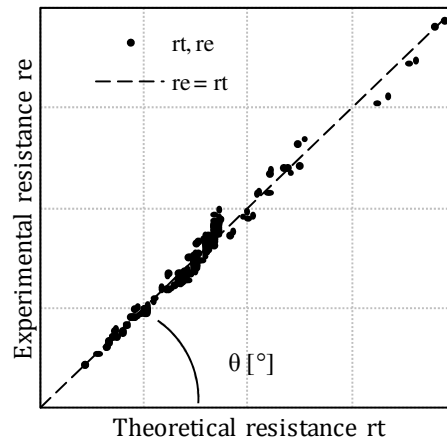


Figure 117: Comparison of experimental (numerical) and theoretical values
Slika 117: Primerjava eksperimentalnih (numeričnih) in teoretičnih vrednosti

If the gradient of mean values is known, the coefficient of variation of the model is expressed through:

- Error term δ_i of each experimental value r_{ei} :

$$\delta_i = \frac{r_{ei}}{b \cdot r_{ti}} \quad (58)$$

- Logarithm of the error terms δ_i :

$$\Delta_i = \ln(\delta_i) \quad (59)$$

- Mean value $\bar{\Delta}$ of logarithm of the error terms:

$$\bar{\Delta} = \frac{1}{n} \sum_{i=1}^n \Delta_i \quad (60)$$

- Standard deviation of the error terms:

$$s_{\Delta}^2 = \frac{1}{n-1} \sum_{i=1}^n (\Delta_i - \bar{\Delta})^2 \quad (61)$$

- Finally, the coefficient of variation V_{δ} of the error terms δ_i is defined as:

$$V_{\delta} = \sqrt{\exp(s_{\Delta}^2) - 1} \quad (62)$$

The calculated coefficient of variation V_{δ} takes into account only those uncertainties that were included in the experimental (numerical) analysis. Since all parameters in the numerical analysis were taken as mean values, other uncertainties beside uncertainty of the theoretical model are considered with the coefficient of variation of the basic variables V_{X_i} .

The coefficient of variation may be obtained from the product of the function:

$$V_r^2 = (V_\delta^2 + 1) \cdot \left[\prod_{i=1}^j (V_{Xi}^2 + 1) \right] - 1 \quad (63)$$

or alternatively, for small values of V_δ^2 and V_{Xi}^2 , the following approximation for V_r^2 may be used:

$$V_r^2 = V_\delta^2 + \sum_{i=1}^j V_{Xi}^2 \quad (64)$$

If a large number of tests ($n > 100$) is available, the characteristic resistance r_k and design resistance r_d , which correspond to 5% and 1% fractil of the probability distribution, may be obtained from:

$$r_k = b \cdot g_r(X_m) \cdot \exp(-k_\infty \cdot Q - 0.5 \cdot Q^2) \quad (65)$$

$$r_d = b \cdot g_r(X_m) \cdot \exp(-k_{d,\infty} \cdot Q - 0.5 \cdot Q^2) \quad (66)$$

with:

$$\begin{aligned} Q &= \sigma_{\ln(r)} = \sqrt{\ln(V_r^2 + 1)} \\ k_\infty &= 1.64 \\ k_{d,\infty} &= 3.04 \end{aligned} \quad (67)$$

Finally the partial safety factor can be determined as:

$$\gamma_M = \frac{r_k}{r_d} = \frac{b \cdot g_r(X_m) \cdot \exp(-k_{d,\infty} \cdot Q - 0.5 \cdot Q^2)}{b \cdot g_r(X_m) \cdot \exp(-k_\infty \cdot Q - 0.5 \cdot Q^2)} = \frac{\exp(-k_{d,\infty} \cdot Q - 0.5 \cdot Q^2)}{\exp(-k_\infty \cdot Q - 0.5 \cdot Q^2)} \quad (68)$$

The partial safety factor is determined for the theoretical model that does not coincide with the numerical calculations. The final reduction factor γ_M^* is then determined by considering the mean value correction factor b :

$$\gamma_M^* = \frac{\gamma_M}{b} \quad (69)$$

7.5.2 Uncertainties in the model - determination of V_{Xi}

The following uncertainties which are of basic importance for the determination of γ_M should be taken into account:

- Uncertainty of resistance model V_δ .
- Uncertainty of geometry.
- Uncertainty of material properties.
- Uncertainty of numerical model.

The uncertainty of material properties and geometry are determined on the basis of prior knowledge. The following coefficients of variations were taken from literature [6]:

- $V_{width} = 0.005$ variation coefficient for the width of the plate
- $V_{thickness} = 0.05$ variation coefficient for the thickness of the plate
- $V_{yield} = 0.07$ variation coefficient for the yield strength

Additionally, the variation coefficient for the vertical position of the stiffener was assumed:

- $V_{hwi} = 0.005$ variation coefficient for the position of the longitudinal stiffener

The partial safety factor evaluated according to EN 1990, Annex D is determined on the basis of experimental results. In this work the experimental results are determined with numerical simulations. Since the results of numerical simulations do not exactly coincide with the experimental results, a coefficient of variation of numerical simulation V_{FEM} is introduced to the calculation of partial safety factor. The calculation of coefficient is given in Table 20 with the following expressions:

$$b = \frac{\sum_i F_{r,exp} \cdot F_{r,num}}{\sum_i F_{r,num}^2} = 0.9773 \quad (70)$$

$$\delta_i = \frac{F_{R,exp}}{b \cdot F_{R,num}} \quad (71)$$

$$\Delta_i = \ln(\delta_i) \quad (72)$$

$$\Delta = \frac{1}{n} \sum_{i=1}^n \Delta_i = -0.0005 \quad (73)$$

$$s_{\Delta}^2 = \frac{1}{n-1} \cdot \sum_{i=1}^n (\Delta_i - \Delta)^2 = 0.0002 \quad (74)$$

$$V_{FEM} = \sqrt{\exp(s_{\Delta}^2) - 1} = 0.0149 \quad (75)$$

Preglednica 20: Izračun vrednosti V_{FEM}

Table 20: Calculation of V_{FEM}

| TEST | $F_{r,exp}$ [kN] | $F_{r,num}$ [kN] | $F_{r,exp} \times F_{r,num}$ | $F_{r,num}^2$ | δ_i | Δ_i | $(\Delta_i - \Delta)^2$ |
|------|------------------|------------------|------------------------------|---------------|------------|--------------------------|-------------------------|
| SO | 1934 | 1991 | 3850594 | 3964081 | 0.994 | -0.006 | 0.0000 |
| SC | 2049 | 2134 | 4372566 | 4553956 | 0.982 | -0.018 | 0.0003 |
| UO | 2173 | 2168 | 4750178 | 4778596 | 1.017 | 0.017 | 0.0003 |
| UC | 2087 | 2125 | 4434875 | 4515625 | 1.005 | 0.005 | 0.000 |
| | | Σ | 17408213 | 17812258 | $\Delta =$ | -0.0005 | 0.0007 |
| | | b = | | 0.9773 | | V_{FEM} = | 0.0149 |

7.5.3 Resistance models

Five resistance models: two interaction models, one gross cross-section resistance model and two combined models were evaluated to determine partial safety factors. The interaction models were evaluated at sections 1-1 and 2-2 as shown in Figure 118, while the check to gross cross-section

bending resistance is performed at section 0-0. The first resistance model $r_{t,1}$ corresponds to the interaction check according to EN 1993-1-5. Since the interaction formulation does not fit the shape of interaction, a new resistance model was introduced in Chapter 7.4 and is denoted as resistance model $r_{t,2}$. When the interaction check is performed in the panel, EN 1993-1-5 requires an additional check of bending resistance of gross cross-section at the most stressed edge of the panel (section 0-0). Therefore, the third resistance $r_{t,3}$ model which represents the bending check of the gross cross-sections was evaluated. Finally the last two combined $r_{t,4}$ and $r_{t,5}$ models were defined as a minimum resistance calculated with the interaction model and bending check of the gross cross-section.

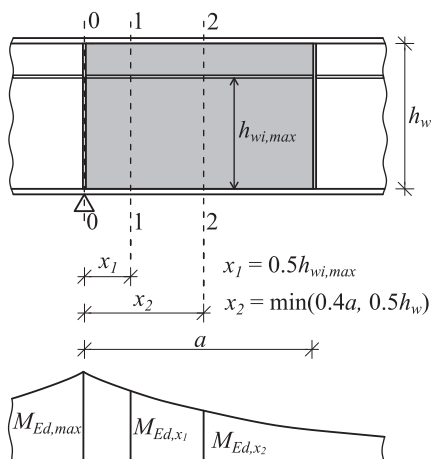


Figure 118: Position of interaction check (sections 1-1 and 2-2) and gross cross-section check (section 0-0)

Slika 118: Pozicija interakcijske kontrole (prezez 1-1 in 2-2) in kontrola nosilnosti prereza (prezez 0-0)

The first theoretical model is the current M-V interaction formula given by equation (49) in Chapter 7.2.3:

$$r_{t,1} = V = \left(1 + \left(\frac{M_{pl,c} - M}{M_{pl,c} - M_{f,c}} \right)^{0.5} \right) \cdot \frac{V_{bw,c}}{2} \quad (76)$$

For the calculation of bending resistance ($M_{f,c}$ and $M_{pl,c}$) of the cross-section, the material partial safety factor was as in EN 1993-1-5 set to $\gamma_{M0} = 1.0$.

The second numerical model is a new proposed M-V interaction formula determined with equation (55) in Chapter 7.4:

$$r_{t,2} = V = \left(1 + \left(\frac{M_{el,eff,c} - M}{M_{el,eff,c} - M_{f,c}} \right) \right) \cdot \frac{V_{bw,c}}{2} \quad (77)$$

The third resistance model is defined as elastic bending resistance of a cross-section checked at the edge of the panel:

$$r_{t,3} = V = \frac{M_{el,c}}{l}, \quad (78)$$

where l is the distance between zero bending point and the point where $M_{el,c}$ is obtained.

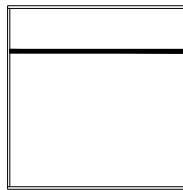
The last two combined models were evaluated at both distances from the most stressed edge and are defined as:

$$r_{t,4} = \min (r_{t,1}; r_{t,3}) \quad (79)$$

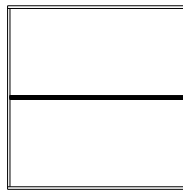
$$r_{t,5} = \min (r_{t,2}; r_{t,3}) \quad (80)$$

As already mentioned, the first two models and the last two models are evaluated at two different distances from the most stressed edge of the panel, while the third resistance model is evaluated at the edge of the panel where the maximum bending moment is present. The models were evaluated for the following sub-sets:

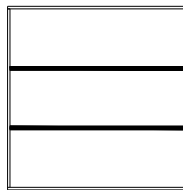
- Sub-set I: All analysed girders - 582 data.
- Sub-set II: Only girders stiffened with longitudinal stiffener at $h_w / 4$.



- Sub-set III: Only girders stiffened with longitudinal stiffener at $h_w / 2$.



- Sub-set IV: Only girders stiffened with two equally spaced longitudinal stiffeners.



In Figure 119 to Figure 123 the numerical results for different resistance models are plotted. Two additional lines, one denoting the line where experimental resistance is equal to resistance model $r_e = r_t$ and the other one denoting the mean value of numerical resistance $r_e = b \cdot r_t$, are plotted. The results that are plotted above the line $r_e = r_t$ prove higher resistance than determined with resistance model, and vice versa, the results below this line prove smaller resistance than obtained with the model.

In Figure 119 the results are evaluated for interaction resistance models $r_{t,1}$ and $r_{t,2}$ through the entire numerical database – sub-set I. The inclination of the mean line is higher for resistance model $r_{t,2}$ than for resistance model $r_{t,1}$. Also the scattering of the results is smaller for model $r_{t,2}$ than for model $r_{t,1}$.

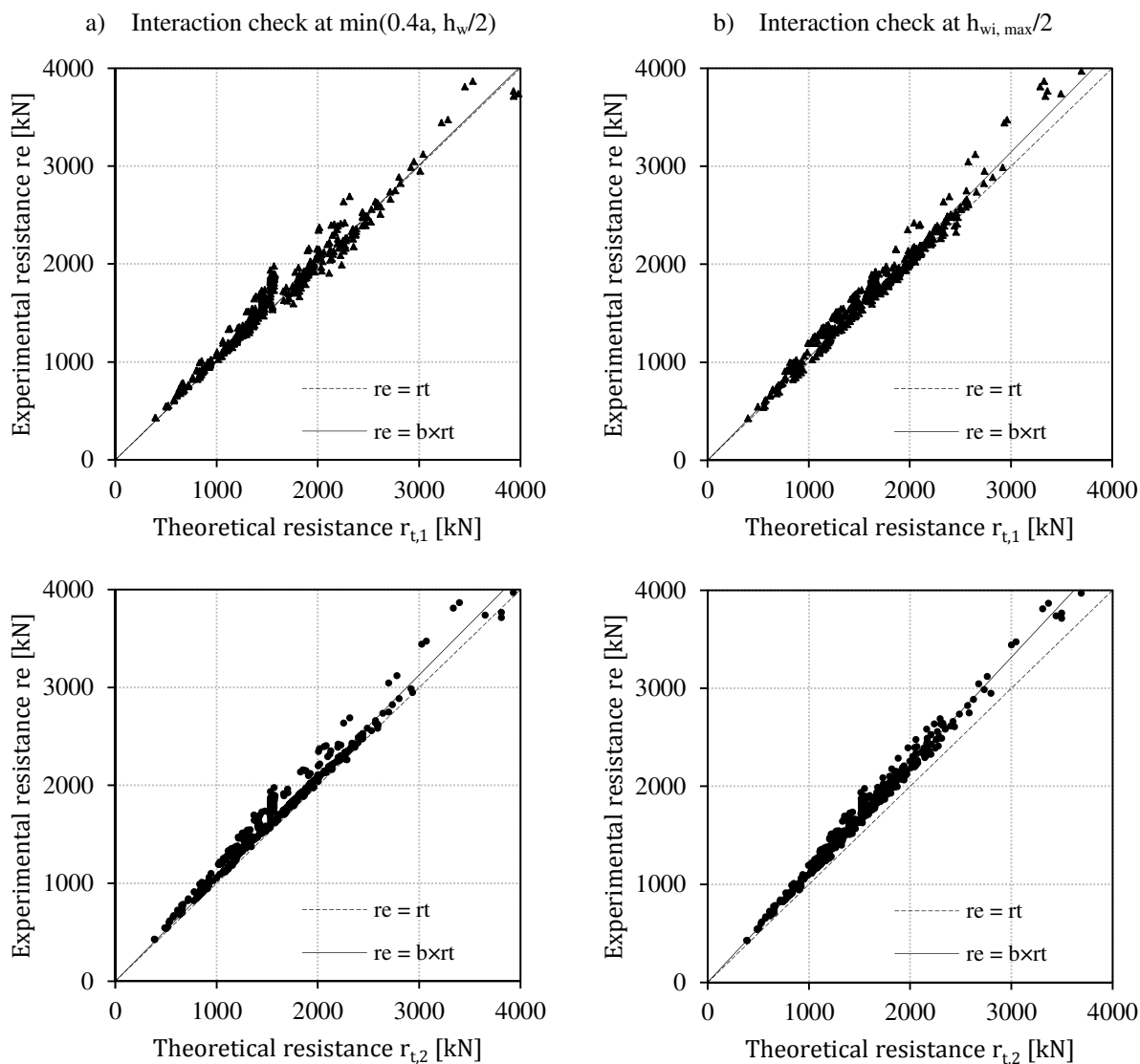


Figure 119: Statistical evaluation of sub-set I for resistance models $r_{t,1}$ and $r_{t,2}$
Slika 119: Statistično ovrednotenje podskupine I za model odpornosti $r_{t,1}$ in $r_{t,2}$

The results of statistical evaluation of resistance models $r_{t,1}$ and $r_{t,2}$ for sub-set II are plotted in Figure 120. For this group all experimental resistances are above the theoretical resistance for both resistance models and for both positions of interaction check. The reason for this is a favourable effect of tension stresses in the critical subpanel which increase shear resistance. The scattering of the results is found slightly smaller for resistance model $r_{t,2}$.

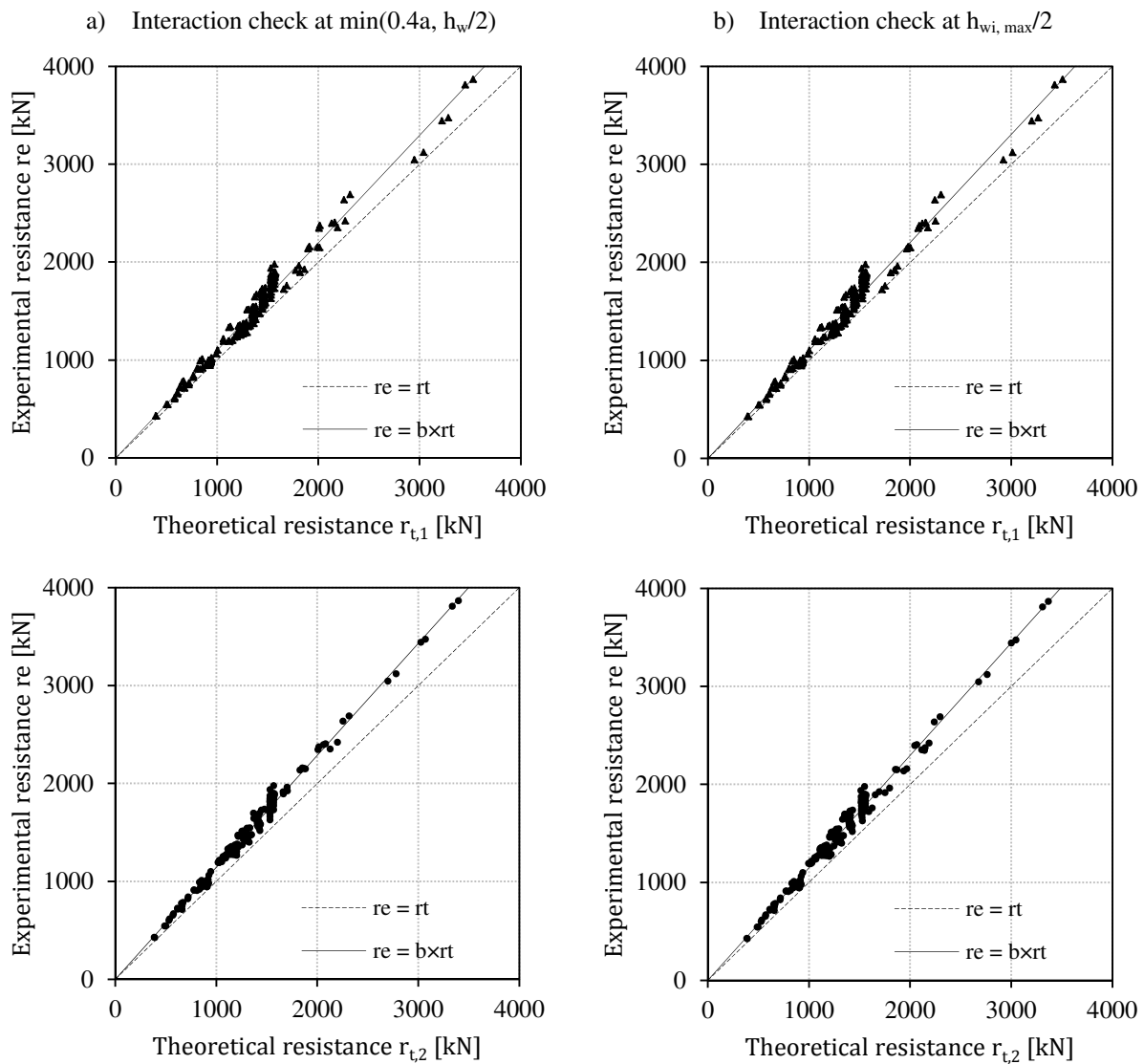


Figure 120: Statistical evaluation of sub-set II for resistance models $r_{t,1}$ and $r_{t,2}$
Slika 120: Statistično ovrednotenje podskupine II za modela odpornosti $r_{t,1}$ in $r_{t,2}$

In the third sub-set the results of girders stiffened with one stiffener in the mid web depth are statistically evaluated. The results for resistance models $r_{t,1}$ and $r_{t,2}$ are plotted in Figure 121. When the resistance model $r_{t,1}$ at a distance of $\min(0.4a, h_w/2)$ is used in statistical evaluation, most of the results are found on unsafe side and the scatter of the results is also very high for this case. This leads to a large partial safety factor. All other models give results mostly on the safe side and also the scatter of the results is much smaller.

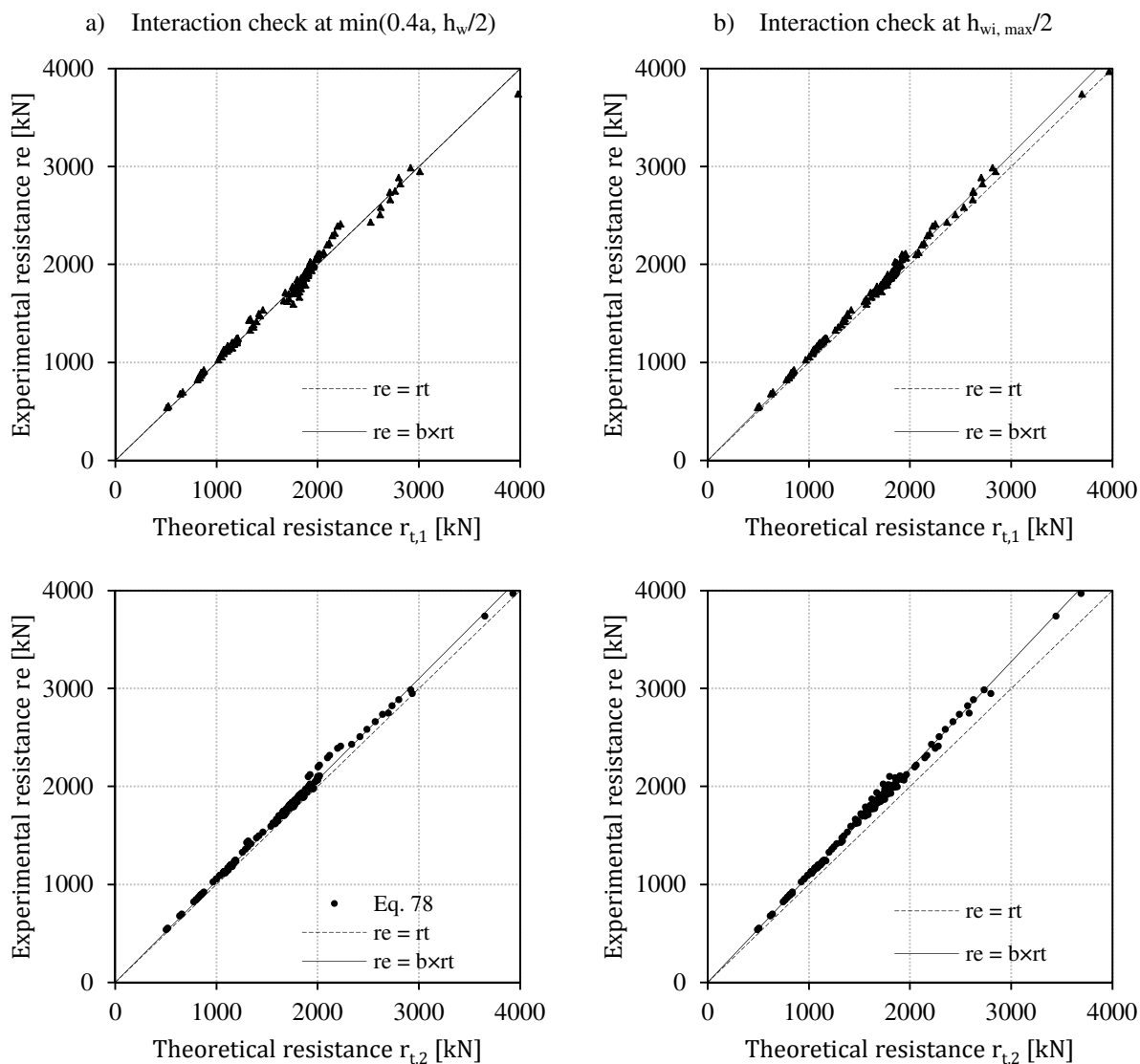


Figure 121: Statistical evaluation of sub-set III for resistance models $r_{t,1}$ and $r_{t,2}$
Slika 121: Statistično ovrednotenje podskupine III za modela odpornosti $r_{t,1}$ in $r_{t,2}$

In Figure 122 the results of girders stiffened with two equidistant stiffeners are plotted. In this situation both resistance models $r_{t,1}$ as well as $r_{t,2}$ give on average nonconservative results, when the interaction is performed at a distance of $\min(0.4a, h_w/2)$. When the interaction check is performed at $h_{wi,max}/2$ from the most stressed edge, all experimental results are higher than defined with resistance model. The final partial safety factor depends on the inclination of the line $r_e = b \cdot r_t$ and the scatter of the results which is found larger for the resistance model $r_{t,1}$ than for the model $r_{t,2}$.

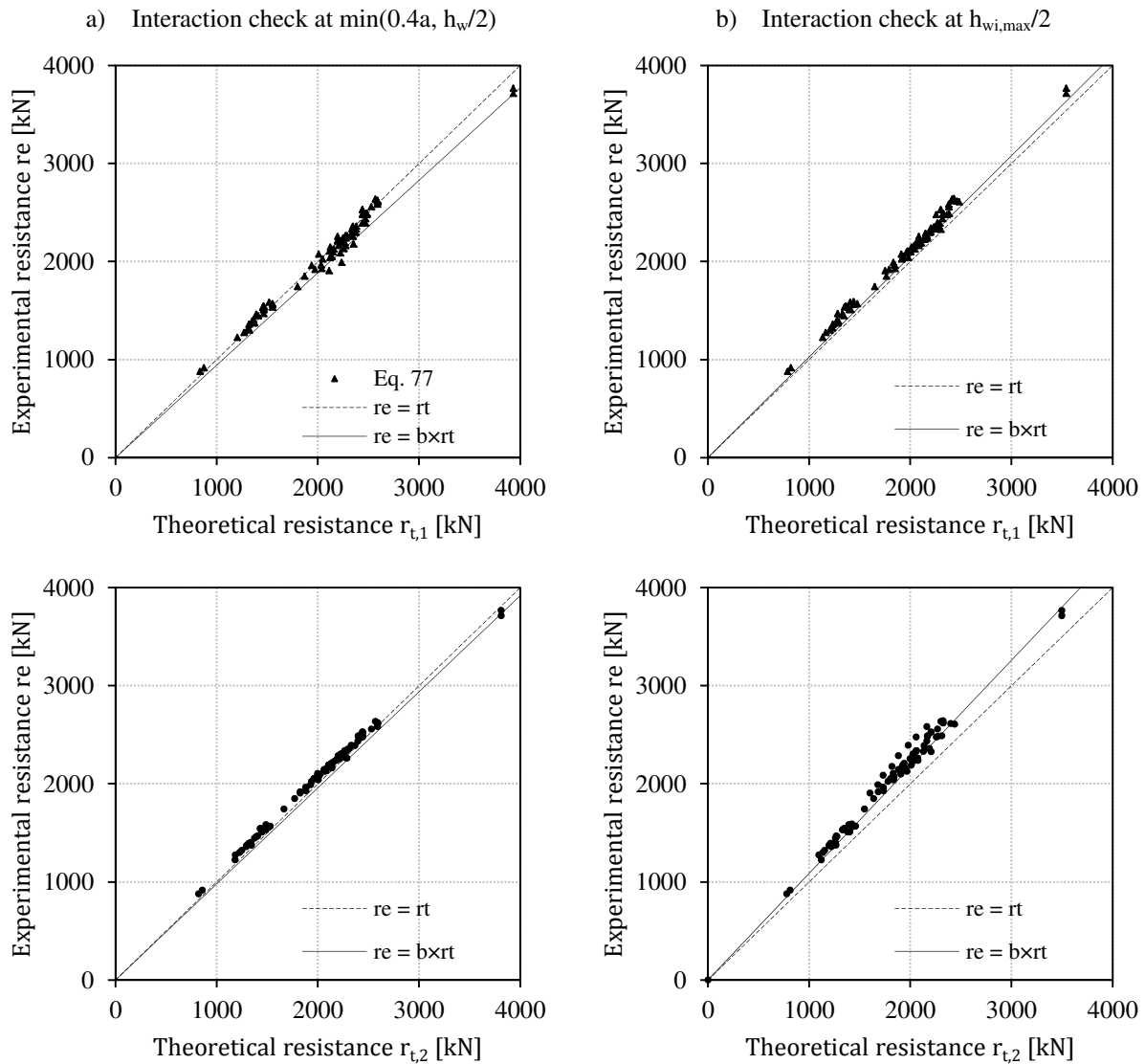


Figure 122: Statistical evaluation of sub-set IV for resistance models $r_{t,1}$ and $r_{t,2}$

Slika 122: Statistično ovrednotenje podskupine IV za modela odpornosti $r_{t,1}$ in $r_{t,2}$

The statistical evaluation of resistance model $r_{t,3}$ for all four sub-sets is plotted in Figure 123. The largest scatter between resistance model and experimental results is found for sub-set I. When the results are further divided in another sub-set, the scatter becomes much smaller. In all cases most of experimental values r_e are on the safe side.

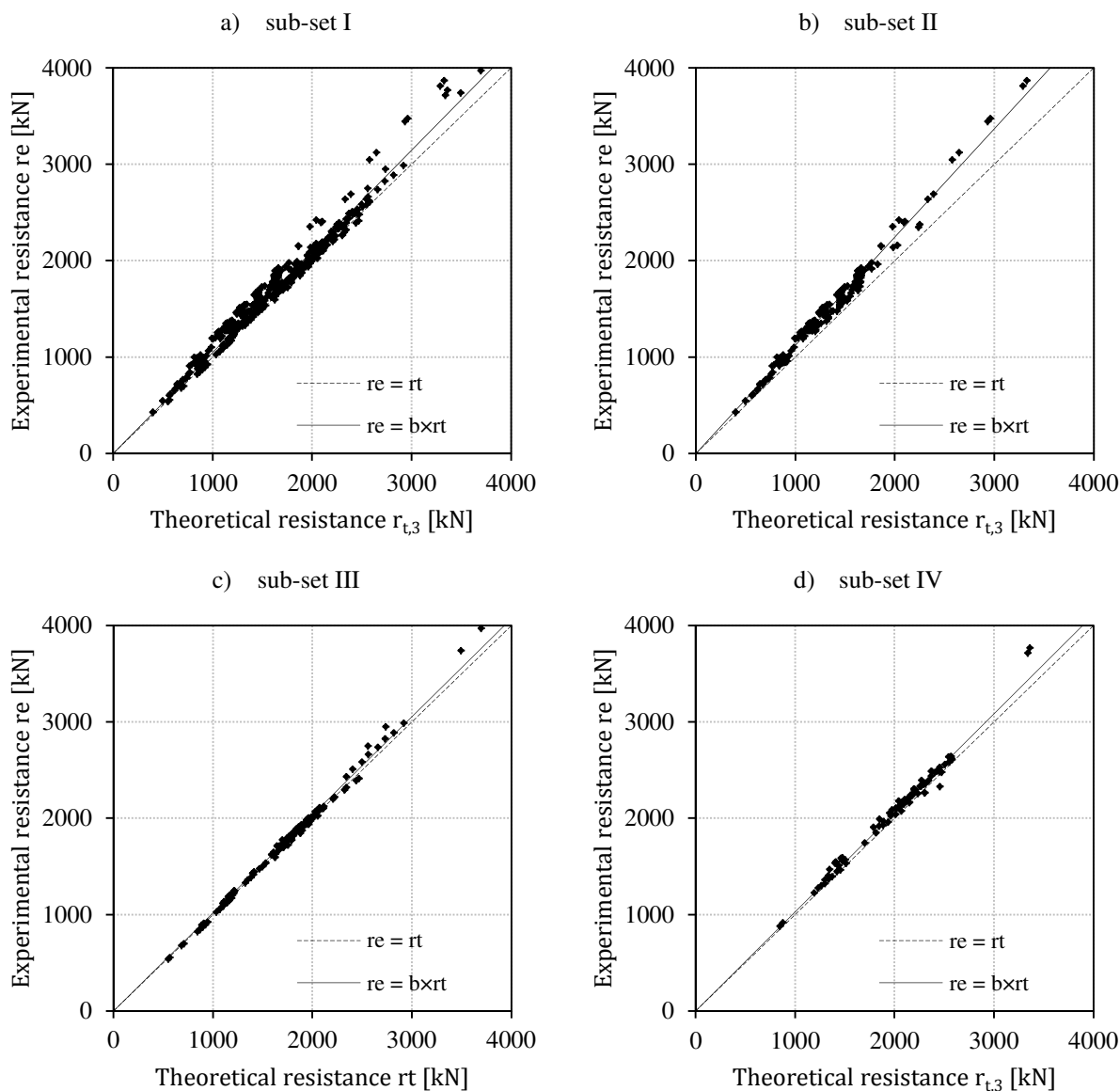


Figure 123: Statistical evaluation for resistance models $r_{t,3}$
 Slika 123: Statistično ovrednotenje za model odpornosti $r_{t,3}$

7.5.4 Comparison and evaluation of results

The results of the evaluated partial safety factors are gathered in Table 21 to Table 25. The partial safety factors were determined for five theoretical models on four sub-sets. The largest partial safety factor is found for interaction model $r_{t,1}$ on sub-set IV, where the results of girders stiffened with two longitudinal stiffeners are treated. The new proposed interaction formula results in smaller partial safety factors for all sub-sets.

When the interaction resistance model is checked at a distance of $\min(0.4a, h_w/2)$, the partial safety factor is smaller than partial safety factor $\gamma_{M1} = 1.1$ given in EN 1993-1-5 only for sub-set II for both models (1.048 and 0.999, see Table 21) and for sub-set III for resistance model $r_{t,2}$ (1.096, see Table 21). In all other cases the partial safety factor is above $\gamma_{M1} = 1.1$, especially for sub-set IV. The lowest partial safety factor is found for girders stiffened with one stiffener in compression zone. This is due to the fact that the resistance model does not consider the increase of shear resistance due to tension stresses in the lower larger sub-panel.

The partial safety factors evaluated for the interaction check at a distance of $h_{wi,max}/2$ from the most stressed edge are gathered in Table 22. For this interaction check location the partial safety factors are logically smaller. If all experimental results are evaluated, the partial safety factor for resistance model $r_{t,1}$ is 1.103 and for model $r_{t,2}$ 1.033 (see Table 22, sub-set I). The largest factor is obtained for sub-set IV where $\gamma_M = 1.113$ for resistance model $r_{t,1}$ and $\gamma_M = 1.051$ for resistance model $r_{t,2}$. The difference between partial safety factors evaluated for all sub-sets is for the interaction check at $h_{wi,max}/2$ much smaller than for the check at a distance of $\min(a, h_w/2)$.

The partial safety factors evaluated for resistance model $r_{t,3}$ where the maximum load is defined with bending moment resistance of gross cross-section are gathered in Table 23. The partial safety factor for gross cross-section control in EN 1993-1-5 is equal to $\gamma_{M0} = 1.0$. For all sub-sets the determined partial safety factors for model $r_{t,3}$ were found higher than the one given in EN 1993-1-5. The maximum factor $\gamma_M = 1.113$ is found for sub-set III. This can be attributed to disregarding of shear and probably the assumption that cross-sections at the transverse stiffeners are fully effective is too optimistic.

Preglednica 21: Izračunane vrednosti faktorja γ_M^* za modela odpornosti $r_{t,1}$ in $r_{t,2}$ pri $\min(a, h_w/2)$

Table 21: Calculated γ_M^* values for resistance models $r_{t,1}$ and $r_{t,2}$ at $\min(a, h_w/2)$

| Sub-set | b | | V_δ | | V_r | | γ_M^* | |
|---------|-----------|-----------|------------|-----------|-----------|-----------|--------------|--------------|
| | $r_{t,1}$ | $r_{t,2}$ | $r_{t,1}$ | $r_{t,2}$ | $r_{t,1}$ | $r_{t,2}$ | $r_{t,1}$ | $r_{t,2}$ |
| I | 1.0050 | 1.0430 | 0.060 | 0.056 | 0.106 | 0.104 | 1.157 | 1.111 |
| II | 1.0997 | 1.1445 | 0.049 | 0.036 | 0.101 | 0.095 | 1.048 | 0.999 |
| III | 0.9993 | 1.0340 | 0.031 | 0.017 | 0.093 | 0.089 | 1.140 | 1.096 |
| IV | 0.9432 | 0.9803 | 0.048 | 0.040 | 0.100 | 0.096 | 1.221 | 1.168 |

Preglednica 22: Izračunane vrednosti faktorja γ_M^* za modela odpornosti $r_{t,1}$ in $r_{t,2}$ pri $h_{wi,max}/2$

Table 22: Calculated γ_M^* values for resistance models $r_{t,1}$ and $r_{t,2}$ at $h_{wi,max}/2$

| Sub-set | b | | V_δ | | V_r | | γ_M^* | |
|---------|-----------|-----------|------------|-----------|-----------|-----------|--------------|--------------|
| | $r_{t,1}$ | $r_{t,2}$ | $r_{t,1}$ | $r_{t,2}$ | $r_{t,1}$ | $r_{t,2}$ | $r_{t,1}$ | $r_{t,2}$ |
| I | 1.0491 | 1.1067 | 0.055 | 0.037 | 0.103 | 0.095 | 1.103 | 1.033 |
| II | 1.1033 | 1.1485 | 0.050 | 0.040 | 0.101 | 0.096 | 1.045 | 0.998 |
| III | 1.0408 | 1.0925 | 0.019 | 0.016 | 0.090 | 0.089 | 1.089 | 1.037 |
| IV | 1.0264 | 1.0881 | 0.036 | 0.037 | 0.095 | 0.095 | 1.113 | 1.051 |

Preglednica 23: Izračunane vrednosti faktorja γ_M^* za modela odpornosti $r_{t,3}$

Table 23: Calculated γ_M^* values for resistance model $r_{t,3}$

| Sub-set | B | V_δ | V_r | γ_M^* |
|---------|--------|------------|-------|--------------|
| I | 1.0493 | 0.054 | 0.103 | 1.103 |
| II | 1.1240 | 0.035 | 0.094 | 1.016 |
| III | 1.0184 | 0.017 | 0.089 | 1.113 |
| IV | 1.0280 | 0.029 | 0.092 | 1.107 |

In Table 24 and Table 25 the partial safety factors evaluated for resistance models $r_{t,4}$ and $r_{t,5}$ are gathered. With these two models the lowest partial safety factors will be obtained because the theoretical resistance is defined as the minimum value of interaction check at a distance of $h_{wi,max}/2$ or $\min(0.4a, h_w/2)$ and gross cross-section resistance to bending moment at the edge of the panel. The partial safety factor is below 1.1 for all cases except for sub-set IV when the interaction check is performed at a distance of $\min(0.4a, h_w/2)$. The difference in values of partial safety factors for both models $r_{t,4}$ and $r_{t,5}$ is much smaller than for resistance models $r_{t,1}$ and $r_{t,2}$.

Preglednica 24: Izračunane vrednosti faktorja γ_M^* za modela odpornosti $r_{t,4}$ in $r_{t,5}$ pri $\min(a, h_w/2)$
 Table 24: Calculated γ_M^* values for resistance models $r_{t,4}$ and $r_{t,5}$ at $\min(a, h_w/2)$

| Sub-set | b | | V_δ | | V_r | | γ_M^* | |
|---------|-----------|-----------|------------|-----------|-----------|-----------|--------------|--------------|
| | $r_{t,4}$ | $r_{t,5}$ | $r_{t,4}$ | $r_{t,5}$ | $r_{t,4}$ | $r_{t,5}$ | $r_{t,4}$ | $r_{t,5}$ |
| I | 1.0590 | 1.0688 | 0.056 | 0.053 | 0.104 | 0.103 | 1.094 | 1.082 |
| II | 1.1425 | 1.1545 | 0.037 | 0.034 | 0.095 | 0.094 | 1.001 | 0.988 |
| III | 1.0302 | 1.0451 | 0.017 | 0.014 | 0.089 | 0.089 | 1.100 | 1.083 |
| IV | 1.0293 | 1.0310 | 0.028 | 0.028 | 0.092 | 0.092 | 1.105 | 1.104 |

Preglednica 25: Izračunane vrednosti faktorja γ_M^* za modela odpornosti $r_{t,4}$ in $r_{t,5}$ pri $h_{wi,max}/2$
 Table 25: Calculated γ_M^* values for resistance models $r_{t,4}$ and $r_{t,5}$ at $h_{wi,max}/2$

| Sub-set | b | | V_δ | | V_r | | γ_M^* | |
|---------|-----------|-----------|------------|-----------|-----------|-----------|--------------|--------------|
| | $r_{t,4}$ | $r_{t,5}$ | $r_{t,4}$ | $r_{t,5}$ | $r_{t,4}$ | $r_{t,5}$ | $r_{t,4}$ | $r_{t,5}$ |
| I | 1.0737 | 1.1099 | 0.047 | 0.037 | 0.099 | 0.095 | 1.071 | 1.030 |
| II | 1.1430 | 1.1563 | 0.038 | 0.037 | 0.096 | 0.095 | 1.001 | 0.989 |
| III | 1.0496 | 1.0929 | 0.017 | 0.016 | 0.089 | 0.087 | 1.079 | 1.037 |
| IV | 1.0477 | 1.0913 | 0.031 | 0.037 | 0.093 | 0.087 | 1.087 | 1.047 |

The new formulation of interaction formula for bending-shear interaction is more consistent than the formulation in EN 1993-1-5. Therefore, the scatter of results is smaller which also results in smaller partial safety factor, but the results are more conservative. From the evaluation of partial safety factor it can be concluded, that the most proper interaction check for longitudinally stiffened girders is at a distance of $h_{wi,max}/2$ from the most stressed edge. The difference between partial safety factors between different groups is much smaller than for the check at $\min(a, h_w/2)$.

The interaction check at $\min(a, h_w/2)$ with partial safety factor $\gamma_{M1} = 1.1$ given in EN 1993-1-5 does not satisfy reliability conditions given in EN 1990 for both resistance models, because the minimum required partial safety factor to fulfil reliability conditions for all sub-sets is 1.221 for resistance model $r_{t,1}$ and 1.168 for resistance model $r_{t,2}$.

If the resistance of girders is defined with interaction check at a distance of $h_{wi,max}/2$ with partial safety factor $\gamma_{M1} = 1.1$, the reliability conditions are fulfilled for resistance model $r_{t,2}$. The required minimal partial safety factor 1.113 is needed for resistance model $r_{t,1}$ to fulfil reliability conditions. Because the difference between the required and the given partial safety factor $\gamma_{M1} = 1.1$ is very small, less than 1.2%, resistance model $r_{t,1}$ with factor $\gamma_{M1} = 1.1$ may also be acceptable. By checking M-V interaction at a distance of $h_w/2$ or $h_{wi,max}/2$ from the most stressed edge of the panel a favourable effect of the moment gradient is accounted for. The moment distribution used in the analysis was realistic and it corresponds exactly to high bending moments and shear forces. It is also important to note that the interaction resistance models were expressed as a shear force resistance influenced by the bending moments in the panel. For bending moments the characteristic value was considered (or the design value with $\gamma_M = 1.0$). The evaluated partial safety factor $\gamma_{M1} = 1.1$ means that for $r_{t,1}$ the validity of the existing resistance model from EN 1993-1-5 is confirmed.

When the moment gradient is considered in the interaction check, EN 1993-1-5 demands also to perform the elastic bending resistance of the gross cross-section at one edge of the panel. The recommended value of the partial safety factor for this check in EN 1993-1-5 is equal to $\gamma_{M0} = 1.0$. The minimum required partial safety factor to fulfil reliability conditions according to EN 1990 and to cover moment-shear interaction is 1.113. Also in this case slightly smaller value of $\gamma_{M1} = 1.1$ could be used to determine the bending –shear interaction resistance. This does not automatically mean that the same partial safety factor should be used for resistance check to normal stresses with effective cross-section characteristic according to Chapter 4 of EN 1993-1-5.

If the interaction check and gross cross-section check are performed as in EN 1993-1-5, then the resistance of girder is defined with minimum value of both controls. Therefore, models $r_{t,4}$ and $r_{t,5}$ were also evaluated for partial safety factor. For these two models the reliability conditions of EN 1990 are met with partial safety factor of $\gamma_{M1} = 1.1$ for all sub-sets at the distance $h_{wi,max}/2$.

8 INTERMEDIATE TRANSVERSE STIFFENERS

8.1 Introduction

The plated girders are usually stiffened with a set of transverse stiffeners. Traditionally, a transverse stiffener is designed to have moment of inertia that adequately provides a simply supported boundary condition to the web panel along the juncture, when the web panel buckles. The intermediate transverse stiffener is subjected to different loads:

- External load.
- Load due the tension field formation.
- Load due to normal stresses (deviation forces).

The design provisions for the design of transverse stiffener take into account the Basler's assumption where the tension field formation is anchored by flanges and transverse stiffener. In this way the transverse stiffener is loaded with large compression force arising from tension field formation.

Recent studies regarding the design of transverse stiffeners show that the Basler's formulation appears to be questionable. An extended study considering the influence of stiffness of transverse stiffener was established by Lee et al. [8, 9]. In this work the influence is studied for transversally stiffened girder under shear load. The result of their work is a new model which describes the post-buckling behaviour called "shear cell analogy" and a new proposal for the stiffness of transverse stiffener requirement.

The test results on transverse stiffener of Basler et al. [26] and Evans et al. [75] were evaluated by Höglund and compared against rules in EN 1993-1-5. The formulation in EN 1993-1-5 for determination of axial force from tension field action was found conservative.

An extended numerical investigation on transversally stiffened girders was established by Presta et al. [13, 14]. A new proposal for designing the transverse stiffener considering the influence of tension field action was given.

In order to investigate the influence of intermediate transverse stiffener, two additional experimental tests on symmetrical tested girder (see Figure 124) were performed and verified against numerical model. On the basis of numerical model a parametric study considering stiffness of transverse stiffener was performed.

8.2 Requierments in EN 1993-1-5

The transverse stiffeners may be rigid or flexible. When flexible transverse stiffeners are used in the calculation of elastic critical stress their stiffness should be taken into account to assess the correct slenderness. In design practice the transverse stiffeners are assumed to be rigid, to provide support to the plate out of its plane.

In Eurocode EN 1993-1-5 [19] transverse stiffeners are designed to resist the loads coming from tension field action and destabilizing forces arising from normal stresses in the plane of the stiffened panel. Two requirements have to be fulfilled:

- a) The resistance check: $\sigma_{\max} \leq f_y / \gamma_{M1}$.

b) The stiffness check: $w \leq h_w / 300$.

The force coming from the tension field action is according to EN 1993-1-5 determined with the following expression:

$$N_{st,ten} = V_{Ed} - \frac{1}{\bar{\lambda}_w^2} \cdot t \cdot h_w \cdot \frac{f_{yw}}{\sqrt{3} \cdot \gamma_{M1}} \quad (81)$$

where V_{Ed} is a design shear force in the adjacent panels and $\bar{\lambda}_w$ is a slenderness of the panel adjacent to the stiffener.

The additional minimum stiffness requirement to prevent buckling of the stiffener due to shear stress in the web plate is defined as:

$$I_{st} \geq \frac{1.5 \cdot h_w^3 \cdot t^3}{a^2} \text{ for } \alpha = \frac{a}{h_w} \leq \sqrt{2} \quad (82)$$

$$I_{st} \geq 0.75 \cdot h_w \cdot t^3 \text{ for } \alpha = \frac{a}{h_w} \geq \sqrt{2}$$

where I_{st} is the second moment of the area of a stiffener for the axis parallel to the web plate. This requirement results in very small stiffeners.

8.3 Experimental investigation

Two additional tests were performed to investigate the behaviour of the transverse stiffener. The tests were performed on the girder where M-V interaction tests SO and SC were previously performed. The layout of the girder and the load positions for tests S1 and S2 are shown in Figure 124. The intermediate transverse stiffener was designed to the effects of deviation forces and half of the effect of tension field action according to EN 1993-1-5. The transverse stiffeners under consideration are marked with blue (test S1, load position S1) and red line (test S2, load position S2) in Figure 124.

The test procedure was the same as described in Chapter 3.1.4. The material characteristics of the plates are given in Chapter 3.1.3. The out-of-plane displacements in the panel as well as in the investigated transverse stiffener were measured in discrete points by LVDT as shown in ANNEX B: Layout of tested girders N1 - S1 and N1 - S2. Aside of displacements also strains were measured in the transverse stiffener and in the web plate in the vicinity of the stiffener. They were observed in three cross sections under the longitudinal stiffener as shown in ANNEX B: Layout of tested girders N1 - S1 and N1 - S2 and in Figure 128.

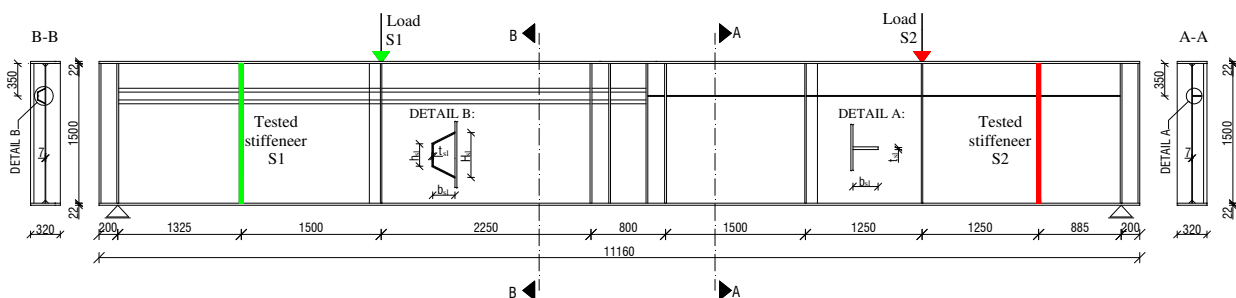


Figure 124: Layout of the tested girder and loading positions for tests S1 and S2

Slika 124: Podpiranje in obremenjevanje nosilca za izvedo testa S1 in S2

8.3.1 Test results

This chapter presents physical quantities that were measured during test execution. In Figure 125 the load-deflection curves are plotted for tests S1 and S2. First, test S1 was performed. The girder was loaded up to 50 mm of vertical deflection with the load of 2572 kN. The test was stopped before the maximum capacity of the girder was reached. Test S2 was loaded over the maximum capacity and so the full load-deflection curve was obtained. In this case the maximum static capacity of 2659 kN was observed from the load deflection curve.

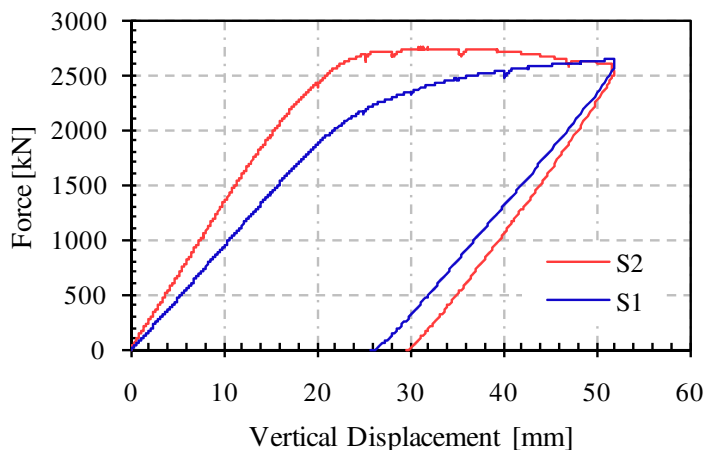


Figure 125: Load-deflection curves for tests S1 and S2

Slika 125: Krivulje sila-pomik za testa S1 in S2

In Figure 126a the strains measured in the stiffener and in the web for each section are plotted. The maximum tension strains are obtained on the edge of transverse stiffener (L1A, L1B, L5A, L5B, L9A and L9B). In all other measured points the strains were negative. The minimum strain was measured in point L12B. In all three sections, where the strains were measured, similar evolution of strains was observed. If the strains were transformed into stresses, the absolute maximum stress of -330 MPa was obtained on one side of the plate, which is below the yield stress of the material $f_y(15 \text{ mm}) = 342 \text{ MPa}$.

The membrane strains in the transverse stiffener are plotted in Figure 126b. The maximum membrane stress is obtained in the position of strain gauge L12 in the web plate with value of -210 MPa . By moving away from the tension field anchoring area the strains and compression stresses in the web and in the stiffener decrease.

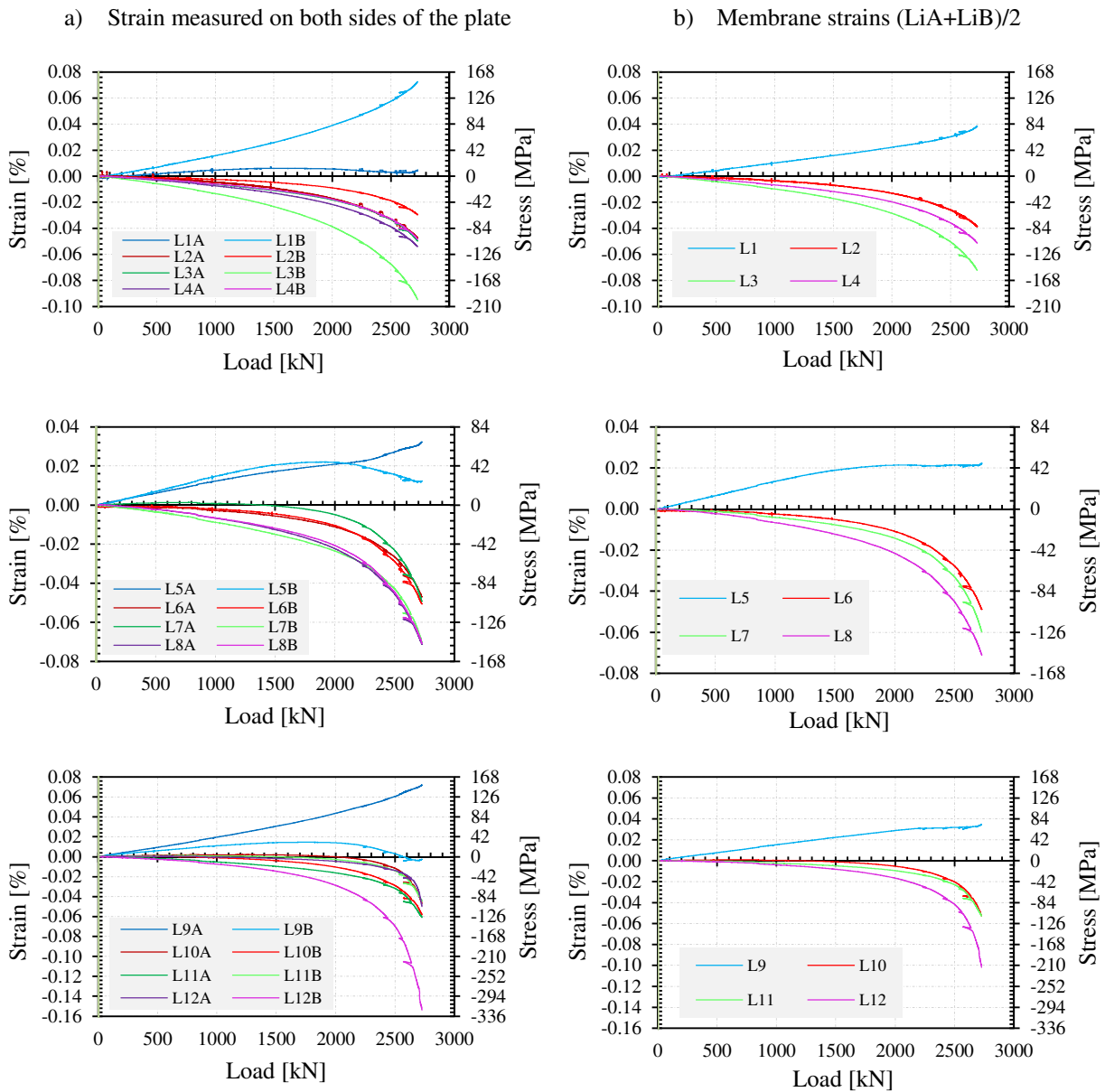


Figure 126: Strain measurements in the transverse stiffener - test S1

Slika 126: Razvoj deformacij v prečni ojačitvi – test S1

The strains measured in the transverse stiffener of test S2 are shown in Figure 127a. The strains are plotted for three sections. Like in the previous test, tension strains are obtained only at the edge of the stiffener. In all other points negative strains are observed with minimum value in point denoted with L11A. In this case the strains exceed the yield strain. The minimum and the maximum strains are measured in the section closest to the area where the tension field action develops.

In Figure 127b the membrane strains in the transverse stiffeners and in the effective parts of the web plate are plotted. The maximum strain, which is also above the yield strain was measured in point L11 is 0.47%. In all other positions the strains are much below the yield strain. Also in this case, by the moving from the anchoring area of tension field action, the strains are decreasing rapidly.

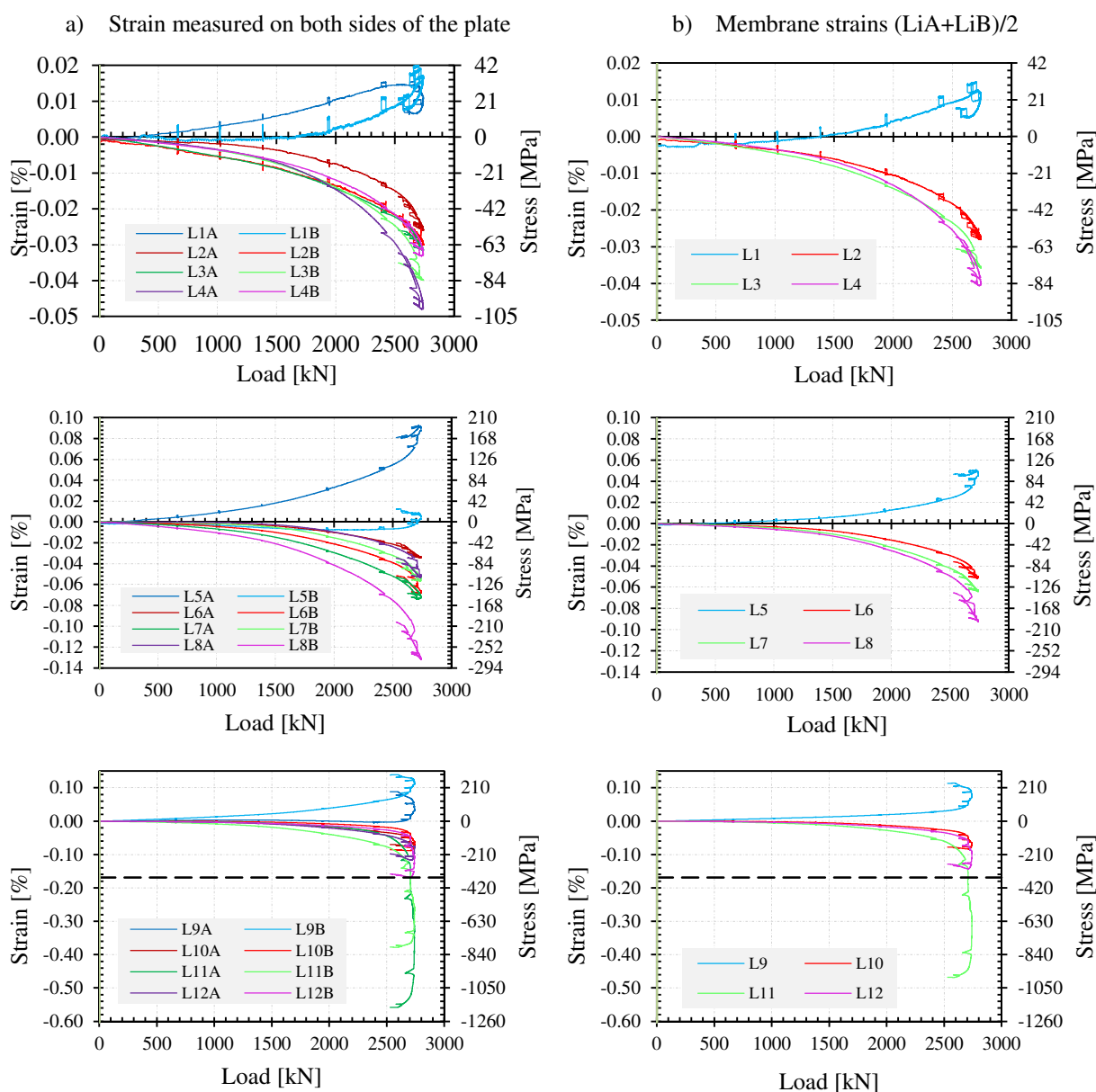


Figure 127: Strain measurements in the transverse stiffener - test S2

Slika 127: Razvoj deformacij v prečni ojačitvi – test S2

In Table 26 the axial force in the transverse stiffener evaluated with measured membrane strains are summarized for all three sections. For comparison 100% (100% TFA) and 50% (50% TFA) of axial force coming from tension field action according to EN 1993-1-5 is given. As it can be seen the maximal compression is obtained in section 1-1 (see Figure 128), where the anchoring of the tension field was observed. In the middle section 2-2 the axial force is much smaller, while the smallest value is obtained in section 3-3. The question that arises is which load is appropriate for designing the transverse stiffener due to tension field action. This may depend on the stiffness of longitudinal stiffener. In this particular case, where the stiffeners are relatively stiff, the value in cross-section 2-2 is found the most appropriate, because it reflects the average force in the stiffener. The actual axial force in the stiffener which is relevant for the design is in section 2-2 and its value presents only 56% of the calculated axial force (equation (81)) which arises from tension field action.

Preglednica 26: Osna sila v prečni ojačitvi in sodelujočem delu stojine ($15\epsilon_{tw}$) pri maksimalni nosilnosti nosilca
Table 26: Axial force in the transverse stiffener at maximal girder resistance, taking into account effective part of the web $15\epsilon_{tw}$

| N_{ten} [kN] | Stiffener S1 | | | Stiffener S2 | | |
|----------------|--------------|----------------|---------|--------------|----------------|---------|
| SECTION | 1-1 | 2-2 | 3-3 | 1-1 | 2-2 | 3-3 |
| TEST | - 329.1 | - 290.0 | - 223.4 | - 653.9 | - 280.7 | - 160.4 |
| 100% TFA | | - 514 | | | - 504 | |
| 50% TFA | | - 257 | | | - 252 | |

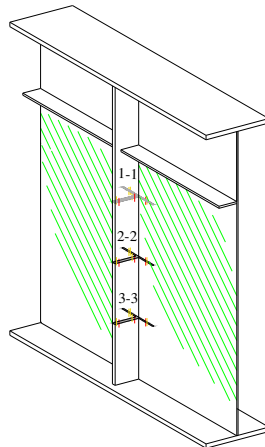


Figure 128: Cross-sections in the stiffener where the axial forces were evaluated
Slika 128: Prerezi v ojačitvi, kjer so bile izračunane osne sile

8.3.2 Model verification

To numerically simulate experimental tests S1 and S2 the numerical model, with which the resistance of SO and SC was assessed, was used. The numerical features described in Chapter 4 were used. To verify the numerical model the load-deflection curves and out-of-plane displacement of the transverse stiffener were inspected.

In Figure 129 the load deflection curves of test S2 are plotted. The initial elastic stiffness is in case of numerical simulation slightly higher than in the experiment. The transition from elastic to plastic zone is very similar in both cases. The comparison of the maximum capacities could not be performed, since the experiment had been stopped before the maximum capacity was reached. Generally, in the sense of load-deflection curve the numerical simulation fits the experimental response.

Larger difference in the numerical simulation and the experiment is obtained for test S2 (see Figure 130). Here the initial numerical stiffness and the plastic response are similar to experimental ones. However, the capacity gained with numerical simulation is lower. The difference of 3.7% compared to static resistance is found.

The comparison of out-of-plane displacements of the transverse stiffener for the test S1 and S2 are plotted in Figure 131. The shape of out-of-plane displacement calculated with numerical model is similar to that obtained by experimental test. This is established for both stiffeners S1 and S2. The difference between numerical simulation and experimental test refers the maximum amplitude of the out-of-plane displacement. For tested girder S1 the maximum amplitude of numerical simulation was - 3.4 mm, while the experimentally obtained value was -2.4 mm. The opposite situation is observed for test S2, where the maximum test amplitude of 4.1 mm is higher than the numerical one which is 2.6 mm.

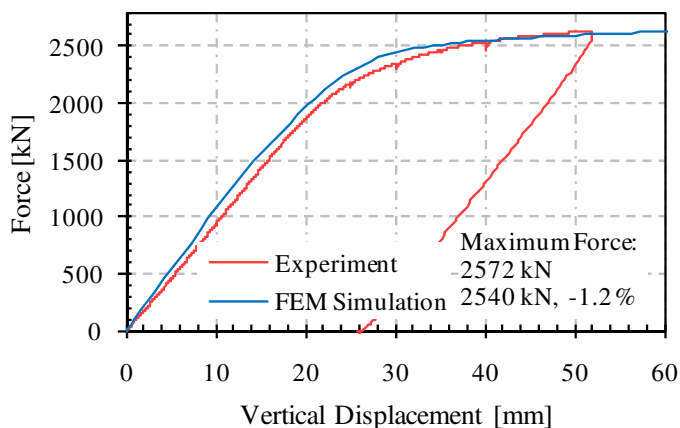


Figure 129: Comparison of load-deflection curves for test S1
Slika 129: Primerjava krivulj sila-pomik za test S1

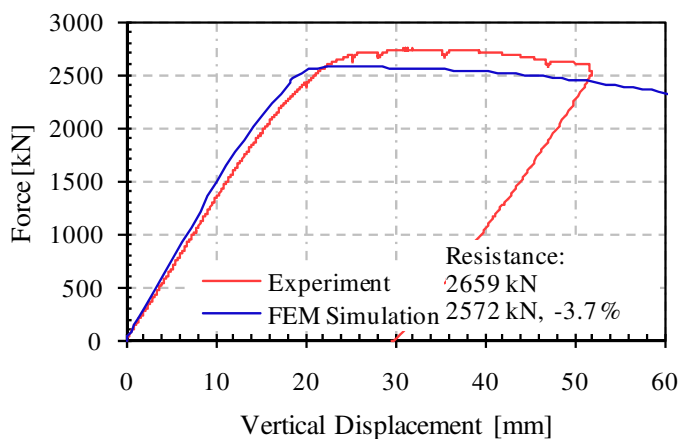


Figure 130: Comparison of load-deflection curves for test S2
Slika 130: Primerjava krivulj sila-pomik za test S2

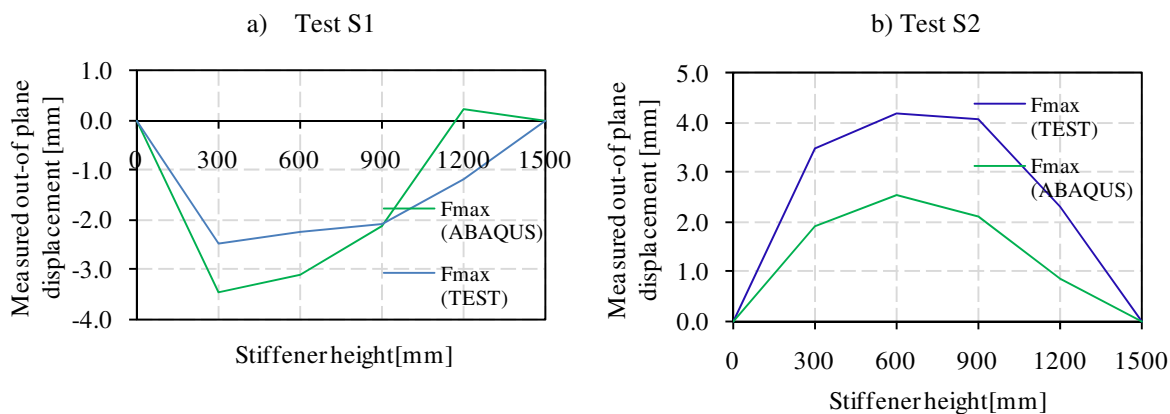


Figure 131: Comparison of the out-of-plane displacement of transverse stiffener
Slika 131: Primerjava pomikov ojačitve izven ravnine

8.3.3 Discussion

Two tests mainly loaded in shear were performed to investigate behaviour of the transverse stiffener. The stiffener was designed as rigid according to EN 1993-1-5 taking into account only 50% of axial force developed from the tension field action. For the design the maximum deflection $w = h_w / 300 = 5 \text{ mm}$ of the stiffener was decisive.

The stresses in the effective width of the stiffener are higher than predicted only in the area where the tension field action was formed. In all other cross sections the stresses were much lower. The assumption that the tension field action is fully anchored by the transverse stiffener is conservative. This was found also by Lee et al. [8, 9].

8.4 Numerical simulation

The parametric study was performed to study the influence of the stiffness of transverse stiffener on the girder resistance and development of the out-of-plane displacement of the web. The numerical calculations were performed by using FEM tools ABAQUS. Two sets of numerical analysis were performed. First the stiffener's stiffness was studied on tested girders S1 and S2. The second series was established on girders loaded with the combination of high bending and high shear loads, where M-V interaction is present. The numerical model is presented and described in Chapter 5.5.

The bilinear material model with yield strength of $f_y = 355 \text{ MPa}$ was used in the parametric studies and sinusoidal imperfection shape over the stiffener height with the maximum amplitude of $w_0 = h_w / 300$ was defined. Each neighbouring stiffener was straight; the imperfection of the web was then assumed as linear interpolation between both stiffeners.

8.4.1 Parameters

When numerical simulation on test girders S1 and S2 was performed, the stiffeners stiffness was varied. In Table 28 the dimensions and the normalized stiffnesses of applied stiffeners are summarized. The stiffnesses are normalized with minimum requested stiffness given by equation (82) and with stiffness required to fulfil displacement and stress conditions taking into account effect of tension field action and deviation forces (see Table 27). The required stiffness to fulfil stress and displacement criterion is calculated with simplified static model given in Johansson et al. [71]. Both effects, tension field action as well as deviation forces were considered in the design of the stiffener.

Preglednica 27: Zahtevana togosti prečnih ojačitev

Table 27: Required stiffener's stiffness consider different requirements

| I_{req} (cm ⁴) | EN 1993-1-5 (82) | 100% TFA | 50% TFA |
|------------------------------|------------------|----------|---------|
| S1 | 115.2 | 545.4 | 179.4 |
| S2 | 165.9 | 522.4 | 161.2 |

Preglednica 28: Variacija dimenzij prečnih ojačitev za test S1 in S2

Table 28: Stiffness variation of transverse stiffeners of tests S1 and S2

| TESTSTIFFENER | I1 | I2 | I3 | I4 | I5 | I6 | I7 | I8 |
|--------------------------|--------|--------|--------|--------|--------|--------|--------|--------|
| S1- b_{st}/t_{st} [mm] | 110/11 | 120/12 | 130/13 | 140/14 | 150/15 | 158/16 | 158/20 | 158/30 |
| I/I_{req} | 2.90 | 3.92 | 5.15 | 6.63 | 8.37 | 10.06 | 11.75 | 15.64 |
| I/I_{req} 100% TFA | 0.61 | 0.83 | 1.09 | 1.40 | 1.77 | 2.12 | 2.48 | 3.30 |
| I/I_{req} 50% TFA | 1.86 | 2.52 | 3.31 | 4.26 | 5.38 | 6.46 | 7.55 | 10.05 |
| S2- b_{st}/t_{st} [mm] | 60/6 | 70/7 | 80/8 | 100/10 | 120/12 | 140/14 | 150/15 | 158/16 |
| I/I_{req} Eq. (82) | 0.23 | 0.40 | 0.65 | 1.44 | 2.72 | 4.60 | 5.81 | 6.99 |
| I/I_{req} 100% TFA | 0.07 | 0.13 | 0.21 | 0.46 | 0.86 | 1.46 | 1.85 | 2.22 |
| I/I_{req} 50% TFA | 0.24 | 0.42 | 0.67 | 1.49 | 2.80 | 4.74 | 5.98 | 7.19 |

In the second parametric analysis the following varied parameters were considered: the stiffness of transverse stiffener, the web slenderness, the ratio of flange area over web area and the panel aspect ratio. Seven different geometries of girder cross-section were analysed. The basic geometry of the girder (girder G1 in Table 30) is defined with the following parameters: $h_w / t_w = 250$, $A_f / A_w = 0.7$, $\gamma / \gamma^* = 3.0$, $\alpha = a / h_w = 1.0$. In all the other girders (G2-G8) only one parameter is changed, comparing to the basic girder.

In Table 29 the stiffness requirements of transverse stiffener are summarized. The stiffness requirement is calculated according to AASHTO, EN 1993-1-5 Eq. (82) and in the last two columns according to stress and displacement control assuming deviation forces and forces due to tension field action. 100% TFA denotes that full tension field action was considered, and 50% TFA denotes that only 50% of tension field action was taken into account.

Preglednica 29: Zahtevana togost prečnih ojačitev
 Table 29: Required stiffener's stiffness considering different requirements

| I_{req} (cm ⁴) | AASHTO | EN 1993-1-5 (82) | 100% TFA | 50% TFA |
|------------------------------|--------|------------------|----------|---------|
| G1-G5 | 51.2 | 153.6 | 3617.4 | 887.1 |
| G6 | 409.6 | 614.4 | 1696.0 | 697 |
| G7 | 237.0 | 711.1 | 710.2 | 349.6 |
| G8 | 18.7 | 56.0 | 2529.7 | 753.8 |

Preglednica 30: Upoštevani parametri za nosilce obremenjene z veliko strižno silo in upogibnim momentom
 Table 30: Parameters taken into account for girders loaded with high bending and shear load

| STIFFENER | I1 | I2 | I3 | I4 | I5 | I6 | I7 | I8 |
|----------------------|---------------|---------------|---------------|------------------------|------------------------|--------------|---------------|---------------|
| b_{st}/t_{st} [mm] | 20/2 | 40/4 | 60/6 | 80/8 | 100/10 | 120/12 | 150/15 | 200/20 |
| GIRDER | G1 | G2 | G3 | G4 | G5 | G6 | G7 | G8 |
| | $h_w/t_w=250$ | $A_f/A_w=0.3$ | $A_f/A_w=1.1$ | $\gamma/\gamma^*=0.30$ | $\gamma/\gamma^*=1.00$ | $\alpha=0.5$ | $h_w/t_w=150$ | $h_w/t_w=350$ |

8.4.2 Results

In this chapter the results investigating the influence of transverse stiffener on girder resistance and behaviour are discussed. The following results are presented:

- The evolution of out-of-plane displacements along the transverse stiffener.
- The amplitude of the maximal displacement for different stiffnesses of transverse stiffeners.
- The maximum capacity of girders with varied stiffnesses.

The out-of-plane displacements obtained at the maximum force for numerical simulation of tests S1 and S2 are shown in Figure 132. On the right side, the results for girder S1 are plotted. Here the shape of out-of-plane displacement of the transverse stiffener was the same for all stiffeners' stiffnesses, with the only difference in maximum amplitude. In this case the lowest stiffness of the transverse stiffener considered in numerical simulation was 2.90 of minimum required stiffness according to Eq.(82). Therefore, the maximum out-of-plane displacement was relatively small. In simulations of girder S2 much lower stiffnesses of the transverse stiffener were applied. The "S" shape of out-of-plane displacement of flexible stiffeners was observed (I1, I2). By increasing the stiffness of transverse stiffener the shape was transformed from the "S" shape to the "C" shape with much smaller amplitudes. This already happens with transverse stiffener I3. If the stiffener is flexible, the buckling due to the shear progresses over the transverse stiffener onto the adjacent subpanel. Therefore, the "S" shape was observed at smaller stiffnesses of the transverse stiffener. The maximum amplitude of 6.2 mm for the most flexible stiffener was found.

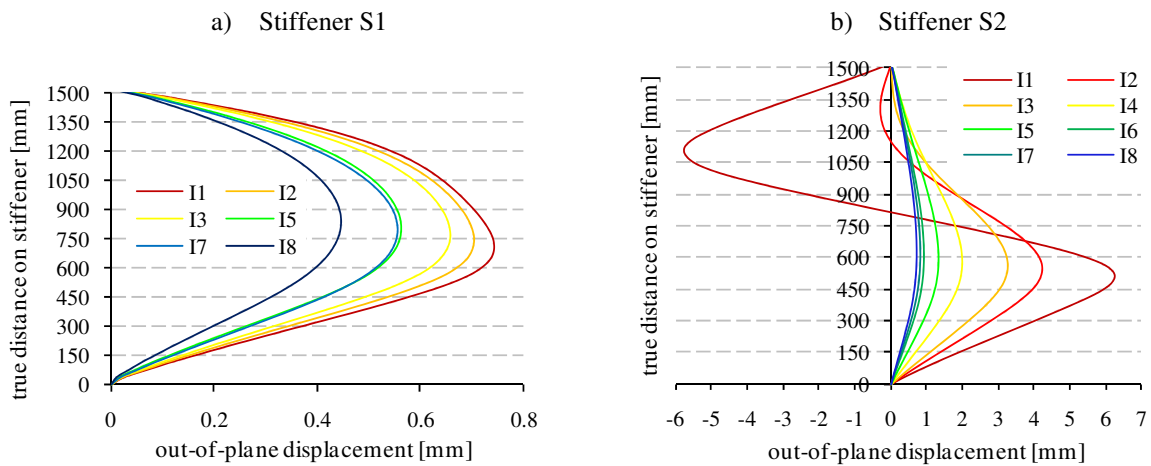


Figure 132: Evolution of the out-of-plane displacement of the transverse stiffener

Slika 132: Razvoj pomikov ojačitve izven ravnine

Figure 133 shows the influence of stiffness of transverse stiffener on maximum resistance and maximum amplitude of out-of-plane displacement. On horizontal axis the actual stiffness of transverse stiffener is normalized with stiffness I_{req} , calculated as:

- a) Minimum stiffener requirement according to Eq. (82).
- b) Required stiffness calculated to fulfil stress and displacement condition including deviation forces and tension filed action on transverse stiffener.
- c) Required stiffness calculated to fulfil stress and displacement condition including deviation forces and 50% of tension filed action on transverse stiffener.

An instantaneous decrease of maximum out-of-plane displacement and increase of girder’s capacity of girder S2 is found already at small ratios I / I_{req} . The increase of girder’s capacity is very small, the difference between maximal and minimal value is only 2%. As it can be seen from the diagram, the maximum displacement of the stiffener is below than required already for small stiffener I2 (see Table 28). To fulfil the displacement criterion ($w \leq h_w/300$) in case a) 40 % of the required stiffness is needed, in case b) 13% and in case c) 42%. The influence of applied stiffeners is small, the difference in girder resistance for smallest and biggest stiffener is below 2%.

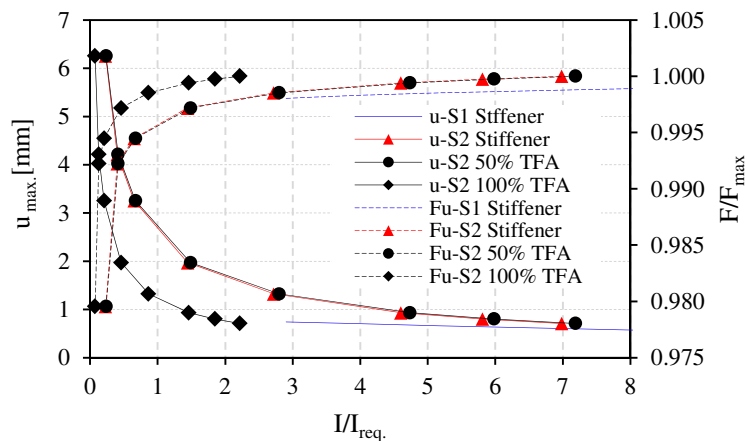


Figure 133: Influence of stiffness of transverse stiffener on girder resistance and out-of-plane displacement of stiffener

Slika 133: Vpliv togosti prečne ojačitve na nosilnost nosilca in na pomike ojačitve izven ravnine

The deflections of transverse stiffeners loaded with high combination of shear force and bending moment are plotted in Figure 134. The curves are plotted for girders with the following parameters: $h_w/t_w = 250$, $A_f/A_w = 0.7$, $\gamma/\gamma^* = 3.0$, $\alpha = a/h_w = 1.0$. Each of the curves corresponds to different stiffnesses of transverse stiffener given in Table 30. The deflection shape depends on the stiffness of the stiffener. By increasing the stiffener's stiffness the deflection of the stiffener is transformed from the "S" shape to the "C" shape.

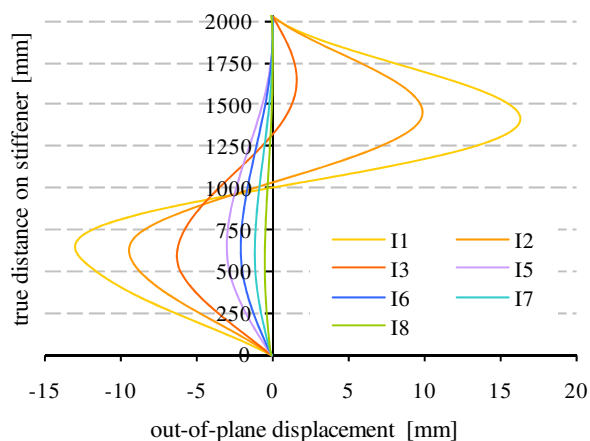


Figure 134: Out-of-plane displacement evolution over transverse stiffener for girder $h_w/t_w=250$, $\alpha=1$, $\gamma/\gamma^*=3.0$, $A_f/A_w=0.7$

Slika 134: Razvoj pomikov ojačitve izven ravnine za nosilec $h_w/t_w=250$, $\alpha=1$, $\gamma/\gamma^*=3.0$, $A_f/A_w=0.7$

In Figure 135 the normalised resistance of girder obtained at deflection of $h_w/300 = 6.67 \text{ mm}$ versus normalised stiffness is plotted. The resistance was normalized with maximal force obtained within all analysed girders of the same cross-section properties, while the actual stiffness is normalized with the required stiffness given by Eq. (82) and with required stiffness to fulfil stress and displacement condition taking into account 50% and 100% of tension field action. From these diagrams the needed stiffeners stiffness is determined to get the resistance when the deflection condition is fulfilled. As it can be seen, the current minimum stiffness requirement is satisfactory.

In Figure 136 the influence of the stiffness of transverse stiffener on maximum girder resistance is shown. It can be seen that the transverse stiffener stiffness does not influence the girder resistance that much, and that maximum capacity is achieved with very small transverse stiffeners.

According to EN 1993-1-5, the transverse stiffener should be designed considering deviation forces and axial force due to tension field action. The current model used for predicting axial force in transverse stiffener is very conservative. This model gives extremely high forces which consequently demand large transverse stiffener, especially if stiffeners are one-sided. On the other hand a minimum stiffness of the stiffener is required in EN 1993-1-5. By increasing minimum stiffness requirement Eq. (82) with factor 3 the stress and displacement condition given in EN 1993-1-5 are met in all cases.

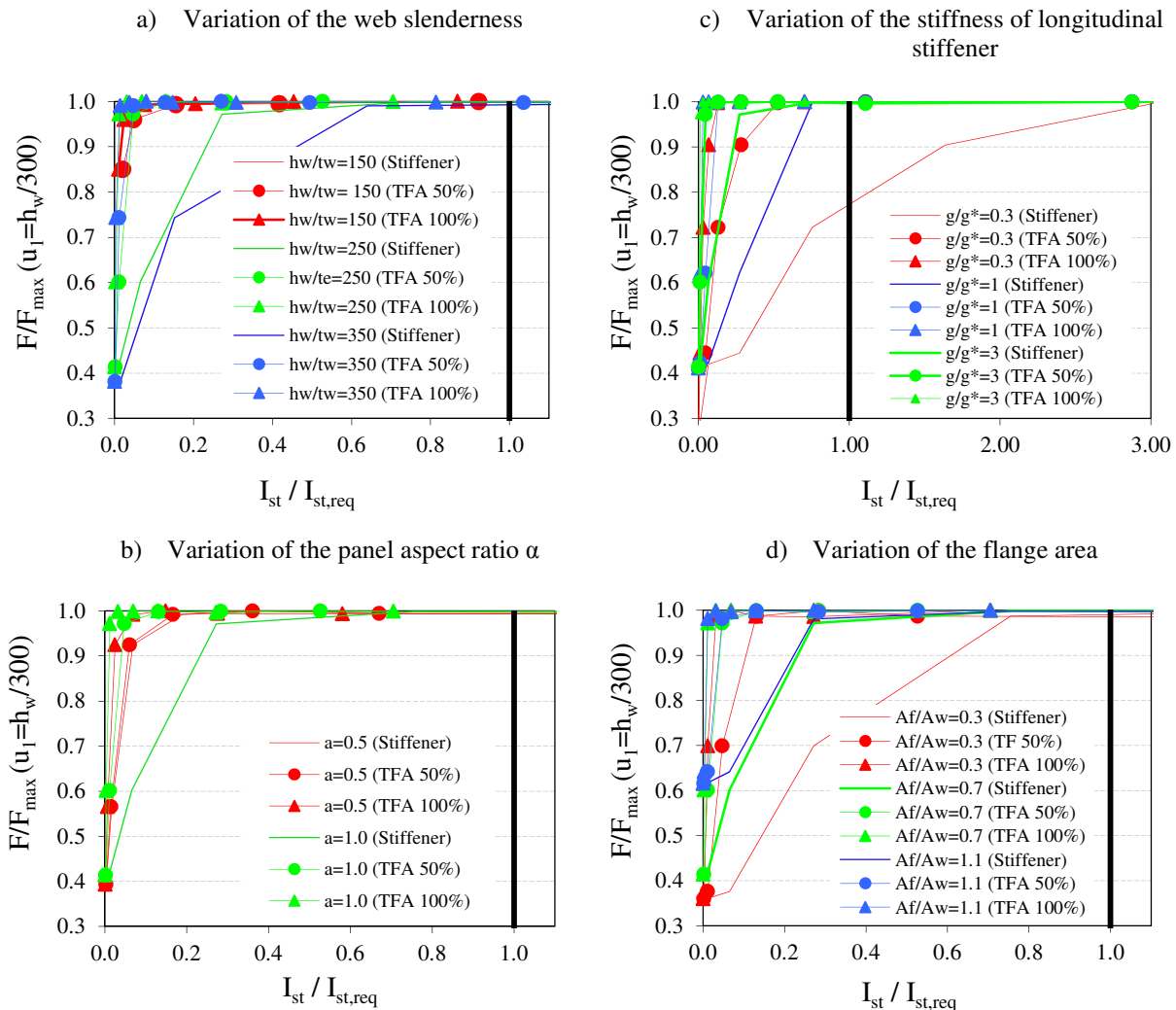


Figure 135: The normalized force obtained at out-of-plane displacement of $h_w/300$ for different stiffness of stiffener

Slika 135: Normirana sila odčitana pri pomiku ojačitve izven ravnine $h_w/300$ za različne zogosti prečne ojačitve

Preglednica 31: Potrebna togost prečne ojačitve da zadostimo pogoju pomika ($w < h_w/300$)

Table 31: Transverse stiffness needed to achieve displacement condition ($w < h_w/300$)

| $I_{needed}/I_{req.}$ | G1 | G2 | G3 | G4 | G5 | G6 | G7 | G8 |
|-----------------------|------|------|------|------|------|------|------|------|
| EN Eq. (82) | 0.27 | 0.75 | 0.27 | 3.04 | 0.27 | 0.19 | 0.08 | 0.64 |
| TFA 50% | 0.05 | 0.13 | 0.05 | 0.53 | 0.05 | 0.17 | 0.16 | 0.05 |
| TFA 100% | 0.01 | 0.03 | 0.01 | 0.13 | 0.01 | 0.07 | 0.08 | 0.01 |

Preglednica 32: Potrebna togost prečne ojačitve, da dosežemo maksimalno nosilnost nosilca

Table 32: Transverse stiffness needed to achieve maximal girder's capacity

| $I_{needed}/I_{req.}$ | G1 | G2 | G3 | G4 | G5 | G6 | G7 | G8 |
|-----------------------|------|------|------|------|------|------|------|------|
| EN Eq. (82) | 0.75 | 1.64 | 0.75 | 1.64 | 0.75 | 0.41 | 0.45 | 0.64 |
| TFA 50% | 0.13 | 0.28 | 0.13 | 0.53 | 0.13 | 0.36 | 0.92 | 0.05 |
| TFA 100% | 0.03 | 0.07 | 0.03 | 0.27 | 0.03 | 0.15 | 0.45 | 0.01 |

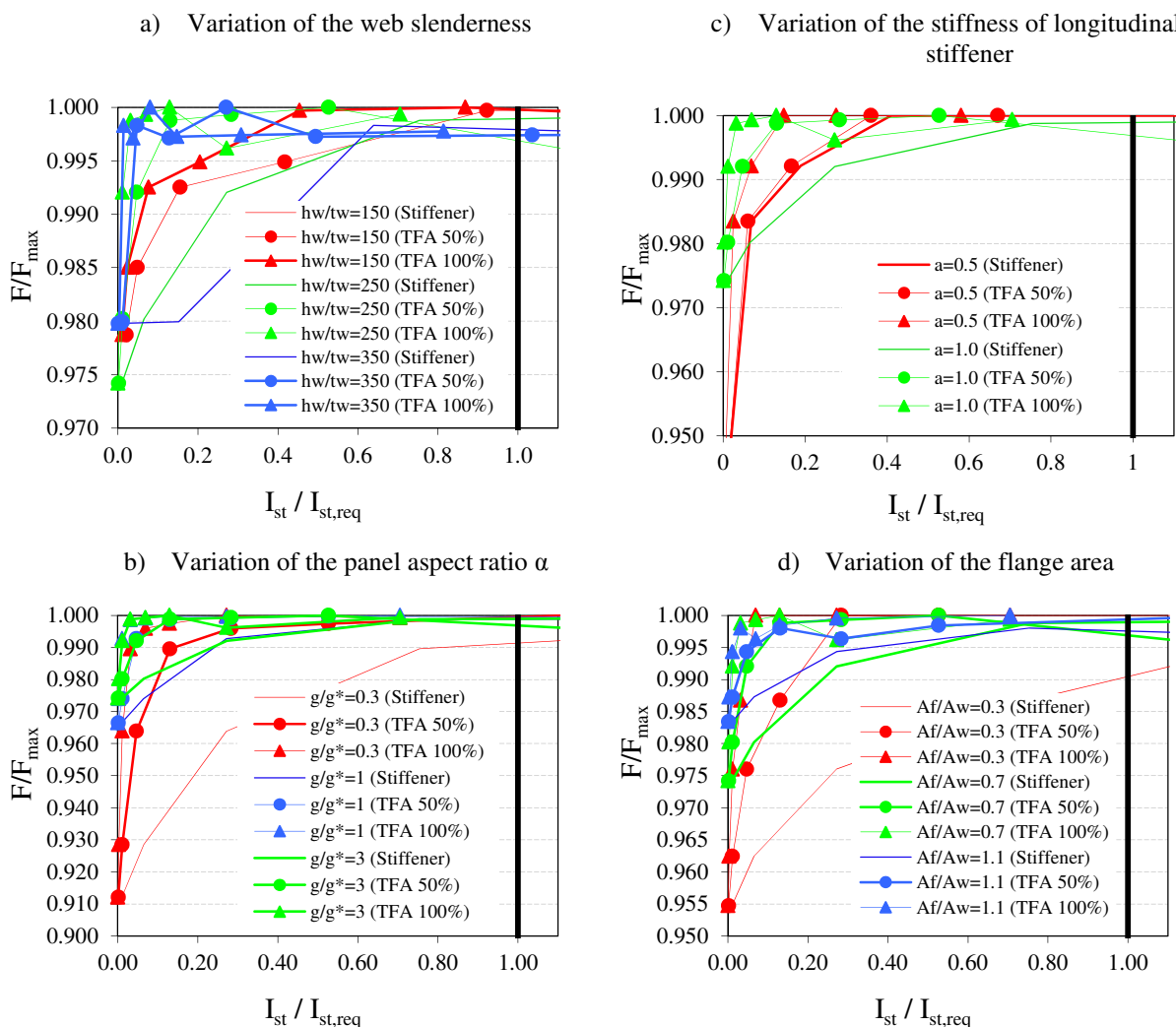


Figure 136: Influence of stiffness on girder's capacity
 Slika 136: Vpliv gostote ojačitve na maksimalno nosilnost nosilca

8.5 Discussions

This chapter brings an overview of experimental and numerical simulations on transverse stiffeners of longitudinally stiffened girders.

The numerical model is verified against experimental results. The following parameters were compared: elastic stiffness of the stiffener, the load-deflection curve and the deflection of transverse stiffeners. The numerical model gives very good results when the capacity, initial stiffness and load-deflection curves are compared. Larger difference is found when the deflections of transverse stiffeners are compared.

Finally, a numerical parametric study was performed to study the influence of stiffness of transverse stiffeners on the behaviour and resistance of the girder. From this analysis the required stiffness of the transverse stiffener to reach maximum resistance and to fulfil design requirements was determined.

If the stiffener is designed to deviation forces and axial forces resulting from the tension field action according to EN 1993-1-5, this results in much bigger stiffener than was obtained by numerical simulations. This comes from overestimation of axial forces due to the tension field action. The actual force, measured in the stiffeners represents 56% of the force calculated according to equation (81).

However, further investigation showed that all the strength and stiffness criteria are met if the minimum stiffness requirement for shear buckling (see Eq. (81)) is multiplied by factor 3:

$$\begin{aligned} I_{st} &\geq \frac{4.5 \cdot h_w^3 \cdot t^3}{a^2} \text{ for } \alpha = \frac{a}{h_w} \leq \sqrt{2} \\ I_{st} &\geq 2.25 \cdot h_w \cdot t^3 \text{ for } \alpha = \frac{a}{h_w} \geq \sqrt{2} \end{aligned} \quad (83)$$

The stiffness of longitudinal stiffener has an important influence on the behaviour and development of out-of-plane displacement of the transverse stiffener. When strong stiffeners are used, they present support to the transverse stiffener and the effect of axial forces is much smaller than for the slender longitudinal stiffeners.

9 CONCLUSIONS AND SUGGESTIONS FOR FURTHER WORK

9.1 Summary and conclusions

One of the main characteristics of plate girders is the post-buckling behaviour where additional resistance is obtained after buckling has occurred. Different models were developed to assess post-buckling resistance of plates. For plates subjected to shear stresses the additional post-buckling resistance is achieved with the formation of the tension field, while for plates subjected to normal stresses the post-buckling resistance is achieved with redistribution of stresses from the buckled parts of the plate to the stiffened or supported parts. In real design situations the plated girders are subjected to various loading conditions with simultaneous presence of bending moments and shear forces.

The aim of this dissertation was to give a general view on the behaviour of longitudinally and transversally stiffened girders subjected to high bending moment and shear load, and to compare the results with the existing resistance model in EN 1993-1-5 and the new proposed model. The load capacity as well as the failure mode of the girders strongly depend on initial imperfections; therefore appropriate and reasonable imperfection shapes and amplitudes have to be considered in the nonlinear analysis to get reliable results.

The design model in EN 1993-1-5 for transverse stiffeners was found conservative by many researchers due to overestimation of axial force in the stiffener due to tension field formation. Therefore, another goal of this dissertation was to study the influence of stiffness of transverse stiffeners on the behaviour of girders.

Four experimental tests were performed on two girders stiffened with open and closed longitudinal stiffeners. These tests represent a major contribution to the available experimental results on longitudinally stiffened plated girders subjected to the combination of high bending moment and shear force. Through load-deflection curve large ductility was obtained for three girders, while girder UC showed smaller ductility due to buckling of the longitudinal stiffener which was in class 4 cross-section. Important results of experimental tests reflected in the evolution of out-of-plane displacements of the investigated web panels. The final resistance of girders was achieved with the formation of the tension field and local buckling of the flanges. The tested girders showed much higher resistance than was obtained by EN 1993-1-5. The reason for this is the stabilizing effect of tension stresses in the largest subpanel which is not considered in the resistance model.

On the basis of experimental results a numerical model was built and verified. The numerical model considered actual geometric properties (width, length and thickness of the plate), geometric initial imperfections and measured material properties. The behaviour, failure mode, initial stiffness and resistance of numerically simulated tests correspond to the experimentally obtained results. In all studied cases numerical model resulted in slightly higher stiffness and resistance (0.6% to 4.1%). Furthermore, a simplified model was developed for numerical simulations and verified against the original model. The average reduction of 0.2% was found for modified numerical model.

The influence of initial geometric imperfections and residual stresses on the girder behaviour and resistance was studied. For all four tests the out-of-plane imperfections were determined by using photogrammetric method. The measured imperfection amplitudes of stiffeners and subpanels were always much below the tolerances. The worst imperfection of the stiffener was found for girder UO and the maximum amplitude of 50.9% of the tolerance was found. Slightly higher out-of-plane

imperfections were found in panel UC. In this case the actual amplitude exceeds tolerances by 24%. The imperfection was caused with preliminary test of neighbour panel UO.

The residual stresses measured in the web plate were found relatively small compared to the other steel elements. The maximum tension stress 246 MPa in the web was measured 15 mm from the flange. The average compression stress 40.60 MPa was larger in the smallest subpanel than in the largest subpanel, i.e. 7.89 MPa. Because of the high slenderness of the panel most of the residual stresses are transformed into out-of-plane deformation of the web.

The imperfection sensitivity analysis was performed taking into account the measured initial imperfections, imperfection shapes according to EN 1993-1-5 and deformed shapes calculated with GMNIA analysis of perfect girder. Within each imperfection shape the maximum amplitudes were varied. The higher amplitude of initial imperfection was applied, the higher reduction in girder resistance was obtained. The deformed shape determined in post-peak range was found as the worst initial imperfection for all studied cases. The reduction of 2.8% to 4.4% was found for all studied girders. The second most unfavourable imperfection was defined as an equivalent combination of a global and local buckling of the plate.

The influence of residual stresses was studied with a simplified stress field distribution. Additional reduction of 0.7% was found when the expected residual stresses were modelled in combination with geometrical imperfections.

In general, initial imperfections have an evident influence on the resistance and behaviour of the element. In particular case the imperfection sensitivity is not so significant, because of the non-symmetry of cross-sections around the weak axis due to single sided longitudinal stiffeners. This results in additional bending moments in longitudinal stiffeners, even when initial imperfections are not present.

An extensive parametric FE study of longitudinally stiffened girders under high bending and shear load was performed to obtain the behaviour and resistance of girders. The considered parameters are given in Chapter 6.2. The study includes 630 girder simulations, of which 520 were stiffened with one stiffener and 110 with two longitudinal stiffeners. In all cases the collapse of girders was characterised by the combination of the yielding over girder height and the yielding of tension field. For flexible stiffeners the tension field was formed over the whole web, otherwise only through a subpanel.

The numerical resistance was compared against the resistance given in EN 1993-1-5. The characteristic resistance was determined at a distance of $\min(0.4a, h_w / 2)$ and $h_{wi,max} / 2$ from the most stressed edge, where a denotes panel length, h_w the web height and $h_{wi,max}$ the maximum height of the subpanel. These distance take into account positive effect of bending gradient and is explained in Chapter 7.2.3. Some discrepancy between numerically obtained capacities and those obtained by current formulation in EN 1993-1-5 is found. The largest difference is found for girders stiffened with one stiffener in compression zone. In these cases the numerical results are much higher due to the positive effect of tension stresses in the largest subpanel. When the stiffener is positioned in the mid-web depth, the obtained resistance is in most cases smaller than predicted with EN 1993-1-5 for interaction check evaluated at a distance of $\min(0.4a, h_w / 2)$. If the interaction check according to EN 1993-1-5 is evaluated at a distance of $h_{wi,max} / 2$, the obtained resistance is higher.

The shape of the interaction diagram according to EN 1993-1-5 generally does not follow numerically obtained results for longitudinally stiffened girders. Therefore, new bending-shear interaction in the web is proposed and verified. Current interaction formula is quadratic, while the obtained response of numerical simulation is for most cases linear. The new interaction formula gives the same resistance only when bending load is equal to bending capacity of flanges. For all other load combinations, the

new proposition result in lower resistance. With newly formulated equation most of numerical results are on safe side and in most cases the coefficient of variation is much smaller.

An important result of this work is also reliability analysis of design resistance formulas, which was performed according to the procedure described in Annex D, EN 1990. Five different resistance models were considered in the reliability analysis. The first two models are bending-shear interaction models (current formulation and new proposal), the third is bending resistance at the most stressed edge and the last two are defined as minimum resistance of interaction check and gross cross-section check. The analysis was performed on different sub-sets which were defined depending on the position of longitudinal stiffener and number of longitudinal stiffeners.

The new formulation of interaction formula for bending-shear interaction is more consistent than the formulation in EN 1993-1-5, but also more conservative. Therefore, the scatter of results is smaller which also results in smaller partial safety factors.

The reliability analysis of design resistance models showed that interaction models $r_{t,1}$ and $r_{t,2}$ do not fulfil reliability conditions with partial safety factor $\gamma_{M1} = 1.1$ when interaction check is performed at a distance of $\min(0.4a, h_w / 2)$. When the interaction check is performed at a distance of $h_{wi,max} / 2$ from the most stressed edge, the reliability conditions are fulfilled for resistance model $r_{t,2}$, while for resistance model $r_{t,1}$ slightly larger partial safety factor of 1.113 is required. Because the difference is very small, resistance model $r_{t,1}$ may be acceptable to determine the resistance of girders under M-V interaction.

Another possibility is to determine resistance of longitudinally stiffened girders with resistance model $r_{t,3}$, which represents bending gross cross-section check at the edge of the panel. The partial safety factor of 1.113 was found in reliability analysis to fulfil conditions given in EN 1990. Also in this case the partial safety factor $\gamma_{M1} = 1.1$ may be acceptable for the design of girders under M-V, considering only bending resistance of gross cross-section at the stiffener. This result is very important from the simplification point of view, because the interaction check can be completely replaced with the much simpler gross cross-section check at the edge of the panel with the maximum value of a bending moment.

Finally, the combination of interaction model and gross cross-section model was used to define girder resistance. For these models the reliability conditions are fulfilled with partial safety factor $\gamma_{M1} = 1.1$.

The influence of stiffness of transverse stiffeners on girder behaviour was also studied. Additional two experimental tests were performed to study the behaviour of rigid transverse stiffener in longitudinally stiffened panel. The test layout and experimental results are presented in Chapter 8. The numerical model that was developed for bending-shear interaction was also verified against these two experiments. The difference of 1.2% and 3.7% compared to static resistance was found. Furthermore, 80 numerical simulations were performed with different stiffnesses of transverse stiffener.

Experimental tests showed that maximum force in the stiffener, which may be decisive for the design of transverse stiffener, is equal to 56% of that predicted in EN 1993-1-5. Further on, numerical investigations, where different stiffnesses of transverse stiffener were studied, showed that the actual stiffness could be much smaller to meet both stress and displacement criteria in EN 1993-1-5. However, all criteria given in EN 1993-1-5 can be fulfilled for all cases, if the minimum stiffness requirement for shear buckling is multiplied by factor 3. With this replacement the unreliable calculation of axial forces in transverse stiffeners due to the tension field action can be completely omitted and the stiffener check is simplified as much as possible.

The size of transverse stiffener is importantly influenced also by the stiffness of longitudinal stiffeners. For flexible longitudinal stiffeners the out-of-plane displacement of the transverse stiffener is much larger than for stiff longitudinal stiffener. Stiff longitudinal stiffeners represent the out-of-plane support to transverse stiffener.

9.2 The original contributions

The original contributions of the present work can be summarized as follows:

- Result from four experimental tests on longitudinally stiffened girders loaded with interaction of high bending moment and shear load.
- First two test on longitudinally and transversally stiffened girders loaded with high shear load to study the influence of tension field action on intermediate rigid transverse stiffener.
- First systematic numerical study of 630 longitudinally stiffened girders subjected to high bending moment and shear load that showed the influence of bending moment on post-critical shear resistance.
- New proposal for interaction resistance model which gives more consistent results.
- Reliability analysis of studied resistance models for M-V interaction.
- Systematic numerical parametric study of the behaviour of intermediate rigid transverse stiffener in longitudinally stiffened girders subjected to high bending moment and shear load.
- Simplified approach to the design of rigid intermediate transverse stiffener based on the minimum stiffness requirement.

9.3 Suggestions for further work

Concerning M-V interaction of longitudinally stiffened girders the following questions arise through this work that might be interesting for further research work:

- The influence of realistic web boundary conditions (flanges and transverse stiffeners) on shear and bending resistance of girders.
- The bending-shear interaction should be studied also for flanges close to the cross-section Class 3 limit.
- The influence of closed Class 4 longitudinal stiffeners on the behaviour of plate girders should also be studied.
- The optimal position of one longitudinal stiffener to maximize shear resistance is not exactly at the mid web depth because of normal stress distribution in the web plate. It would be interesting to define the optimal position of longitudinal stiffener considering influence of normal stresses in compression and tension.

I. UVOD

Uporaba tankih jeklenih pločevin je močno razširjena v letalstvu, strojništvu in v gradbeništvu. V gradbeništvu tanke pločevine predstavljajo del nosilnega elementa. Najbolj pogosto uporabo teh pločevin srečamo v varjenih I nosilcih in škatlastih nosilcih. Varjeni I oziroma polnostenski nosilec je običajno sestavljen iz vitke stojine in kompaktnih pasnic, medtem ko škatlasti profil sestavljajo dve pasnici in dve stojini. Običajna višina takšnih nosilcev je od 1,5 m pa do 4 m in več. Z višino nosilca se močno poveča upogibna nosilnost elementa. Da se zmanjša lastna teža nosilca, se za stojine uporabi vitke pločevine, ki pa so občutljive na izbočenje. Nosilnost takšnih nosilcev se dodatno poveča s prečnimi in vzdolžnimi ojačitvami na stojini. Same ojačitve predstavljajo bodisi togo, bodisi elastično podporo pločevini, s čimer se lahko močno povečata elastična kritična napetost pločevine in nosilnost celotnega nosilca.

Posebnost polnostenskih nosilcev je izkazovanje velike post-kritične nosilnosti, t.j. dodatne nosilnosti, ki jo element izkazuje potem, ko se pločevina že izboči. Post-kritično nosilnost je že davnega leta 1886 opisal Wilson, vendar pa so se polnostenski elementi do leta 1960 projektirali le na kritično uklonsko obtežbo. Po letu 1960 je bilo opravljenih veliko teoretičnih, eksperimentalnih in numeričnih študij, katerih namen je bila določitev modelov za pravilen opis post-kritične nosilnosti. Večina raziskav je bilo usmerjenih v določitev samo strižne ali samo upogibne nosilnosti elementa, medtem ko interakcija hkrati delujočih vplivov upogibnega momenta in strižne sile ni bila tako dobro raziskana. V literaturi lahko zasledimo, da je bilo v 70-ih in 80-ih letih v območju interakcije velikih strižnih sil in upogibnih momentov vsega skupaj opravljenih le 9 eksperimentalnih testov na vzdolžno in prečno ojačanih polnostenskih nosilcih. Glavna pomanjkljivost že izvedenih testov so pomanjkljivi rezultati, ki jih potrebujemo za numerično verifikacijo modela.

Da bi bolje razumeli obnašanje vzdolžno ojačanih nosilcev, obremenjenih z velikimi strižnimi silami in upogibnimi momenti, ter določili vpliv interakcije na post-kritično nosilnost, smo izvedli eksperimentalne raziskave na štirih nosilcih realnih dimenzij. Rezultati eksperimentalnih testov so uporabljeni za verifikacijo numeričnega modela, s katerim smo opravili obširno parametrično študijo, ki da vpogled na vpliv interakcije tudi pri drugačnih geometrijah nosilcev.

Namen doktorskega dela je spoznati in določiti obnašanje vzdolžno ojačanih polnostenskih nosilcev, obremenjenih z visokim nivojem strižnih sil in upogibnih momentov. Na podlagi raziskav je podan modificiran model odpornosti, ki temelji na obstoječem modelu, iz EN 1993-1-5.

Poleg študije interakcijske upogib-strig pri polnostenskih nosilcih je narejena tudi študija vpliva diagonalnega nateznega polja na razvoj osne sile v prečnih ojačitvah. Trenutni model, podan v EN 1993-1-5, predpostavlja nerealno velike osne sile, ki pri enostranskih ojačitvah zahtevajo pretirano velike ojačitve. Eksperimentalne in numerične raziskave, ki so jih opravili Presta [14] in Lee et al. [8, 9], ter Höglundove obdelave eksperimentalnih raziskav od Basler et al. [75, 84] in Evans et al. [75] so pokazale, da je osna sila zaradi razvoja nateznega polja bistveno manjša, kot jo predlaga osnovni model, podan v EN 1993-1-5.

Doktorsko delo je osnovano na eksperimentalnih raziskavah, na podlagi katerih je razvit numeričen model za obširno parametrično študijo. Glavni cilji doktorske disertacije so:

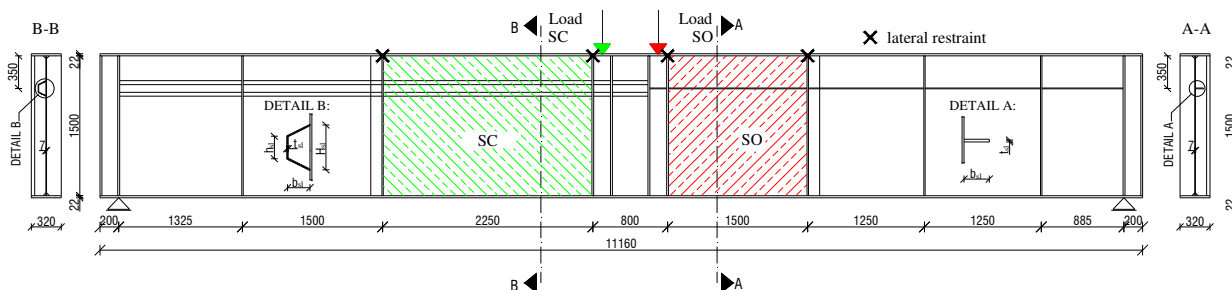
- izvedba eksperimentalnih testov vzdolžno ojačanih nosilcev v območju interakcije velikih strižnih sil in upogibnih momentov,
- verificirati numerični model z rezultati eksperimentalnih testov,

- določiti vpliv začetnih nepopolnosti na obnašanje in nosilnost nosilcev,
- obširna nelinearna parametrična študija nosilcev, obremenjenih z interakcijo strižne sile in upogibnega momenta, ter primerjava numeričnih odpornosti z odpornostmi, določenimi po EN 1993-1-5,
- določitev novega interakcijskega modela in določitev prereza, kjer se izvede kontrola nosilnosti,
- določitev osne sile v prečnih ojačitvah zaradi formacije nateznega polja in študija vpliva togosti prečne ojačitve na nosilnost nosilca.

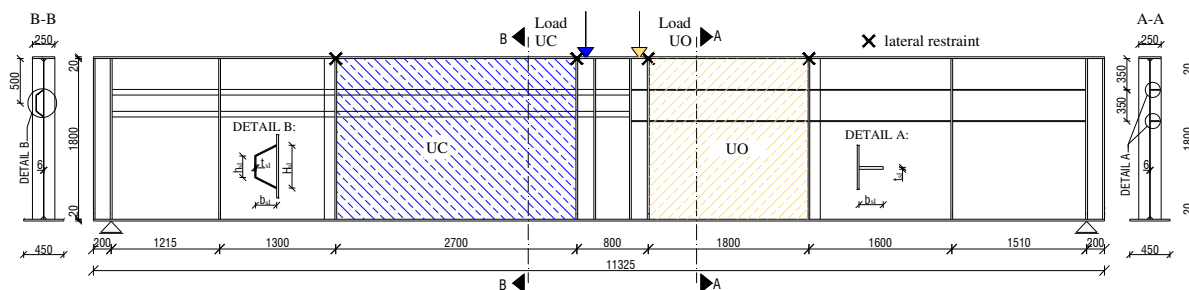
II. EKSPERIMENTALNI TESTI

V območju velikih upogibnih in strižnih obremenitev so bili izvedeni štiri testi na dveh nosilcih. Osnovni prerez prvega nosilca je bil simetričen, drugega pa nesimetričen. Parametri, ki smo jih spreminjali, so sledeči: lega ojačitve, število ojačitev, oblika ojačitve, razmerje stranic panela in vitkost stojine. Prečne ojačitve so bile dimenzionirane z računskim modelom podanim v Johansson et al. [71], upoštevajoč deviacijske sile in sile od nateznega polja. Dolžina nosilca je bila določena tako, da je bilo doseženo zahtevano razmerje med upogibnim momentom in strižno silo v panelu. Togost prečnih ojačitev je bila vedno večja od tiste, ki je potrebna, da je lokalna strižna nosilnost posamezne pločevine med ojačitvami enaka strižni nosilnosti celotnega panela.

Dolžina testnega nosilca s simetričnim prerezom je bila 11,160 m, nosilca z nesimetričnim prerezom pa 11,325 m. Paneli, ki so bili testirani, so z barvnimi šrafurami označeni na sliki 1 in sliki 2. Na nosilcu s simetričnim prerezom (slika 1) in skupno višino 1544 mm sta bila izvedena testa na panelu SO, ojačanem z odprto ojačitvijo, in na panelu SC, ojačanem z zaprto ojačitvijo. Poleg razlike v geometriji vzdolžne ojačitve se panela razlikujeta tudi po razmerju stranic panela, pri čemer je to razmerje za test SO enako $\alpha = 1,0$ in za panel SC $\alpha = 1,5$. Težišče vzdolžne ojačitve je bilo v obeh primerih na razdalji 350 mm od tlačene pasnice. Debelina stojine je bila v območju testnih panelov 7 mm, izven tega območja pa je bila debelina povečana na 8 mm. Med obema testnima paneloma je bila stojina dodatno ojačana s pločevino debeline 7 mm. Prav tako so bili nosilci zaključeni s parom obojestranskih ojačitev, s čimer je bilo zagotovljeno ustrezno sidranje nateznega polja. Vmesne prečne ojačitve so bile dimenzionirane upoštevajoč zahteve EN 1993-1-5 na deviacijske sile in 50% sile zaradi razvoja nateznega polja. Pri izračunu sile od nateznega polja je bila kot obremenitev privzeta čista nosilnost panela.



Slika 1: Geometrija nosilca – simetričen prerez



Slika 2: Geometrija nosilca – nesimetričen prerez

Preostala dva testa sta bila izvedena na nesimetričnem nosilcu skupne višine 1840 mm (slika 2). Panel UO z razmerjem stranic panela $\alpha = 1,0$ je bil ojačan z dvema odprtima ojačitvama. Ojačitvi sta bili postavljeni v tlačno cono, in sicer 350 mm in 750 mm od tlačene pasnice. Panel UC z razmerjem $\alpha = 1,5$ je bil ojačan z eno zaprto ojačitvijo v tlačeni coni na oddaljenosti 500 mm od roba pasnice.

Debelina stojine testnih panelov je bila 6 mm, izven testnega območja pa je bila debelina ojačitve povečana na 7 mm. Nesimetričen prerez je bil izbran z namenom povečanja tlačne cone v stojini. Osnovni parametri geometrije obeh nosilcev so zbrani v preglednici 1.

Preglednica 1: Nominalna geometrija preizkušancev

| Specimen | Stojina | | Pasnica zgoraj | | Pasnica spodaj | | Vzdolžna ojačitev | | | | |
|----------|---------------|---------------|----------------|------------------|------------------|------------------|-------------------|------------------|------------------|------------------|------------------|
| | h_w [mm] | t_w [mm] | a [mm] | b_{f1} [mm] | t_{f1} [mm] | b_{f2} [mm] | t_{f2} [mm] | H_{sl} [mm] | h_{sl} [mm] | b_{sl} [mm] | t_{sl} [mm] |
| SO | 1500 | 7 | 1500 | 320 | 22 | 320 | 22 | / | / | 90 | 10 |
| SC | 1500 | 7 | 2250 | 320 | 22 | 320 | 22 | 160 | 80 | 80 | 5 |
| UO | 1800 | 6 | 1800 | 250 | 20 | 450 | 20 | / | / | 100 | 10 |
| UC | 1800 | 6 | 2700 | 250 | 20 | 450 | 20 | 300 | 180 | 80 | 5 |

Da je bila mogoča izvedba obeh testov, je bil osrednji del nosilca med testnima paneloma dodatno ojačan. V fazi prvega testa je bil sosednji panel ojačan z leseno diagonalo in s tem preprečena nepričakovana porušitev tega panela. V naslednji fazi je bil porušen panel ojačan z vzdolžnimi jeklenimi ojačitvami, test pa je bil izveden na drugem panelu, pri čemer se je točka vnosa sile med obema fazama zamaknila za 600 mm na stran testiranega panela. Bočna zvrnitev tlačene pasnice je bila preprečena z bočnimi podporami, kot je prikazano na sliki 1 in sliki 2.

MATERIAL

Nosilca sta bila izdelana iz osmih različnih pločevin. Za vsako pločevino so bili pripravljene trije natezni preizkušanci, pri čemer sta bila dva natezna testa izvedena v skladu z EN 10002-1, tretji natezni test pa je bil izveden tako, da smo dobili statične vrednosti krivulje napetosti – deformacija. V preglednici 2 so zbrani rezultati nateznih testov pločevin. Napetost tečenja je za posamezno debelino pločevin določena kot srednja vrednost, statična meja plastičnosti pa nato kot povprečno zmanjšanje standardne napetosti tečenja.

Preglednica 2: Rezultati nateznih preizkusov pločevine

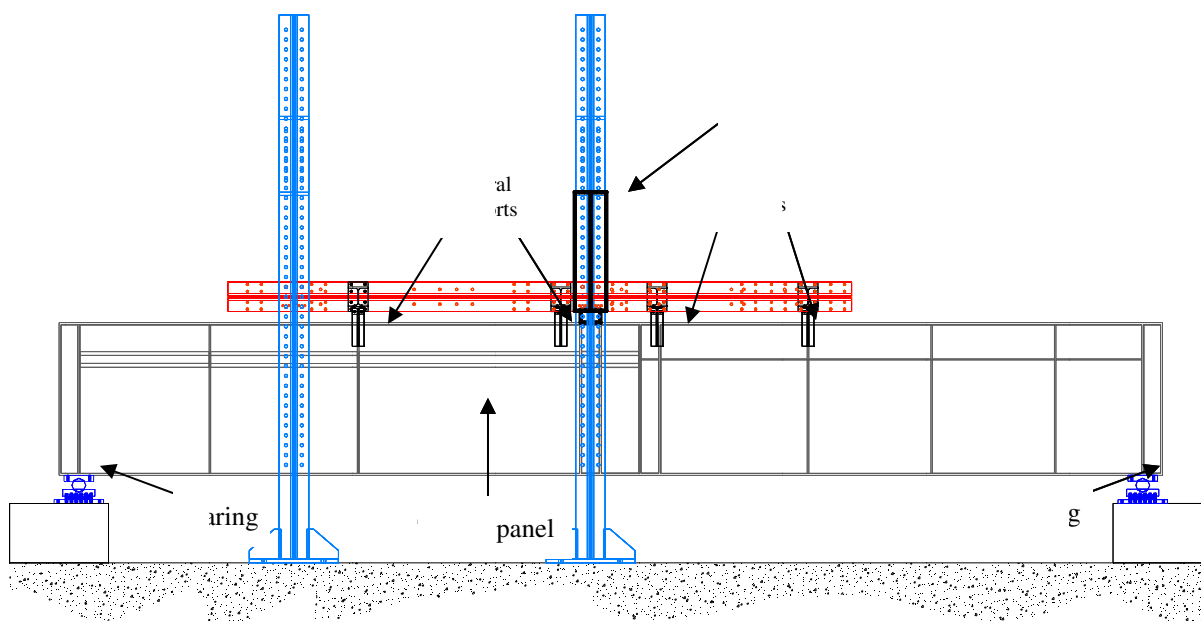
| Pločevina | $R_{p0.02}$ Napetost tečenja [MPa] | R_m Natezna napetost [MPa] | f_u/f_y | Povprečno zmanjšanje $R_{p0.02}$ [%] | Statična napetost tečenja [MPa] |
|-----------|------------------------------------|------------------------------|-----------|--------------------------------------|---------------------------------|
| 5 mm | 385 | 539 | 1.40 | 7.19 | 357 |
| 6 mm | 405 | 539 | 1.33 | | 376 |
| 7 mm | 391 | 561 | 1.44 | | 363 |
| 8 mm | 399 | 552 | 1.38 | | 371 |
| 10 mm | 395 | 542 | 1.37 | | 367 |
| 15 mm | 369 | 520 | 1.41 | | 342 |
| 20 mm | 375 | 543 | 1.45 | | 348 |
| 22 mm | 354 | 536 | 1.52 | | 328 |

IZVEDBA TESTOV

Preizkusi nosilcev so bili zasnovani kot tri-točkovni upogibni testi. Podpori na obeh koncih sta omogočali zasuk okoli osi pravokotno na stojino in pomik v vzdolžni smeri nosilca. Obremenitev je bila vnesena preko hidravličnega bata s kapaciteto 3000 kN, kot je prikazano na sliki 3 in sliki 4. Po postavitvi nosilca v testni položaj smo nosilec obremenili v elastičnem območju do 15% predvidene kapacitete in ga nato razbremenili. Predobremenitev nosilca je služila statični kontroli nosilca, kontroli inštrumentov in tudi zato, da se je nosilec pravilno namestil v testni položaj.



Slika 3: Postavitev testa v laboratoriju

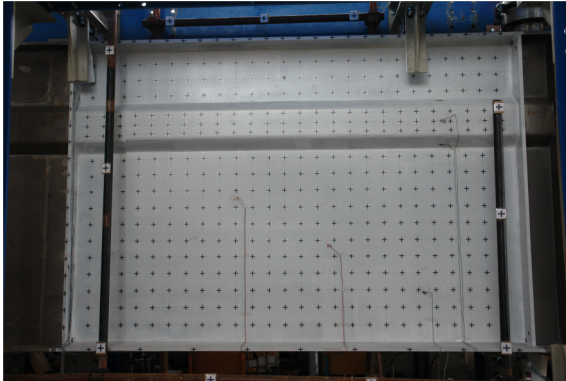


Slika 4: Postavitev testa

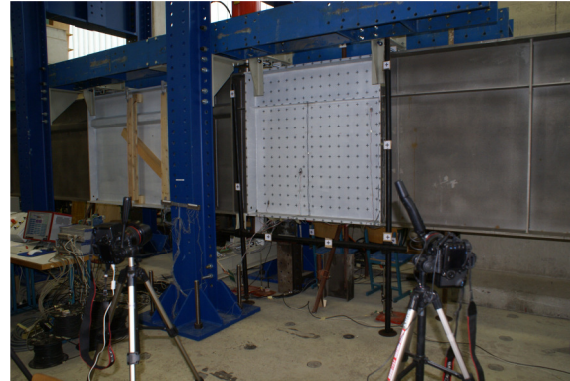
Sledil je test nosilca do porušitve in sicer po sledečem protokolu obremenjevanja: hitrost obremenjevanja v elastičnem področju je bila 0,05 mm/s in povišana v plastičnem področju na 0,10 mm/s. Med samim testom se je v določenih točkah obremenjevanje ustavilo, da so se določile statične vrednosti odziva nosilca. V elastičnem področju so bili časovni postanki dolgi 60 s, v plastičnem pa 300 s. Med postanki so bile opravljene fotogrametrične meritve.

Med izvedbo testov smo neprestano merili silo, pomike in deformacije. V pasnicah, prečni in vzdolžni ojačitvi so se deformacije merile z linijskimi merilnimi lističi, medtem ko so se deformacije v stojini merile z rozetami. V stojinah, vzdolžnih odprtih ojačitvah in v prečnih ojačitvah so se meritve izvajale na obeh straneh pločevine, medtem ko so se deformacije v pasnicah in v zaprtih vzdolžnih ojačitvah merile le na eni strani pločevine. Pomiki panela izven ravnine so bili za posamezne obtežne korake določeni z uporabo fotogrametričnih metod. Za ta namen je bil panel predhodno pobarvan z belo barvo in označen z črnimi križi. Oznake so označevale presečišča mreže 100×100 mm. Da so se pomiki

lahko določili z uporabo fotogrametričnih metod, so bile v prostor okoli testnega panela postavljene dodatne neodvisne referenčne točke (glej slika 5). Dodatno so se pomiki merili z induktivnimi merilci in digitalnimi uricami. Za primerjavo so trije induktivni merilci merili pomik v panelu izven ravnine. Ti rezultati so služili za kontrolo pomikov, izmerjenih s fotogrametrijo.



a) oprema panela s tarčami – črni križi



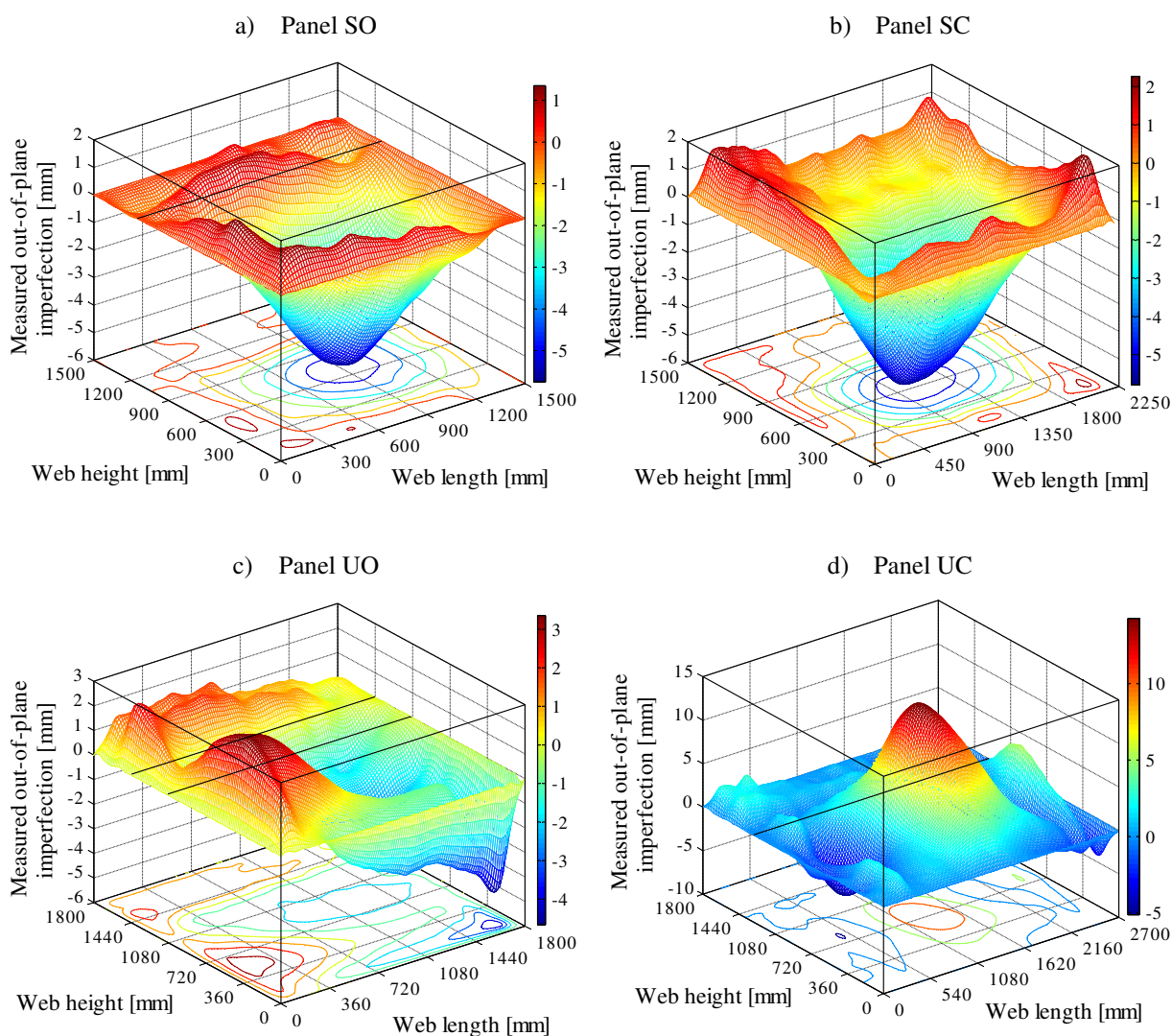
b) pozicija dveh digitalnih kamer Canon EOS 5D

Slika 5: Priprava panelov in postavitev kamer za fotogrametrijo

ZAČETNE NEPOPOLNOSTI

Začetne nepopolnosti imajo lahko pomemben vpliv pri določitvi nosilnosti elementa. Pri klasičnem dimenzioniranju se vpliv začetnih nepopolnosti zajame z uporabo uklonskih krivulj. Alternativa temu je, da se dimenzioniranje elementov izvede z nelinearno geometrijsko in materialno analizo z upoštevanjem začetnih nepopolnosti. Pri polnostenskih nosilcih poznamo dve vrsti nepopolnosti: geometrijsko nepopolnost in zaostale napetosti. V numeričnem modelu lahko obe nepopolnosti modeliramo neodvisno, vendar se zaradi kompleksnosti modeliranja zaostalih napetosti pogosto oba vpliva nadomestita samo z nadomestnimi geometrijskimi nepopolnostmi.

Da smo z eksperimenti lahko ustrezno verificirali numerični model, smo torej potrebovali natančne meritve začetnih nepopolnosti. V testnih panelih smo geometrijske nepopolnosti določili s pomočjo fotogrametrije. Globalno nepopolnost celotnega nosilca smo določili z ročnim merjenjem, pri čemer smo med skrajnima točkama napeli vrvico in nato odmerjali razdaljo med vrvico in robom pasnice. V nadaljevanju so predstavljene le lokalne nepopolnosti panela. Merjenja začetnih nepopolnosti so pokazala, da so vse nepopolnosti, ki so posledica izdelave nosilcev, pod mejami dovoljenih toleranc. Nepopolnosti, izmerjene v panelu UC, so presegle meje toleranc, vendar te nepopolnosti niso izhajale le iz procesa izdelave nosilca, temveč iz predhodno opravljenega testa na panelu UO. Največje amplitude začetnih nepopolnosti so bile izmerjene v največjem pod panelu (glej slike 6a-d). Primerjave izmerjenih amplitud in toleranc so zbrane v preglednici 3.



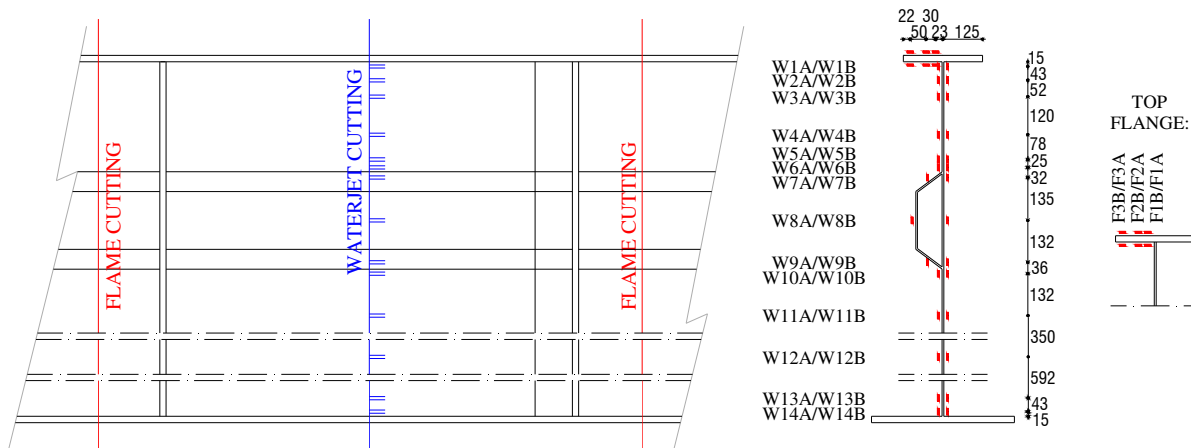
Slika 6: Izmerjene začetne nepopolnosti v panelih

Preglednica 3: Primerjava izmerjenih amplitude panela s tolerancami podanimi v EN 1090-2

| | Izmerjeno | Toleranca | 0.8×Toleranca | Izmerjeno/Toleranca |
|-----------------|-----------|-------------------|---------------|---------------------|
| PANEL SO | | | | |
| Ojačitev | 0.92 mm | $a/400 = 3.75$ mm | 3.00 mm | 0.245 |
| Večji podpanel | - 5.75 mm | $b/100 = 11.5$ mm | 9.20 mm | 0.500 |
| PANEL SC | | | | |
| Ojačitev | 1.49 mm | $a/400 = 5.63$ mm | 4.50 mm | 0.164 |
| Večji podpanel | - 5.79 mm | $b/100 = 10.7$ mm | 8.56 mm | 0.537 |
| Manjši podpanel | 1.85 mm | $b/100 = 2.70$ mm | 2.16 mm | 0.685 |
| PANEL UO | | | | |
| Ojačitev | 2.29 mm | $a/400 = 4.50$ mm | 3.60 mm | 0.509 |
| Večji podpanel | - 4.67 mm | $b/100 = 11.0$ mm | 8.56 mm | 0.425 |
| Manjši podpanel | 2.51 mm | $b/100 = 3.50$ mm | 2.80 mm | 0.717 |
| PANEL UC | | | | |
| Ojačitev | 2.49 mm | $a/400 = 6.75$ mm | 5.40 mm | 0.369 |
| Večji podpanel | 14.27 mm | $b/100 = 11.5$ mm | 9.20 mm | 1.241 |
| Manjši podpanel | -3.08 mm | $b/100 = 3.50$ mm | 2.80 mm | 0.880 |

Zaostale napetosti, prisotne v nosilcu, so pri polnostenskih varjenih nosilcih predvsem posledica neenakomerne plastifikacije med varjenjem. V območju zvarov tako dobimo velike natezne napetosti, kjer lahko največje vrednosti dosežejo vrednosti, enake napetosti tečenja, v preostalem območju pa dobimo tlačne napetosti. Te napetosti so uravnotežene, kar pomeni, da je integral napetosti po površini prereza enak nič.

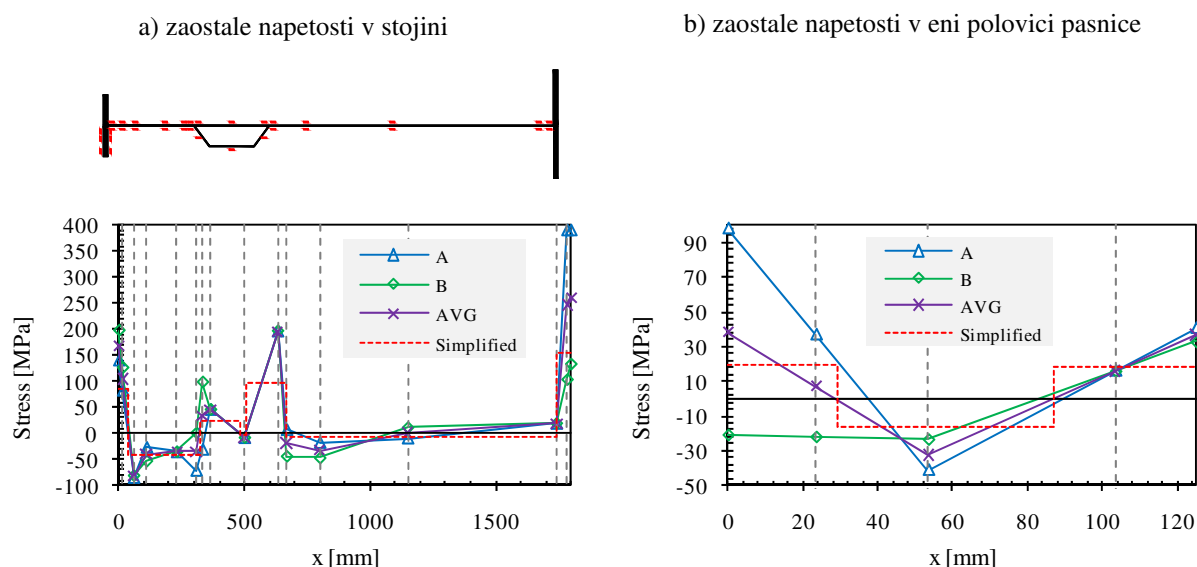
Potek zaostalih napetosti po prerezu smo določili na nesimetričnem nosilcu z uporabo destruktivne metode razreza pločevine. Zaostale napetosti smo merili na delu nosilca, ki med mehanskimi testi ni bil obremenjen preko plastičnih deformacij. Merjenje smo izvedli v stojini in v eni polovici manjše pasnice, kot je prikazano na sliki 7.



Slika 7: Lokacija merilnih mest zaostalih deformacij

Proces merjenja zaostalih napetosti je bil sledeč: v prvi fazi smo del panela, kjer smo merili deformacije, izrezali z avtogenim rezanjem. Sledilo je abrazivno rezanje nosilca ob nameščenih merilnih lističih, in sicer najprej po višini nosilca in nato v vzdolžni smeri ob obeh straneh merilnega lističa. Deformacije smo merili skozi celoten proces rezanja pločevine in ga zaključili, ko v meritvah ni bilo zaznati več nobene spremembe. Rezultati meritev zaostalih napetosti za izbran prerez so prikazani na sliki 8. Potek zaostalih napetosti po prerezu stojine je pričakovan. V območju zvarov smo tako izmerili natezne napetosti z največjo vrednostjo 246 MPa, in sicer 15 mm od roba spodnje pasnice. Povprečna vrednost tlačnih napetosti v manjšem podpanelu je 40,60 MPa, kar predstavlja 10,25 % izmerjene napetosti tečenja. V večjem podpanelu znaša povprečna vrednost izmerjenih tlačnih napetosti 7.89 MPa. Natezne zaostale napetosti v pasnici zasledimo v območju zvara, in tudi na robu pasnice, kar pa je posledica plamenskega rezanja pločevine. Največja povprečna izmerjena natezna zaostala napetost znaša le 38.35 MPa.

Izmerjene zaostale napetosti v varjenem polnostenskem nosilcu so razmeroma majhne, še posebno če jih primerjamo z zaostalimi napetostmi, ki so prisotne pri vroče valjanih profilih. Največji vpliv na zaostale napetosti ima razmerje med vhodno energijo in maso materiala, ki ga spajamo. V primeru polnostenskih nosilcev je to razmerje majhno. Drugi pomemben faktor, ki tudi vpliva na zaostale napetosti, pa je vitkost elementov. Bolj kot so elementi vitki, večji del zaostalih napetosti se prelevi v geometrijske nepopolnosti. To lahko vidimo tudi iz rezultatov, saj so zaostale napetosti v večjem podpanelu bistveno manjše kot v manjšem podpanelu, posledično pa so izmerjene večje geometrijske nepopolnosti v večjem podpanelu.

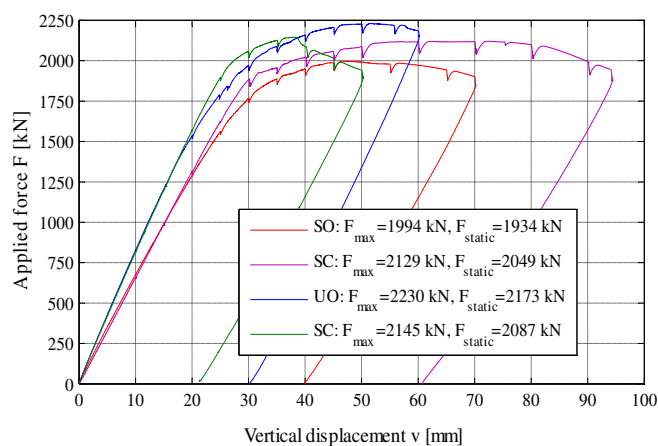


Slika 7: Izmerjene zaostale napetosti

REZULTATI TESTOV

V tem poglavju so na kratko predstavljeni najbolj pomembni rezultati, kot so krivulje sila-pomik in razvoj pomikov izven ravnine. Pomiki izven ravnine natančno pokažejo obnašanje nosilcev, obremenjenih s kombinacijo velikih prečnih sil in upogibnih momentov. Prikazani in komentirani so tudi rezultati izmerjenih deformacij v stojini, pasnicah in v prečni ojačitvi.

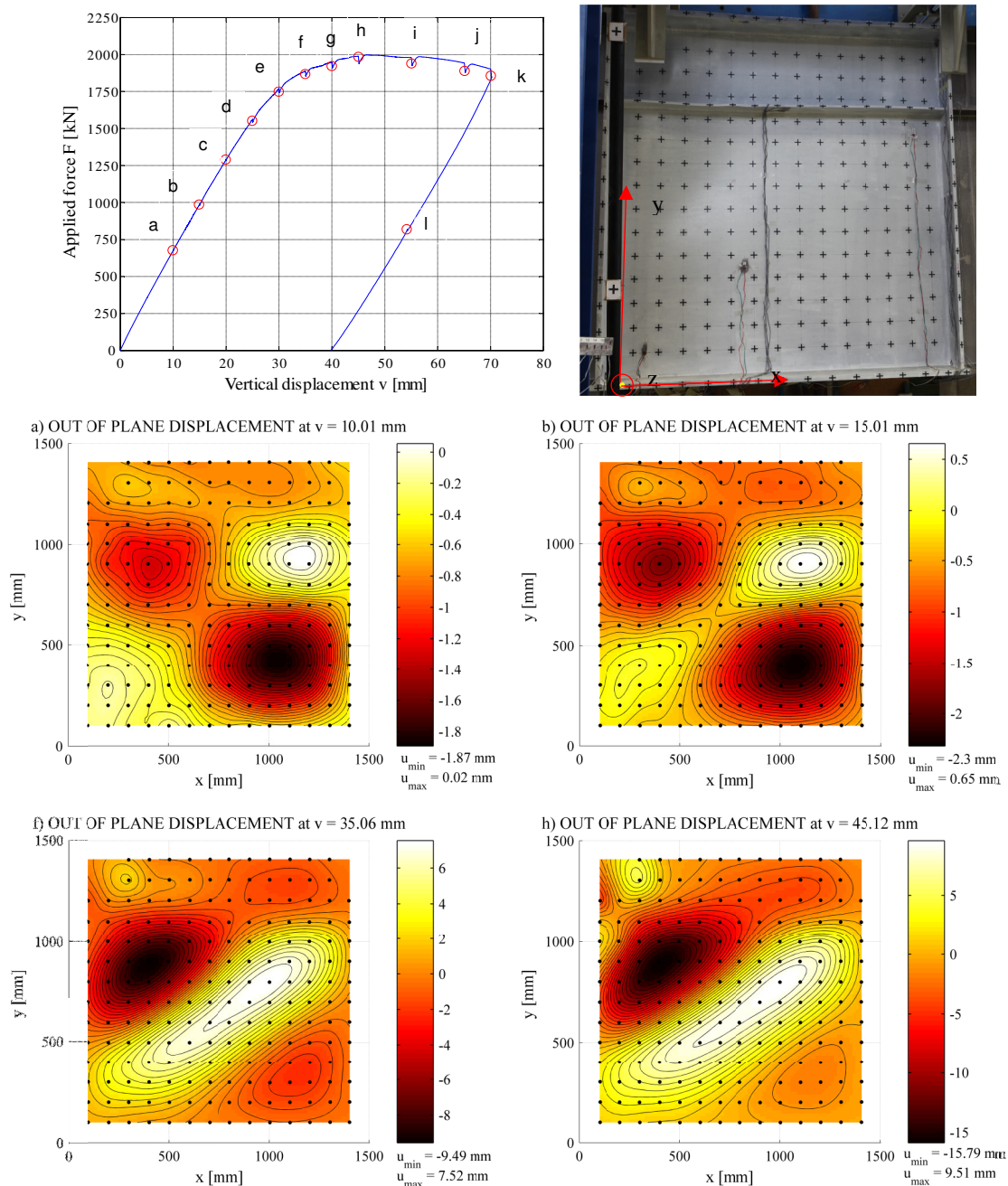
Na sliki 8 so prikazane krivulje sila-pomik za vse štiri nosilce. Največjo nosilnost smo izmerili pri panelu UO in najmanjšo pri panelu SO. Pri vseh krivuljah je lepo viden padec nosilnosti med 300 s postanki med izvedbo testa. Po postanku se je test nadaljeval z enako hitrostjo kot pred postankom. Spodnje točke krivulje predstavljajo statičen odziv nosilca pri nični hitrosti naraščanja deformacij.



Slika 8: Krivulje sila – pomik za vse štiri teste

Razvoj pomikov izven ravnine za testni panel SO je predstavljen na sliki 9. Pomiki so prikazani za obtežna stanja, ki so na krivulji sila-pomik označena z rdečimi krogi in črkami. Že pri majhni obremenitvi ($v = 10$ mm), kjer je obremenitev manjša od kritične strižne sile panela, smo zaznali pomike izven ravnine. Že v naslednjem koraku pri $v = 15$ mm lahko opazimo čisto strižno izbočenje panela z razvojem nateznega polja. V tem koraku zaznamo tudi prvo izbočenje v manjšem podpanelu

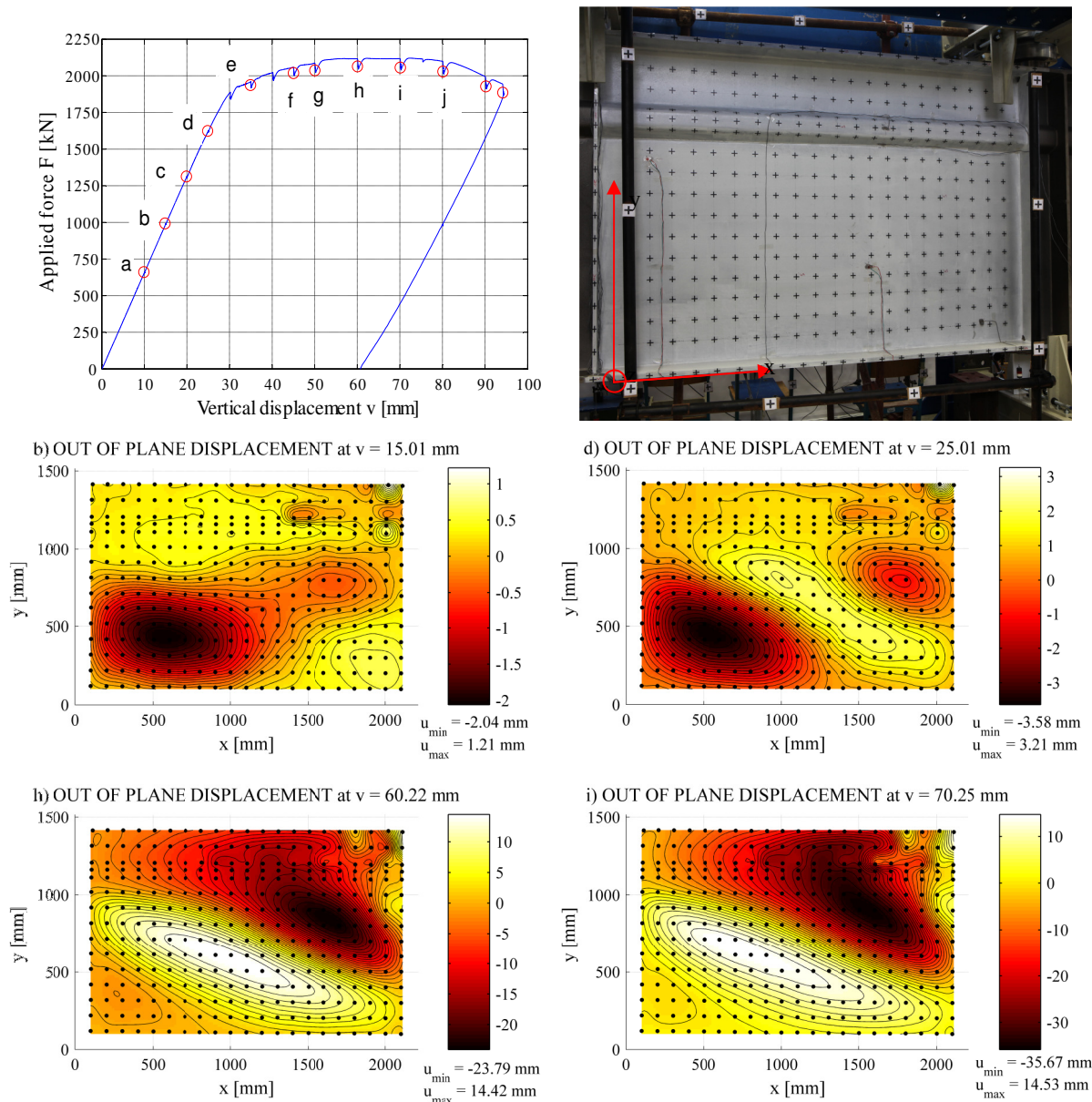
zaradi tlačnih napetosti. Z večanjem obremenjevanja ostane oblika izbočenja enaka, spreminja se le amplituda. Pri pomiku $v = 35$ mm se prične spreminjati tudi oblika izbočenja, in sicer iz treh simetričnih valov v dva nesimetrična. Največja nosilnost nosilca je izkazana pri pomiku $v = 45$ mm. V tej točki smo med testom opazili tudi izbočenje tlačne pasnice. Končna porušna oblika panela je kombinacija izbočenja zaradi upogibnega momenta in strižne sile.



Slika 9: Razvoj pomikov izven ravnine, panel SO

Za drugi panel SC, ki je bil testiran na istem nosilcu kot panel SO, je razvoj pomikov izven ravnine prikazan na sliki 10. V začetnem elastičnem področju so prirastki pomikov izven ravnine relativno majhni. Večje prirastke zasledimo pri obremenitvi, ki je večja od strižne kritične sile ($v = 25$ mm). Tu lahko razločno vidimo strižno izbočenje podpanela in s tem razvoj nateznega polja. V elastičnem območju obremenjevanja v vzdolžni ojačitvi ni bilo zaznani večjih pomikov izven ravnine. Prav tako ni bilo večjih pomikov izven ravnine v zgornjem, manjšem podpanelu, ki spada za izbrano napetostno stanje v 3. razred kompaktnosti. Do globalnega izbočenja panela pride pri obtežbi pri $v = 60$ mm, kjer

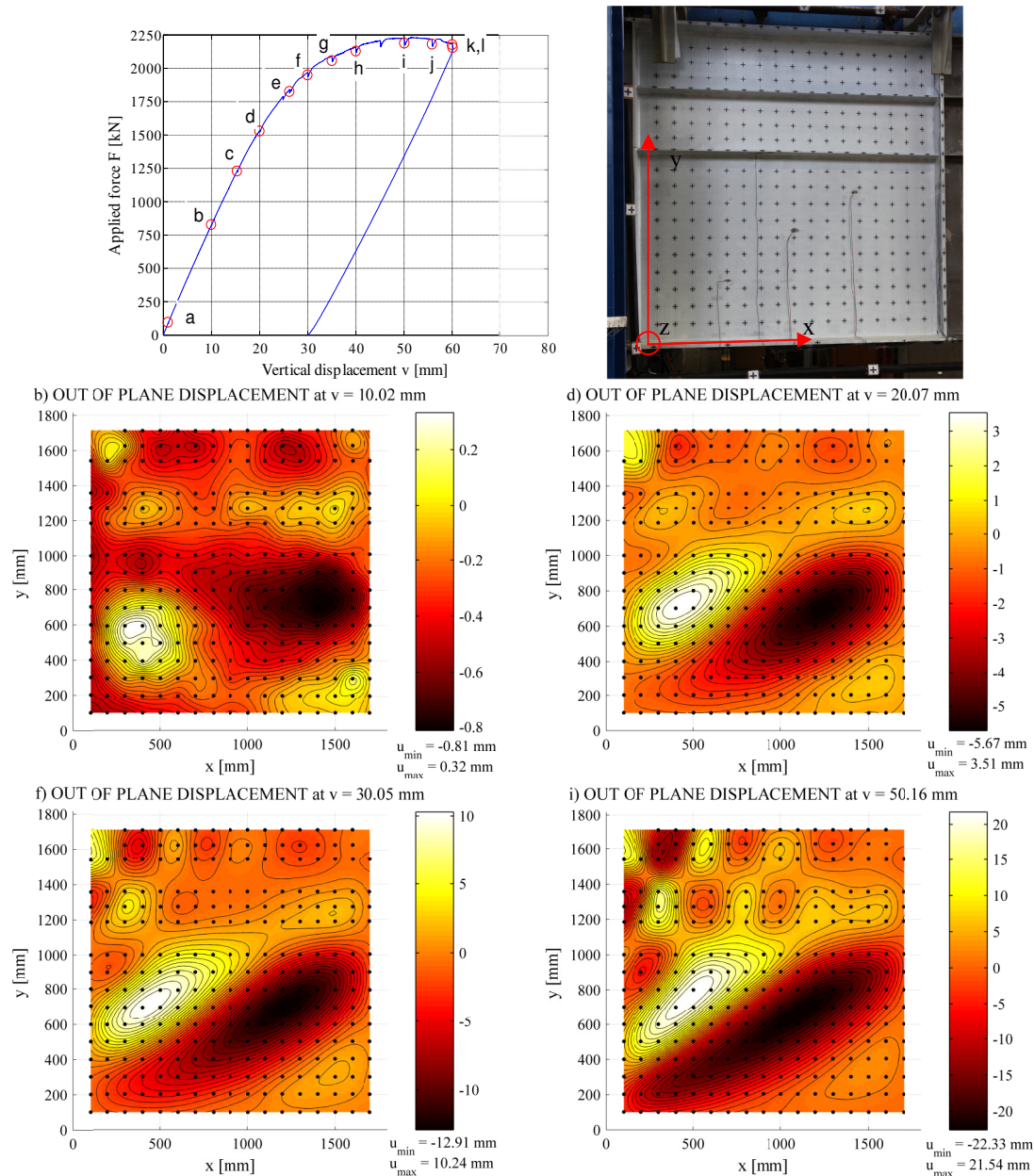
zaznamo večje pomike izven ravnine vzdolž ojačitve. Z nadaljnjim obremenjevanjem nosilnost panela le še pada. Tudi v tem primeru je končna porušna oblika kombinacija globalnega izbočenja zaradi upogibnega momenta in strižne sile.



Slika 10: Razvoj pomikov izven ravnine, panel SC

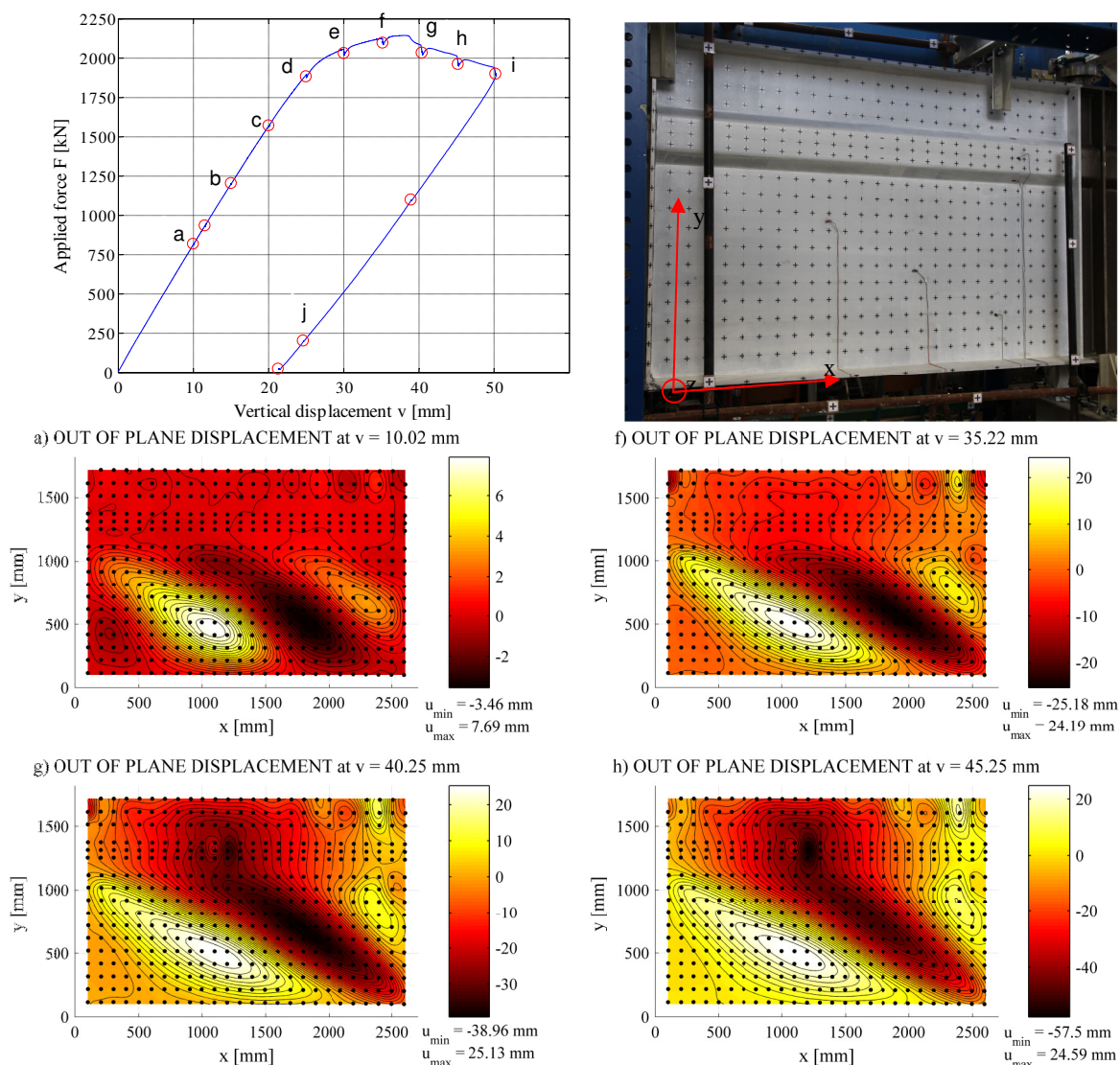
Naslednja dva testa sta bila izvedena na nosilcu z nesimetričnem prerezom. Rezultati razvoja pomikov izven ravnine v panelu UO so prikazani na sliki 11. Pri sili, ki je manjša od elastične kritične strižne sile izbočenja, so pomiki izven ravnine majhni. Strižno obliko izbočenja panela najprej opazimo pri vertikalnem pomiku $v = 20$ mm oziroma pri sili, ki je nekoliko večja od 1500 kN. Amplituda največjega pomika izven ravnine je pri tej obtežbi 5.67 mm. Pri tej obremenitvi lahko tudi že opazimo lokalno izbočenje v obeh manjših podpanelih zaradi tlačnih napetosti, ki so posledica upogibnega momenta. Prve znake globalnega izbočenja zasledimo pri pomiku $v = 50$ mm, kjer se izbočenje večjega podpanela razširi tudi preko srednjega podpanela. Končna oblika porušitve je v tem primeru kombinacija strižnega izbočenja večjega panela, ki se je delno razširil tudi preko srednjega podpanela, in lokalnega izbočenja v manjših podpanelih zaradi tlačnih napetosti. Porušna oblika vzdolžnih

ojačitev je kombinacija globalnega uklona in lokalne nestabilnosti. V plastičnem območju se lokalno ukloni tudi tlačena pasnica.



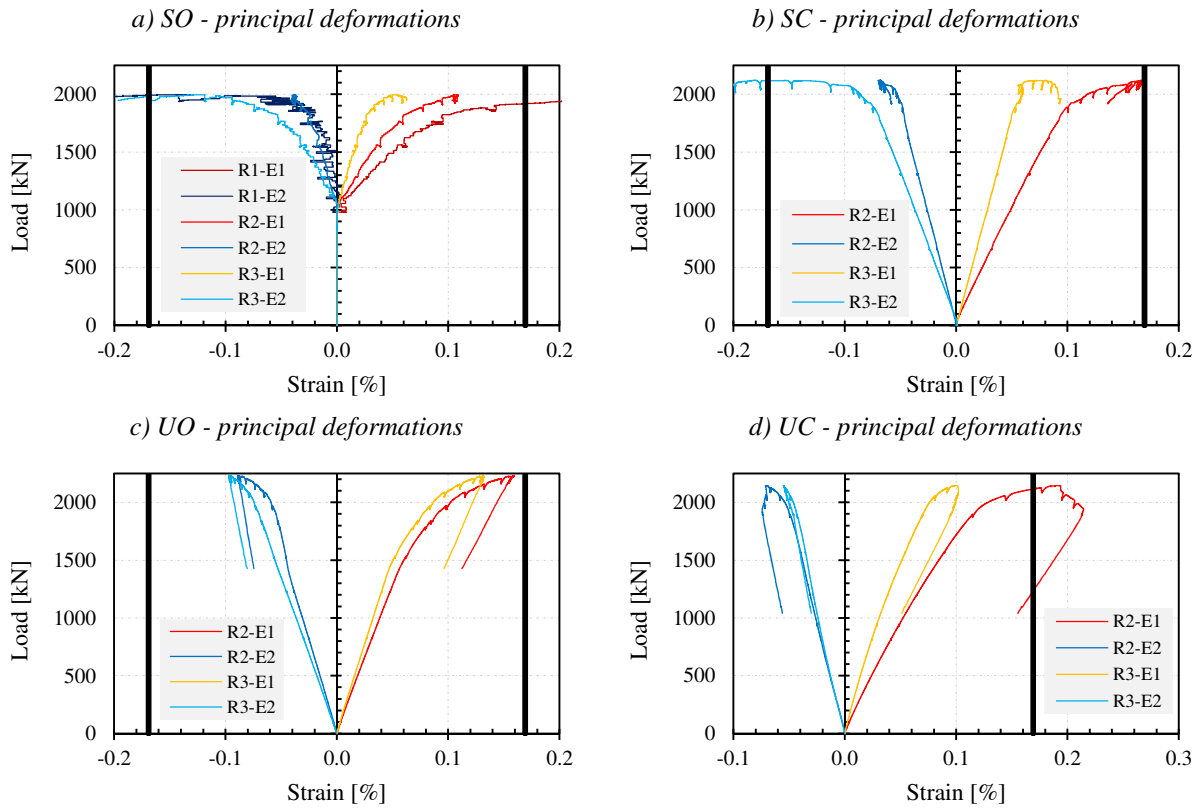
Slika 11: Razvoj pomikov izven ravnine, panel UO

Zadnji test je bil izveden na panelu UC, ki je imel za razliko od ostalih testov bistveno večje začetne geometrijske nepopolnosti. Te nepopolnosti so bile posledica predhodnega testa na panelu UO. Tako zasledimo strižno obliko izbočenja (glej sliko 12) že pri zelo majhnem nivoju obremenitve, $v = 10$ mm. Večji podpanel se izboči v treh diagonalnih valovih z maksimalno amplitudo na mestu najmanjšega upogibnega momenta. V manjšem podpanelu opazimo lokalno izbočenje pri obremenitvi 1200 kN. Z večanjem obtežbe se povečujejo pomiki izven ravnine in tako tudi vplivi drugega reda. Zaradi teh vplivov in velike osne sile, s katero je obremenjena vzdolžna ojačitev, se le-ta ukloni. Uklon ojačitve se zgodi med pomikoma $v = 35$ mm in $v = 40$ mm, kar je razvidno tudi iz krivulje sila-pomik (hipen padec nosilnosti).



Slika 12: Razvoj pomikov izven ravnine, panel UC

Kot že omenjeno, so bile deformacije merjene v stojini, pasnicah in prečni ojačitvi. V stojini so bile deformacije merjene z rozetami, tako smo lahko določili smer in velikost glavnih deformacij. Za vse štiri izvedene teste je razvoj glavnih deformacij prikazan na sliki 13. V vseh primerih je natezna deformacija v točki R2 večja kot tlačna deformacija. Prav tako so glavne natezne deformacije usmerjene v smeri formiranja nateznega polja. V točki R3 je deformacijsko stanje zaradi različnih vplivov, kot so sidranje nateznega polja, kombinacija tlačnih in strižnih obremenitev in bližina obeh ojačitev, bistveno bolj kompleksno. Pri testih SC in SO so tlačne deformacije večje kot natezne in obratno pri testih OU in OC.

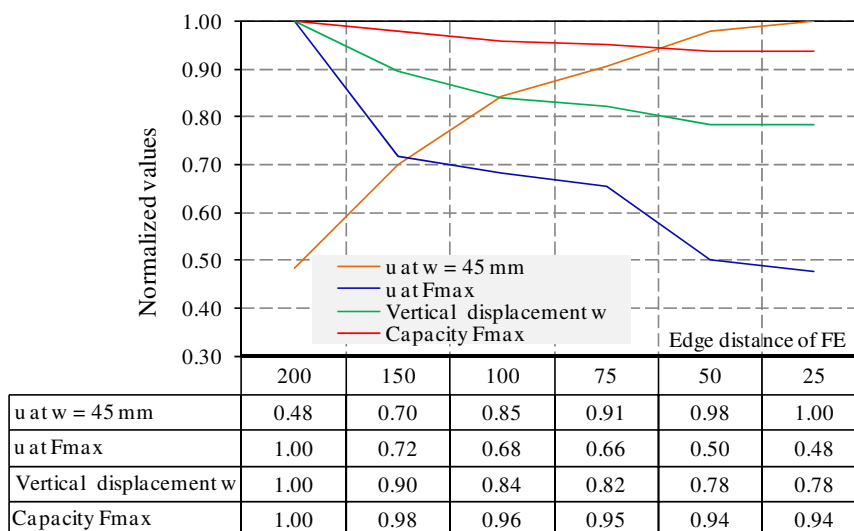
Slika 13: Glavne membranske deformacije v stojini ($\epsilon_1 = E1$, $\epsilon_2 = E2$)

III. NUMERIČNI MODEL

V tem poglavju je poleg predstavitve numeričnega modela in njegove verifikacije s testnimi rezultati prikazana tudi študija vplivov različnih nepopolnosti in amplitud na mejno nosilnost polnostenskega nosilca.

Preizkuse smo numerično modelirali s končnimi elementi v okolju ABAQUS. Uporabljeni so bili 4 vozliščni lupinasti končni elementi z reducirano integracijo. Na nekaterih mestih so bili zaradi geometrije nosilca uporabljeni tudi 3 vozliščni končni elementi. Za verifikacijo numeričnega modela smo uporabili modificirane materialne modele iz nateznih preizkusov, za ostale numerične simulacije pa bilinearen diagram z minimalno utrditvijo. V parametrični študiji smo uporabili material S355 z napetostjo na meji tečenja 355 MPa in elastičnim modulom $E = 210000$ MPa.

Velikost končnih elementov, ki smo jih uporabili v numerični analizi, smo določili s konvergenčno študijo. Zadovoljive rezultate nosilnosti nosilca smo dosegli že pri večjih velikostih končnih elementov (Slika 14). Pri pomikih izven ravnine se je pokazalo, da je njihova amplituda močno odvisna od velikosti mreže. Na podlagi dobljenih rezultatov smo vse nadaljnje numerične simulacije izvajali s končnimi elementi, katerih rob je manjši od 50 mm.

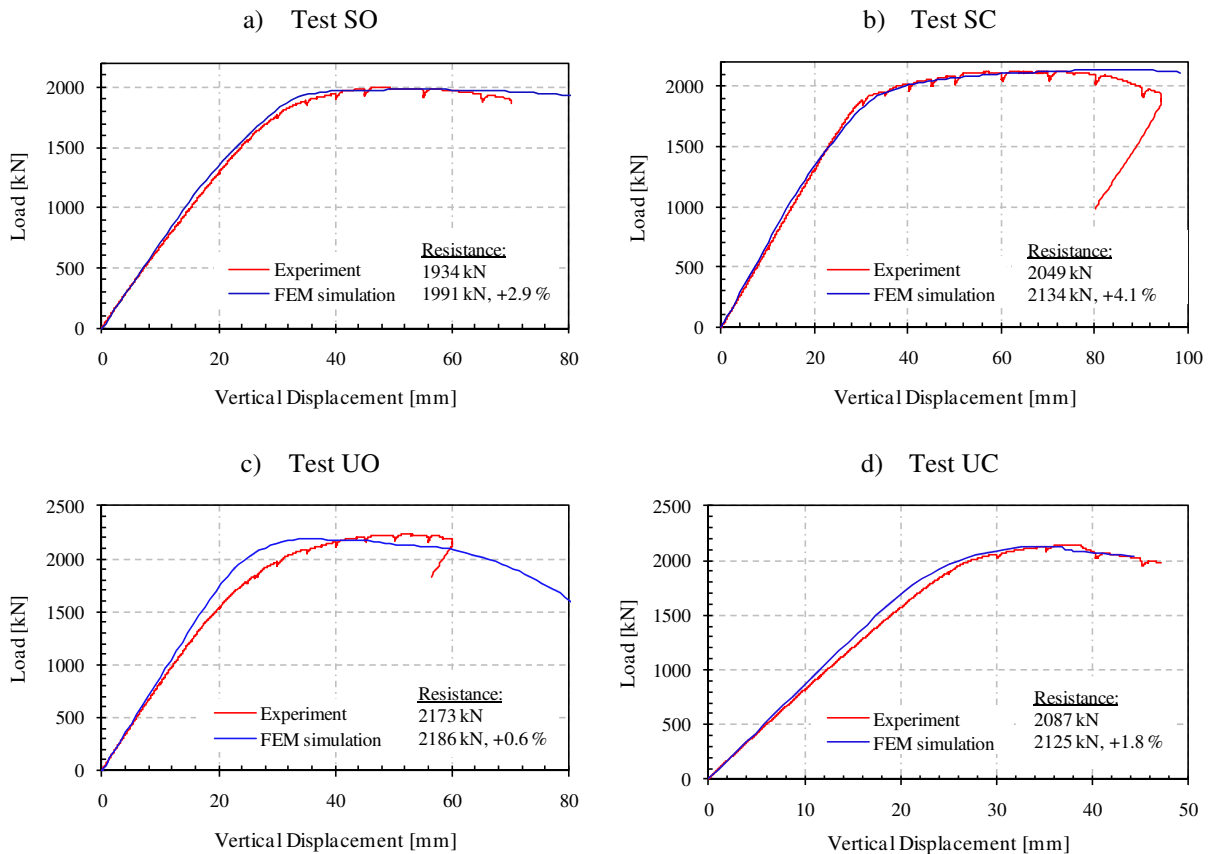


Slika 14: Vpliv gostote mreže na pomike in nosilnost nosilca

Pri numerični simulaciji testov smo modelirali tudi dejanske izmerjene začetne geometrijske nepopolnosti v testnem panelu, medtem ko smo v ostalih panelih nepopolnost določili v skladu s priporočili Dodatka C v SIST EN 1993-1-5. Dobljene numerične rezultate, kot so nosilnost, globalni odziv nosilca in razvoj pomikov izven ravnine, smo primerjali z rezultati testov.

Primerjava odzivov numeričnega modela in testa SO je prikazana na sliki 15a. Numerični model izkazuje malenkost večjo togost kot test. Poleg tega je območje med elastičnim in plastičnim delom v primeru testa daljše, kar je posledica zaostalih napetosti v nosilcu. Nosilnost numeričnega modela je povsem primerljiva in znaša le 2,9% več od nosilnosti, izmerjene v testu. Nekoliko večje razlike med simulacijo in testom lahko opazimo pri velikostih pomikov izven ravnine. Oblika pomikov izven ravnine je povsem primerljiva z izmerjenimi, razlika je torej le v vrednostih. Večje odstopanje opazimo pri majhnih pomikih, medtem ko se z večanjem obtežbe ta razlika zmanjšuje.

Na sliki 15b so prikazane krivulje sila-pomik za test SC. Z numerično simulacijo smo dobili zelo podoben odziv vse do pomika 65 mm. Od tu dalje numerični model še vedno izkazuje enako nosilnost, medtem ko začne le-ta v testu padati. Tudi v tem primeru je nosilnost, dobljena z numerično simulacijo, nekoliko večja od nosilnosti po testu, in sicer za 4,1%.



Slika 15: Primerjava krivulj sila-pomik

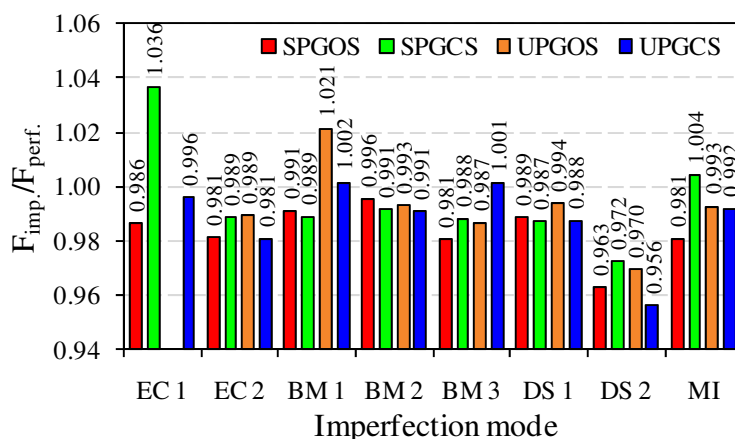
Pri nosilcu UO se globalni odziv simulacije glede na test bistveno bolj razlikuje kot v ostalih primerih. Na sliki 15c lahko vidimo, da je začetna togost numeričnega modela večja od dejanske togosti. Kot pri testu SO je tudi tukaj bistveno hitrejši prehod med elastičnim in plastičnim obnašanjem v primeru numerične simulacije. Tako je maksimalna nosilnost nosilca v primeru simulacije dosežena prej kot v primeru testa. Kljub temu je razlika med obema nosilnostma le 0,6%.

Tudi primerjava zadnjega testa UC kaže, da je numerični model ustrezen, saj je razlika tako med odzivoma kot tudi med nosilnostima minimalna (1,8%, glej sliko 15d). Manjšo razliko opazimo v začetni togosti, ki je nekoliko večja v primeru numerične simulacije.

Pokazali smo, da lahko s predstavljenim numeričnim modelom zadovoljivo simuliramo realne vzdolžno ojačane polnostenske nosilce. Razlika med numerično nosilnostjo in nosilnostjo po testih je bila med 0,6 in 4,1%. Primerljivi pa so bili tudi ostali rezultati, kot so začetna togost nosilcev, celoten odziv in razvoj pomikov izven ravnine.

V numeričnih simulacijah smo upoštevali dejanske izmerjene nepopolnosti. Ker običajno geometrijske nepopolnosti niso znane vnaprej, jih moramo v nelinearnih numeričnih analizah predpostaviti. Da smo z rezultati na varni strani, moramo predpostaviti takšno začetno nepopolnost, s katero bomo dobili najmanjšo nosilnost. Sama oblika nepopolnosti mora biti realna in omejena z največjo vrednostjo amplitude. Vpliv začetnih nepopolnosti na nosilnost nosilca je predstavljena v Sinur et al. [77]. Kljub

temu smo v tem delu vpliv nepopolnosti numerično raziskali na testnih nosilcih. Pri tem smo upoštevali 8 različnih oblik nepopolnosti, ki so bile določene kot pozitivne izbočne oblike (3 oblike), kot deformacijske oblike predhodne numerične simulacije nosilca (2 oblike), kot izmerjene nepopolnosti (1 oblika) in kot začetne geometrijske nepopolnosti, ki jih podaja Dodatek C v EN 1993-1-5. V izračunih so bile upoštewane različne amplitude in smeri začetnih nepopolnosti. V vseh štirih primerih se je izkazalo, da je najbolj neugodna začetna nepopolnost, določena z deformirano obliko predhodne numerične analize. Redukcija nosilnosti za vse štiri nosilce se je gibala med 2,8 in 4,4 % (glej sliko 16). Druga najbolj neugodna nepopolnost, z redukcijo nosilnosti med 1,1 in 1,9%, je nepopolnost EC2, ki je določena po SIST EN 1993-1-5. V nadaljnji numerični parametrični študiji smo vplive nepopolnosti zajeli z začetno nepopolnost EC2.

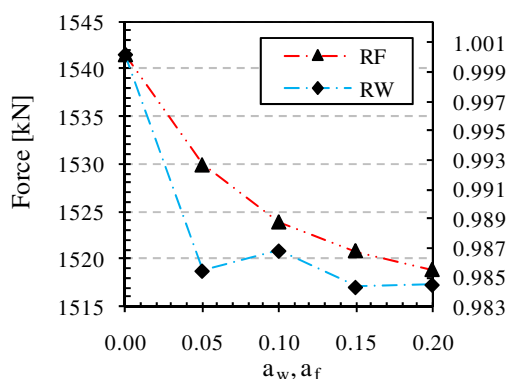


Slika 16: Redukcija nosilnosti nosilca za različne začetne nepopolnosti

Poleg začetnih geometrijskih nepopolnosti smo opravili tudi študijo vpliva zaostalih napetosti na nosilnost in obnašanje nosilca, pri čemer smo spreminjali različne nivoje zaostalih napetosti (glej preglednica 4). Redukcija nosilnosti in odziv nosilca za različne nivoje zaostalih napetosti je prikazana na slikin17. Največje zmanjšanje (1,5%) zaznamo pri največji vrednosti tlačnih zaostalih napetostih, ki so bistveno večje od izmerjenih. Redukcija nosilnosti pri primerljivih zaostalih napetostih znaša le 0,7%. Zaradi zanemarljivega vpliva zaostalih napetosti na nosilnost nosilca smo v numerični študiji upoštevali le geometrijske nepopolnosti EC2.

Preglednica 4: Upoštevani nivoji zaostalih napetosti v ojačanih nosilcih

| MODEL | k_w | k_f | MODEL | k_w | k_f |
|-------|-------|-------|-------|-------|-------|
| RW005 | 0.05 | | RF005 | | 0.05 |
| RW010 | 0.10 | 0.20 | RF010 | 0.05 | 0.10 |
| RW015 | 0.15 | | RF015 | | 0.15 |
| RW020 | 0.20 | | RF020 | | 0.20 |



Slika 17: Redukcija nosilnosti nosilca za različne nivoje zaostalih napetosti

IV. PARAMETRIČNA ŠTUDIJA IN PRIMERJAVA Z RAČUNSKIMI MODELI

Parametri numerične študije

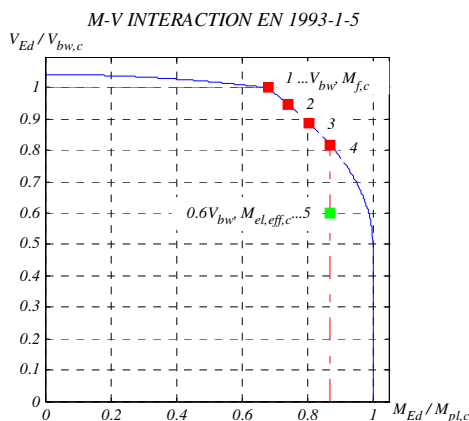
Eksperimentalni testi so služili za verifikacijo numeričnega modela. Da bi lahko širše ovrednotili interakcijsko enačbo, podano v EN 1993-1-5, potrebujemo več testov, oz. numeričnih simulacij testov. V parametrični analizi smo tako razširili bazo rezultatov s spreminjanjem sledečih parametrov: razmerje površin pasnice in stojine A_f/A_w , vitkost stojine h_w/t_w , razmerje stranic panela a , število in geometrijo vzdolžnih ojačitev, togost vzdolžne ojačitve, vertikalna lega vzdolžne ojačitve in razmerje upogibnega momenta in strižne sile v panelu. Vsi parametri so zbrani v preglednici 5.

Preglednica 5: Parametri numeričnih simulacij

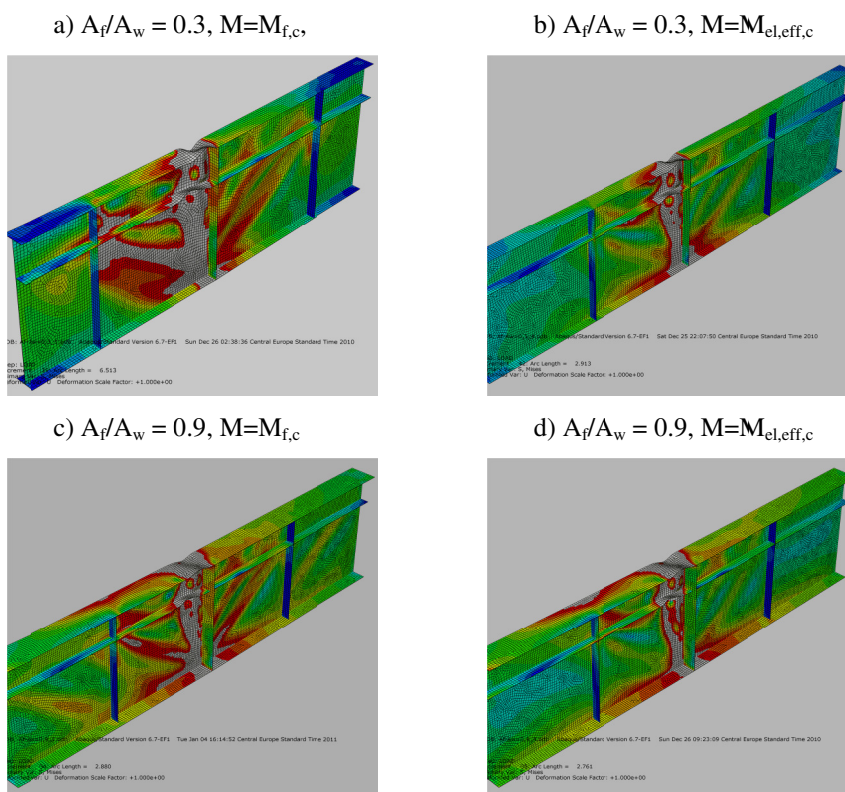
| Parameter | SKUPINA | | | |
|------------------------------|---------|---------------------------------------|---------|---------|
| | I | II | III | IV |
| A_f/A_w | 0.3 | | | |
| | 0.5 | | | |
| | 0.7 | | | |
| | 0.9 | 0.7 | 0.7 | 0.7 |
| | 1.1 | | | |
| | 1.5 | | | |
| h_w/t_w | | 150 | | |
| | | 200 | | |
| | 250 | 250 | 250 | 250 |
| | | 300 | | |
| | | 350 | | |
| | | 400 | | |
| a | | | 1000 | |
| | 2000 | 2000 | 2000 | 2000 |
| | | | 3000 | |
| | | | 4000 | |
| | | | 5000 | |
| $\gamma\gamma^*$ | | | | 0.3 |
| | | | | 0.75 |
| | 3 | 3 | 3 | 1 |
| | | | | 2 |
| | | | | 3 |
| | | | | 4 |
| Oblika ojačitve | Odrpta | Odrpta | Odrpta | Odrpta |
| | Zaprta | Zaprta | Zaprta | Zaprta |
| | | | | |
| Pozicija ojačitve | $h_w/4$ | $h_w/4$ | $h_w/4$ | $h_w/4$ |
| | $h_w/2$ | $h_w/2$ | $h_w/2$ | $h_w/2$ |
| | $h_w/3$ | $h_w/3$ | / | $h_w/3$ |
| Število vzdolžnih ojačitev | 1 | 1 | 1 | 1 |
| | 2 | 2 | | 2 |
| Obtežba | | Case 1: $M_{f,c} + V_{bw,c}$ | | |
| | | Case 2: $(2M_{f,c} + M_{el,eff,c})/3$ | | |
| | | Case 3: $(M_{f,c} + 2M_{el,eff,c})/3$ | | |
| | | Case 4: $M_{el,eff,c}$ | | |
| | | Case 5: $M_{el,eff,c} + 0.6V_{bw,c}$ | | |
| Število numeričnih simulacij | 140+40 | 120+30 | 100 | 160+40 |
| Skupno število simulacij | 630 | | | |

V analizi smo upoštevali 5 različnih razmerij upogibnega momenta in strižne obremenitve. Upoštevani nivoji upogibnega momenta in strižne sile za posamezno analizo so prikazani na sliki 18. Štiri kombinacije obremenitev so odgovarjale interakciji, podani v EN 1993-1-5, ena obremenitev pa je bila določena izven interakcije, v območju, kjer je potrebna le kontrola upogibne nosilnosti elementa. V poglavju 6 so za posamezno skupino parametrov predstavljeni rezultati numeričnih analiz z vidika

razporeditve primerjalnih Misesovih napetosti pri maksimalni sili. V večini primerov lahko pri majhnem nivoju upogibnih momentov zaznamo plastifikacijo nateznega polja ter plastifikacijo po višini prereza (glej sliko 19). Z večanjem upogibnega momenta se plastifikacija pojavi le po višini prereza.



Slika 18: Upoštevane obtežne situacije v numeričnih simulacijah (rdeči pravokotniki označujejo točke v območju interakcije po EN 1993-1-5, zelen pravokotnik označuje točko, kjer je izvedena le kontrola upogibne nosilnosti)



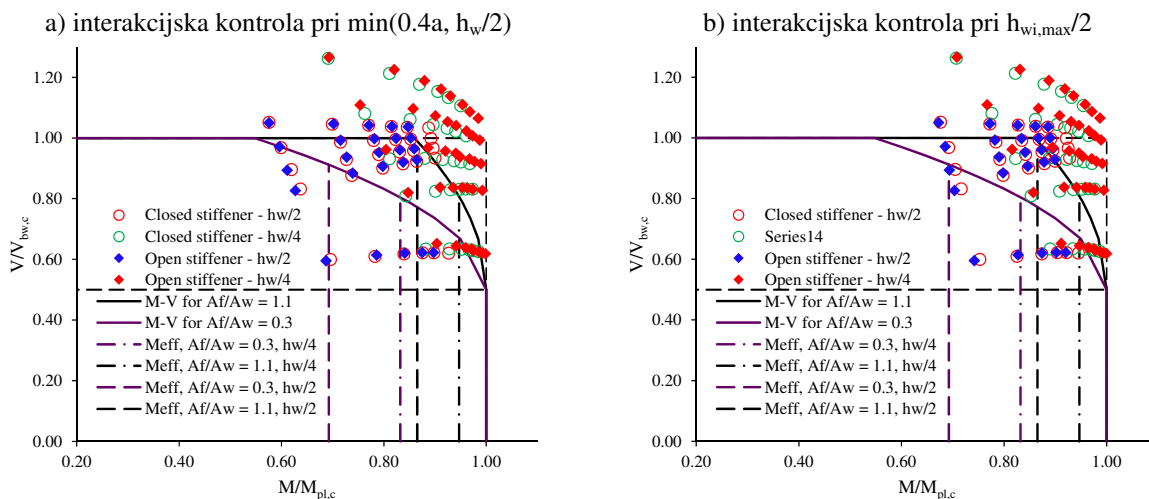
Slika 19: Misesove primerjalne napetosti za nosilec ojačan z eno odprto ojačitvijo na $h_w/4$

Primerjava nosilnosti po EN 1993-1-5

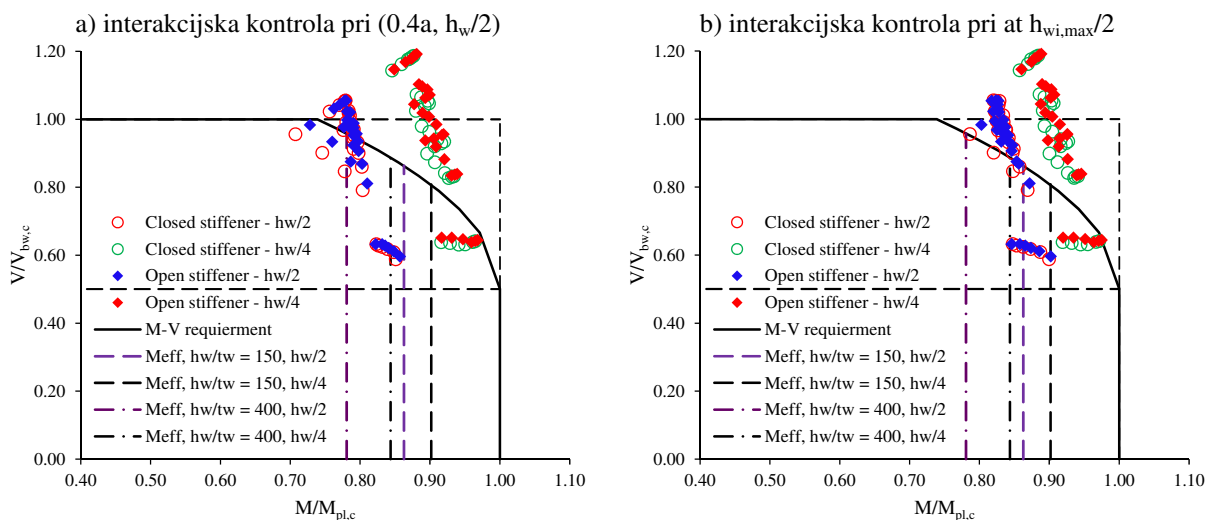
Nosilnosti, ki smo jih določili kot največje vrednosti na krivulji sila-pomik, smo primerjali z nosilnostmi, ki smo jih določili z modelom, podanim v EN 1993-1-5. V poglavju 7.2 so podane podrobnosti izračuna upogibne nosilnosti, strižne nosilnosti nosilca in formulacija interakcije. EN

1993-1-5 predlaga, da se kontrolo interakcije za vzdolžno neojačane nosilce izvede na oddaljenosti $h_w/2$ od roba z največjimi obremenitvami, medtem ko za vzdolžne ojačane nosilce prerez kontrole interakcije ni podan. Johansson et al. [71] predlagajo, da se interakcija izvede na oddaljenosti $h_{wi,max}/2$ od najbolj obremenjenega roba panela. V disertaciji smo predlagali, da se kontrola izvede na oddaljenosti $\min(0,4a; h_w/2)$. Na ta način je interakcija za vse možne načine ojačanja vedno definirana na istem prerezu, pri čemer vedno upoštevamo isti gradient. Poleg tega so v primeru globalnega uklona vplivi teorije drugega reda največji na mestu največje izbočitve, kar pomeni blizu sredine nosilca. Predlog $h_{wi,max}/2$ bi pri velikem številu vzdolžnih ojačitev privedel do kontrole na robu prereza, s čimer bi zanemarili ugoden vpliv gradienta momentov in strigov na končno nosilnost. V nalogi smo upoštevali obe možni definiciji prereza, kjer se izvede interakcijska kontrola.

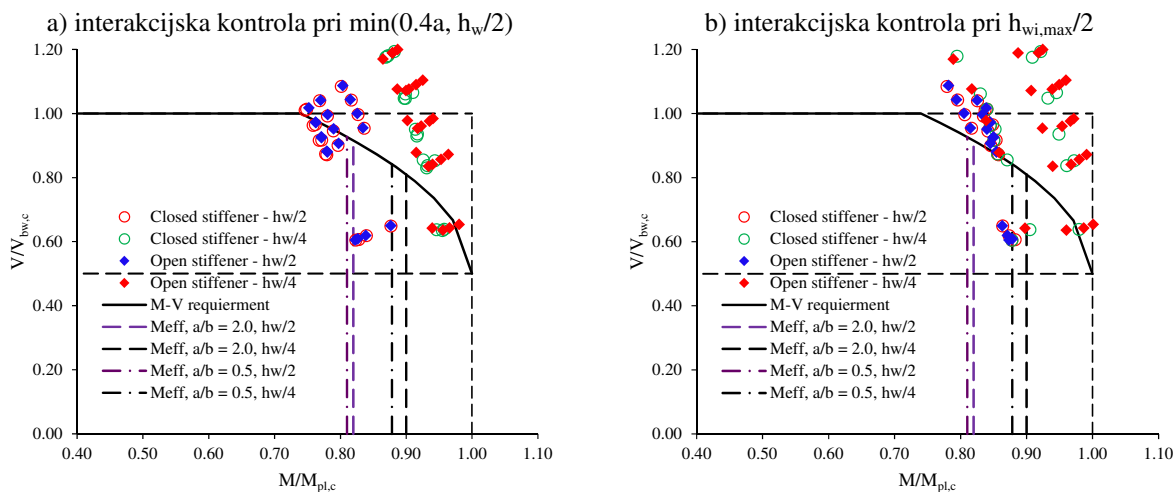
Rezultati numeričnih analiz skupaj z interakcijskimi krivuljami so za posamezne skupine prikazani na slikah 20 do 23. Vse numerične vrednosti, ki so izven območja interakcijske krivulje, izkazujejo večjo nosilnost, kot jo določa EN 1993-1-5. Rezultati kažejo, da vsi nosilci, ki so bili ojačani z ojačitvijo v tlačni coni, izkazujejo bistveno večjo nosilnost. Pri teh nosilcih je bil večji podpanel, ki je merodajen za strižno nosilnost, obremenjen z nateznimi napetosti, ki so posledica upogibnega momenta. Te napetosti povečajo nosilnost strižnega podpanela in s tem tudi strižno nosilnost. Ker ugodnega vpliva interakcijski model ne zajema, je zato numerična odpornost večja. Za nosilce z vzdolžno ojačitvijo na sredini panela so rezultati bistveno bližje interakcijski krivulji. Kadar je interakcija kontrolirana na $\min(0,4a; h_w/2)$, večino vrednosti pade na notranjo stran interakcijske krivulje, kar pomeni, da interakcijski model preceni nosilnost. Bistveno boljše rezultate dobimo, kadar interakcijo izvedemo na oddaljenosti $h_{wi,max}/2$. V tem primeru večino rezultatov leži izven območja interakcije.



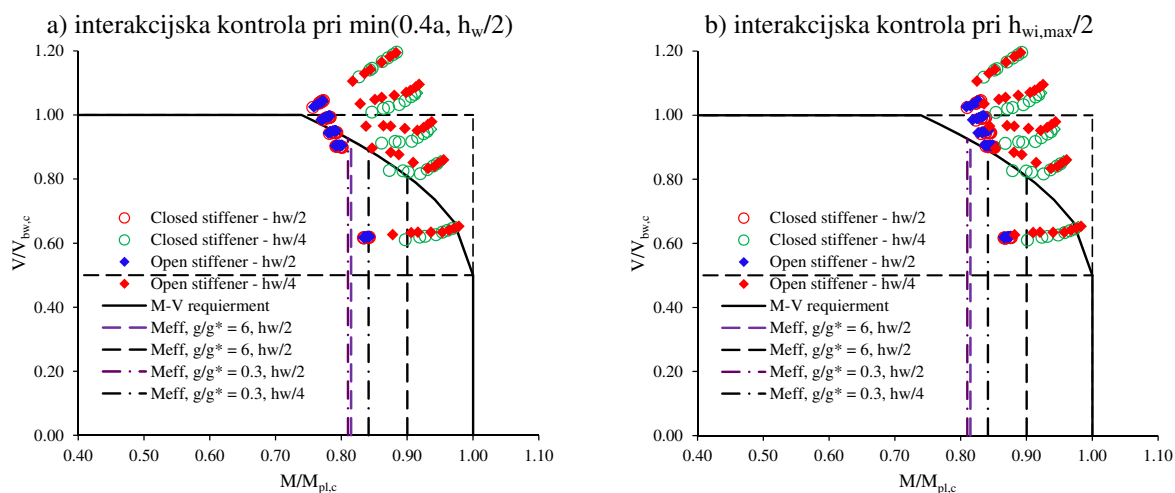
Slika 20: Prikazani numerični rezultati na obstoječi M-V formulaciji - SKUPINA I



Slika 21: Prikazani numerični rezultati na obstoječi M-V formulaciji - SKUPINA II



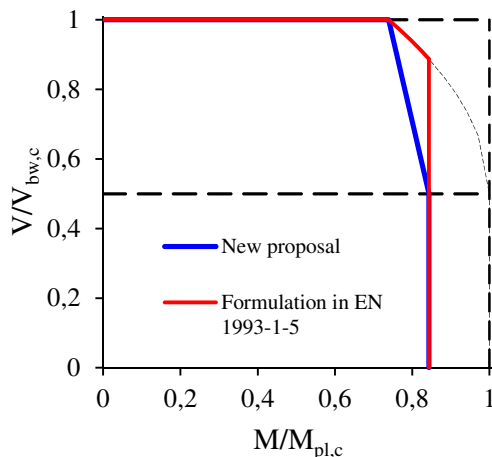
Slika 22: Prikazani numerični rezultati na obstoječi M-V formulaciji - SKUPINA III



Slika 23: Prikazani numerični rezultati na obstoječi M-V formulaciji - SKUPINA IV

PREDLAGAN INTERAKCIJSKI MODEL

Iz interakcijskih diagramov lahko vidimo, da je oblika interakcije povsem drugačna, kot je podana v EN 1993-1-5. Izkaže se, da je v večini primerov, kjer je vitkost stojine večja od $h_w/t_w = 200$, oblika interakcije linearna. Nelinearno obliko lahko opazimo le pri manjših vitkostih stojine, npr. $h_w/t_w = 150$. Na podlagi rezultatov smo predlagali nov interakcijski model (enačba(56)). Oba interakcijska modela sta prikazana na sliki 24. Z novim interakcijskim modelom večino točk prestavimo izven območja interakcije, razen tistih z majhno vitkostjo stojine, in zmanjšamo raztros, saj je razlika med izračunanimi vrednostmi in interakcijskim modelom bolj konsistentna.



Slika 24: Primerjava M-V interakcijskih modelov

DOLOČITEV DELNEGA VARNOSTNEGA FAKTORJA

Namen statistične analize je bila določitev ustreznosti modelov odpornosti in delnega faktorja γ_M , ki je definiran kot količnik med karakteristično vrednostjo in projektno vrednostjo. Izračun projektnih vrednosti in delnega faktorja je bil določen po Dodatku D standarda EN 1990. Podrobni opis je podan v poglavju 7.5. Pri določitvi delnega faktorja γ_M smo upoštevali naslednje nezanesljivosti:

- nezanesljivost numeričnega modela,
- nezanesljivost geometrije,
- nezanesljivost materiala in
- nezanesljivost numeričnega modela.

V analizi smo obravnavali pet modelov odpornosti. Prvi model je interakcijski model odpornosti, ki je definiran v EN 1993-1-5 in je podan z enačbo:

$$r_{t,1} = V = \left(1 + \left(\frac{M_{pl,c} - M}{M_{pl,c} - M_f} \right)^{0.5} \right) \cdot \frac{V_{bw}}{2}.$$

Drugi model odpornosti je nov interakcijski model, ki je definiran z enačbo:

$$r_{t,2} = V = \left(1 + \left(\frac{M_{el,eff} - M}{M_{el,eff} - M_f} \right) \right) \cdot \frac{V_{bw}}{2}.$$

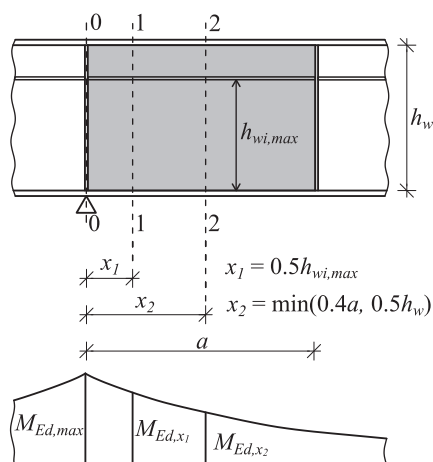
V EN 1993-1-5 je predpisano, da se izvede dodatna kontrola upogibne nosilnosti bruto prereza, kadar je kontrola interakcije striga in upogiba izvedena v panelu, upoštevajoč redukcijo notranjih sil. Tako je tretji model odpornosti definiran kot kontrola upogibne nosilnosti bruto prereza na robu panel (prerez 0-0, Slika 25):

$$r_{t,3} = V = \frac{M_{ed}}{l}$$

Glede na to, da EN 1993-1-5 zahteva obe kontroli je maksimalna nosilnost določena kot minimalna vrednost interakcije in bruto nosilnosti. Tako smo definirali še dva modela, ki predstavljata kombinacijo interakcijskega modela in modela bruto nosilnosti prereza in sta definirana kot:

$$r_{t,4} = \min(r_{t,1}; r_{t,3}),$$

$$r_{t,5} = \min(r_{t,2}; r_{t,3})$$



Slika 25: Pozicija interakcijske kontrole (prerez 1-1 in 2-2) in kontrola nosilnosti prereza (prerez 0-0)

Interakcijska modela $r_{t,1}$ in $r_{t,2}$ smo statistično ocenili za prerez 1-1 in prerez 2-2, kot je prikazano na sliki 25. Pri tem smo vse rezultate razvrstili v več skupin:

- Skupina I: vsi rezultati,
- Skupina II: rezultati z ojačitvijo na $h_w/4$,
- Skupina III: rezultati z ojačitvijo na $h_w/2$ in
- Skupina IV: rezultati z dvema ojačitvama.

Rezultati statistične analize so predstavljeni v preglednicah 6 do 10. Interakcijski model $r_{t,1}$ izpolnjuje zahteve zanesljivosti po standardu EN 1990 le za skupino II, kadar je interakcija upoštevana na oddaljenosti $\min(0,4x_a; h_w/2)$, saj je zahtevani delni faktor $\gamma_M = 1,048$ manjši od $\gamma_{M,1} = 1,1$. V primeru, da je kontrola interakcije izvedena na oddaljenosti $h_{wi,max}/2$, interakcijski model $r_{t,1}$ izpolnjuje zahteve zanesljivosti za skupino II in III, kjer sta zahtevana faktorja varnosti $\gamma_M = 1,045$ in $1,089$ manjša od vrednosti $\gamma_{M,1} = 1,1$. Za skupino IV pa delni faktor $1,113$ za malenkost presega vrednost $\gamma_{M,1} = 1,1$.

Z interakcijskim modelom $r_{t,2}$ na oddaljenosti $\min(0,4x_a; h_w/2)$ so zahteve zanesljivosti izpolnjene za skupini II in III, kjer sta faktorja $\gamma_M = 0,999$ in $1,096$ manjša od vrednosti $1,1$. Za ostali dve skupini so

zahteve zanesljivosti izpolnjene, kadar je delni faktor za skupino I enak $\gamma_M = 1,111$ in za skupino $\gamma_M = 1,168$. Interakcijski model $r_{t,2}$ na oddaljenosti $h_{w_i,max}/2$ izpolnjuje zahteve zanesljivosti za vse štiri skupine, saj so delni varnostni faktorji $\gamma_M = 1,033; 0,998; 1,037$ in $1,051$ manjši od $\gamma_{M,1} = 1,1$.

Model odpornosti $r_{t,3}$ je definiran kot upogibna nosilnost prereza, kjer EN 1993-1-5 predpostavlja delni varnostni faktor $\gamma_{M,0} = 1,0$. Za vse podane skupine je zahtevani delni varnostni faktor (glej preglednico 8) večji od $\gamma_{M,0}$, kar pomeni, da model odpornosti $r_{t,3}$ ne dosega zahtevane zanesljivosti, določene po standardu EN 1990.

V primeru, da je nosilnost določena kot minimalna vrednost interakcijskega modela in modela za upogibno nosilnost bruto prereza so delni varnostni faktorji nekoliko nižji kot pri ostalih modelih odpornosti. Izkazuje se, da je najmanjši varnostni faktor, ki ga potrebujemo za zahtevano zanesljivost, za odpornostni modela $r_{t,4}$ enak 1.105 in za model $r_{t,5}$ enak 1.104, kadar interakcijo izvedemo na oddaljenosti $\min(a, h_w/2)$. Če interakcijo izvedemo na oddaljenosti $h_{w_i,max}/2$ pa so varnostni faktorji za oba modela odpornosti $r_{t,4}$ in $r_{t,5}$ in za vse skupine pod vrednostjo 1.1.

Preglednica 6: Izračunane vrednosti faktorja γ_M^* za modela odpornosti $r_{t,1}$ in $r_{t,2}$ pri $\min(a, h_w/2)$

| Skupina | b | | V_δ | | V_r | | γ_M^* | |
|---------|-----------|-----------|------------|-----------|-----------|-----------|--------------|--------------|
| | $r_{t,1}$ | $r_{t,2}$ | $r_{t,1}$ | $r_{t,2}$ | $r_{t,1}$ | $r_{t,2}$ | $r_{t,1}$ | $r_{t,2}$ |
| I | 1,0050 | 1,0430 | 0,060 | 0,056 | 0,106 | 0,104 | 1,157 | 1,111 |
| II | 1,0997 | 1,1445 | 0,049 | 0,036 | 0,101 | 0,095 | 1,048 | 0,999 |
| III | 0,9993 | 1,0340 | 0,031 | 0,017 | 0,093 | 0,089 | 1,140 | 1,096 |
| IV | 0,9432 | 0,9803 | 0,048 | 0,040 | 0,100 | 0,096 | 1,221 | 1,168 |

Preglednica 7: Izračunane vrednosti faktorja γ_M^* za modela odpornosti $r_{t,1}$ in $r_{t,2}$ pri $h_{w_i,max}/2$

| Skupina | b | | V_δ | | V_r | | γ_M^* | |
|---------|-----------|-----------|------------|-----------|-----------|-----------|--------------|--------------|
| | $r_{t,1}$ | $r_{t,2}$ | $r_{t,1}$ | $r_{t,2}$ | $r_{t,1}$ | $r_{t,2}$ | $r_{t,1}$ | $r_{t,2}$ |
| I | 1,0491 | 1,1067 | 0,055 | 0,037 | 0,103 | 0,095 | 1,103 | 1,033 |
| II | 1,1033 | 1,1485 | 0,050 | 0,040 | 0,101 | 0,096 | 1,045 | 0,998 |
| III | 1,0408 | 1,0925 | 0,019 | 0,016 | 0,090 | 0,089 | 1,089 | 1,037 |
| IV | 1,0264 | 1,0881 | 0,036 | 0,037 | 0,095 | 0,095 | 1,113 | 1,051 |

Preglednica 8: Izračunane vrednosti faktorja γ_M^* za modela odpornosti $r_{t,3}$

| Skupina | B | V_δ | V_r | γ_M^* |
|---------|--------|------------|-------|--------------|
| I | 1,0493 | 0,054 | 0,103 | 1,103 |
| II | 1,1240 | 0,035 | 0,094 | 1,016 |
| III | 1,0184 | 0,017 | 0,089 | 1,113 |
| IV | 1,0280 | 0,029 | 0,092 | 1,107 |

Preglednica 9: Izračunane vrednosti faktorja γ_M^* za modela odpornosti $r_{t,4}$ in $r_{t,5}$ pri $\min(a, h_w/2)$

| Skupina | b | | V_δ | | V_r | | γ_M^* | |
|---------|-----------|-----------|------------|-----------|-----------|-----------|--------------|--------------|
| | $r_{t,4}$ | $r_{t,5}$ | $r_{t,4}$ | $r_{t,5}$ | $r_{t,4}$ | $r_{t,5}$ | $r_{t,4}$ | $r_{t,5}$ |
| I | 1,0590 | 1,0688 | 0,056 | 0,053 | 0,104 | 0,103 | 1,094 | 1,082 |
| II | 1,1425 | 1,1545 | 0,037 | 0,034 | 0,095 | 0,094 | 1,001 | 0,988 |
| III | 1,0302 | 1,0451 | 0,017 | 0,014 | 0,089 | 0,089 | 1,100 | 1,083 |
| IV | 1,0293 | 1,0310 | 0,028 | 0,028 | 0,092 | 0,092 | 1,105 | 1,104 |

Preglednica 10: Izračunane vrednosti faktorja γ_M^* za modela odpornosti $r_{t,4}$ in $r_{t,5}$ pri $h_{w_i,max}/2$

| Skupina | b | | V_δ | | V_r | | γ_M^* | |
|---------|-----------|-----------|------------|-----------|-----------|-----------|--------------|--------------|
| | $r_{t,4}$ | $r_{t,5}$ | $r_{t,4}$ | $r_{t,5}$ | $r_{t,4}$ | $r_{t,5}$ | $r_{t,4}$ | $r_{t,5}$ |
| I | 1,0737 | 1,1099 | 0,047 | 0,037 | 0,099 | 0,095 | 1,071 | 1,030 |
| II | 1,1430 | 1,1563 | 0,038 | 0,037 | 0,096 | 0,095 | 1,001 | 0,989 |
| III | 1,0496 | 1,0929 | 0,017 | 0,016 | 0,089 | 0,087 | 1,079 | 1,037 |
| IV | 1,0477 | 1,0913 | 0,031 | 0,037 | 0,093 | 0,087 | 1,087 | 1,047 |

Tako model $r_{t,1}$ kot tudi model $r_{t,2}$ z delnim varnostnim faktorjem $\gamma_{M,1} = 1,1$ ne odgovarjata kriterijem zanesljivosti po EN 1993-1-5 ob upoštevanju gradienta notranjih sil na oddaljenosti $\min(a, h_w/2)$. Pri interakciji na $h_{w,i,max}/2$ odpornostni model $r_{t,2}$ z varnostnim faktorjem $\gamma_{M,1} = 1,1$ odgovarja kriterijem zanesljivosti za vse štiri skupine, medtem ko odpornostni model $r_{t,1}$ ne odgovarja tem kriterijem le za skupino IV, kjer je zahtevani delni varnostni faktor enak 1,113. Glede na to, da je zahtevani varnostni faktor večji le za 1,1% od predpisanega $\gamma_{M,1} = 1,1$ je model $r_{t,1}$ z varnostnim faktorjem $\gamma_{M,1} = 1,1$ tudi ustrezen za določitev mejne nosilnosti.

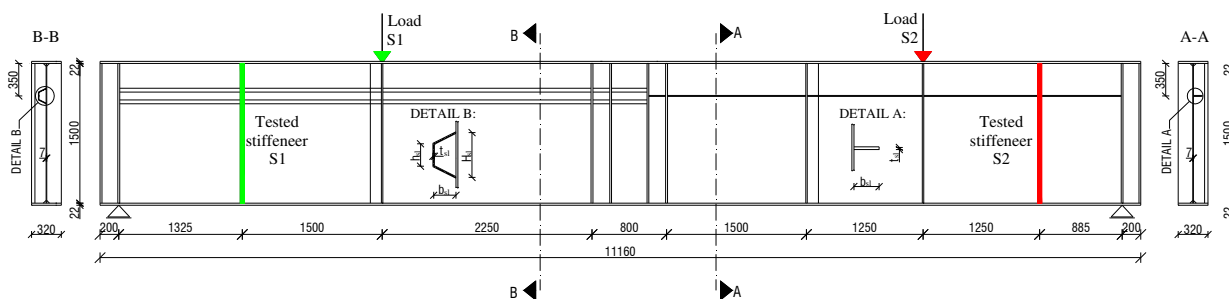
Modelom odpornosti $r_{t,3}$ z delnim varnostnim faktorjem $\gamma_{M,0} = 1,0$ ne zadosti kriterijem zanesljivosti. V primeru, da je nosilnost nosilca določena le z elastično upogibno kontrolo bruto preseza je potreben večji varnostni faktor in sicer 1,1, da zadostimo kriterijem zanesljivosti.

EN 1993-1-5 zahteva, da se kontrolo bruto preseza izvede takrat, ko se v interakciji upošteva vpliv gradientov notranjih sil v panelu. Modela $r_{t,4}$ in $r_{t,5}$ upoštevata obe kontroli. V primeru, da nosilnost določimo s kombinacijo dveh modelov, zadostimo pogojem zanesljivosti za oba kombinacijska modela z delnim varnostnim faktorjem $\gamma_{M,1} = 1,1$.

V. TOGOST PREČNE OJAČITVE

Pri dimenzioniranju prečnih ojačitev moramo zadostiti trem pogojem, in sicer pogoju nosilnosti, upogibne togosti in minimalne togosti za strižno izbočenje. Za izpolnitev prvih dveh pogojev moramo izvesti nelinearno analizo oz. uporabiti poenostavljene računske modele, s katerimi izračunamo napetosti v ojačitvi in pomike ojačitve. Pogoj minimalne togosti je enostavno določen z geometrijo ojačitve.

Za izpolnitev prvih dveh pogojev moramo poznati sile, ki delujejo na ojačitev. Ojačitve so običajno obremenjene z deviacijskimi silami, z zunanjo obtežbo in s silami od nateznega polja. Na podlagi študij drugih avtorjev se je izkazalo, da je model, ki določa velikost osne sile v ojačitvi od nateznega polja, konservativen. V sklopu doktorske disertacije smo tako izvedli dva eksperimentalna testa (Slika 26), kjer smo določili vpliv nateznega polja na prečne ojačitve.



Slika 26: Podpiranje in obremenjevanje nosilca za izvedo testa S1 in S2

Osne sile, ki smo jih določili s pomočjo merjenih deformacij v ojačitvi in sodelujočem delu stojine (preglednica 11), so primerljive le v območju sidranja nateznega polja, medtem ko sile na sredini nosilca predstavljajo le 56% sile, ki jo določa model v EN 1993-1-5. Na podlagi testnih rezultatov smo opravili numerično analizo različnih togosti ojačitev, s katero smo ugotovili, da je potrebna velikost, in s tem togost ojačitev, da izpolnimo kriterij pomikov in napetosti, bistveno manjša, kot je določena z izračunom po EN 1993-1-5. Na podlagi numeričnih simulacij smo pokazali, da zadostimo kriterijem pomikov, napetosti in minimalne togosti po EN 1993-1-5, če povečamo minimalno zahtevano togost za strižno izbočenje s faktorjem 3 (enačba 83).

Preglednica 11: Osna sila v prečni ojačitvi in sodelujočem delu stojine ($15t_w$) pri maksimalni nosilnosti nosilca

| SECTION | Stiffener S1 | | | Stiffener S2 | | |
|----------|--------------|----------------|---------|--------------|----------------|---------|
| | 1-1 | 2-2 | 3-3 | 1-1 | 2-2 | 3-3 |
| TEST | - 329,1 | - 290,0 | - 223,4 | - 653,9 | - 280,7 | - 160,4 |
| 100% TFA | | - 514 | | | - 504 | |
| 50% TFA | | - 257 | | | - 252 | |

VI. ZAKLJUČEK

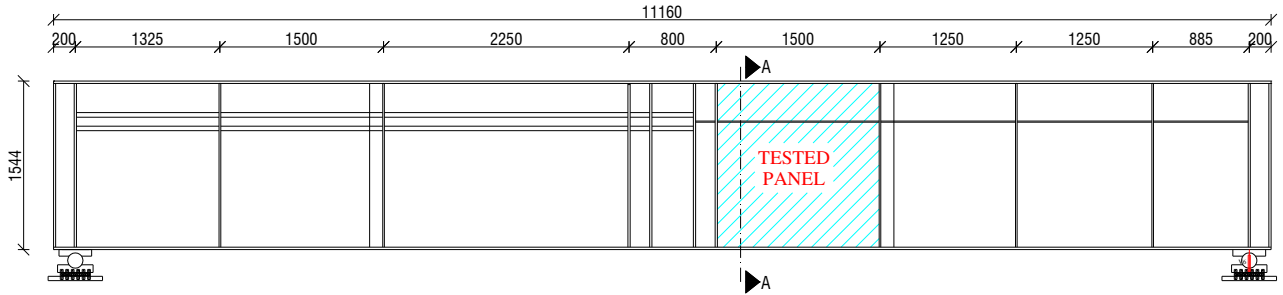
Na podlagi eksperimentalnih testov in numeričnih simulacij, s katerimi smo študirali vpliv interakcije velikih upogibnih momentov in strižnih sil na obnašanje vzdolžno ojačanih nosilcev, lahko zaključke strnemo v naslednjih točkah:

- Vsi eksperimentalni testi, ki smo jih izvedli, so izkazovali višjo nosilnost, kot jo določa EN 1993-1-5. Pri vseh nosilcih je zaznati daljši plastični plato, kar kljub problemu lokalne stabilnosti panela dokazuje solidno rotacijsko kapaciteto nosilcev. Izmerjene geometrijske nepopolnosti so bile za vse relevantne primere pod velikostjo dovoljenih toleranc. Nivo zaostalih tlačnih napetosti, ki smo jih izmerili v stojini, znaša v manjšem podpanelu 11,4% f_y in v večjem podpanelu le 2,2% f_y .
- Z numerično analizo začetnih nepopolnosti smo pokazali, da je najbolj neugodna začetna oblika nepopolnosti definirana kot deformacijska oblika predhodno izvedene nelinearne numerične analize, ki je določena v plastičnem območju po doseženi maksimalni sili. Redukcija nosilnosti je tako znašala med 2,8 in 4,4 %. Opravili smo tudi študijo vpliva zaostalih napetosti, kjer se je izkazalo, da je redukcija nosilnosti z upoštevanjem zaostalih napetosti v modelu minimalna.
- Določili smo nov model M-V interakcije v območju velikih obremenitev, ki daje bolj konsistentne rezultate in manjše raztrose, je pa nekoliko bolj konzervativen.
- Z interakcijskima modeloma $r_{t,1}$ in $r_{t,2}$ določenima na oddaljenosti $h_{wi,max}/2$ zadostimo pogojem zanesljivosti če uporabimo delni varnostni faktor $\gamma_{M,1} = 1,1$.
- Pokazali smo, da je potreben delni varnostni faktor za kontrolo bruto elastične upogibne nosilnosti prerezov ob prečni ojačitvi enak enak 1,1 in ne $\gamma_{M,0} = 1,0$, kot je definiran v EN 1993-1-5. Glavni razlog je verjetno neupoštevanje prečnih sil in pa dejstvo, da je predpostavka o polni nosilnosti prereza preoptimistična, saj ta kontrola v celoti pokriva interakcijo moment-strig obravnavanega panela.
- Na podlagi eksperimentalnih testov in numeričnih simulacij smo predlagali poenostavljen postopek kontrole vmesnih prečnih ojačitev pri vzdolžno ojačanih nosilcih.

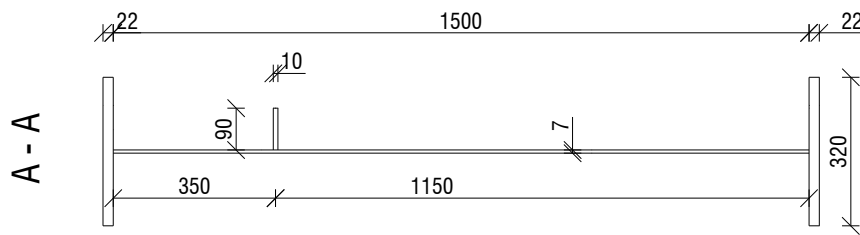
ANNEX A: Layout of tested girders under M-V interaction

TEST SO

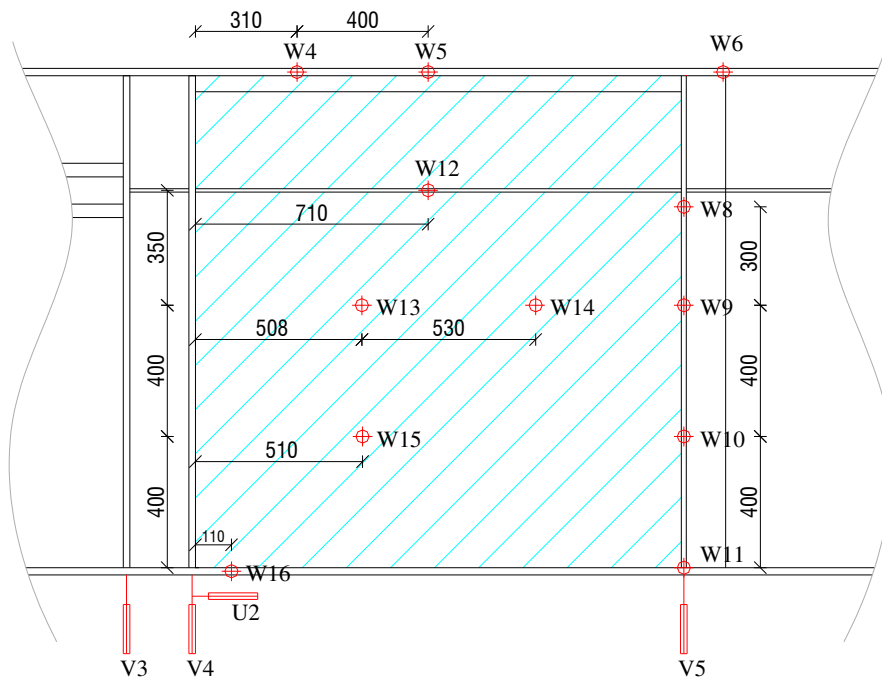
- Layout of tested girder



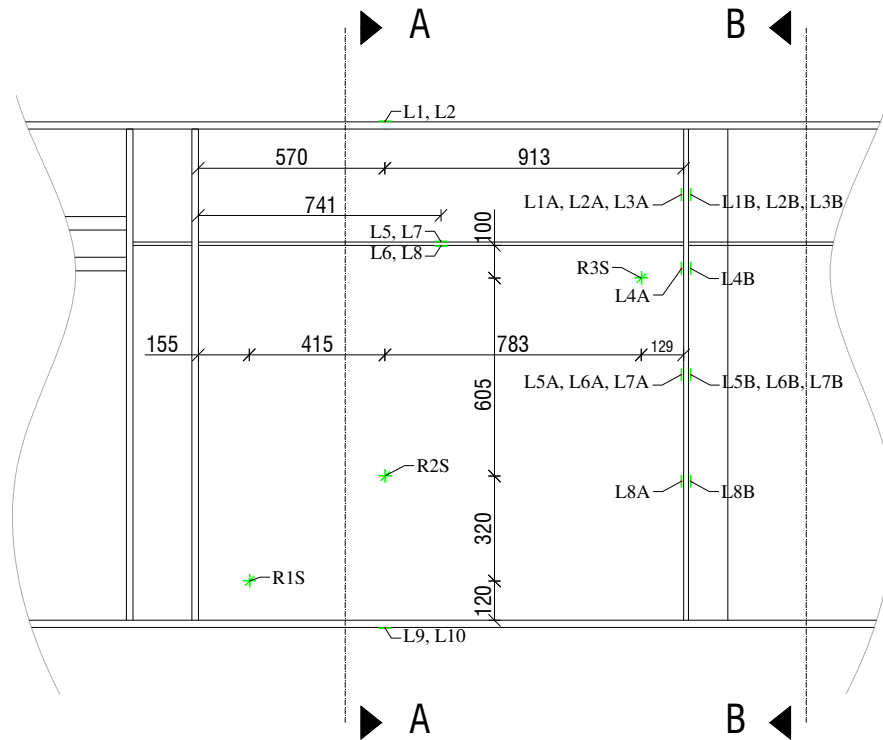
- Cross-section in the tested panel



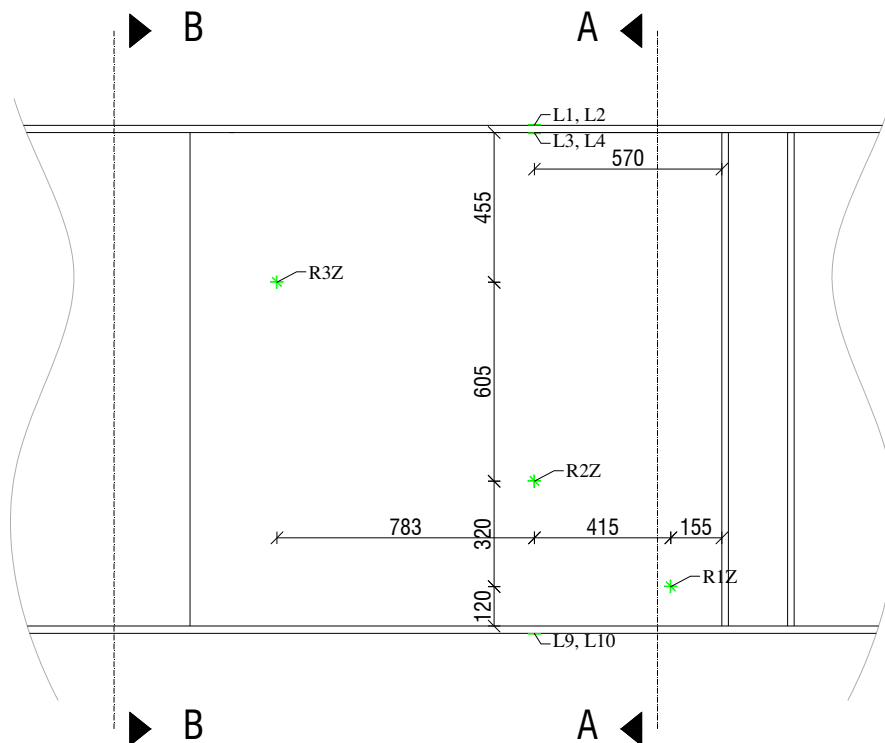
- Position of measured points in the panel



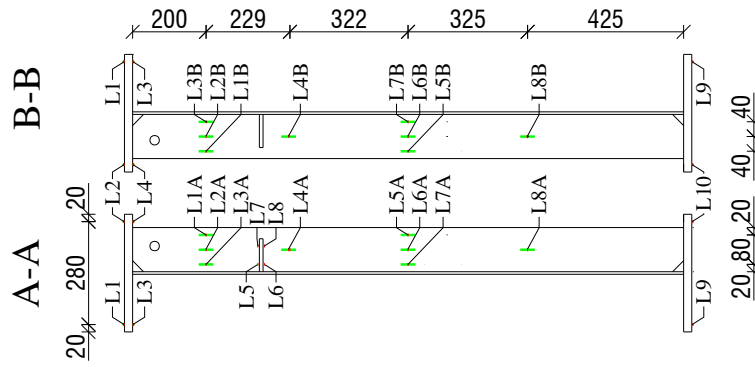
- Position of strain gauges – front side



- Position of strain gauges – back side

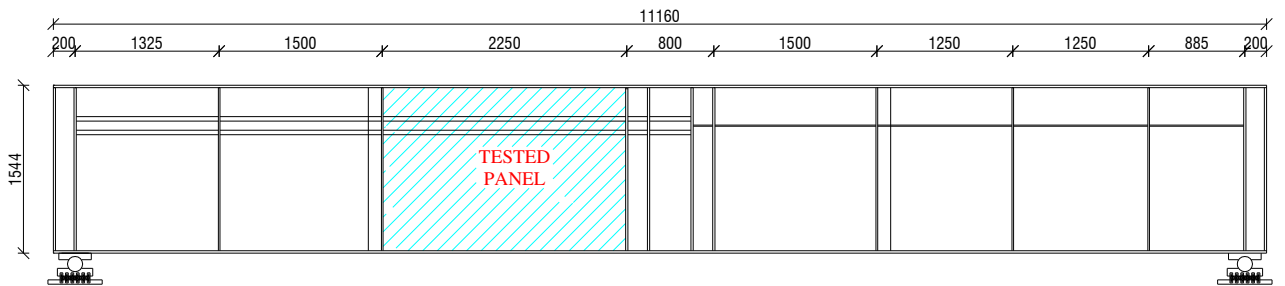


- Position of strain gauges – view A-A and B-B

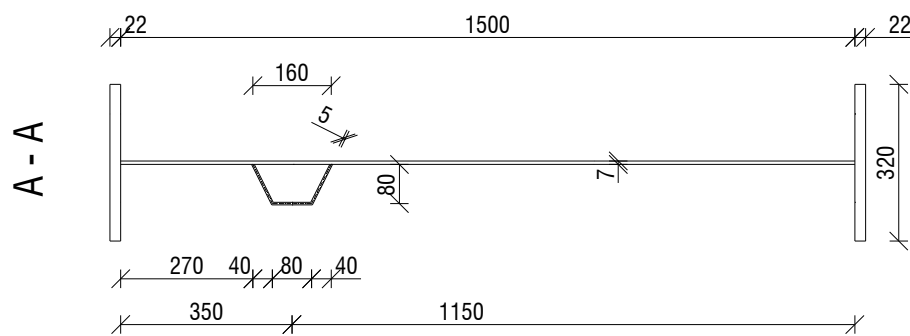


TEST SC

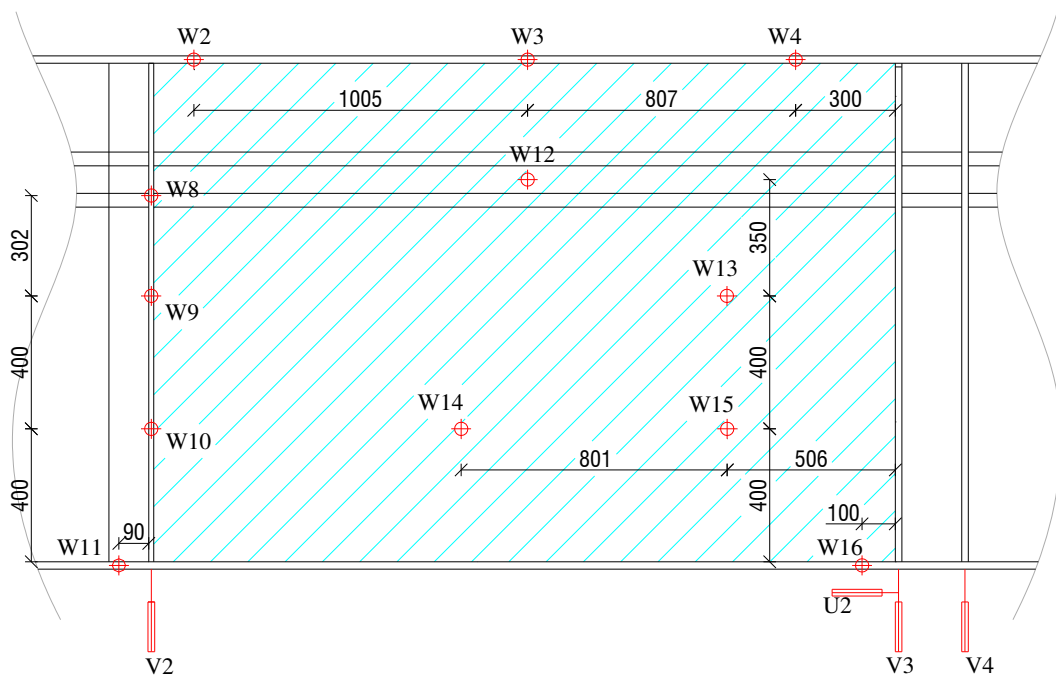
- Layout of tested girder



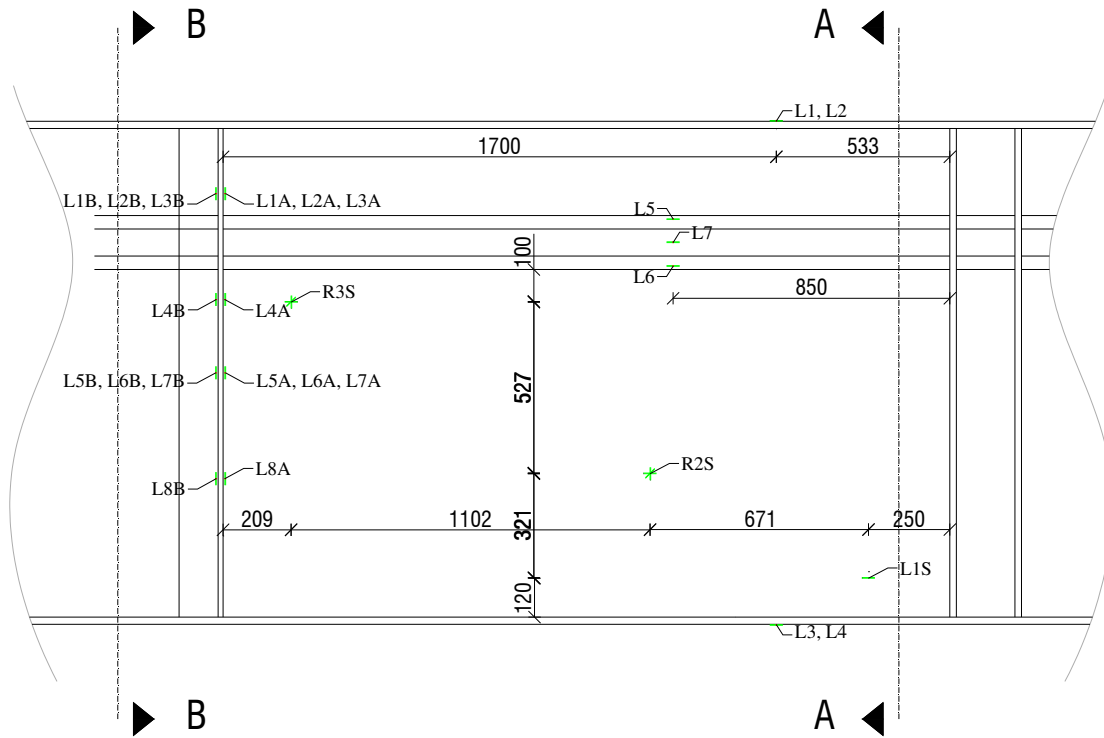
- Cross-section in the tested panel



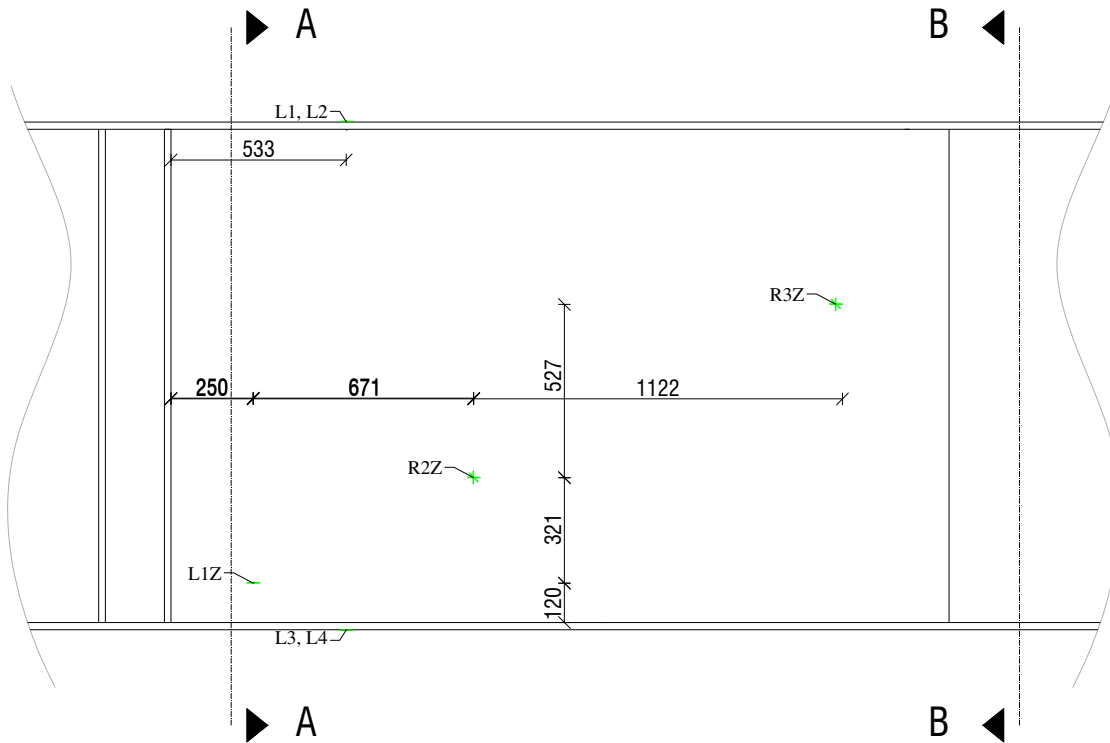
- Position of measured points in the panel



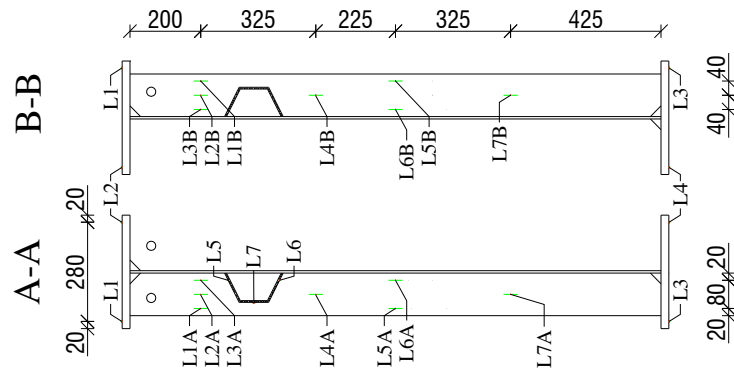
- Position of strain gauges – front side



- Position of strain gauges – back side

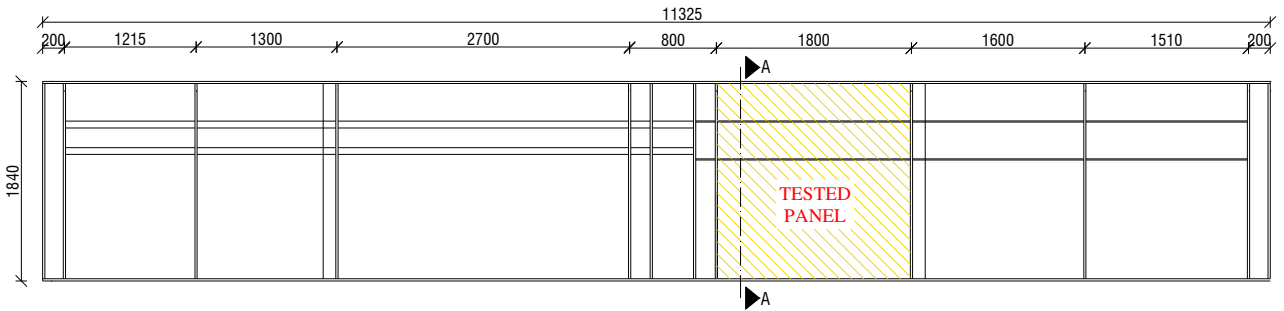


- Position of strain gauges – view A-A and B-B

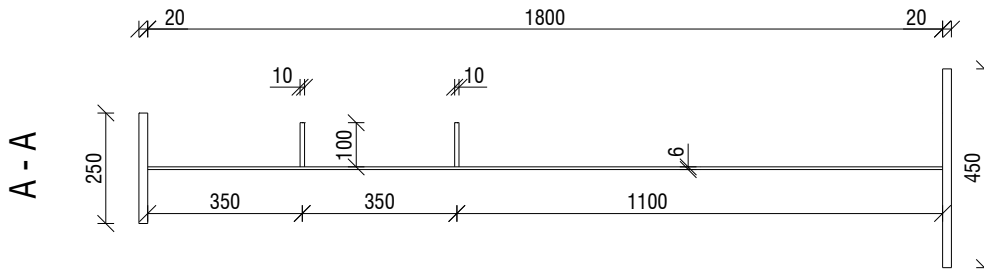


TEST UO

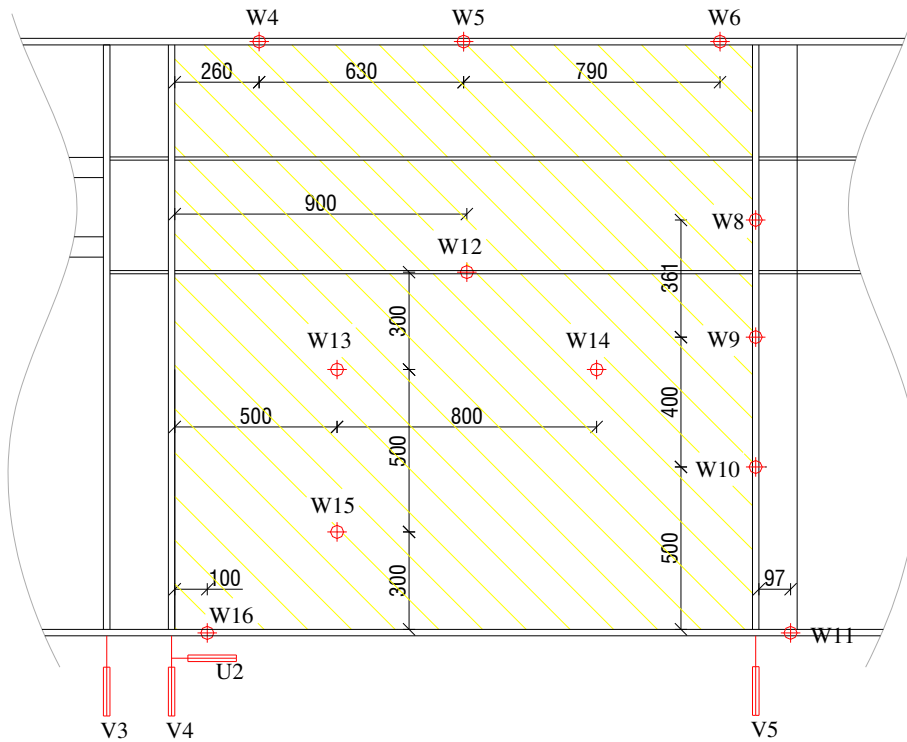
- Layout of tested girder



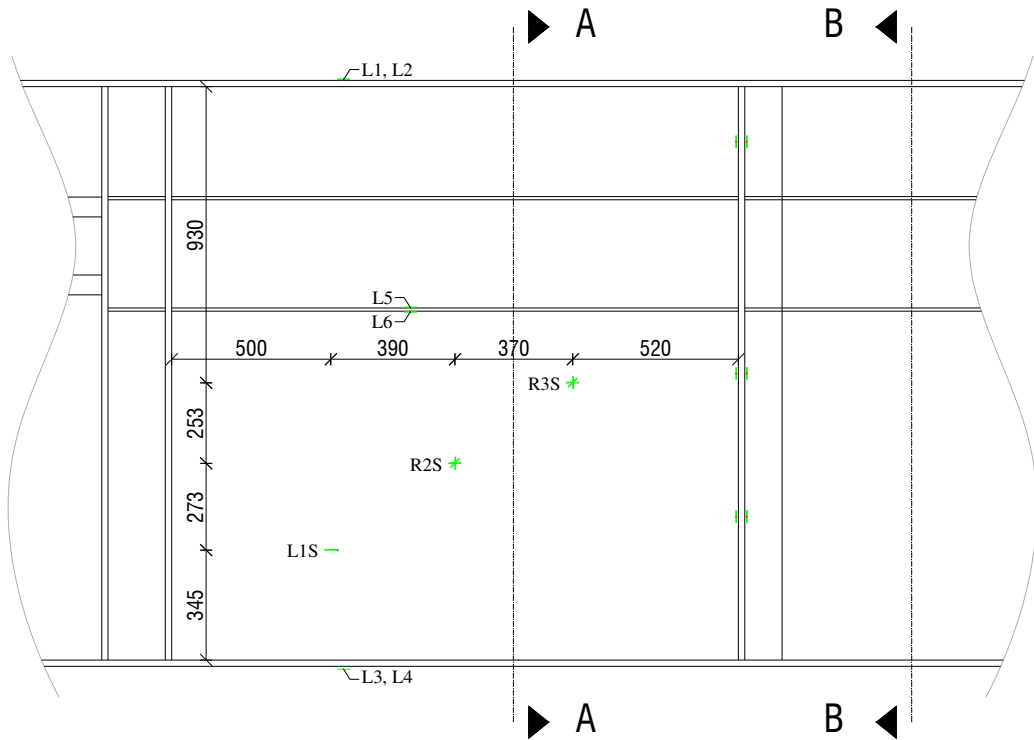
- Cross-section of tested panel



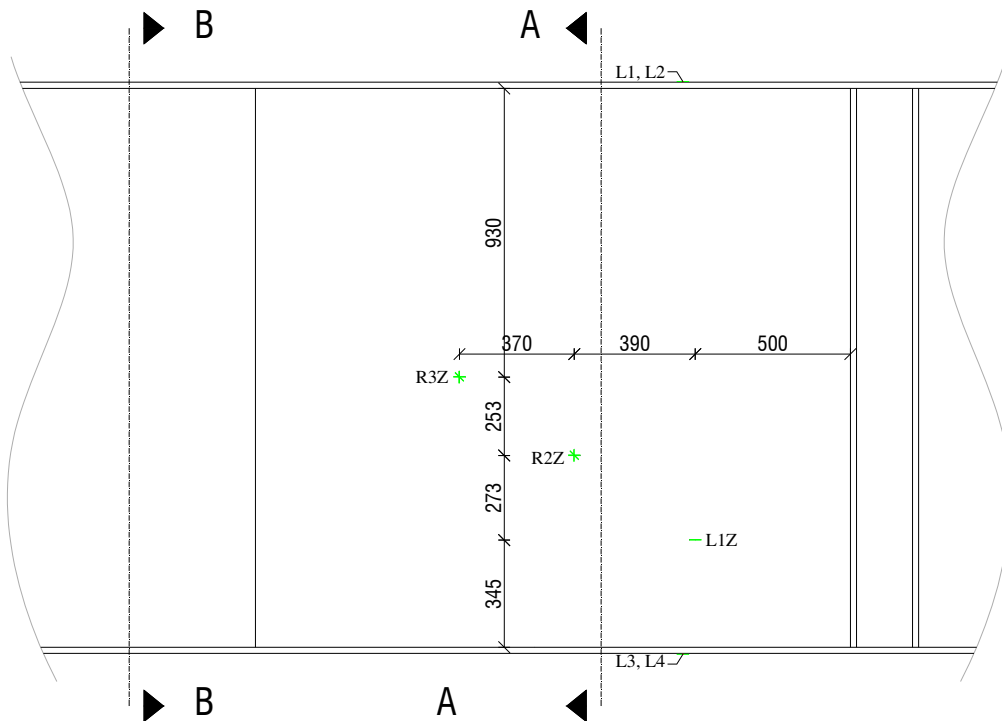
- Position of measured points in the panel



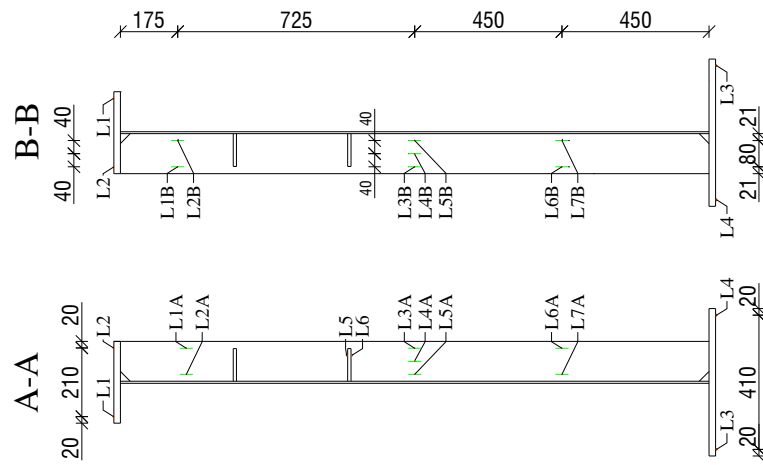
- Position of strain gauges – front side



- Position of strain gauges – back side

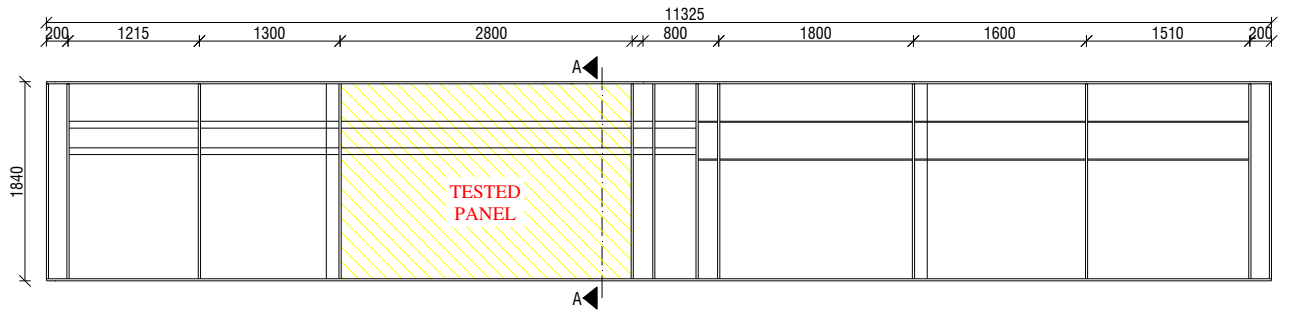


- Position of strain gauges – view A-A and B-B

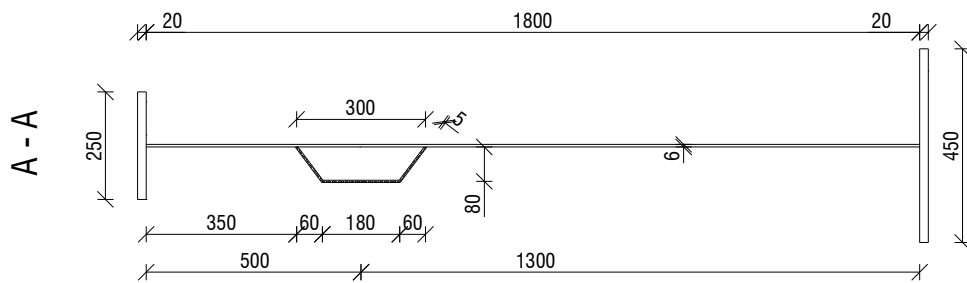


TEST UC

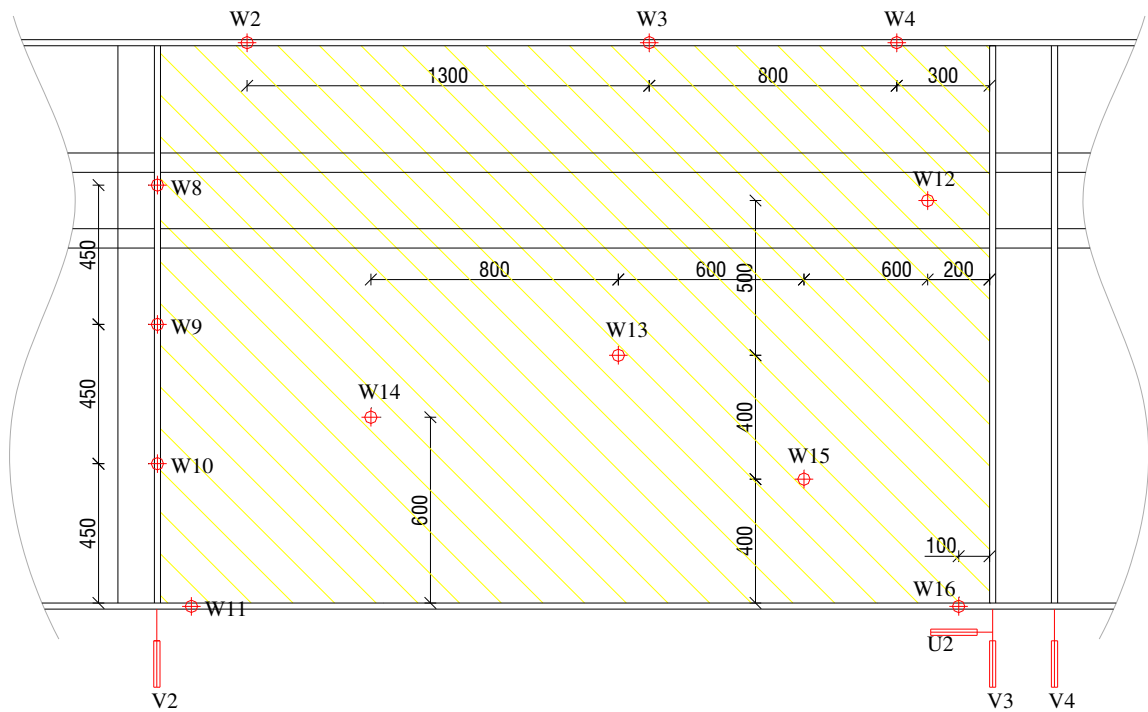
- Layout of tested girder



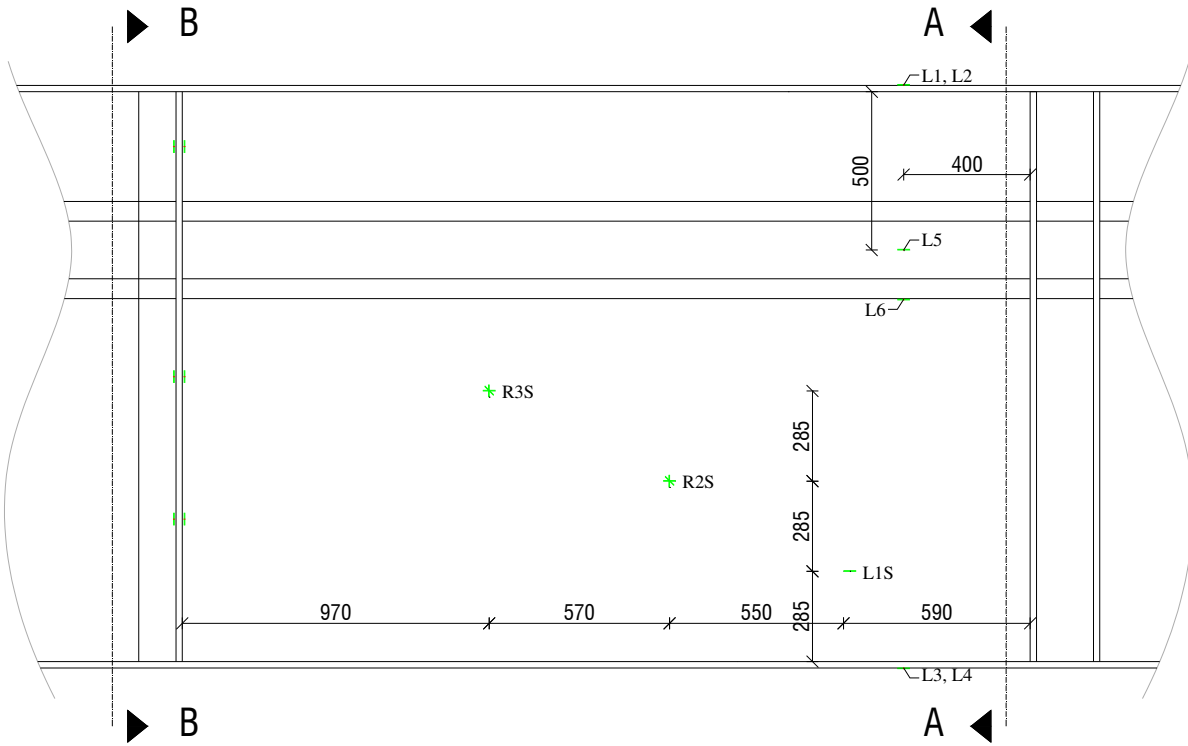
- Cross-section of tested panel



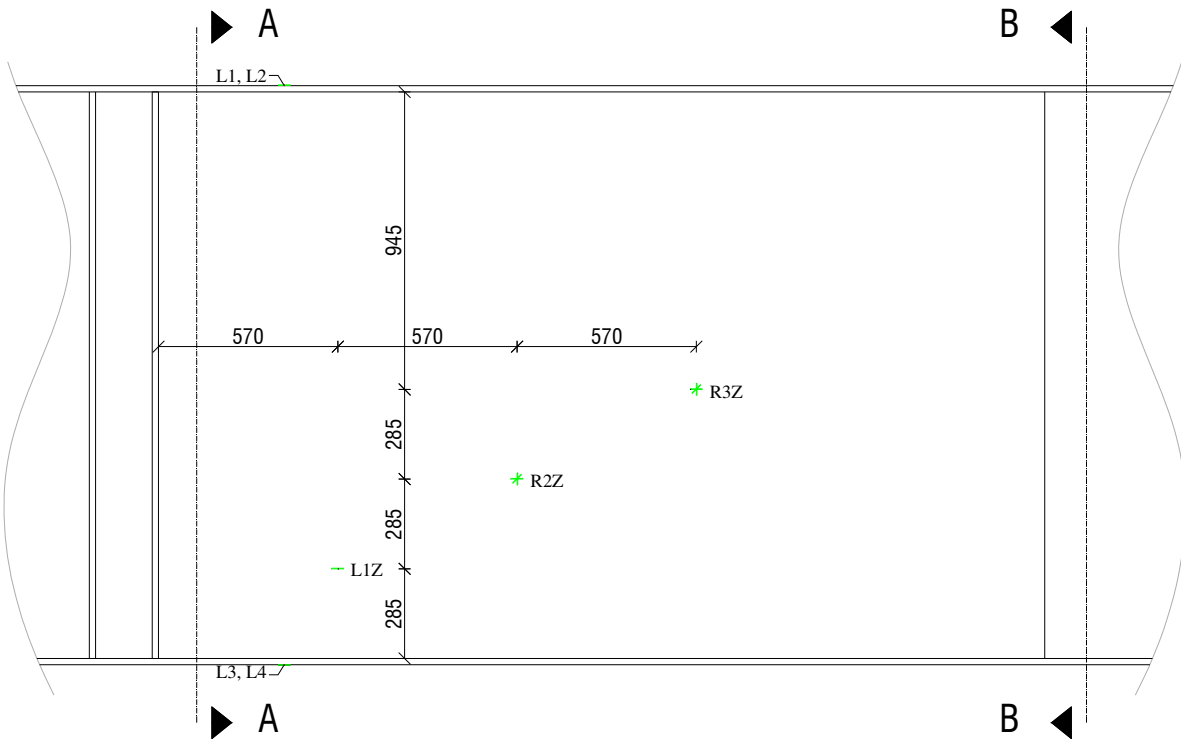
- Position of measured points in the panel



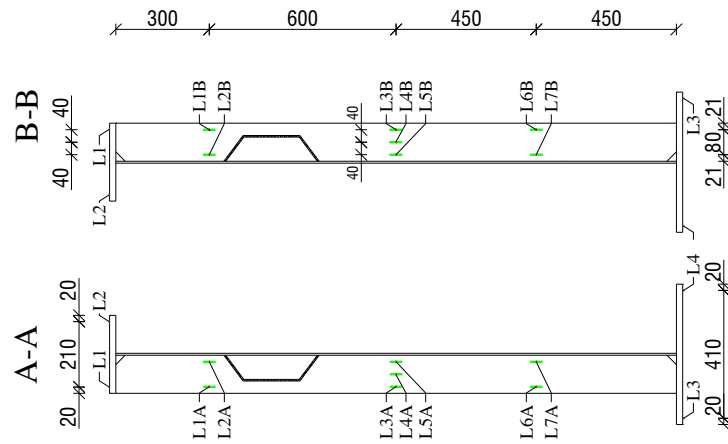
- Position of strain gauges – front side



- Position of strain gauges – back side

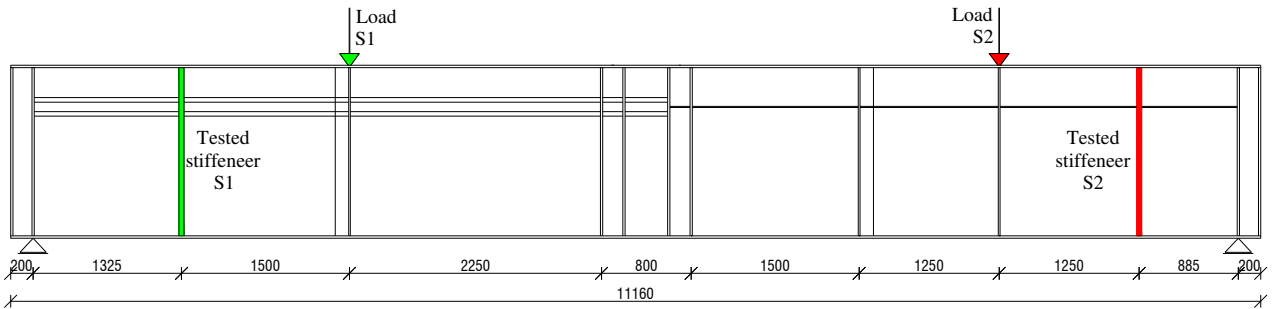


- Position of strain gauges – view A-A and B-B

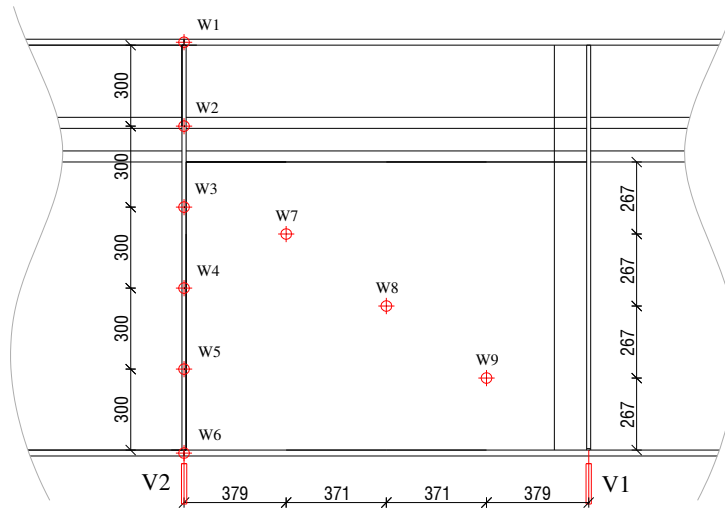


ANNEX B: Layout of tested girders N1 - S1 and N1 - S2

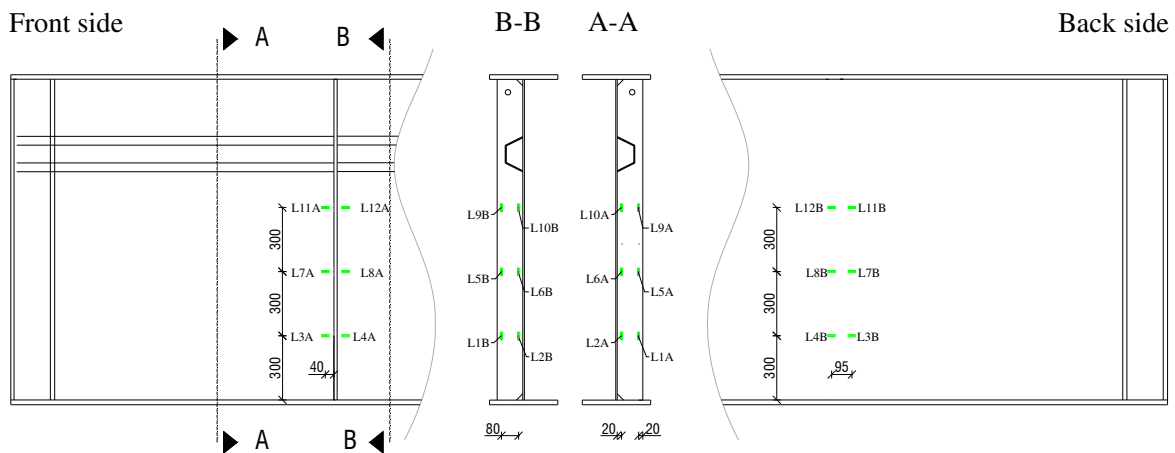
- Layout of tested girder



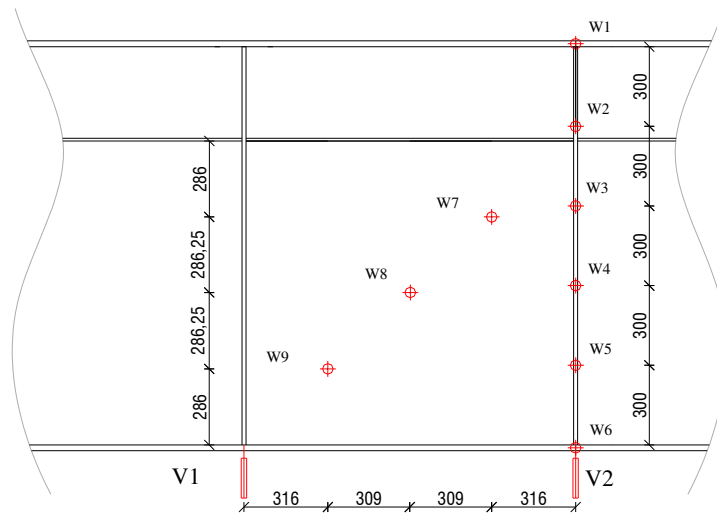
- Position of measured points for test S1



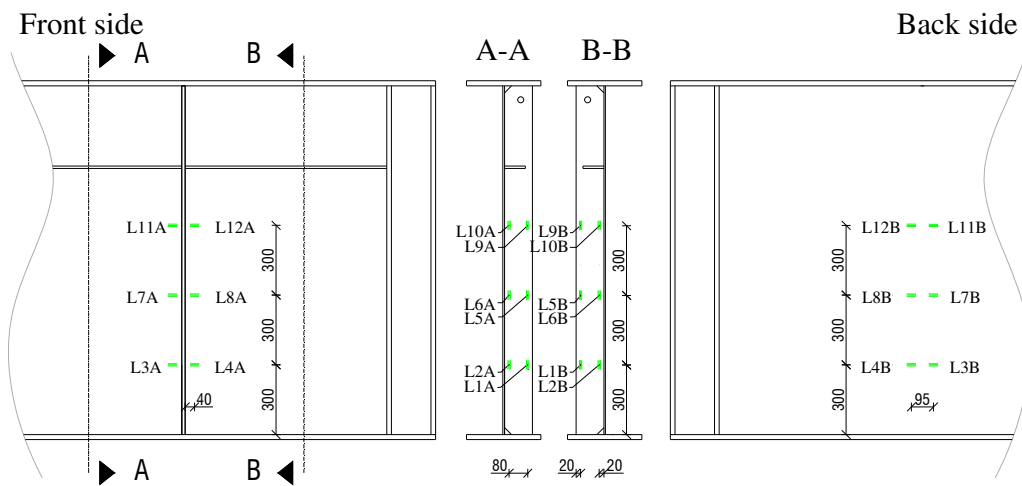
- Position of strain gauges for tests S1



- Position of measured points for test S1



- Position of strain gauges for tests S1



REFERENCES

- [1] Lagerqvist, O. 1994. Patch loading, Resistance of steel girders subjected to concentrated forces. Doctoral Thesis. Lulea, Sweden, Division of Steel structures Lulea University of Technology, Department of Civil Engineering: p. 159.
- [2] Lagerqvist, O. and Johansson, B. 1996. Resistance of I-girders to concentrated loads. *Journal of Constructional Steel Research*, vol. 39, 2: p. 87-119.
- [3] Davaine, L., Raoul, J. and Aribert, J.M. 2004. Patch loading resistance of longitudinally stiffened bridge girders. In: *Steelbridge 2004: International symposium on steel bridges*. Millau, France, june 23-25, 2004. OTUA.
- [4] Kuhlmann, U. and Seitz, M. 2004. Longitudinally Stiffened Girder Webs Subjected to Patch Loading. In: *Steelbridge 2004: International symposium on steel bridges*. Millau, France, june 23-25, 2004. OTUA.
- [5] Chacon, F.R. 2009. Resistance of transversally stiffened hybrid plated girders to concentrated loads. Ph. D. Thesis. Universitat Politècnica de Catalunya: p. 220.
- [6] Kövesdi, B. 2010. Patch Loading Resistance of Girders with Corrugated Webs. Doctoral Thesis. Budapest, Budapest University of Technology and Economics: p. 109.
- [7] Braun, B. 2010. Stability of steel plates under combined loading. Doctoral Thesis. Stuttgart, Universität Stuttgart: p. 226.
- [8] Lee, S.C., Yoo, C.H. and Yoon, D.Y. 2002. Behaviour of Intermediate Transverse Stiffeners Attached on Web Panels. *Journal of Structural Engineering*, vol. 128, 3: p. 337-345.
- [9] Lee, S.C., Yoo, C.H. and Yoon, D.Y. 2003. New Design Rule for Intermediate Transverse Stiffeners Attached on Web Panels. *Journal of Structural Engineering*, vol. 129, 12: p. 1607-1614.
- [10] Xie, M. and Chapman, J.C. 2003. Design of web stiffeners: axial forces. *Journal of Constructional Steel Research*, vol. 59, 8: p. 1035-1056.
- [11] Xie, M. and Chapman, J.C. 2004. Design of web stiffeners: local panel bending effects. *Journal of Constructional Steel Research*, vol. 60, 10: p. 1425-1452.
- [12] Xie, M., Chapman, J.C. and Hobbs, R.E. 2007. A rational design model for transverse web stiffeners. *Journal of Constructional Steel Research*, vol.
- [13] Hendy, C.R. and Presta, F. 2008. Transverse web stiffeners and shear moment interaction for steel plate girder bridges. In: *International Conference on Steel Bridges*. Guimarães, Portugal, june 04-06, 2008. ECCS: p. 8.
- [14] Presta, F. 2007. Post-buckling behaviour of transversely stiffened plate girders. Doctoral Thesis. Cosenza, Università degli studi della Calabria: p. 164.
- [15] Pavlovčič, L., Beg, D. and Kuhlmann, U. 2007. Shear resistance of longitudinally stiffened panels - Part 2: Numerical parametric study. *Journal of Constructional Steel Research*, vol. 63, 3: p. 351-364.

- [16] Pavlovčič, L., Detzel, A., Kuhlmann, U. and Beg, D. 2007. Shear resistance of longitudinally stiffened panels - Part 1: Tests and numerical analysis of imperfections. *Journal of Constructional Steel Research*, vol. 63, 3: p. 337-350.
- [17] COMBRI 2006. Schlussbericht des RFCS -Forschungsprojekts RFS-CR-03018 "Competitive Steel and Composite Bridges by Improved Steel Plated Structures". p. 154.
- [18] Veljkovic, M. and Johansson, B. 2001. Design for buckling of plates due to direct stress. In: *Nordic Steel Construction Conference*. Helsinki, Finland, June 18-20.
- [19] EN 1993-1-5: 2006. - Eurocode 3: Design of steel structures - Part 1-5: Plated structural elements. Brussels, European Committee for Standardisation
- [20] Sinur, F. and Beg, D. 2009. Numerical investigation on moment-shear interaction of longitudinally stiffened girders. In: *Nordic Steel Construction Conference*. Malmö, Sweden, September 02-04, 2009.
- [21] Sinur, F. and Beg, D. 2009. Upogibno-strižna interakcija vzdolžno ojačanih nosilcev. In: 31. zborovanje gradbenih konstruktorjev Slovenije. Rogaška Slatina, oktober 8-10, 2009.
- [22] Galambos, V.T. 1998. *Guide to Stability Design Criteria for Metal Structures*. 5th ed: John Wiley & Sons, inc.
- [23] Wilson, J.M. 1886. On specifications for strength of iron bridges. *Trans. ASCE*, vol. 15, 1: p. 401-403, 489-490.
- [24] Wagner, H. 1929. Eben blechwandträger mit sehr dünnen Stegblechen. *Zeitschr. Flugtechn. Motorluftschiffahrt*, vol. 20: p. 200-306.
- [25] Wagner, H. 1931. Flat Sheet Metal Girder with Very Thin Metal Plates. *NACA Tech. Memo*. Nos. 604, 605, 606, vol.
- [26] Basler, K., et al. 1960. Web buckling tests on welded plate girders. *Welding research council, Bulletin No 64*, New York, vol.
- [27] Basler, K. 1961. Strength of plate girders in shear. *Journal of the Structural Division*, vol. 87, ST 7.
- [28] Gaylord, E.H. 1963. Discussion of K. Basler 'Strength of Plate Girders in Shear'. *Trans. ASCE*, vol. 128, 2.
- [29] Selberg, A. 1973. On the shear capacity of girder webs. *Univ. Trondheim*.
- [30] Takeuchi, T. 1964. Investigation of the load carrying capacity of plate girders. *M.Sc. Thesis*. University of Kyoto.
- [31] Konishi, I. 1965. Theories and experiments on the load carrying capacity of plate girders (Report). *Western Japan Research Society for Bridges, Steel Frames and Welding*.
- [32] Fujii, T. 1968. On an improved Theory for Dr. Basler's Theory. In: *IABSE*: New York.
- [33] Fujii, T. 1968. On ultimate strength of Plate Girders. *Jpn. Shipbuild. Mar.*, vol.

- [34] Fujii, T. 1971. A comparison between theoretical values and experimental results for the ultimate shear strength of plate girders. In: Proceedings of Colloquium on design of plate and box girders for ultimate strength. London, March 25-26. IABSE: p. 161-172.
- [35] Fujii, T., Fukomoto, Y., Nishino, F. and Okumura, T. 1971. Research works on ultimate strength of plate girders and Japanese provisions on plate girder design. In: Proceedings of Colloquium on design of plate and box girders for ultimate strength. London, March 25-26. IABSE: p. 21-48.
- [36] Chern, C. and Ostapenko, A. 1969. Ultimate strength of plate girders under shear (Report). Fritz Engineering Laboratory, Lehigh University Institut of Research.
- [37] Komatsu, S. 1971. Ultimate strength of stiffened plate girders subjected to shear. In: Proceedings of Colloquium on design of plate and box girders for ultimate strength. London, March 25-26. IABSE: p. 49-57.
- [38] Rockey, K.C. and Škaloud, M. 1972. The Ultimate Load Behaviour of Plate Girders Loaded in Shear. *The Structural Engineer*, vol. 50, 1: p. 29-47.
- [39] Porter, D.M., Rockey, K.C. and Evans, H.R. 1975. The Collapse Behaviour of Plate Girders Loaded in Shear. *Structural Engineering*, vol. 53, 8: p. 313-325.
- [40] Höglund, T. 1971. Behaviour and strength of the web of thin plate I-girders (in Swedish). In: Bulletin No.93 of the Division of Building Statics and Structural Engineering. The Royal Institute of Technology: Stockholm, Sweden. p. 13-30.
- [41] Höglund, T. 1971. Simply supported thin plate I-girders without web stiffeners subjected to distributed transverse load. In: Proceedings of Colloquium on design of plate and box girders for ultimate strength. London, March 25-26. IABSE: p. 85-98.
- [42] Höglund, T. 1973. Design of thin-plate I Girders in Shear and Bending. In: Bulletin No.94 of the Division of Building Statics and Structural Engineering. The Royal Institute of Technology: Stockholm, Sweden. p. 13-30.
- [43] Cooper, P.B. 1967. Strength of Longitudinally Stiffened Plate Girders. *J. Struct. Div. ASCE*, vol. 93, 2: p. 419-452.
- [44] Chern, C. and Ostapenko, A. 1971. Strength of Longitudinally Stiffened Plate Girder Under Shear and Moment. Fritz Engineering Laboratory, Lehigh University Institute of Research.
- [45] Höglund, T. 1997. Shear buckling resistance of steel and aluminium plate girders. *Thin-Walled Structures*, vol. 29: p. 13-30.
- [46] Karman, T., Sechler, E.E. and Donell, L.H. 1932. Strength of thin plates in compression. *Trans. A.S.M.E.*, vol. 54: p. 53.
- [47] Winter, G. 1947. Strength of Thin Steel Compression Flanges. *Trans. ASCE*, vol. 112: p. 527-544.
- [48] Winter, G., Lansing, W. and McCalley, R.B. 1950. Four papers on the performance of thin walled steel structures. In: *Eng. Exp. Strn. Rep. No. 33*. Cornell University, Ithaca, N. Y. p. 27-32, 51-57.
- [49] Basler, K. and Thürlimann, B. 1963. Strength of plate girders in bending. In: ASCE.

- [50] Fujii, T. and Akita, Y. 1968. On ultimate strength of plate girders. Japan Shipbuilding and Marine Engineering, vol.: p. 7-16.
- [51] Chern, C. and Ostapenko, A. 1970. Bending strength of Unsymmetrical Plate Girders (Report). Fritz Engineering Laboratory, Lehigh University Institute of Research.
- [52] Basler, K. 1961. Strength of plate girders under combined bending and shear. Journal of the Structural Division, vol. 87, ST 7.
- [53] Herzog, M. 1974. Ultimate static strength of plate girders from tests. J. Struct. Div. ASCE, vol. 100, ST5: p. 849-864.
- [54] Herzog, M. 1974. Die Traglast unversteifer und versteifer, dünnwandiger Blechträger unter reinem Schub und Schub mit Biegung nach Versuchen. Bauingenieur, vol.
- [55] Rockey, K.C. 1971. An Ultimate Load Method for the Design of Plate Girders. In: Proceedings of Colloquium on design of plate and box girders for ultimate strength. London, March 25-26. IABSE: p. 253-268.
- [56] Rockey, K.C., Evans, H.R. and Porter, D.M. 1973. Ultimate Load Capacity of Stiffened Webs Subjected to Shear and Bending. In: Proc. Conf. Steel Box Girders. London.
- [57] Schueller, W. and Ostapenko, A. 1970. Tests on transversally stiffened and on longitudinally stiffened unsymmetrical plate girders. Welding research council, vol. 156.
- [58] Evans, H.R. 1986. An approach by full-scale testing of new design procedures for steel girders subjected to shear and bending. In: Proceedings of the Institute of Civil Engineers: p. 175-189.
- [59] 1987. Public Works Research Institute, Report of load resistance tests on plate girders. Public Works Research Institute Technical Report No. 2533.
- [60] Cooper, P.B., Lew, H.S. and Yen, B.T. 1964. Welded constructional alloy steel plate girders. J. Struct. Div. ASCE, vol. 90, ST 1: p. 1-36.
- [61] Rockey, K. and Skaloud, M. 1969. Influence of the flexural rigidity of flanges upon the load-carrying capacity and failure mechanism in shear. Acta Technica CSAV, vol. 3: p. 295-300.
- [62] Carskaddan, P.S. 1968. Shear buckling of unstiffened hybrid beams. J. Struct. Div. ASCE, vol. 94, ST 8: p. 1965-1992.
- [63] Nishino, F. and Okumura, T. 1968. Failure tests of plate girders using large-sized models. In: Proceedings of 8th Congress: On wearing surfaces for steel bridge decks of lightweight construction. New York, September 07. IABSE.
- [64] Okumura, T., Fujii, T. and Fukumoto, Y. 1967. Failure tests on plate girders. In: Structural Engineering Laboratory Report, Department of Civil Engineering. University of Tokyo.
- [65] Okumura, T. and Nishino, F. 1966. Failure tests of plate girders using large-sized models. In: Structural Engineering Laboratory Report, Department of Civil Engineering. University of Tokyo.
- [66] Wargsjö, A. 1991. Plastic rotation capacity of welded steel girders. Licentiate Thesis. Lulea university of Technology, Sweden: p. .

- [67] Axhag, F. 1998. Plastic Design of Slender Steel Bridge Girders. Doctoral Thesis. Lulea University of Technology: p. 116.
- [68] Vigh, L.G. 2006. Virtual and real test based analysis and design of non-conventional thin-walled metal structures. Doctoral Thesis. Budapest, Budapest University of technology and Economics, Hungary: p. 117.
- [69] Stein, M. and Fralich, R.W. 1950. Critical shear stress of infinitely long simply supported plate with transverse stiffeners. Journal of Aeronautic Science, vol. 17.
- [70] AASHTO: 1996. - Standard specifications for highway bridges. Washington, D.C., American Association of State Highway and Transportation Officials
- [71] Johansson, B., Maquoi, R., Sedlacek, G., Müller, C. and Beg, D. 2007. Commentary and worked examples to EN 1993-1-5 "Plated Structural Elements". In: JRC Scientific and Technical Reports.
- [72] EN 10002-1: 2004. - Metallic materials - Tensile testing - Part 1: Method of test at ambient temperature. Brussels, European Committee for Standardisation
- [73] MATLAB 2007b. MathWorks. Natick, Massachusetts USA.
- [74] EN 1090-2: 2008. - Execution of steel structures and aluminium structures - Part 2: Technical requirements for steel structures. Brussels, European Committee for Standardisation
- [75] Evans, H.R. and Tang, K.H. 1981. A report on five tests carried out on a large-scale transversely stiffened plate girder - TRV3. University College, Cardiff.
- [76] SIMULIA 2008. Abaqus Online Documentation: Version 6.7. EF1. In: Deassault Systemes.
- [77] Sinur, F. and Beg, D. 2010. Imperfection Sensitivity Analysis of Longitudinally Stiffened Plated Girders Subjected to Bending - Shear Interaction. In: Stability and Ductility of Steel Structures. Rio, Brazil, September, 08-10: p. 787-794.
- [78] Beg, D., Kuhlmann, U., Davaine, L. and Braun, B. 2010. Eurocode 3: Design of Steel Structures, Part 1-5-Design of Plated Structures. 1st. ed, ed. ECCS. Vol. 1: Ernst & Sohn Wiley Company: p. 272.
- [79] Winter, G. 1947. Strength of Thin Steel Compression Flanges. Transaction ASCE, vol. 112: p. 527-544.
- [80] Klöppel, K. and Möller, K.H. 1968. Beulwerte ausgesteifer Rechteckplatten (Band II). Ernst & Sohn Verlag, Berlin.
- [81] Klöppel, K. and Scheer, J. 1960. Beulwerte ausgesteifer Rechteckplatten (Band I). Ernst & Sohn Verlag, Berlin.
- [82] EBPlate 2007. Centre Technique Industriel de la Construction Metallique. France, www.cticm.com.
- [83] EN 1990: 2004. - Eurocode-Basis of Structural Design. Brussels, European Committee for Standardisation
- [84] Basler, K. 1961. Strength of plate girders in shear. Journal of the Structural Division, ASCE, vol. 87, ST 7: p. 151-180.